SCUOLA NORMALE SUPERIORE

Classe di Scienze
Perfezionamento in Fisica
PhD Thesis

# Bindings in the Dark

## Bound States in Dark Matter Phenomenology


Candidate:

**Andrea Mitridate**


Thesis submitted for the degree of
Doctor of Philosophy in Physics


Advisor:
Prof. Roberto Contino


2018/2019

# Contents

# The hunt for the missing piece

It is almost a century now since data implying the presence of nonluminous matter in the Universe surfaced: in 1932 Oort [1] observed that the number of stars near the sun was $30-50\%$ less than the number necessary to explain their velocities; then, in 1933, Zwicky [2] pointed out that the velocity dispersion of galaxies in the Coma cluster required 10 to 100 times more mass than the one accounted for the luminous galaxies themselves. The same Zwicky called this unseen matter *dunkle materie* (dark matter). These observations were practically ignored for almost four decades until a large number of new evidences corroborating the claim of Oort and Zwicky emerged.

Nowadays evidences advocating the existence of Dark Matter (DM) range from the galactic scale, where DM is needed to explain the observed stellar dynamics, to cosmological scales, DM being one of the pillars of the ΛCDM model. However, despite its central role, the nature of the DM remains unknown. This ignorance, which mostly stems from our inability to detect non-gravitational interactions between dark and baryonic matter, together with the fact that DM is one of the few phenomenological flaws of the Standard Model (SM) has driven a huge activity in the theoretical community.[1] However, if the lack of information about the DM properties makes quite easy is to come up with plausible theoretical solutions it also makes very hard to proof or disproof them. Thus it is crucial to keep pushing the experimental frontiers in parallel with the theoretical efforts. In the following we summarize the (few) experimental informations we have about the DM, and the experimental endeavors that the community is undergoing in the attempt to unveil some of its key features.

## Energy density

The only thing we know with a high degree of accuracy about the DM is its cosmological abundance, $\Omega_{\rm DM} \equiv \rho_{\rm DM}/\rho_0$, where $\rho_{\rm DM}$ and $\rho_0$ are respectively the DM and the critical energy densities. Up to now, the more accurate determination of $\Omega_{\rm DM}$ comes from fitting the parameters of the ΛCDM model to the CMB power spectrum [6]:

$$\Omega_{\rm DM} h^2 = 0.1186 \pm 0.0020\,, \tag{1}$$

where $h$ is the Hubble constant in units of $100\,\mathrm{Km}/(\,\mathrm{s\,Mpc})$.

## Mass

While the DM energy density is known with an high degree of accuracy, its number density $n_{\rm DM} = \rho_{\rm DM}/M_{\rm DM}$, or equivalently its mass, is very poorly constrained.

The lower bound on the DM mass depends on whether it is a fermionic or a bosonic particle. In the bosonic case, this lower limit comes from the requirement that DM has to behave classically

[1] The lack of non-gravitational signals, not only limits our investigating power, also raises the doubt that the DM could be just a manifestation of some modified theory of gravity. This possibility seemed to be ruled out by the observation of two galaxies lacking DM [3, 4], however a recent work [5] showed that the apparent lack of DM was due to a misestimate of the galaxis' distances. Therefore the doubt remains.

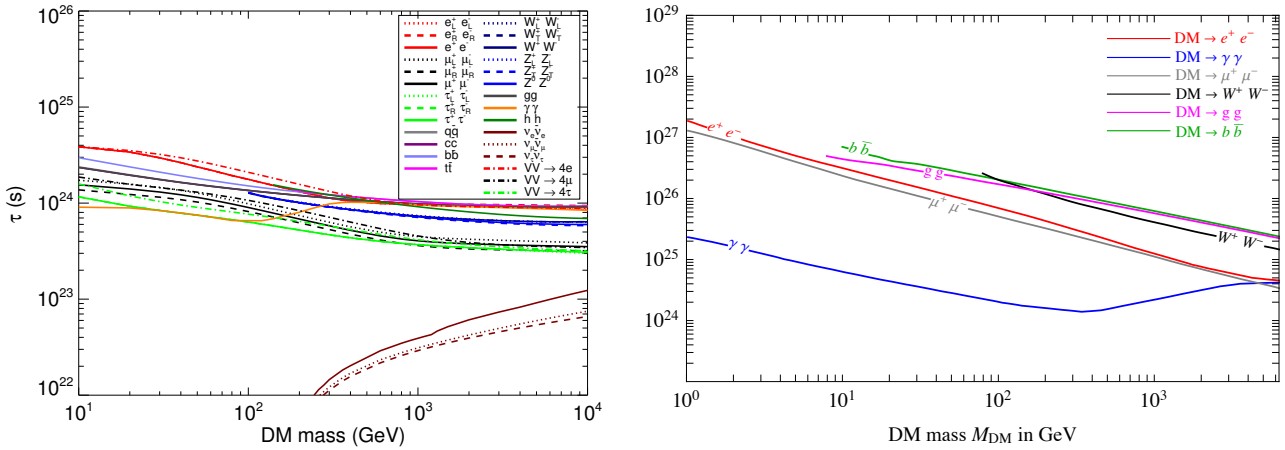


Figure 1: *Bounds on the DM lifetime from measurements of the CMB power spectrum (left panel) [12], and 21-cm absorption signal (right panel) [13], assuming different decay channels. Both bounds are provided up to DM masses of* $\mathcal{O}(10\,\mathrm{TeV})$. *The ones coming from CMB are expect to remain constant at higher masses, while further studies are needed to extend the ones coming from* $21-cm$ *line observables. At masses below the* MeV *significant bounds can be placed only assuming a decay channel into photons.*

on galactic scales, *i.e.* its de Broglie wavelength, $\lambda_{\rm DM} = h/(M_{\rm DM} v_{\rm DM})$ has to be smaller than galactic length scales ($\sim 10\,\mathrm{Kpc}$). From this requirement, and taking $v_{\rm DM} \sim 200\,\mathrm{Km/s}$ (the typical DM velocity in our galaxy), we find the lower bound $M_{\rm DM} \gtrsim 10^{-22}\,\mathrm{eV}$. For fermionic DM we also have to require that the degeneracy pressure does not prevent galaxy formation. The space density of fermions cannot exceed the value $f = gh^{-3}$, where $g$ is the number of internal degrees of freedom [7]. Assuming the dark-matter distribution to be an isothermal sphere with core radius $r_c = (9\sigma^2/4\pi G\rho_c)^{1/2}$, where $\rho_c$ is the central density and $\sigma$ is the Maxwellian one-dimensional velocity dispersion, the corresponding maximum phase-space density is $f = \rho_c M_{\rm DM}^{-4}(2\pi\sigma^2)^{-3/2}$ [8]. Requiring that this maximum value is smaller than $gh^{-3}$ and taking a Milky Way type galaxy ($\sigma = 150\,\mathrm{Km/s}$ and $\rho_c >$ GeV $\mathrm{cm}^{-3}$) we get $M_{\rm DM} > 25\,\mathrm{eV}$.

For what concern the largest possible value for the DM mass, several analysis seem to rule out DM candidates with masses above $\sim 10-100 M_\odot$ (see for example the bounds from disruption of compact stellar system [9, 10]). However, is important to emphasize that many of these analysis are plagued by astrophysical uncertainties. Recently it has been pointed out [11] that pulsar timing measurements will provide an astrophysical clean constrain in the near future.

To summarize, we are able to constraint the DM mass within 79 orders of magnitude for bosonic candidates and 56 orders of magnitudes for fermionic ones.

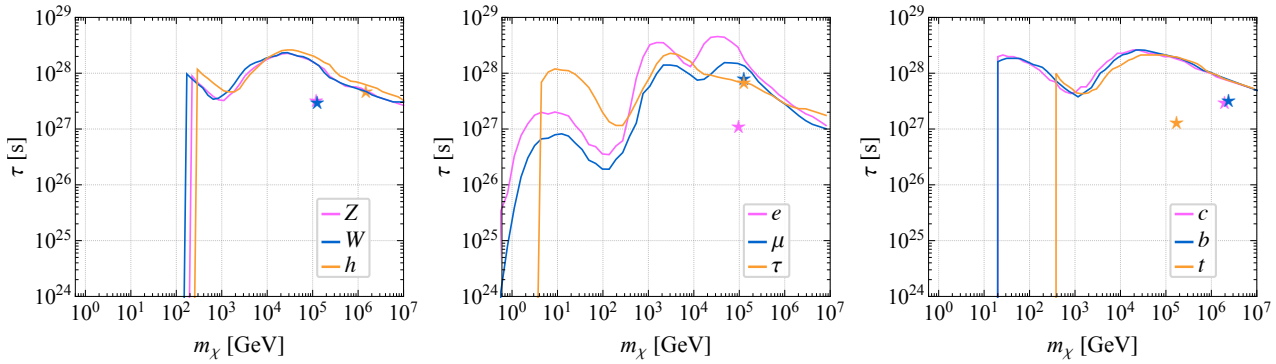


Figure 2: *Bounds on the DM lifetime from indirect searches for different decay channels [14]. In the mass range* $\sim 10^7$ *to* $10^9$ GeV *the IceCube experiments provide stronger bounds, see for example [15].*

## Lifetime

The DM has to be present both in the early Universe, where it provides the seeds for structure formation, and in the present-day Universe, where it dictates the stellar dynamics in galaxies. Therefore, we can readily state that its lifetime has to be at least of the order of the Universe: $\tau_{\rm DM} \gtrsim 10^{17}$ s. However, much stronger constraints can be placed looking for the effects of the energy released in DM decays [2].

Decays during the recombination epoch inject highly energetic particles in the baryon-photon plasma at a rate which is proportional to $\tau_{\rm DM}$. These particles heat the gas and -more importantly- ionize hydrogen atoms, modifying the location and the thickness of the last scattering surface (LSS). The shift of LSS location translate in a shift of the CMB acoustic peak, while the broadening of the LSS induces a suppression of the CMB modes with $l \gtrsim 3$. Therefore, measurements of the CMB power spectrum can be used to constrain $\tau_{\rm DM}$ [12], as shown in the left panel of Fig. 1.

The recently observed absorption line in the low energy tail of the CMB spectrum [16] allows us to put an upper bound on the temperature of the intergalactic medium (IGM) at redshift $z \sim 17$. Decays of DM particles during the dark ages (*i.e.* the epoch which goes from recombination, $z \sim 1100$, to reionization, $z \sim 10$) are constrained, mainly because they inject energy in the IGM heating it, erasing or reducing the absorption line [17, 18, 13]. The bounds obtained in this way are stronger than the ones derived from observations of the CMB power spectrum (see the right panel of Fig. 1) and will became even stronger as soon as the experimental error on the amplitude of the absorption line is reduced.

[2] Here (and in the following discussion about the DM annihilation cross section) we assume that DM either decays (annihilates) into SM or that its decay (annihilation) products decay into SM on cosmologically short timescales. This is the case in the vast majority of DM models but scenarios in which both this assumptions are violated can be engineered (consider for example DM decaying into dark photons of a completely decoupled dark sector). In this case, bounds on the DM lifetime and annihilation cross section have to be revised.

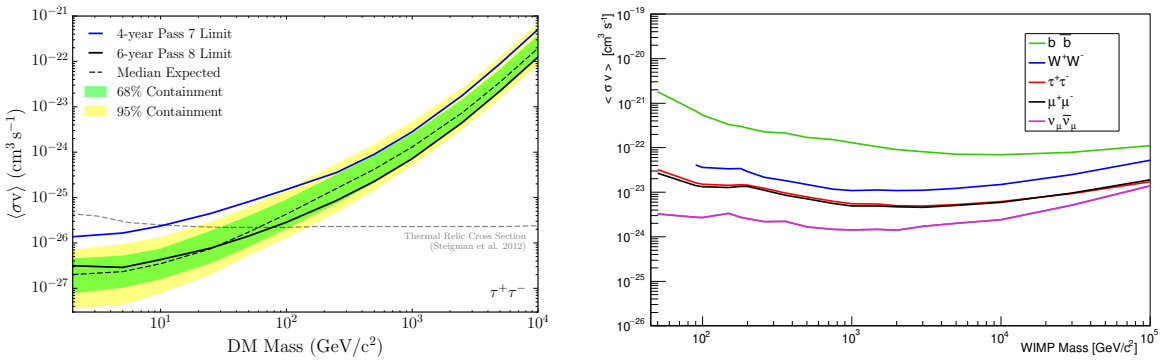


Figure 3: *Bounds on the DM annihilation cross section from indirect searches for different decay channels. The left panel shows an example of bound for masses around the weak scale [19], the right panel shows bounds at higher masses from the ANTARES neutrino telescope [20].*

Finally, products of DM decays in the present-day Universe give an excess over the predicted flux of particles from astrophysical objects. Experiments looking at these flux can then be used to constraint the DM lifetime (see for example [14] and Fig. 2 where some of their results are reported).

## Annihilation cross section

If the DM abundance is not generated by a primordial asymmetry, residual annihilations of DM particles can release energy in the Universe giving rise to effects similar to the ones generated by DM decays. Therefore, CMB observables [22] together with 21-cm [21] and indirect detection experiments can be use to constrain the DM annihilation cross section, see Fig. 3 and 4 (for DM masses around the weak scale see for example [19, 23] for searches of gamma rays in Dwarf spheroidal galaxies and the Milky Way galactic halo, and [24] for searches of antiprotons; for DM above the TeV the strongest bound are provided by HESS [25] and neutrino telescopes, *e*.g. [20]).

Despite the bounds provided by the three methods above mentioned are in the same ballpark, it is important to stress that the ones coming from the 21-cm signal are free from astrophysical uncertainties (that plague the ones coming from indirect detection) and model independent (differently from the ones from CMB observables, which rely on a global fit that assumes ΛCDM).

## Interactions with the SM

One of the most promising way to shed some light on the particle nature of the DM is to directly detect it. A long-standing strategy to achieve this goal is to look for interactions between DM particles of the galactic halo and terrestrial detectors. Since the typical velocity of DM particles in our galaxy is fixed ($v_{\rm DM} \sim 10^{-3}$), the typical kinetic energy carried by a DM particle changes

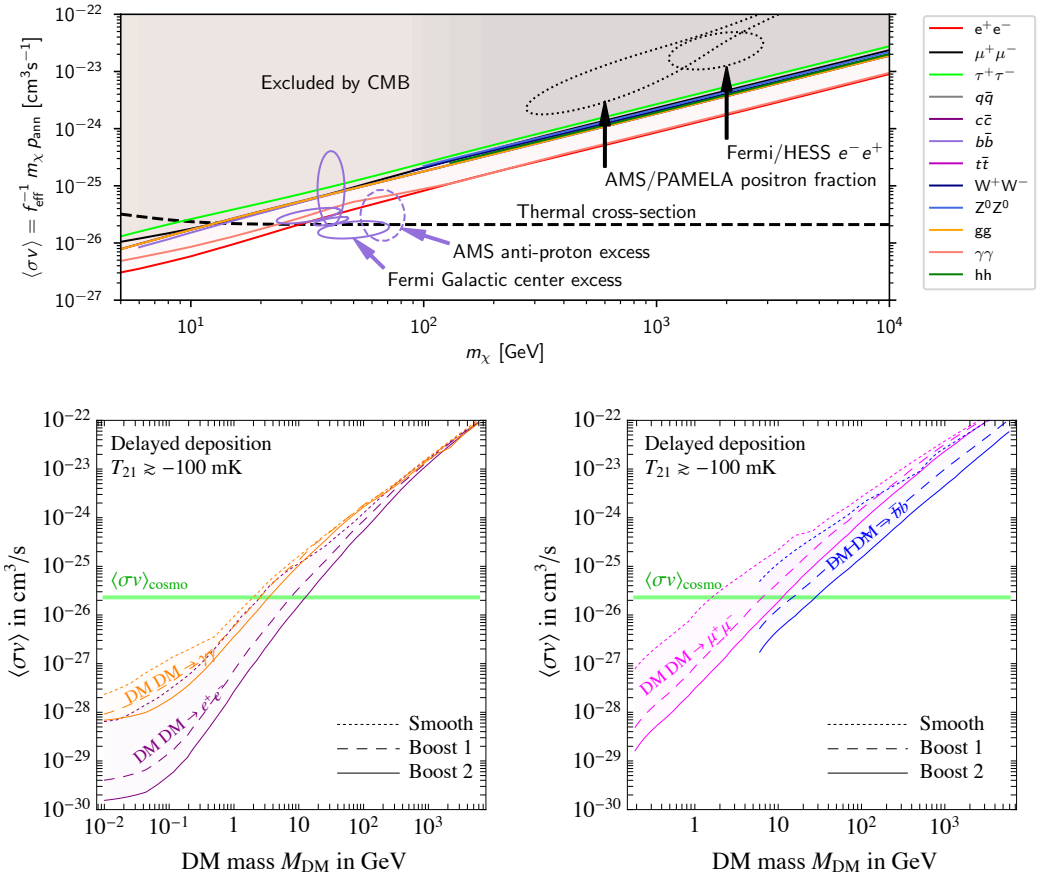


Figure 4: *Bounds on the DM annihilation cross section from measurements of the CMB power spectrum (top panel) [6], and 21-cm absorption signal (lower panels) [21], assuming different dacey channels. Both the CMB and the 21-cm bounds are expect to continue the linear scaling at higher DM masses. At masses below the* MeV*, as for the decay, significant bounds can be placed only assuming annihilations into photons.*

with its mass. Therefore, different experiments sensitive to different energy ranges are required to test different DM masses.

For a long time the weakly interacting massive particle (WIMP) scenario has dominated the direct detection program, partly because of its theoretical attractiveness (especially in its supersymmetric realization) and partly because of its fairly well defined target region in the parameter space (*i.e.* a mass around the weak scale, $1\,\text{GeV} \lesssim M_{\rm DM} \lesssim 10\,\text{TeV}$, and a scattering cross section with nucleons in the range $10^{-50}\,\text{cm}^2 \lesssim \sigma_{\rm DM-n} \lesssim 10^{-45}\,\text{cm}^2$). This lead to the development of several experiments aimed to detect nuclear recoils induced by scatterings of DM particles; which, with a typical energy threshold of order 10 KeV, were sensitive to DM masses $\gtrsim 10\,\text{GeV}$. Up to now, no scattering events have been observed, and we can only place upper bounds on the DM-nucleon scattering cross sections. The strongest ones (for masses above 10 GeV) are provided by the XENON1T experiment [26], whose results are summarized in Fig. 5.

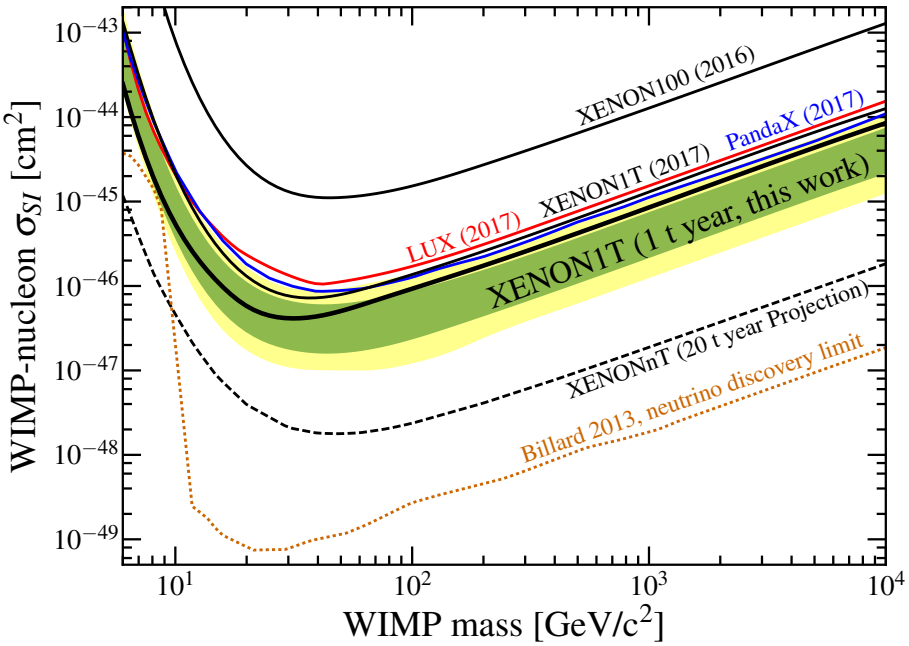


Figure 5: *Reproduced from [26]. Solid lines show present bounds on the spin-independent (SI) cross section for DM-nucleon scattering. The black dashed line shows a projection of the bounds that will be placed by XENONnT in the case of a null detection, while the yellow dashed line shows the neutrino floor.*

The lack of a detection signal in experiments looking for WIMP-like particles gave rise, in the last decade, to a blossoming of new DM candidates that, like WIMP ones, are highly motivated by theoretical results and/or experimental data, but live in different (typically sub GeV) mass ranges. A broad and partially incomplete classification can be made dividing them in two categories: *hidden-sectors* and *ultra-light* candidates.

Hidden sectors candidates are a natural generalization of WIMP candidates to include interaction with a new force rather than just with SM ones. In this scenario interactions with the SM may be only gravitational, or mediated by new forces that interact only very feebly with the dark and/or visible sectors. Thanks to the interplay between the SM and dark dynamic, hidden sectors are viable over a broader mass range than WIMP, roughly going from KeV to tens of TeV. The technological challenge in detecting sub GeV candidates is the size of the detectable signal. If we consider a nuclear recoil, for example, the maximum energy which can be deposited in the detector is given by

$$E_{\max} = \frac{2\mu^2 v_{\rm DM}^2}{M_N} \lesssim 190\,\text{eV} \left(\frac{M_{\rm DM}}{500\,\text{MeV}}\right)^2 \left(\frac{16\,\text{GeV}}{M_N}\right) \tag{2}$$

where $\mu$ is the DM-nucleus reduced mass and $M_N$ is the nucleus mass. From this equation we see that the maximum deposited energy decreases quadratically with the DM mass when

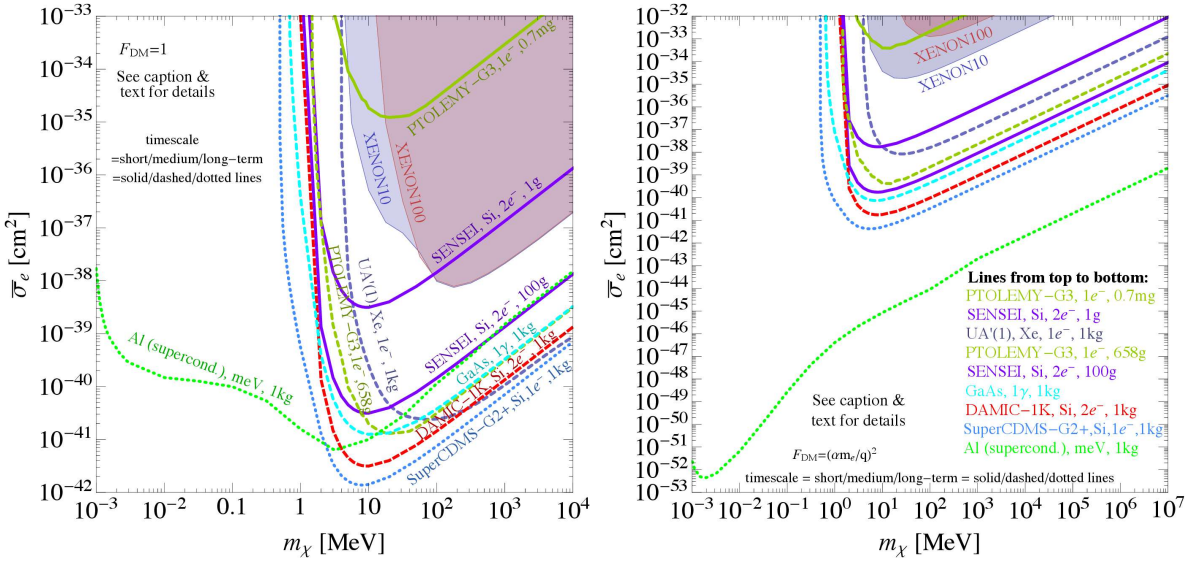


Figure 6: *Present (shaded regions) and future (solid/dashed/dotted lines for short/medium/long timescales) bounds on the DM-electron scattering cross section of ultra-light DM candidates [27]. Left (right) panel assumes a momentum-independent (dependent) interaction.*

this is lowered below the GeV scale, rapidly going below the threshold of most current DM detectors. Right now, the only experiments already probing the sub GeV region (down to $\sim 10\,\text{MeV}$) are XENON10 and XENON100. The experimental apparatus is the same searching for WIMP-like candidates but, instead of looking for nuclear recoil, they look for electron recoils. These processes have a much smaller energy threshold ($\sim 10 \div 100\,\text{eV}$) and, as long has the DM mass is heavier than the electron, they can access to a much larger fraction of the DM kinetic energy [28]. Because of the poor knowledge of the background for few-electron events, the bounds provided by these experiments (shown in Fig. 6) are less stringent than the ones in the WIMP mass range. However, using the annual modulation of the signal to reduce the background could lead to a sizable improvement of these bounds [28]. Candidates as light as the MeV can be probed by looking for excitations of electrons from the valence to the conduction band in semiconductors. The challenge here is to reduce dark counts and increase sensitivity to energy depositions three orders of magnitude below the WIMP targets. This program is well under way in silicon targets, and is actively being pursued in collaborations such as SENSEI [29], DAMIC [30] and SuperCDMS [31] whose projected sensitivities are shown in Fig. 6. To test even lighter candidates, down to the KeV scale, small gap materials have been identified as the best targets. They include superconductors [32] and Dirac materials for the case of electrons excitations, and superfluid Helium [33] and polar materials [34] when the DM couples to nuclei or ions.

Below the KeV scale we enter the realm of ultra-light DM candidates. They include scalars, pseudoscalars and vector bosons produced during inflation or high-temperature phase transitions;

the most famous being the axion. Bosonic candidates down to the meV scale can be tested by looking for their absorption in superconductor through single phonon emission [35], or in a semiconductor through emission of one [36, 37] or more [36] phonons. For masses below the eV, bosonic DM in the galaxy starts to behave as an oscillating classical field with a high occupation number and frequency $\nu = M_{\rm DM}/2\pi$. For sub-meV masses, corresponding to frequencies less than THz, this property can be used to detect these ultra-light candidates looking for continuous signals rather than impulse ones. Different experiments, relying on different couplings of the oscillating DM field to the SM, plan to explore the entire mass range: from the meV scale down to $10^{-22}$ eV. Experiments sensitive to electromagnetic coupling will explore the mass range $10^{-12} \div 10^{-5}$ eV, the ones looking for coupling to gluons will test the range $10^{-12} \div 10^{-6}$ eV, while the lowest mass range $10^{-22} \div 10^{-15}$ can be tested by state-of-the-art torsion balances and atomic interferometers (for a brief summary of the experiments see Table 1).

In addition to detect interactions with DM particles in the galactic halo, we can also directly probe the DM by producing it at colliders. Collider searches are particularly well suited to test models where the DM abundance is fixed by a thermal freeze-out of annihilations into SM particles (either directly, like for ordinary WIMP, or through some portal, like in the case of hidden sectors). In this case a lower bound can be placed on the annihilation cross section of the DM, and this translates in a minimum expected rate at colliders. Compared to direct detection experiments, colliders have advantages (reduced dependence on the DM particle nature, capability to explore the dark sector structure by producing the mediators, ecc...) and disadvantages (difficulties to test non thermal models, like freeze-in scenarios, where the annihilation cross sections are extremely small). The experimental approaches used in collider searches can be broadly divided in three chathegories: missing mss(/energy/momentum) searches, where we look for the missing mass associated to the undetected DM particles. Dark photon production, where we look for SM decays of the hypothetical mediator of the dark sector. And searches in electron and proton beam dump, where the DM is produced in electron or proton decays and detected through a scattering in a downstream detector. For a review of on-going and future experimental efforts in DM searches a colliders see [38].

## Self-interactions

One of the best way to constrain DM self interactions is to study merging clusters, with the most famous being the "Bullet clusters" [45, 46] (for other methods see *e.g.* [47] and [48]). Clusters mergers are characterized by three components: galaxies that, because of their small self-scattering cross section, behave as collisionless particles; intercluster medium (ICM) gas that, because of the drag forced induced by the ram pressure, is dissociated by any collisionless component; and DM which provides the larger contribution to the total cluster mass. If the DM is collisionless its distribution, reconstructed through strong and weak gravitational lensing, should coincide with the one of galaxies after the merger. While if it has non-negligible self interaction we expect to see an offset between the DM and galactic components. In the archetypical merger provided by the "Bullet clusters" the center of the galactic and mass distribution are offset by

| Experiment | Coupling | Sensitivity |
|---|---|---|
| ADMX | E&M | $500\,\text{MHz} \div 10\,\text{GHz}$ |
| HAYSTAC [39] | E&M | $2.5\,\text{GHz} \div 12\,\text{GHz}$ |
| LC circuits [40] | E&M | $3\,\text{MHz} \div 30\,\text{MHz}$ |
| ABRACADABRA [40] | E&M | $1\,\text{Hz} \div 100\,\text{MHz}$ |
| CASPEr [41] | QCD & Spin | $200\,\text{Hz} \div 200\,\text{MHz}$ |
| Torsion balances [42, 43] | Spin & Scalar | $10^{-8}\,\text{Hz} \div 10^{-1}\,\text{Hz}$ |
| Atomic interferometers (MAGIS) [44] | Spin & Scalar | $0.1\,\text{Hz} \div 10\,\text{Hz}$ |

Table 1: Experiments that are going to probe the ultra-light mass landscape. The first column indicates the coupling between the oscillating DM field and the SM exploited by the experiments, while the second one reports the frequency window in which the experiments operate.

$25 \pm 29\,\text{Kpc}$, implying that DM behaves as collisionless within experimental uncertainties [49]. Specifically, this observations constrains the self-interaction cross section to be smaller than $\sigma_{\text{self}}/M_{\text{DM}} \lesssim 1.25\,\text{cm}^2/\text{g}$ [49].

This bound is quite weak and leaves room for non negligible self-interactions between DM particles. For example DM at the electro-weak scale is allowed to have a self scattering cross section just one or two orders of magnitude smaller than the neutron capture cross section. Those hypothetical self-interactions have sometimes been advocated to solve some tensions in small scale structures observables. Indeed, while collisionless DM successfully explains distribution of matter on large scales ($\gtrsim$ Mpc), a few problems seem to arise when we try to explain small scale distributions (for a recent review see [50]). Among them the biggest ones are: the *cusp to core* problem; *i.e.* the tension between the observed DM core profile ($\rho_{DM} \propto r^0$) [51] and the cusp profile ($\rho_{\text{DM}} \propto r^{-1}$) expected by numerical simulation assuming no self interactions [52]. The *diversity problem*; *i.e.* the clash between the large scatter observed in the density profile of dwarf galaxies with equal maximum rotation speed [53], and the small scatter obtained by numerical simulations [52]. The *too-big-to-fail problem*; *i.e.* the tension between the Milk Way's satellites masses inferred from observed stellar dynamics with respect to the values predicted by numerical simulations of a $10^{12} M_\odot$ cold DM halo with no self interactions [54]. However, it must be emphasized that it is still unclear wether these discrepancies are due to some unexpected properties of the DM or to the limited accuracy of the N-body simulations used to make predictions on the small scale distribution of matter (like, for example, the lack of baryonic feedback).

It is clear from what we have said so far that the DM issue is far from being solved. Experimental and theoretical efforts are still needed, with the former providing new hints for the model building and the latter identifying motivated target regions for experiments.

Theoretical works on the subject broadly divide in two categories: model independent studies and model building works. In the first category fall -for example- works trying to infer properties of the DM using astrophysical and cosmological data, or to understand what kind of mechanism may have generated the abundance of DM that we observe in the Universe. In the second category there are works that, motivated by theoretical puzzles and/or experimental evidences, propose new viable DM candidates. The content of this thesis touches both these categories with the *fil rouge* being the study of DM bound states.

Bound states are a common feature of theories with long-range or confining forces. In the former case bound states are perturbative objects resembling atoms of QED, while in the latter they are more similar to hadrons of QCD. Bound states are one of the main characters in the cosmological history of the visible part of the Universe from recombination up today, and it is interesting to wonder if they could play a crucial role also in the dark sector.

The thesis is divided in two parts. The first one, which is mainly based on [55, 56], is devoted to a model independent study of bound state effects on DM thermal relics. Specifically, we discuss how the relic abundance of DM candidates produced through thermal freeze-out is modified by the additional annihilation channel provided by formation and subsequent decay of unstable DM bound states. The second part, based on [57–59], is model building oriented. There, we present some models where the DM candidate is not an elementary particle but a composite state of some confining dynamic (either a new dark force or the strong dynamic of the SM).

# Part I

# Bound States and thermal relics

On the road to unveil the nature of the Dark Matter, the knowledge of its cosmological abundance is one of the few experimental evidences guiding us. Requiring that this cosmological abundance is reproduced is a common way to constrain the parameter space of a DM model and provide target regions for experiments. Thus, it is crucial to compute this quantity accurately.

Even though the mechanism that sets the abundance of DM in the Universe is still unknown, among the many proposals thermal freeze-out is one of the most known and studied. In this framework, the final abundance only depends on how efficiently the DM annihilates. It has been notice long ago [60–62] that long range interactions between DM particles can significantly enhance or suppress this annihilation rate, through an effect that goes under the name of Sommerfeld enhancement. More recently [63–67], it has been shown that formation and subsequent decay of unstable DM bound states, providing a new annihilation channel, can also significantly enhance the annihilation rate. So far, this effect have been mostly considered in models where the DM is charged under a speculative abelian extra 'dark force'. In the following two chapters we present a formalism that allows one to include this effect in the case of a thermal relic charged under SM interactions.

# Chapter 1

# Including bound states in the cosmological history

In this chapter we present generic formulæ for computing how Sommerfeld corrections together with bound-state formation affect the thermal abundance of Dark Matter with non-abelian gauge interactions. We then apply these results to two benchmark DM candidates: an electroweak triplet and quintuplet. In the latter case bound states raise the DM mass required to reproduce the cosmological DM abundance from 9 to 14 TeV and give new indirect detection signals such as (for this mass) a dominant $\gamma$-line around 85 GeV. We conclude considering DM co-annihilating with a colored particle, such as a squark or a gluino, finding that bound state effects are especially relevant in the latter case.

The chapter is structured as follows. In section 1.1 we show how the system of Boltzmann equations for DM freeze-out can be reduced to a single equation with an effective annihilation cross section that takes into account Sommerfeld corrections and bound state formation. In section 1.2 we review how the Sommerfeld correction can be computed for non-abelian gauge interactions, and how the effect of non-zero vector masses can be approximated analytically. In section 1.3 we summarise the basic formulæ for bound state formation, showing how the effects of non-abelian gauge interactions can be encoded into Clebsh-Gordon-like factors, and how the main effect of massive vectors is kinematical. In section 1.4 we provide formulæ which describe the main properties of the bound states, such as annihilation rates and decay rates. All these quantities are needed at finite temperature: in section 1.5 we discuss the issue of thermal corrections, showing that the breaking of gauge invariance lead to the loss of quantum coherence. Finally, in section 1.6 we perform concrete computations in interesting models of Dark Matter charged under $\mathrm{SU}(2)_L$ (a wino triplet, a quintuplet) and of co-annihilation with particles charged under $\mathrm{SU}(3)_c$ (squarks and gluinos). We find that bound state effects can be sizeable, as summarized in the conclusion, section 1.7.

## 1.1 Boltzmann equations

We assume that the DM, $\chi_i$, lies in the representation $R$ (if real) or $R \oplus \overline{R}$ (if $R$ is complex) of a gauge group $G$ with gauge coupling $g$. We define $\alpha = g^2/4\pi$ and $g_\chi$ as the number of degrees of freedom of the DM system. The evolution of the DM number density, $n_{\rm DM}$, together with the one of the various bound states, $n_I$, is described by a set of coupled Boltzmann equations. In this section we show how this system can be reduced to a single equation for the DM density with an effective DM annihilation cross section. In what follows, each DM bound states is identified by an index $I$ which collectively denotes its various quantum numbers: angular momentum, spin, gauge group representation. etc.

The Boltzmann equation for the total DM density is

$$sHz\frac{dY_{\rm DM}}{dz} = -2\gamma_{\rm ann}\left[\frac{Y_{\rm DM}^2}{Y_{\rm DM}^{\rm eq2}} - 1\right] - 2\sum_I \gamma_I\left[\frac{Y_{\rm DM}^2}{Y_{\rm DM}^{\rm eq2}} - \frac{Y_I}{Y_I^{\rm eq}}\right] \tag{1.1}$$

where $Y_{\rm DM} = n_{\rm DM}/s$, $s$ is the entropy density and $z = M_\chi/T$. We define as $n^{\rm eq}$ and $Y^{\rm eq}$ the value that each $n$ or $Y$ would have in thermal equilibrium, and $\gamma$ is the space-time density of interactions in thermal equilibrium. The first term describes DM DM annihilations to SM particles; the extra term describes formation of bound state $I$. The expression of $\gamma_{\rm ann}$ is related to the annihilation cross section by [68]:

$$\gamma_{\rm ann} = \frac{T}{64\pi^4}\int_{4M^2}^{\infty} ds\, s^{1/2} K_1\left(\frac{\sqrt{s}}{T}\right)\hat{\sigma}(s) \tag{1.2}$$

where $K_1$ is a modified Bessel function, and $\hat{\sigma}$ is the adimensional reduced annihilation cross section:

$$\hat{\sigma}(s) = \int_{-s}^{0} dt \sum \frac{|\mathcal{A}|^2}{8\pi s} \tag{1.3}$$

with $s, t$ being the Madelstam variables and the sum running over all DM components and over all the annihilation channels into all SM vectors, fermions and scalars, assuming that SM masses are negligibly small. For bound state formation, the explicit value of $\gamma_I$ is give in eq.(1.9).

We next need the Boltzmann equation for the number density of bound state $I$, $n_I(t)$:

$$\frac{\dot{n}_I + 3Hn_I}{n_I^{\rm eq}} = \langle\Gamma_{I\rm break}\rangle\left[\frac{n_{\rm DM}^2}{n_{\rm DM}^{\rm eq2}} - \frac{n_I}{n_I^{\rm eq}}\right] + \langle\Gamma_{I\rm ann}\rangle\left[1 - \frac{n_I}{n_I^{\rm eq}}\right] + \sum_J \langle\Gamma_{I\to J}\rangle\left[\frac{n_J}{n_J^{\rm eq}} - \frac{n_I}{n_I^{\rm eq}}\right]. \tag{1.4}$$

The first term accounts for formation from DM DM annihilations and breaking: $\langle\Gamma_{I\rm break}\rangle$ is the thermal average of the breaking rate of bound state $I$ due to its collisions with the plasma. The second term contains $\langle\Gamma_{I\rm ann}\rangle$, which is the thermal average of the decay rate of the bound state $I$ into SM particles, due to annihilation of its DM components. The third term describes decays to lower bound states $J$ or from higher states $J$, as well as the inverse excitation processes. They are both accounted in a single term if we define $\Gamma_{J\to I} = -\Gamma_{I\to J}$. For decays, the thermal average of

the Lorentz dilatation factor of a particle with total mass $M$ gives $\langle\Gamma\rangle = \Gamma K_1(M/T)/K_2(M/T)$, which equals to the decay width at rest $\Gamma$ in the non-relativistic limit $T \ll M$. The thermal rate for breaking has a different dependence on $T$. In the models we consider at least some decay or annihilation rates is much faster than the Hubble rate, $\Gamma \gg H$. Therefore, the left-handed side of eq. (1.4) can be neglected, and the system of differential equations reduces to a system of linear equations that determine the various $n_I/n_I^{\rm eq}$. This can be shown formally by rewriting eq. (1.4) for $n_I(t)$ into an equivalent Boltzmann equation for $Y_I(z)$

$$sHz\frac{dY_I}{dz} = n_I^{\rm eq}\left\{\langle\Gamma_{I\rm break}\rangle\left[\frac{Y_{\rm DM}^2}{Y_{\rm DM}^{\rm eq2}} - \frac{Y_I}{Y_I^{\rm eq}}\right] + \langle\Gamma_{I\rm ann}\rangle\left[1 - \frac{Y_I}{Y_I^{\rm eq}}\right] + \sum_J\langle\Gamma_{I\to J}\rangle\left[\frac{Y_J}{Y_J^{\rm eq}} - \frac{Y_I}{Y_I^{\rm eq}}\right]\right\}. \quad (1.5)$$

Inserting the values of $n_I$ or $Y_I$ into eq. (1.1), it becomes one differential equation for the DM abundance with an effective cross section

$$sHz\frac{dY_{\rm DM}}{dz} = -2\gamma_{\rm eff}\left[\frac{Y_{\rm DM}^2}{Y_{\rm DM}^{\rm eq2}} - 1\right]. \quad (1.6)$$

For example, in the case of a single bound state $I = 1$ one finds

$$\gamma_{\rm eff} = \gamma_{\rm ann} + \gamma_1{\rm BR}_1, \qquad {\rm BR}_1 = \frac{\langle\Gamma_{1\rm ann}\rangle}{\langle\Gamma_{1\rm ann} + \Gamma_{1\rm break}\rangle}. \quad (1.7)$$

Namely, the rate of DM DM annihilations into the bound state gets multiplied by its branching ratio into SM particles.[1] The breaking rate $\Gamma_{I\rm break}$ is related to the space-time density formation rate $\gamma_I$ by the Milne relation:

$$\gamma_I = n_I^{\rm eq}\langle\Gamma_{I\rm break}\rangle. \quad (1.9)$$

This relation is derived by taking into account that 2 DM particles disappear whenever a DM-DM bound state forms, such that $Y_{\rm DM} + Y_I/2$ is conserved by this process, and by comparing eq. (1.5) with eq. (1.1).

Next, the space-time densities $\gamma$ for DM-DM process can be written in the usual way in terms of the cross sections $\sigma v_{\rm rel}$, averaged over all DM components.[2] In the non-relativistic limit one has

$$2\gamma \overset{T\ll M_\chi}{\simeq} (n_{\rm DM}^{\rm eq})^2\langle\sigma v_{\rm rel}\rangle. \quad (1.10)$$

[1] In the case of two bound states 1 and 2 one finds

$$\gamma_{\rm eff} = \gamma_{\rm DM\to SM} + \frac{\gamma_1(\langle\Gamma_{1\rm ann}\rangle\langle\Gamma_2\rangle + \langle\Gamma_{12}\rangle\langle\Gamma_{1\rm ann} + \Gamma_{2\rm ann}\rangle) + \gamma_2(\langle\Gamma_{2\rm ann}\rangle\langle\Gamma_1\rangle + \langle\Gamma_{12}\rangle\langle\Gamma_{1\rm ann} + \Gamma_{2\rm ann}\rangle)}{\langle\Gamma_1\rangle\langle\Gamma_2\rangle + \langle\Gamma_{12}\rangle\langle\Gamma_1 + \Gamma_2\rangle} \quad (1.8)$$

where $\Gamma_I \equiv \Gamma_{I\rm ann} + \Gamma_{I\rm break}$.

[2] If DM is a real particle (e.g. a Majorana fermion) this is the usual definition of a cross section. If DM is a complex particle (e.g. a Dirac fermion) with no asymmetry, the average over the 4 possible initial states is $\sigma \equiv \frac{1}{4}(2\sigma_{\chi\overline{\chi}} + \sigma_{\chi\chi} + \sigma_{\overline{\chi}\overline{\chi}})$. In many models only $\chi\overline{\chi}$ annihilations are present, so that $\sigma = \frac{1}{2}\sigma_{\chi\overline{\chi}}$.

The Boltzmann equation for the DM abundance can then be written in the final form

$$\frac{dY_{\rm DM}}{dz} = -\frac{\langle\sigma_{\rm eff} v_{\rm rel}\rangle s}{Hz}(Y_{\rm DM}^2 - Y_{\rm DM}^{\rm eq2}) = -\frac{\lambda\, S(z)}{z^2}(Y_{\rm DM}^2 - Y_{\rm DM}^{\rm eq2}), \tag{1.11}$$

where $S$ is the tempeature-dependent correction due to higher order effects (Sommerfeld enhancement, bound-state formation, ...) with respect to a reference cross section $\sigma_0$ computed at tree level in $s$-wave

$$S(z) = \frac{\langle\sigma_{\rm eff} v_{\rm rel}\rangle}{\sigma_0}, \qquad \lambda = \left.\frac{\sigma_0 s}{H}\right|_{T=M_\chi} = \sqrt{\frac{g_{\rm SM}\pi}{45}}\sigma_0 M_{\rm Pl} M_\chi \tag{1.12}$$

where $g_{\rm SM}$ is the number of degrees of freedom in thermal equilibrium at $T = M_\chi$ ($g_{\rm SM} = 106.75$ at $T \gg M_Z$) and $M_{\rm Pl} = G_N^{-1/2} = 1.22 \times 10^{19}$ GeV. In the non-relativistic limit the Milne relation becomes

$$\langle\Gamma_{I\rm break}\rangle = \frac{g_\chi^2}{g_I}\frac{(M_\chi T)^{3/2}}{16\pi^{3/2}} e^{-E_{B_I}/T}\langle\sigma_I v_{\rm rel}\rangle \tag{1.13}$$

where $E_{B_I} > 0$ is the binding energy of the bound state under consideration, $g_I$ is the number of its degrees of freedom, and $\langle\sigma_I v_{\rm rel}\rangle$ is the thermal average of the cross section for bound-state formation (computed in section 1.3). The branching ratio in eq. (1.7) approaches 1 at small enough temperature. For a single bound state one has the explicit result

$$S(z) = S_{\rm ann}(z) + \left[\frac{\sigma_0}{\langle\sigma_I v_{\rm rel}\rangle} + \frac{g_\chi^2\sigma_0\, M_\chi^3}{2 g_I\, \Gamma_{\rm ann}}\left(\frac{1}{4\pi z}\right)^{3/2} e^{-z\, E_{B_I}/M_\chi}\right]^{-1} \tag{1.14}$$

where $S_{\rm ann}$ is the Sommerfeld correction to the annihilation cross section (computed in section 1.2), and the second term is the contribution from the bound state $I$. Its effect is sizeable if $\sigma_I$, $E_{B_I}$ and $\Gamma_{I\rm ann}$ are large.

## 1.2 Sommerfeld enhancement

### 1.2.1 DM annihilation at tree level

The tree-level (co)annihilation cross section of DM particles into SM particles can be readily computed. We consider two main classes of models. In both cases we assume that the DM mass is much heavier than all SM particles. A posteriori, this will be consistent with the DM cosmological abundance.

First, we assume that DM is the neutral component of a fermionic $n$-plet of $\mathrm{SU}(2)_L$ with hypercharge $Y = 0$ and mass $M_\chi$. The $s$-wave annihilation cross section into SM vectors,

fermions and Higgses is [69]

$$\sigma v_{\rm rel} = \frac{g_2^4(2n^4+17n^2-19)}{256\pi g_\chi M_\chi^2} = \frac{\pi\alpha_2^2}{M_\chi^2} \times \begin{cases} 37/12 & n=3 \\ 207/20 & n=5 \end{cases} \tag{1.15}$$

where $g_\chi = 2n$ is the number of degrees of freedom of the DM multiplet. The $p$-wave contribution is suppressed by an extra $v_{\rm rel}^2$ factor. Similar formulæ apply for fermions with $Y \neq 0$ and for a degenerate scalar multiplet [69]. Related interesting models have been proposed along similar lines [70].

Next, we consider co-annihilations of a DM particle $\chi$ with a colored state $\chi'$ in the representation $R$ of $\mathrm{SU}(3)_c$, mass $M_{\chi'} = M_\chi + \Delta M$ and $g'_\chi$ degrees of freedom. In supersymmetric models $\chi$ can be a neutralino and $\chi'$ can be the gluino or a squark. Assuming that co-annihilations are dominant one has an effective cross-section [71]

$$\sigma v_{\rm rel} = \sigma(\chi'\chi' \to \text{SM particles}) v_{\rm rel} \times \left[1 + \frac{g_\chi}{g_{\chi'}} \frac{\exp(\Delta M/T)}{(1+\Delta M/M_\chi)^{3/2}}\right]^{-2} . \tag{1.16}$$

Assuming that $\chi'$ lies in the representation $R$ of color $\mathrm{SU}(3)_c$ one has the $s$-wave cross sections [71]

$$\sigma(\chi'\chi' \to gg) v_{\rm rel} = \frac{2d_R C_R^2 - 12 T_R}{g_{\chi'} d_R} \frac{\pi\alpha_3^2}{M_{\chi'}^2} , \tag{1.17}$$

$$\sigma(\chi'\chi' \to q\overline{q}) v_{\rm rel} = \frac{48 T_R}{g_{\chi'} d_R} \frac{\pi\alpha_3^2}{M_{\chi'}^2} \times \begin{cases} 1 & \text{if } \chi' \text{ is a fermion} \\ 0 & \text{if } \chi' \text{ is a boson} \end{cases} . \tag{1.18}$$

where we summed over all SM quarks and $d_3 = 3$, $T_3 = 1/2$, $C_3 = 4/3$; $d_8 = 8$, $T_8 = C_8 = 3$, $C_{10} = C_{\overline{10}} = 6$, $C_{27} = 8$, etc. The number of degrees of freedom of $\chi'$ is $g_{\chi'} = 6$ for a scalar triplet, 8 for a scalar octet, 12 for a fermion triplet, 16 for a fermion octet.

As discussed in the next sections, all these tree-level cross sections get significantly affected by Sommerfeld corrections and by bound-state formation due to SM gauge interactions.

### 1.2.2 Sommerfeld corrections

We consider an arbitrary gauge group with a common vector mass $M_V$. Non-abelian interactions among particles in the representations $R$ and $R'$ give rise to the non-relativistic potential

$$V = \alpha \frac{e^{-M_V r}}{r} \sum_a T_R^a \otimes T_{R'}^a \tag{1.19}$$

which is a matrix, if written in $R, R'$ components. As long as the group is unbroken, its algebra allows one to decompose the processes into effectively abelian sub-sectors, $R \otimes R' = \sum_J J$, as

$$V = \alpha \frac{e^{-M_V r}}{2r} \left[ \sum_J C_J \mathbb{I}_J - C_R \mathbb{I}_R - C_R \mathbb{I}_{R'} \right]. \tag{1.20}$$

In each sub-sector one gets an effective abelian-like potential described by a numerical constant $\lambda_J$.

$$V_J = -\alpha_{\rm eff} \frac{e^{-M_V r}}{r}, \qquad \alpha_{\rm eff} = \lambda_J \alpha, \qquad \lambda_J = \frac{C_R + C_{R'} - C_J}{2} \tag{1.21}$$

such that $\alpha_{\rm eff} > 0$ and $\lambda_J > 0$ for an attractive channel $J$.

We specialise to the two classes of models considered in section 1.2.1.

Isospin $\mathrm{SU}(2)_L$ is broken, and gets restored by thermal effects at $T \gtrsim 155\,\mathrm{GeV}$, where degenerate vector thermal masses $M_V$ respect the group decomposition. The Casimir of the $\mathrm{SU}(2)_L$ irreducible representations with dimension $n$ is $C_n = (n^2-1)/4$. A two-body state decomposes as $n \otimes \overline{n} = 1 \oplus 3 \oplus \ldots \oplus 2n-1$. The potential is $V = (I^2 + 1 - 2n^2)\alpha_2/8r$ within the two-body sector with an isospin representation of dimension $I$. The most attractive channel is the singlet $I = 1$: $V = -2\alpha_2/r$ for $n = 3$ ($\alpha_{\rm eff} = 0.066$), $V = -6\alpha_2/r$ for $n = 5$ ($\alpha_{\rm eff} = 0.2$).

Color is unbroken. The Casimirs $C_R$ of SU(3) irreducible representations have been listed below eq.(1.17), such that the singlet state has $V = -4\alpha_3/3r$ if made of $3 \otimes \overline{3}$ ($\alpha_{\rm eff} = 0.13$) and $V = -3\alpha_3/r$ if made of $8 \otimes 8$ ($\alpha_{\rm eff} = 0.3$).

The Sommerfeld correction can be computed from the distortion of the wave function of the initial state. In the center of mass frame of the incoming two 2 fermions, the stationary Schroedinger equation is

$$-\frac{\nabla^2 \psi}{M_\chi} + V\psi = E\psi. \tag{1.22}$$

As usual we can decompose the wave function in states of given orbital angular momentum

$$\psi(r,\theta,\varphi) = R_\ell(r) Y_\ell^m(\theta,\varphi) = \frac{u_\ell(r)}{r} Y_\ell^m(\theta,\varphi) \tag{1.23}$$

where $Y_\ell^m$ are spherical harmonics and the radial wave function $u_\ell(r)$ satisfies

$$-\frac{u_\ell''}{M_\chi} + \left[ V + \frac{\ell(\ell+1)}{M_\chi r^2} \right] u_\ell = E u_\ell. \tag{1.24}$$

The Schroedinger equation admits discrete solutions with negative energy and continuum solutions with $E = M_\chi v_{\rm rel}^2/4$ equal to the kinetic energy of the two DM particles in the center-of-mass frame, where each DM particle has velocity $\beta$, such that their relative velocity is $v_{\rm rel} = 2\beta$. For identical particles, one must only consider a wave function (anti)symmetric under their exchange.

The deflection of the initial wave function from a plane wave leads to the Sommerfeld

enhancement. For $s$-wave annihilation,[3] the Sommerfeld factor that enhances the tree-level cross section can be computed as $S = |u(\infty)/u(0)|^2$ where $u$ has outgoing boundary condition $u'(\infty)/u(\infty) \simeq iM_\chi v_{\rm rel}/2$. For the potential of eq. (1.21) and $s$-wave scattering one gets

$$S = \frac{2\pi\alpha_{\rm eff}/v_{\rm rel}}{1 - e^{-2\pi\alpha_{\rm eff}/v_{\rm rel}}} \qquad \text{for } M_V = 0. \tag{1.25}$$

In the case of a massive vector, an analytic solution is obtained by approximating the Yukawa potential with a Hulthen potential

$$\frac{e^{-M_V r}}{r} \approx \frac{\kappa\, M_V e^{-\kappa M_V r}}{1 - e^{-\kappa\, M_V r}}\,. \tag{1.26}$$

This potential approximates the Yukawa behaviour best if $\kappa$ is chosen as $\kappa \approx 1.74$. The Sommerfeld factor that enhances an $s$-wave cross section is [73]

$$S = \frac{2\pi\alpha_{\rm eff}\sinh\left(\pi M_\chi v_{\rm rel}/\kappa M_V\right)}{v_{\rm rel}\left(\cosh\left(\pi M_\chi v_{\rm rel}/\kappa M_V\right) - \cosh\left(\pi M_\chi v_{\rm rel}\sqrt{1 - 4\alpha_{\rm eff}\kappa M_V/M_\chi v_{\rm rel}^2}/\kappa M_V\right)\right)}\,. \tag{1.27}$$

This expression reduces to the Coulomb result of eq. (1.25) in the limit of vanishing vector mass $M_V$. $S$ is resonantly enhanced when $M_\chi = \kappa n^2 M_V/\alpha_{\rm eff}$ for integer $n$, which corresponds to a zero-energy bound state, as discussed in section 1.3. $S$ depends only on $\alpha_{\rm eff}/v_{\rm rel}$ and on $y \equiv \kappa M_V/M_\chi\alpha_{\rm eff}$; its thermal average $\langle S\rangle$ depends only on $\alpha_{\rm eff}\sqrt{z}$ and $y$, where $z = M_\chi/T$. At small velocities, $v_{\rm rel} \ll M_V/M_\chi$ as relevant for indirect detection, the formula above reduces to

$$S \overset{v_{\rm rel}\to 0}{\simeq} \frac{2\pi^2\alpha_{\rm eff}M_\chi}{\kappa M_V}\left(1 - \cos 2\pi\sqrt{\frac{\alpha_{\rm eff}M_\chi}{\kappa M_V}}\right)^{-1} \tag{1.28}$$

producing a significant enhancement if $\alpha_{\rm eff}M_\chi/M_V \gtrsim 1$.

## 1.3 Bound state formation

### 1.3.1 Binding energies

As well known, an infinity of bound states with quantum number $n = 1, 2, \ldots$ exist in a Coulomb potential $V = -\alpha_{\rm eff}/r$ with any $\alpha_{\rm eff}$: the binding energies $E_B$ are $E_{n\ell} = \alpha_{\rm eff}^2 M_\chi/4n^2$ and do not depend on the angular momentum $\ell$; their wave functions normalized to unity $\psi_{n\ell m}(r,\theta,\varphi) = R_{n\ell}(r)Y_{\ell m}(\theta,\varphi)$ are summarized in eq. (A.1) in the appendix. In particular, $\psi_{100}(r,\theta,\varphi) = e^{-r/a_0}/\sqrt{\pi a_0^3}$ for the ground state, where $a_0 = 2/\alpha_{\rm eff}M_\chi$ is the Bohr radius.

A Yukawa potential $-\alpha_{\rm eff}e^{-M_V r}/r$ allows a finite number of bound states if the Yukawa screening length, $1/M_V$, is larger than the Bohr radius: $M_V \lesssim \alpha_{\rm eff}M_\chi$. Formation of a bound

[3] The Sommerfeld enhancement also affects $p$-wave cross sections, which remain subleading [72, 73].

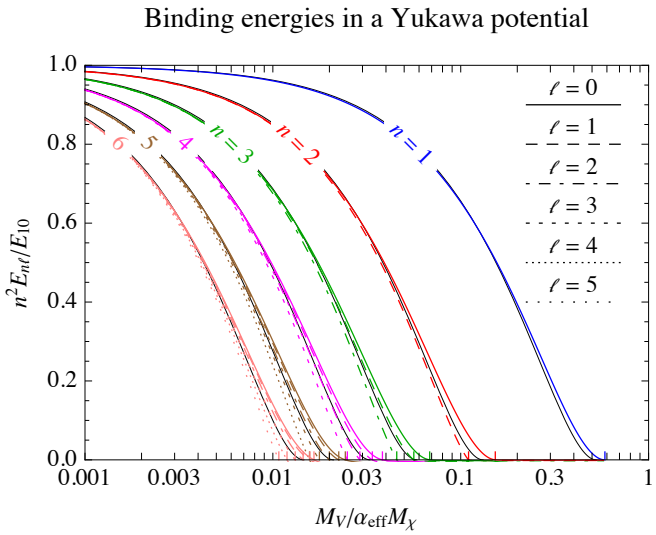


Figure 1.1: *Energies of bound states in a Yukawa potential (colored curves) compared to the Hulthen approximation with* $\kappa = 1.9$ *(black continuous curves).*

state via emission of a vector is kinematically possible if the binding energy $\sim \alpha_{\rm eff}^2 M_\chi$ plus the kinetic energy $M_\chi v_{\rm rel}^2/4$ is larger than the mass of the emitted vector: $M_V \lesssim (\alpha_{\rm eff}^2 + v_{\rm rel}^2) M_\chi$ [64,65].

The binding energies in a Yukawa potential can be exactly computed at first order in $M_V$ by expanding $V = -\alpha_{\rm eff} \exp(-M_V r)/r \simeq -\alpha_{\rm eff}(1/r - M_V)$, finding

$$E_{n\ell} \simeq \frac{\alpha_{\rm eff}^2 M_\chi}{4n^2} - \alpha_{\rm eff} M_V + \mathcal{O}(M_V^2). \tag{1.29}$$

The relative correction becomes of order unity for $M_V \sim \alpha_{\rm eff} M_\chi$ where the Coulomb approximation is unreliable. The shift in energy is equal for ground state and excited levels so that the Coulomb approximation fails earlier for the latter ones.

Fig. 1.1 shows numerical results for the binding energies, obtained by computing the matrix elements of the Yukawa potential in the basis of eq. (A.1) and diagonalising the resulting matrix in each sector with given $\ell$, see also [74, 67]. Analytic expressions for the binding energies are obtained by approximating the Yukawa potential with the Hulthen potential of eq. (1.26), where $\kappa$ is an arbitrary order one constant. For states with $\ell = 0$ one has

$$E_{n0} = \frac{\alpha_{\rm eff}^2 M_\chi}{4n^2} \left[1 - n^2 y\right]^2 \qquad \text{where} \qquad y \equiv \frac{\kappa M_V}{\alpha_{\rm eff} M_\chi} \tag{1.30}$$

which reproduces eq. (1.29) at leading order in $M_V$ for $\kappa = 2$. The bound state exists only when the term in the squared parenthesis is positive, namely for $M_\chi \geqslant \kappa n^2 M_V/\alpha_{\rm eff}$. Fig. 1.1 shows that setting $\kappa \approx 1.90$ better reproduces the generic situation, while $\kappa \approx 1.74$ better reproduces the critical value at which the special $n = 1$ bound state first forms. Bound states with angular

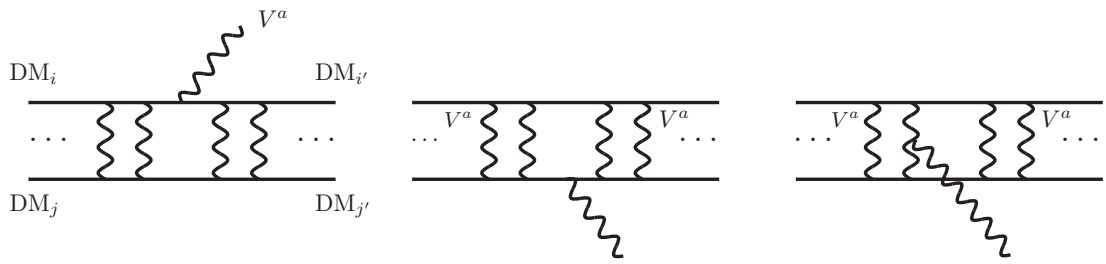


Figure 1.2: *Diagrams relevant for bound state formation. The first two diagrams give the first two terms of eq. (1.35). The third diagrams, which is peculiar of non-abelian interactions, gives rise to the last term.*

momentum $\ell > 0$ have different energy from the corresponding state with $\ell = 0$ only if the Yukawa potential deviates significantly from its Coulomb limit, namely if the second term in the parenthesis is of order one. Analytic solutions are only available making extra simplifications. A comparison with numerical results suggests a relatively minor correction of the form

$$E_{n\ell} \approx \frac{\alpha_{\rm eff}^2 M_\chi}{4n^2}\left[1 - n^2 y - 0.53 n^2 y^2 \ell(\ell+1)\right]^2, \qquad \kappa = 1.74. \tag{1.31}$$

The wave functions for free and bound states, in a Coulomb or Hulthen potential, will be needed later and are listed in Appendix A.

### 1.3.2 Bound state formation

We are interested in the formation of bound states through the emission of a vector $V^a$:

$$\mathrm{DM}_i(P_1) + \mathrm{DM}_j(P_2) \to B_{i'j'} + V^a(K). \tag{1.32}$$

In the non-relativistic limit, we write the 4-momenta as

$$P_1 \simeq (M_\chi + \frac{p_1^2}{2M_\chi}, \vec{p}_1), \qquad P_2 \simeq (M_\chi + \frac{p_2^2}{2M_\chi}, \vec{p}_2), \qquad K = (\omega, \vec{k}) \tag{1.33}$$

with $\omega = \sqrt{k^2 + M_V^2}$ where $M_V$ is the vector mass. In the center-of-mass frame $\vec{p}_2 = -\vec{p}_1$ and the momentum of each DM particle is $p = M_\chi v_{\rm rel}/2$. Conservation of energy reads

$$\frac{p^2}{M_\chi} = \frac{k^2}{2(2M_\chi - E_B)} - E_B + \omega \tag{1.34}$$

where $E_B = 2M_\chi - M_B > 0$ is the binding energy. The first term on the right-hand side is the recoil energy of the bound state that is negligible in what follows, such that energy conservation approximates to $\omega \approx E_B + M_\chi v_{\rm rel}^2/4$.

The diagrams in fig. 1.2 contribute to the amplitude. In the non-relativistic limit the first two diagrams describe the usual dipole approximation, which gives a cross section for bound state formation proportional to $\alpha^5$ times a sizeable Sommerfeld correction, while the third diagram is only present when the gauge interaction is non-abelian [67]. The diagrams of fig. 1.2 generate the non-relativistic Hamiltonian [75–77]

$$H_I = -\frac{g}{M_\chi}\left(\vec{A}^a(x_1)\cdot\vec{p}_1 T^a_{i'i}\delta_{jj'} + \vec{A}^a(x_2)\cdot\vec{p}_2\overline{T}^a_{j'j}\delta_{ii'}\right) + \left(g\alpha\vec{A}^a(0)\cdot\hat{r}\,e^{-M_a r}\right) T^b_{i'i}\overline{T}^c_{j'j}f^{abc} \tag{1.35}$$

where $T$ and $\overline{T}$ are the generators in the representation of particles 1 and 2 respectively; the indexes $a, b, c$ run over the vectors in the adjoint, and the indexes $i, j, i', j'$ over DM components.

In Born approximation we get the following cross section for the formation of a bound state with quantum numbers $n\ell m$:

$$\sigma^{n\ell m}_{\rm bsf} v_{\rm rel} = \sum_a (\sigma^{n\ell m}_{\rm bsf} v_{\rm rel})_a \tag{1.36}$$

where

$$(\sigma^{n\ell m}_{\rm bsf} v_{\rm rel})_a = \frac{2\alpha}{\pi}\frac{k}{M_\chi^2}\int d\Omega_k \sum_\sigma \left|\epsilon^a_\mu(k,\sigma)\mathscr{A}^\mu_{p,n\ell m}\right|^2 . \tag{1.37}$$

The polarization vectors, $\epsilon^a_\mu$, of the massive gauge boson satisfy

$$\sum_\sigma \epsilon^a_\mu \epsilon^{a*}_\nu = -\left(\eta_{\mu\nu} - \frac{K_\mu K_\nu}{M_a^2}\right) , \tag{1.38}$$

while the transition amplitude, $\mathscr{A}^\mu$, satisfies $K_\mu\mathscr{A}^\mu = 0$ because of current conservation. Therefore the unpolarized cross section can be rewritten in terms of the spatial terms as

$$(\sigma^{n\ell m}_{\rm bsf} v_{\rm rel})_a = \frac{2\alpha}{\pi}\frac{k}{M_\chi^2}\int d\Omega_k \left(|\vec{\mathscr{A}}^a_{p,n\ell m}|^2 - \frac{\left|\vec{k}\cdot\vec{\mathscr{A}}^a_{p,n\ell m}\right|^2}{k^2+M_a^2}\right). \tag{1.39}$$

In the dipole approximation,[4] that will be used throughout, the spatial part of the transition matrix in the center-of-mass frame is

$$\vec{\mathscr{A}}^a_{p,n\ell m} = \frac{1}{2}\left(T^a_{i'i}\delta_{jj'} - \overline{T}^a_{j'j}\delta_{ii'}\right)\vec{\mathcal{J}}^{ij,i'j'}_{p,n\ell m} - i\left(T^b_{i'i}\overline{T}^c_{j'j}f^{abc}\right)\vec{\mathcal{T}}^{ij,i'j'}_{p,n\ell m} \tag{1.40}$$

where we have defined the overlap integrals between the initial state wave function $\phi_{p\ell,ij}(\vec{r})$ and

[4] The dipole approximation is valid if the wave-length of the photon is larger than the size of the bound state. As discussed in [78] the most relevant bound states are approximately Coulomb-like so that the binding energy is $\alpha_{\rm eff}^2 M_\chi/(4n^2)$ and the size the Bohr radius $a_0 = 2n^2/(\alpha_{\rm eff}M_\chi)$. If follows that when the binding energy dominates over the initial kinetic energy the dipole approximation is always satisfied. The dipole approximation fails for $v_{\rm rel}^2 \gg \alpha_{\rm eff}$. When this condition is verified the value of the cross-section is however small.

the wave function $\psi_{n\ell m,i'j'}(\vec{r})$ of the desired bound-state:

$$\vec{\mathcal{J}}^{ij,i'j'}_{p,n\ell m} \equiv \int d^3r\, \psi^*_{n\ell m,i'j'} \vec{\nabla}\, \phi_{p,ij} \tag{1.41}$$

$$\vec{\mathcal{T}}^{ij,i'j'}_{p,n\ell m} \equiv \frac{\alpha M_\chi}{2} \int d^3r\, \psi^*_{n\ell m,i'j'}\, \hat{r}\, e^{-M_a r}\, \phi_{p,ij}\,. \tag{1.42}$$

The dipole approximation imposes the selection rule $\Delta L = 1$. Since in the non-relativistic limit spin is also conserved this implies that $s$-wave bound states can only be produced from two DM particles in an initial $p$-wave state. Furthermore, $p$-wave bound states can be produced from $s$ and $d$-waves. With this in mind we get the following overlap integrals for the production of bound states in $s$-wave configuration:

$$\vec{\mathcal{J}}^{ij,i'j'}_{p,n00} = -\frac{1}{\sqrt{3}} \left( \int r^2 dr R_{p1,ij}(r) \partial_r R^*_{n0,j'i'}(r) \right) (\hat{e}_0 + \hat{e}_+ + \hat{e}_-), \tag{1.43a}$$

$$\vec{\mathcal{T}}^{ij,i'j'}_{p,n00} = \frac{\alpha M_\chi}{2\sqrt{3}} \left( \int r^2 dr R_{p1,ij}(r) e^{-M_a r} R^*_{n0,j'i'}(r) \right) (\hat{e}_0 + \hat{e}_+ + \hat{e}_-)\,. \tag{1.43b}$$

where $\hat{e}_0 \equiv \hat{z}$ and $\hat{e}_\mp \equiv \pm\frac{1}{\sqrt{2}}(\hat{x} \mp i\hat{y})$. For production of bound states in a $p$-wave configuration starting from an $s$-wave one we get

$$\vec{\mathcal{J}}^{ij,i'j'}_{\mathbf{p},n1\pm1} = \frac{1}{\sqrt{3}} \left( \int r^2 dr R_{p0,ij}(r) \partial_r R^*_{n1,j'i'}(r) \right) \hat{e}_\mp, \tag{1.43c}$$

$$\vec{\mathcal{J}}^{ij,i'j'}_{\mathbf{p},n10} = \frac{1}{\sqrt{3}} \left( \int r^2 dr R_{p0,ij}(r) \partial_r R^*_{n1,j'i'}(r) \right) \hat{e}_0, \tag{1.43d}$$

$$\vec{\mathcal{T}}^{ij,i'j'}_{\mathbf{p},n1\pm1} = \frac{\alpha M_\chi}{2\sqrt{3}} \left( \int r^2 dr R_{p0,ij}(r) e^{-M_a r} R^*_{n1,j'i'}(r) \right) \hat{e}_\mp, \tag{1.43e}$$

$$\vec{\mathcal{T}}^{ij,i'j'}_{\mathbf{p},n10} = \frac{\alpha M_\chi}{2\sqrt{3}} \left( \int r^2 dr R_{p0,ij}(r) e^{-M_a r} R^*_{n1,j'i'}(r) \right) \hat{e}_0\,. \tag{1.43f}$$

The amplitudes for producing a $p$-wave bound state starting from a $d$-wave configuration are

$$\vec{\mathcal{J}}^{ij,i'j'}_{\mathbf{p},n1\pm1} = -\frac{1}{\sqrt{5}} \left[ \int r^2 dr R_{p2,ij}(r) \left( \partial_r - \frac{1}{r} \right) R^*_{n1,j'i'}(r) \right] \left( \sqrt{2}\hat{e}_\pm + \frac{\hat{e}_\mp}{\sqrt{3}} + \hat{e}_0 \right), \tag{1.43g}$$

$$\vec{\mathcal{J}}^{ij,i'j'}_{\mathbf{p},n10} = -\frac{1}{\sqrt{5}} \left[ \int r^2 dr R_{p2,ij}(r) \left( \partial_r - \frac{1}{r} \right) R^*_{n1,j'i'}(r) \right] \left( \hat{e}_+ + \hat{e}_- + \frac{2}{\sqrt{3}}\hat{e}_0 \right), \tag{1.43h}$$

$$\vec{\mathcal{T}}^{ij,i'j'}_{\mathbf{p},n1\pm1} = \frac{\alpha M_\chi}{2\sqrt{5}} \left[ \int r^2 dr R_{p2,ij}(r) e^{-M_a r} R^*_{n1,j'i'}(r) \right] \left( \sqrt{2}\hat{e}_\pm + \frac{\hat{e}_\mp}{\sqrt{3}} + \hat{e}_0 \right), \tag{1.43i}$$

$$\vec{\mathcal{T}}^{ij,i'j'}_{\mathbf{p},n10} = \frac{\alpha M_\chi}{2\sqrt{5}} \left[ \int r^2 dr R_{p2,ij}(r) e^{-M_a r} R^*_{n1,j'i'}(r) \right] \left( \hat{e}_+ + \hat{e}_- + \frac{2}{\sqrt{3}}\hat{e}_0 \right). \tag{1.43j}$$

Plugging these amplitudes in eq. (1.39), performing the angular integral, averaging over initial states and summing over final states we get the cross sections for the formation of $s$-wave bound

states:

$$(\sigma^{n0}_{\rm bsf} v_{\rm rel})^{p\to s}_a = \frac{8}{3}\frac{\alpha k}{M_\chi^2}\left(1-\frac{k^2}{3\omega^2}\right)\times \\ \times\left|\int r^2 dr R_{p1,ij}\left(\frac{1}{2}\left(T^a_{i'i}\delta_{jj'}-\overline{T}^a_{j'j}\delta_{ii'}\right)\partial_r + i\,\frac{\alpha M_\chi}{2}\left(T^b_{i'i}\overline{T}^c_{j'j}f^{abc}\right)e^{-M_a r}\right)R^*_{n0,j'i'}\right|^2 \tag{1.44}$$

For $p$-wave bound states we get

$$(\sigma^{n1}_{\rm bsf} v_{\rm rel})_a = (\sigma^{n1}_{\rm bsf} v_{\rm rel})^{s\to p}_a + (\sigma^{n1}_{\rm bsf} v_{\rm rel})^{d\to p}_a \tag{1.45a}$$

where $(\sigma^{n1}_{\rm bsf} v_{\rm rel})^{s\to p}_a$ and $(\sigma^{n1}_{\rm bsf} v_{\rm rel})^{s\to p}_a$ are the cross sections from initial states in $s$ and $d$-wave respectively. Their explicit values are

$$(\sigma^{n1}_{\rm bsf} v_{\rm rel})^{s\to p}_a = 8\frac{\alpha k}{M_\chi^2}\left(1-\frac{k^2}{3\omega^2}\right)\left|\int r^2 dr R^*_{n1,j'i'} \right. \\ \left.\times\left(\frac{1}{2}\left(T^a_{i'i}\delta_{jj'}-\overline{T}^{a*}_{j'j}\delta_{ii'}\right)\partial_r - i\,\frac{\alpha M_\chi}{2}\left(T^b_{i'i}\overline{T}^c_{j'j}f^{abc}\right)e^{-M_a r}\right)R_{p0,ij}\right|^2 \tag{1.45b}$$

$$(\sigma^{n1}_{\rm bsf} v_{\rm rel})^{d\to p}_a = \frac{16}{5}\frac{\alpha k}{M_\chi^2}\left(1-\frac{k^2}{3\omega^2}\right)\left|\int r^2 dr R_{p2,ij}\times \right. \\ \left.\times\left(\frac{1}{2}\left(T^a_{i'i}\delta_{jj'}-\overline{T}^{a*}_{j'j}\delta_{ii'}\right)\left(\partial_r-\frac{1}{r}\right) + i\,\frac{\alpha M_\chi}{2}\left(T^b_{i'i}\overline{T}^c_{j'j}f^{abc}\right)e^{-M_a r}\right)R^*_{n1,j'i'}\right|^2 \tag{1.45c}$$

If DM are scalars, the wave function is symmetric under exchange of identical scalars. Real (complex) scalars have $g_\chi = d_R$ ($2d_R$) degrees of freedom. Bound states of scalars have $S = 0$. For $s$ ($p$)-wave bound states this implies that the gauge part of the wave function is symmetric (anti-symmetric). The cross-sections for bound state formation are again given by eq. (1.45).

### 1.3.3 Group algebra

Assuming that the global group $G$ is unbroken (such that vectors are either massless or have a common mass), group algebra allows one to simplify the above formulæ. We assume that DM is a particle $\chi_i$ in the representation $R$ of $G$, labeled by an index $i$, and we focus on $\chi_i\overline{\chi}_j$ bound states so that $\overline{T}^a = -T^{a*}$. Both the initial state and each bound state can be decomposed into irreducible representations of $G$, times the remaining spin and spatial part. So the two-body DM states $\chi_i\overline{\chi}_j$ fill the representations $J$ contained in $R\otimes\overline{R} = \sum_J J$. Each representation $J$ is labeled by an index $M$. The change of basis is described the the coefficients $\mathrm{CG}^M_{ij} \equiv \langle J, M|R, i; \overline{R}, j\rangle$ of the group $G$. For $G = \mathrm{SU}(2)_L$ these are the Clebsh-Gordon coefficients usually written as $\langle j, m|j_1, m_1; j_2, m_2\rangle$. For the singlet representation one has $\mathrm{CG}_{ij} = \delta_{ij}/\sqrt{d_R}$ and for the adjoint

representation one has $\mathrm{CG}^a_{ij} = T^a_{ij}/\sqrt{T_R}$. In the new basis, where $ij$ is replaced by $M$ and $i'j'$ by $M'$, the bound-state formation amplitudes of eq. (1.40) becomes

$$\vec{\mathscr{A}}^{aMM'}_{p,n\ell m} = C^{aMM'}_{\mathcal{J}}\vec{\mathcal{J}}_{p,n\ell m} + C^{aMM'}_{\mathcal{T}}\vec{\mathcal{T}}_{p,n\ell m} \tag{1.46}$$

where the group-theory part has been factored out in the coefficients

$$C^{aMM'}_{\mathcal{J}} \equiv \frac{1}{2}\,\mathrm{CG}^M_{ij}\mathrm{CG}^{M'*}_{i'j'}(T^a_{i'i}\delta_{jj'} + T^{a*}_{j'j}\delta_{ii'}) = \frac{1}{2}\,\mathrm{Tr}[\mathrm{CG}^{M'}\{\mathrm{CG}^M, T^a\}] \tag{1.47}$$

$$C^{aMM'}_{\mathcal{T}} \equiv i\,\mathrm{CG}^M_{ij}\mathrm{CG}^{M'*}_{i'j'}(T^b_{i'i}T^c_{jj'}f^{abc}) = i\,\mathrm{Tr}\Big[\mathrm{CG}^{M'}\,T^b\,\mathrm{CG}^M\,T^c\Big]f^{abc} \tag{1.48}$$

that holds separately for each initial channel $J$ and final channel $J'$. In many cases of interest the two tensors are proportional to each other. The overlap integrals $\mathcal{J}$, $\mathcal{T}$ are the same of eq. (1.41), but now containing only the spatial part of the wave functions. With these notations the cross sections of eq. (1.44) and (1.45), in a given channel $(J, M) \to (J', M')$, become

$$(\sigma^{n0}_{\mathrm{bsf}}v_{\mathrm{rel}})^{p\to s}_{aMM'} = \frac{8}{3}\frac{\alpha k}{M_\chi^2}\left(1-\frac{k^2}{3\omega^2}\right)\left|\int r^2 dr R_{p1}\left(C^{aMM'}_{\mathcal{J}}\partial_r - C^{aMM'}_{\mathcal{T}}\frac{\alpha M_\chi}{2}e^{-M_a r}\right)R^*_{n0}\right|^2 \tag{1.49a}$$

$$(\sigma^{n1}_{\mathrm{bsf}}v_{\mathrm{rel}})^{s\to p}_{aMM'} = 8\frac{\alpha k}{M_\chi^2}\left(1-\frac{k^2}{3\omega^2}\right)\left|\int r^2 dr R^*_{n1}\left(C^{aMM'}_{\mathcal{J}}\partial_r + C^{aMM'}_{\mathcal{T}}\frac{\alpha M_\chi}{2}e^{-M_a r}\right)R_{p0}\right|^2 \tag{1.49b}$$

$$(\sigma^{n1}_{\mathrm{bsf}}v_{\mathrm{rel}})^{d\to p}_{aMM'} = \frac{16}{5}\frac{\alpha k}{M_\chi^2}\left(1-\frac{k^2}{3\omega^2}\right)\left|\int r^2 dr R_{p2}\left(C^{aMM'}_{\mathcal{J}}\left(\partial_r - \frac{1}{r}\right) - C^{aMM'}_{\mathcal{T}}\frac{\alpha M_\chi}{2}e^{-M_a r}\right)R^*_{n1}\right|^2. \tag{1.49c}$$

In the special case $1 \to \mathrm{adj}$ (namely, the initial state is a gauge singlet, such that the bound state is an adjoint) the group theory factors are proportional to each other, $C^{aMM'}_{\mathcal{J}} \propto C^{aMM'}_{\mathcal{T}}$, so that the inclusive cross-section remains a perfect square:

$$\sum_{aMM'}\left|C^{aMM'}_{\mathcal{J}} + \gamma C^{aMM'}_{\mathcal{T}}\right|^2 = \frac{T_R d_{\mathrm{adj}}}{d_R}\left|1 \mp \frac{\gamma}{2}T_{\mathrm{adj}}\right|^2. \tag{1.50}$$

The + sign corresponds to the opposite $\mathrm{adj} \to 1$ process. The same simplification holds for any $\mathrm{SU}(2)_L$ representation, because in the product of two $\mathrm{SU}(2)_L$ representations each irreducible representation appears only once. The relevant $\mathrm{SU}(2)_L$ group factors are listed in Table 1.1. Furthermore, the simplification also holds for the $\mathrm{SU}(3)_c$ representations that we will encounter later, and the relevant group $\mathrm{SU}(3)_c$ factors are listed in Table 1.2.

### 1.3.4 Massless vectors

The overlap integrals in the spatial part of the amplitudes for bound state formation can be analytically computed if vectors are massless.

The initial states are assumed to be asymptotically plane-waves with momentum $\vec{p}$, distorted

by the potential in channel $J$ where $\alpha_{\rm eff} = \lambda_i \alpha$ with $\lambda_i = \lambda_J$ given by eq. (1.21). The initial state wave function in a Coulomb-like potential is given in eq. (A.8).

The final states are assumed to be bound states in channel $J'$ in a Coulomb potential with $\alpha_{\rm eff} = \lambda_f \alpha$ and $\lambda_f = \lambda_{J'}$. We use a basis of eigenstates of angular momentum, parameterized by the usual $\ell, m$ indeces. The bound state wave functions are given in eq. (A.1), and are analytic continuations of the free-state wave functions.

Plugging these wave functions into the overlap integrals we get the cross section for the production of the various bound states. We are interested in the cross-section averaged over initial states and summed over final gauge bosons and bound states components. For the lowest lying bound state with $n = 1$, $\ell = 0$ and spin $S$ we get

$$(\sigma v_{\rm rel})^{n=1,\ell=0}_{\rm bsf} = \sigma_0 \lambda_i (\lambda_f \zeta)^5 \frac{2S+1}{g_\chi^2} \frac{2^{11}\pi(1+\zeta^2\lambda_i^2) e^{-4\zeta\lambda_i {\rm arccot}(\zeta\lambda_f)}}{3(1+\zeta^2\lambda_f^2)^3\,(1-e^{-2\pi\zeta\lambda_i})} \times \sum_{aMM'} \left| C_{\mathcal{J}}^{aMM'} + \frac{1}{\lambda_f} C_{\mathcal{T}}^{aMM'} \right|^2 \tag{1.51}$$

where $\sigma_0 = \pi\alpha^2/M_\chi^2$ and $\zeta = \alpha/v_{\rm rel}$. For the bound states with $n = 2$ and $\ell = \{0, 1\}$ we get

$$(\sigma v_{\rm rel})^{n=2,\ell=0}_{\rm bsf} = \sigma_0 \lambda_i \lambda_f^5 \frac{2S+1}{g_\chi^2} \frac{2^{14}\pi\zeta^5\,(\zeta^2\lambda_i^2+1)\, e^{-4\zeta\lambda_i {\rm arccot}(\zeta\lambda_f/2)}}{3\left(\zeta^2\lambda_f^2+4\right)^5 (1-e^{-2\pi\zeta\lambda_i})} \tag{1.52}$$

$$\times \sum_{aMM'} \left| C_{\mathcal{J}}^{aMM'} \left(\zeta^2\lambda_f\,(\lambda_f - 2\lambda_i) - 4\right) + C_{\mathcal{T}}^{aMM'} \left(\zeta^2\,(3\lambda_f - 4\lambda_i) - \frac{4}{\lambda_f}\right) \right|^2 ,$$

$$(\sigma v_{\rm rel})^{n=2,\ell=1}_{\rm bsf} = \sigma_0 \lambda_i \lambda_f^5 \frac{2S+1}{g_\chi^2} \frac{2^{12}\pi\alpha\zeta^7 e^{-4\zeta\lambda_i {\rm arccot}(\zeta\lambda_f/2)}}{9\left(\zeta^2\lambda_f^2+4\right)^5 (1-e^{-2\pi\zeta\lambda_i})} \times$$

$$\times \sum_{aMM'} \left[ \left| C_{\mathcal{J}}^{aMM'} \left( \lambda_f(\zeta^2\lambda_i(3\lambda_f - 4\lambda_i) + 8) - 12\lambda_i \right) + C_{\mathcal{T}}^{aMM'} \left(\zeta^2(-3\lambda_f^2 + 12\lambda_f\lambda_i - 8\lambda_i^2) + 4\right) \right|^2 + \right.$$

$$\left. + 2^5(\zeta^2\lambda_i^2+1)(\zeta^2\lambda_i^2+4) \left| C_{\mathcal{J}}^{aMM'}\lambda_f + 2C_{\mathcal{T}}^{aMM'} \right|^2 \right]. \tag{1.53}$$

In the last equation we have separated the contribution of the $s$-wave and $d$-wave initial state. These formulas apply both for Dirac and Majorana particles, and in all cases relevant for us the sums can be performed as summarized in tables 1.1 and 1.2.

In the limit $\lambda_i = 0$ where the Sommerfeld correction is ignored, the cross section for producing a bound state with $\ell = 0$ is of order $\alpha^2/M_\chi^2$ times a $(v_{\rm rel}/\alpha_{\rm eff})^2$ suppression at $v_{\rm rel} \ll \alpha_{\rm eff}$ as expected for production from a $p-$wave; the cross section for producing a bound state with $\ell = 1$ does not have this suppression for $C_{\mathcal{T}} \neq 0$.

The formulæ above simplify in the limit of large and small velocities. For the ground state

one finds

$$(\sigma v_{\rm rel})^{n=1,\ell=0}_{\rm bsf} = \sigma_0 \frac{2S+1}{g_\chi^2}\frac{2^{11}\pi}{3}\sum_{aMM'}\left|C^{aMM'}_{\mathcal{J}} + \frac{1}{\lambda_f}C^{aMM'}_{\mathcal{T}}\right|^2 \times \begin{cases} \dfrac{\lambda_i^3\alpha}{\lambda_f v_{\rm rel}} e^{-4\lambda_i/\lambda_f} & v_{\rm rel} \ll \lambda_{i,f}\alpha \\ \dfrac{\lambda_f^5\alpha^4}{2\pi v_{\rm rel}^4} & v_{\rm rel} \gg \lambda_{i,f}\alpha \end{cases} \tag{1.54}$$

For large velocities the cross-section is proportional $\alpha\alpha_{\rm eff}^5/v_{\rm rel}^4$.

### 1.3.5 Approximate formulæ for massive vectors

The cross sections for producing bound states in a Yukawa potential can be obtained by computing numerically the wave functions (or using the wave functions in Hulthen approximation, listed in the appendix), and by computing numerically the overlap integrals. As this is somehow cumbersome, we discuss how massless formulæ can be readapted, with minor modifications, to take into account the main effects of vector masses. We start considering the case where the vectors have a common mass $M_V$ and the group theory structure is identical to the massless case.

The initial state wave function remains approximately Coulombian as long as $M_V \ll M_\chi v_{\rm rel}$. Physically, this means that the range of the force $1/M_V$ is much larger than the de Broglie wavelength of Dark Matter $\lambda^{-1} = M_\chi v_{\rm rel}$. One indeed can check that in this limit the Sommerfeld factor in eq. (1.27) is well approximated by its Coulombian limit $M_V = 0$. At finite temperature $v_{\rm rel}^2 \sim T/M_\chi$, so that the Coulombian approximation holds for temperatures $T \gg M_V^2/M_\chi$ which can be much lower than $M_V$. When this condition is violated, the modification of the shape of the potential leads to a scaling of the cross section with velocity as $v_{\rm rel}^{2\ell}$, where $\ell$ is the angular momentum of the initial state wave function. Thus, for the $1s$ bound state, which is created from a $p$ wave state, the scaling is $v_{\rm rel}^2$. Therefore, the cross section is velocity suppressed and small after thermal average at late times. On the other hand $p$-wave bound states which are formed from an $s$-wave initial state approach a constant value.

Next, we consider bound states. Eq. (1.30) shows that bound states are well approximated by the Coulombian $M_V = 0$ limit if $M_V \ll M_\chi\alpha_{\rm eff}$. This condition can be alternatively obtained from the analogous condition for free states by replacing $v_{\rm rel} \to \alpha_{\rm eff}$, since this is the typical velocity in a bound state. In the limit of small $M_V \ll \alpha_{\rm eff}M_\chi$ all binding energies undergo a small common shift $-\alpha_{\rm eff}M_V$ as discussed around eq. (1.29).

In summary for $T \gg M_V^2/M_\chi$ the main effect of vector masses is the kinematical suppression of the cross section for bound-state formation, which blocks the process if $M_V$ is bigger than the total accessible energy. This effect is approximately captured by

$$\frac{\sigma(\chi\chi \to BV)}{\sigma(\chi\chi \to BV)|_{M_V=0}} \approx \frac{3}{2}\frac{k}{\omega}\left(1 - \frac{k^2}{3\omega^2}\right) \qquad \text{for} \qquad x < \frac{M_\chi^2}{M_V^2} \tag{1.55}$$

where $K_\mu = (\omega, \vec{k})$ is the massive vector quadri-momentum as in eq. (1.33). The parenthesis take into account the emission of the third polarization of a massive vector. The bound state formation gets suppressed or blocked when $\omega$ becomes of order $M_V$.

In our applications we will need the cross sections below the critical temperature at which $\mathrm{SU}(2)_L$ gets broken. In this case the masses are not degenerate: one has $M_W \approx M_Z$ and $M_\gamma = 0$. It becomes important to include emission of photons and eq. (1.55) becomes

$$\frac{\sigma(\chi\chi \to BV)}{\sigma(\chi\chi \to BV)|_{M_V=0}} \approx \frac{k}{\omega}\left(1 - \frac{k^2}{3\omega^2}\right)\left(1 + \frac{\cos^2\theta_\mathrm{W}}{2}\right) + \frac{\sin^2\theta_\mathrm{W}}{3}\,, \tag{1.56}$$

where the first term takes into account the emission of the $W$ and $Z$ bosons while the last term corresponds to the photon emission.

One extra effect is that the charged components of the DM electroweak multiplet get split from the neutral component and become unstable. In the cases of interest discussed later, the resulting decay width negligibly affects the cosmological relic DM density.

## 1.4 Annihilations of DM in bound states, and their decays

The two DM particles bound in a potential $V = -\alpha_\mathrm{eff} e^{-M_V r}/r$ can annihilate to SM particles, such that the bound state decays. We will refer to this process as 'annihilation' rather than 'decay'. Analogously to quarkonium in QCD, the rate is

$$\Gamma_\mathrm{ann} \sim \alpha_\mathrm{eff}^3 \alpha_\mathrm{SM}^2 M_\chi \gtrsim 10^{-8} M_\chi. \tag{1.57}$$

This is typically much faster than the Hubble rate

$$H = \sqrt{\frac{4\pi^3 g_\mathrm{SM}}{45}}\frac{T^2}{M_\mathrm{Pl}} \approx 2\ 10^{-18} M_\chi \times \frac{M_\chi}{\mathrm{TeV}} \qquad \text{at } T \approx \frac{M_\chi}{25}. \tag{1.58}$$

Nevertheless breaking of bound states in the thermal plasma can have a rate $\Gamma_\mathrm{break}(T)$ which is as fast as $\Gamma_\mathrm{ann}$ at the freeze-out temperature. So we need to compute the annihilation rates in order to obtain the branching ratios in eq. (1.7). We assume that DM is heavy enough that we can ignore the masses of SM particles produced in annihilations of DM bound states.

The group-theory factors are analogous to the one encountered in section 1.2.2 when computing Sommerfeld-enhanced DM annihilations to SM particles. As already discussed, the DM-DM bound states $\chi_i \overline{\chi}_j$ fill the representations $J$ contained in $R \otimes \overline{R} = \sum_J J$, and the bound state $B_M$ in representation $J$ with index $M$ is given by $\mathrm{CG}_{ij}^M \chi_i \overline{\chi}_j$.

### 1.4.1 Annihilations of spin 0 bound states with $\ell = 0$

We assume that the gauge group is unbroken and that DM is much heavier than SM particles. The annihilation rate of a spin-0 bound state $B^M_{n\ell}$ with $\ell = 0$ into two vectors $V^a V^b$, summed over all their components $a, b$ is

$$\Gamma_{\rm ann} = \Gamma(B^M_{n0} \to VV) = \alpha^2 \frac{|R_{n0}(0)|^2}{F^2 M_\chi^2} \sum_{a,b} {\rm Tr}\left[ {\rm CG}^M \frac{\{T^a_R, T^b_R\}}{2} \right]^2 \tag{1.59}$$

where $T^a_R$ is the generator in the DM representation $R$, and $R_{n\ell}(r)$ is the radial wave function of the bound state normalized as $\int_0^\infty |R_{n\ell}(r)|^2 r^2 dr = 1$; $F = 1(2)$ for distinguishable (identical) DM particles. For Majorana particles the amplitude is 1/2 the one of Dirac particles while the wave function at the origin is $\sqrt{2}$ so that the total rate is 1/2 the one of Dirac particles.

In general $R \otimes \overline{R}$ always contains the singlet and the adjoint representation, so we evaluate explicitly the group-theory factors that determine the annihilation rates of these specific bound states.

- For a gauge-singlet bound state one has ${\rm CG}_{ij} = \delta_{ij}/\sqrt{d_R}$ such that its annihilation rate is

$$\Gamma(B_{n0} \to VV) = \alpha^2 \frac{|R_{n0}(0)|^2}{F^2 M_\chi^2} \frac{T_R^2 d_{\rm adj}}{d_R} \tag{1.60}$$

  where ${\rm Tr}\left[T^a_R T^b_R\right] = T_R \delta^{ab}$.

- For a bound state $B^a$ in the adjoint representation of $G$ one finds

$$\Gamma(B^a_{n0} \to VV) = \alpha^2 \frac{|R_{n0}(0)|^2}{16 F^2 M_\chi^2} \frac{\sum_{abc} d^2_{abc}}{d_{\rm adj}} \tag{1.61}$$

  where $d_{abc} = 2{\rm Tr}\left[{\rm CG}^a \{T^b, T^c\}\right]$. This is zero if $G =$ SU(2). Indeed the triplet bound state for SU(2) has spin-1 and cannot decay into massless vectors.

The annihilation rate into scalars is given by one half of the above expression.

The previous formulas hold for a generic Yukawa potential. In the Coulomb limit the wave functions can be explicitly evaluated, obtaining

$$\frac{|R_{n0}(0)|^2}{M_\chi^2} = F \frac{M_\chi \alpha_{\rm eff}^3}{2n^3}. \tag{1.62}$$

Approximating the Yukawa potential with the Hulthen potential one finds

$$\frac{|R_{n0}(0)|^2}{M_\chi^2} = F \frac{M_\chi \alpha_{\rm eff}^3}{2n^3} \left(1 - \frac{\kappa^2 n^4 M_V^2}{M_\chi^2 \alpha_{\rm eff}^2}\right). \tag{1.63}$$

### 1.4.2 Annihilations of spin 1 bound states

In view of the Landau-Yang theorem, spin-1 bound states cannot annihilate into $VV$. They can annihilate into pairs of SM fermions and scalars (or equivalently longitudinal gauge bosons). For fermions

$$\Gamma(B^M_{n0} \to f_i \overline{f_j}) = \frac{\alpha^2}{6} \frac{|R_{n0}(0)|^2}{F^2 M_\chi^2} \sum_a |\mathrm{Tr}\left[\mathrm{CG}^M T^a_R\right] T^a_{\mathrm{SM}ij}|^2 \tag{1.64}$$

where $T^a_{\mathrm{SM}}$ are the gauge generators of the considered SM fermion. The rate is different from zero only for bound state in the adjoint representation ($\mathrm{CG}^a_{ij} = T^a_{ij}/\sqrt{T_R}$). Summing over the components of $f$ we get

$$\Gamma(B^a_{n0} \to f\overline{f}) = \frac{\alpha^2}{6} \frac{|R_{n0}(0)|^2}{F^2 M_\chi^2} T_R T_{\mathrm{SM}} \tag{1.65}$$

that should be multiplied by the multiplicity of final states: the SM contains $3(3+1)$ fermionic $\mathrm{SU}(2)_L$ doublets. If DM has hypercharge, the annihilation rate receives the extra contribution

$$\Delta\Gamma(B^a_{n0} \to f\overline{f}) = \frac{\alpha_Y^2}{6} \frac{|R_{n0}(0)|^2}{F^2 M_\chi^2} d_R Y_Q Y_f. \tag{1.66}$$

Spin-1 singlet resonances can also decay into three vectors, but with a suppressed rate

$$\Gamma(B_{n0} \to VVV) = \frac{\sum_{abc} d^2_{abc}}{36 d_R} \frac{\pi^2 - 9}{\pi} \alpha^3 \frac{|R_{n0}(0)|^2}{F^2 M_\chi^2}. \tag{1.67}$$

### 1.4.3 Annihilations of bound states with $\ell > 0$

The annihilation rate of bound states with orbital angular momentum $\ell > 0$ is suppressed by higher powers of $\alpha$. For example spin-1 bound states annihilate into vectors as

$$\Gamma(B^M_{n1} \to VV) = 9\alpha^2 \frac{|R'_{n1}(0)|^2}{F^2 M_\chi^4} \frac{1}{d_B} \sum_{a,b} \mathrm{Tr}\left[\mathrm{CG}^M \frac{\{T^a, T^b\}}{2}\right]^2 \tag{1.68}$$

where in the massless limit the derivative of the wave function at the origin contains the suppression factor

$$\frac{|R'_{21}(0)|^2}{M_\chi^4} = F\,\frac{\alpha_{\mathrm{eff}}^5}{24} M_\chi \tag{1.69}$$

Annihilations of spin-0 bound states with $\ell = 1$ into fermions and scalars are similarly suppressed. A greater suppression applies to bound states with $\ell > 1$. We will not need to compute these suppressed annihilation rates because states with $\ell > 0$ undergo faster decays into lower bound states, as discussed in the next section.

### 1.4.4 Decays of bound states

We next consider decays of a DM bound state into another lighter bound state. This is analogous to decays of excited state of the hydrogen atom.[5]

The decay rate of a $2s$ state into the corresponding $1s$ state is suppressed, and negligible with respect to its annihilation rate.

The decay rate of a $2p$ state into the corresponding $1s$ state is unsuppressed, and dominant with respect to its annihilation rate. The formula for the decay rate is related to the cross-section for bound state formation [67]: the only difference is that the initial state is not a free state, but a bound states with wave functions normalized to 1. Explicitly

$$\Gamma(B_{21}^{M} \to B_{10}^{M'} + V^a) = \frac{16}{9}\frac{\alpha k}{M_\chi^2}\left|\int r^2 dr R_{21}\left(C_{\mathcal{J}}^{aMM'}\partial_r - C_{\mathcal{T}}^{aMM'}\frac{\alpha M_\chi}{2}e^{-M_a r}\right)R_{10}^*\right|^2 . \tag{1.70}$$

If $G = \mathrm{SU}(2)_L$ and at temperatures below the scale of electroweak symmetry breaking the released binding energy is usually not enough to emit a massive $\mathrm{SU}(2)_L$ vector $W$ or $Z$, and only the photon can be emitted.

$$\Gamma(2p \to 1s + \gamma) = \alpha_{\rm em}\alpha_2^4 M_\chi\left(\lambda_f^2 - \frac{\lambda_i^2}{4}\right)\frac{512\lambda_i^5\lambda_f^5}{3(\lambda_i + 2\lambda_f)^8} \times \frac{1}{3d_B}\sum_{aMM'}\left|C_{\mathcal{J}}^{aMM'} + \frac{C_{\mathcal{T}}^{aMM'}}{\lambda_f}\right|^2 . \tag{1.71}$$

having assumed that the bound state is well approximated by its Coulombian limit.

## 1.5 Thermal effects

So far we allowed for generic vectors mass. The motivation is that all vectors acquire non-relativistic 'thermal masses' in the early universe at finite temperature. In the non-relativistic limit we are interested in electric potentials, and the relevant masses are the Debye masses, given by

$$m_{\mathrm{U}(1)}^2 = \frac{11}{6}g_Y^2 T^2, \qquad m_{\mathrm{SU}(2)}^2 = \frac{11}{6}g_2^2 T^2, \qquad m_{\mathrm{SU}(3)}^2 = 2g_3^2 T^2. \tag{1.72}$$

This means that an attractive potential with $\alpha_{\rm eff} = \lambda\alpha$ supports bound states with quantum number $n = 1, 2, \ldots$ if

$$\lambda \geqslant \frac{T}{M_\chi/25}n^2 \times \begin{cases} 1.7 & \text{for } \mathrm{SU}(2)_L \\ 1.0 & \text{for } \mathrm{SU}(3)_c \end{cases} . \tag{1.73}$$

Furthermore, the $W^\pm$ and the $Z$ acquire mass from the electro-weak symmetry breaking. Combining $\mathrm{SU}(2)_L$-breaking masses with thermal masses gives a thermal mixing between $\gamma$ and $Z$. At finite temperature the $\mathrm{SU}(2)_L$-breaking Higgs vev $v$ decreases until $\mathrm{SU}(2)_L$ is restored via a

[5] With the important difference that Dark Matter (unlike hydrogen at recombination) has a small number density at freeze-out, such that vectors emitted at bound state formation (unlike photons) or from bound states have a negligible impact on the plasma.

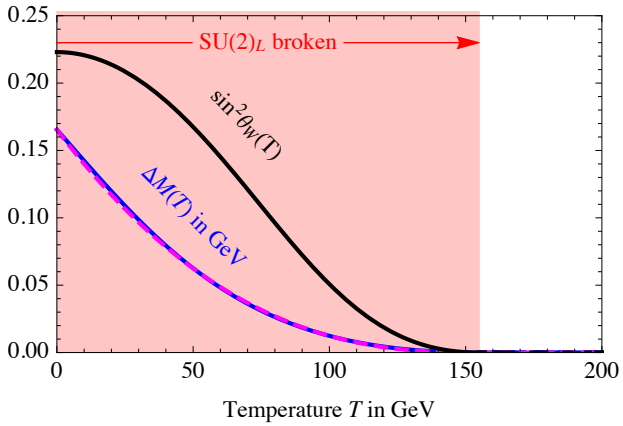


Figure 1.3: *DM mass splitting (blue) and weak angle (black) at finite temperature.*

cross-over at $T > T_{\rm cr} \approx 155\,{\rm GeV}$. This effect can be roughly approximated as

$$v(T) = v\,{\rm Re}(1 - T^2/T_{\rm cr}^2)^{1/2}. \tag{1.74}$$

In reality, thermal corrections are a much more subtle issue. We need to reconsider if/how the above naive approach applies at finite temperature.

### 1.5.1 Sommerfeld enhancement at finite temperature

Evolution of the DM states is affected by the presence of the thermal plasma. At leading order in the couplings to a plasma one gets refraction (in the case of the thermal plasma, this corresponds to thermal masses). At second order one gets interactions with rates $\Gamma$ which exchange energy and other quantum numbers with the plasma, and break quantum coherence among different DM components. Thereby DM forms an open quantum system, which is not described by a wave function, but by a density matrix $\rho$. Its evolution equation has the form

$$\dot\rho = -i[H,\rho] + \sum_L \Gamma_L (L\rho L^\dagger - \frac{1}{2}\{\rho, L^\dagger L\}) \tag{1.75}$$

where $L$ are Lindblad operators that describe the various interactions $\Gamma_L$ [79]. A gauge interaction with the plasma typically gives $\Gamma_L \sim \alpha^2 T^3/M_\chi^2$. Let us discuss breaking of quantum coherencies in the cases of interest.

In the ${\rm SU}(3)_c$ case, the Lindblad operators are proportional to the unit matrix in each 2-body sub-system with given quantum numbers. Thereby coherencies within each sector with given total color is preserved, while contributions from different sectors to the total cross section must be summed incoherently.

In the ${\rm SU}(2)_L$ case, its breaking leads to loss of coherence within the components of a given representation. For example, if DM is a ${\rm SU}(2)_L$ triplet with components $\chi_0$ and $\chi_\pm$, a $\chi_0\chi_0$ state

can become $\chi_0\chi_+$ by interacting with soft $W^\pm$ vectors in the plasma. From the point of view of exactly conserved quantum numbers, such as electric charge, these are different sectors. Thereby one has something intermediate between exact $\mathrm{SU}(2)_L$ (full coherence within each sector with given weak representation) and badly broken $\mathrm{SU}(2)_L$ (coherence only between state with same electric charges). An effect of this type is induced by the mass splitting among $\chi_0$ and $\chi_\pm$, which randomises their relative phase. In a static situation this is equivalent to loss of quantum coherence [81].

So we compute the thermal contribution to the mass splitting between different components of $\mathrm{SU}(2)_L$ multiplets, which was neglected in previous studies. A fermion with mass $M_\chi \gg M_V, T$ receives the following thermal correction to its mass, at leading order in $g$:

$$\Delta M_T = \frac{g^2 C}{4\pi^2}\frac{1}{M_\chi}\int_0^\infty dk\; k^2 \frac{2k^2+3M_V^2}{(k^2+M_V^2)^{3/2}} n_B(\sqrt{k^2+M_V^2}), \qquad n_B(E) = \frac{1}{e^{E/T}-1}. \tag{1.76}$$

This correction is suppressed by $M_\chi$ and can be neglected for our cases of interest. A correction not suppressed by $M_\chi$ arises at higher order in $g$ [82,83], and can be taken into account as follows. In the limit $M_\chi \gg M_V$ the one-loop quantum correction to the mass of a charged particle, as computed from Feynman diagrams, reduces to the classical Coulomb energy $U$ stored in the electric fields. For a single vector $A_\mu$ it is

$$U = \int dV \left[\frac{(\nabla A_0)^2}{2} + \frac{M_V^2}{2}A_0^2\right] = \frac{g^2}{8\pi}M_V + \text{divergent} \qquad \text{where} \qquad A_0 = \frac{g}{4\pi}\frac{e^{-M_V r}}{r}. \tag{1.77}$$

After summing over all SM vectors, the mass difference between two DM components $i$ and $j$ with electric charges $Q_i$ and $Q_j$ in a generic Minimal Dark Matter model is [69]

$$\Delta M_{ij} = \frac{\alpha_2}{2}[(Q_i^2-Q_j^2)s_{\mathrm{W}}^2(M_Z-M_\gamma) + (Q_i-Q_j)(Q_i+Q_j-2Y)(M_W-M_Z)]. \tag{1.78}$$

The higher order thermal contribution is obtained by simply replacing $M_\gamma, M_Z, M_W$ and $s_{\mathrm{W}}$ with their thermal expressions. For $Q_i = 1$, $Q_j = Y = 0$ the mass difference is plotted in Fig. 1.3 and well approximated by

$$\Delta M(T) = 165\,\mathrm{MeV}\,\mathrm{Re}(1-T/T_{\mathrm{cr}})^{5/2}. \tag{1.79}$$

### 1.5.2 Bound-state formation at finite temperature

If thermal masses were naive masses, they could kinematically block bound-state formation $\chi\bar{\chi} \to BV$, when $M_V \sim gT$ is bigger than the binding energy $E_B \sim \alpha^2 M_\chi$.

However thermal masses are not naive masses. Heuristically, one expects that a plasma cannot block the production of a vector with wave-length shorter than its interaction length. Formally, in thermal field theory cross sections get modified with respect to their leading-order value in $g$ by effects suppressed by powers of $g/\pi$. Thermal masses are a resummation of a class of such higher order corrections: those that become large at $E \lesssim gT$. Scatterings at higher order

in $g$ can have extra initial state particles, such as $V\chi\bar{\chi} \to BV$: this means that bound state formation is not blocked by thermal masses. Technically, the same conclusion can be reached in the thermal formalism, by computing the formation rate of bound states $B$ rate as the imaginary part of their propagator $\Pi_{BB}$. Cutted diagrams give an integral over thermal vectors: they have 'poles' (that can get kinematically blocked) as well as 'longitudinal'/'holes' and a 'continuum' below the light cone, which indeed corresponds to processes such as $V\chi\bar{\chi} \to BV$.

Formally, the cross section computed ignoring such 'thermal mass' effects is correct at leading order in $g$. In our cases of interest $g \sim g_3$ and $g \sim g_2$ are of order one, such that higher order effects cannot be neglected. Given that a full thermal computation is difficult and does not seem to give qualitatively new effects such as kinematical blocking of bound state formation, *we compute the $\chi\bar{\chi} \to BV$ cross sections at leading order in $g$ i.e. by ignoring the vector thermal mass $M_V$ in the kinematics.* We take into account vector masses in the Yukawa potentials. This approximation should be correct up to $\mathcal{O}(1)$ thermal corrections, as confirmed by [83], who finds that thermal corrections are small for $g = g_2$ and of order unity for $g = g_3$.

## 1.6 Applications

We now apply our formalism to the computation of the thermal relic abundance of various models previously studied in the literature. We start with DM candidates with SU(2) quantum numbers, such as Minimal Dark Matter scenarios, where the mass of mediators reduce the impact of bound state formation on the relic abundance. We finally consider supersymmetric scenarios with co-annihilation of neutralinos with gluinos or squarks.

### 1.6.1 Minimal Dark Matter fermion triplet (wino)

The first explicit model that we consider is the Minimal DM fermionic triplet [69], which coincides with a supersymmetric wino in the limit where all other sparticles are much heavier. Once $\mathrm{SU}(2)_L$ is broken, the conserved quantum numbers are $L = 0$, $S$ and $Q$. The potential among the neutral states with spin $S = 0$ is [61, 69]

$$V_{Q=0}^{S=0} = \begin{matrix} \\ - \\ 0 \end{matrix} \begin{matrix} \begin{matrix} + & \quad 0 \end{matrix} \\ \begin{pmatrix} 2\Delta M - A & -\sqrt{2}B \\ -\sqrt{2}B & 0 \end{pmatrix} \end{matrix}. \tag{1.80}$$

where $A = \alpha_{\mathrm{em}}/r + \alpha_2 c_{\mathrm{W}}^2 e^{-M_Z r}/r$, $B = \alpha_2 e^{-M_W r}/r$ and $\Delta M$ is the mass splitting produced by electroweak symmetry breaking, equal to $\Delta M = 165\,\mathrm{MeV}$ at $T = 0$ (we use the two-loop result [84, 85]). The charged states with $S = 0$ have [61, 69]

$$V_{Q=1}^{S=0} = \Delta M + B, \qquad V_{Q=2}^{S=0} = 2\Delta M + A. \tag{1.81}$$

| $I_J \rightleftarrows I_{J'}$ | $\sum_{aMM'} \lvert C_{\mathcal{J}}^{aMM'} + \gamma C_{\mathcal{T}}^{aMM'} \rvert^2$ |
|---|---|
| $1 \rightleftarrows 3$ | $2\,\lvert 1 \mp \gamma \rvert^2$ |
| $3 \rightleftarrows 5$ | $\frac{5}{2}\,\lvert 1 \mp 2\gamma \rvert^2$ |

| $I_J \rightleftarrows I_{J'}$ | $\sum_{aMM'} \lvert C_{\mathcal{J}}^{aMM'} + \gamma C_{\mathcal{T}}^{aMM'} \rvert^2$ |
|---|---|
| $1 \rightleftarrows 3$ | $6\,\lvert 1 \mp \gamma \rvert^2$ |
| $3 \rightleftarrows 5$ | $\frac{21}{2}\,\lvert 1 \mp 2\gamma \rvert^2$ |
| $5 \rightleftarrows 7$ | $12\,\lvert 1 \mp 3\gamma \rvert^2$ |
| $7 \rightleftarrows 9$ | $9\,\lvert 1 \mp 4\gamma \rvert^2$ |

Table 1.1: *Group theory factors for formation of a bound state made of two* $\mathrm{SU}(2)_L$ *3plets (left) or quintuplet (right) with total isospin* $I_{J'}$ *from an initial state with total isospin* $I_J$ *and viceversa. The upper sign refers to* $I_J \to I_{J'}$*, the lower sign to* $I_{J'} \to I_J$*.*

Finally, for the states with $S = 1$ one has

$$V_{Q=0}^{S=1} = 2\Delta M - A, \qquad V_{Q=1}^{S=1} = \Delta M - B. \tag{1.82}$$

where $V_{Q=1}^{S=1}$ differs by a sign from the earlier literature [61, 69]. These potentials allow one to compute the Sommerfeld correction, which affects the thermal relic abundance because of the existence of a loosely bound state in the sector with $Q = S = 0$ and $\ell = 0$. The cosmological DM abundance is reproduced for $M_\chi \approx 2.7\,\mathrm{TeV}$, such that the freeze-out temperature $M_\chi/25$ is below the temperature at which $\mathrm{SU}(2)_L$ gets broken, and the $\mathrm{SU}(2)_L$-invariant approximation is not accurate.

Nevertheless it is interesting to discuss the $\mathrm{SU}(2)_L$-invariant limit, which clarifies the controversial sign in eq. (1.82). Ignoring $\mathrm{SU}(2)_L$ breaking, the DM-DM states formed by two triplets of $\mathrm{SU}(2)_L$ decompose in the following isospin channels

$$3 \otimes 3 = 1_S \oplus 3_A \oplus 5_S\,, \tag{1.83}$$

The two DM fermions can make a state with spin $S = 0$ or 1. The total wave function must be anti-symmetric under exchange of the two identical DM fermions: taking into account the spin parity $(-1)^{S+1}$, the space parity $(-1)^\ell$ and the isospin parity $(-1)^{\tilde{I}}$ where $I = 2\tilde{I} + 1$ is the dimension of the representation, only states with $(-1)^{\ell+S+\tilde{I}} = 1$ are allowed. Namely, the allowed states are

| $I$ | $V$ i.e. | $\lambda$ | allowed $\ell$ |
|---|---|---|---|
| 1 | $-2\alpha_2/r$ | $+2$ | even if $S = 0$, odd if $S = 1$ |
| 3 | $-\alpha_2/r$ | $+1$ | even if $S = 1$, odd if $S = 0$ |
| 5 | $+\alpha_2/r$ | $-1$ | even if $S = 0$, odd if $S = 1$ |

(1.84)

The charged components of the 5-plet two-body channel have potentials as in eq. (1.81); the neutral components of the 5 mix with the 1 giving the matrix in eq. (1.80). By computing

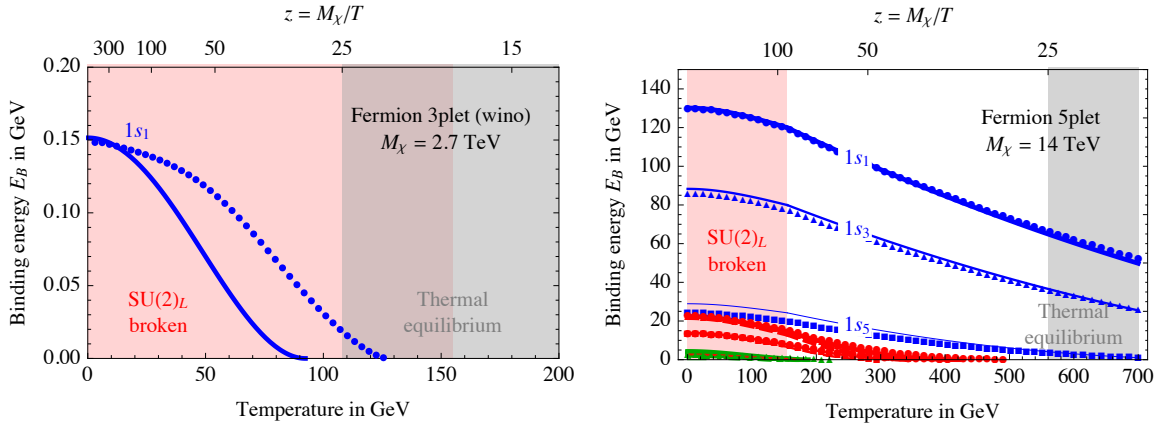


Figure 1.4: *Energies of bound states at finite temperature. made of two triplets (left) or quintuplets (right). Curves show results in* $\mathrm{SU}(2)_L$*-invariant approximation, dots show numerical results in components. In the left panel we consider DM as a* $\mathrm{SU}(2)_L$ *fermion triplet, there is only one bound state and the* $\mathrm{SU}(2)_L$*-invariant approximation is not accurate. In the right panel we consider DM as a* $\mathrm{SU}(2)_L$ *fermion quintuplet, the bound states are identified as follows:* $I = 1$ *(thick),* $I = 3$ *(medium),* $I = 5$ *(thin),* $n = 1$ *(blue),* $n = 2$ *(red),* $n = 3$ *(green),* $\ell = 0$ *(continuous),* $\ell = 1$ *(dashed),* $\ell = 2$ *(dot-dashed).*

its eigenvalues one finds that the correct $\mathrm{SU}(2)_L$-invariant limit is recovered for $\Delta M = 0$ and $A = B$. The components of the $I = 3$ triplet with $S = 1$ have the potentials of eq. (1.82), with a correct $\mathrm{SU}(2)_L$-invariant limit: notice that the $W$-mediated $V_{Q=1}^{S=1}$ has opposite sign to $V_{Q=1}^{S=0}$, unlike what assumed in previous literature. Anyhow, computing the spectrum we notice that this channel is not attractive enough to form a bound state, so that the sign change has a minor impact, as shown by comparing Fig. 1.5a with [61, 69]. The figure also shows the DM abundance as obtained using the simple $\mathrm{SU}(2)_L$-invariant approximation, which turns out not to be accurate. In $\mathrm{SU}(2)_L$-invariant approximation the Sommerfeld-corrected cross section [86] is obtained by decomposing the total $s$-wave annihilation cross-section of eq. (1.15) into isospin channels:

$$\sigma_{\rm ann} v_{\rm rel} = \left[\frac{16}{111} S_2 + \frac{20}{111} S_{-1} + \frac{75}{111} S_1\right] \times \frac{37}{12} \frac{\pi \alpha_2^2}{M_\chi^2}. \tag{1.85}$$

where $S$ is given by eq. (1.27) and the pedix on $S$ indicates the value of $\lambda$. We renormalise $\alpha_2$ at the RGE scale $M$, adopting the value from [87].

We next consider the contribution of bound states. Eq. (1.31) tells that a bound state with given $n$ and $\alpha_{\rm eff} = \lambda \alpha_2$ exists if

$$M_\chi \gtrsim 50 M_V \frac{n^2}{\lambda} \approx 4\,\mathrm{TeV} \frac{n^2}{\lambda} \tag{1.86}$$

where, in the last expression, we inserted the approximated vector mass $M_W \approx M_Z$ at zero temperature. This means that only the ground state $n = 1$, $\ell = 0$ of the $I = 1$ configuration

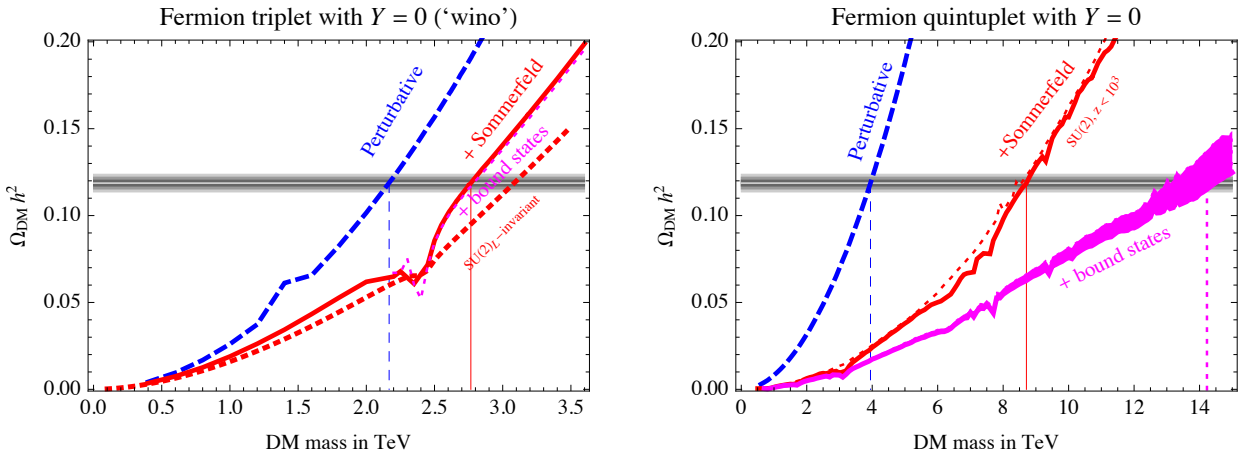


Figure 1.5: *Thermal relic DM abundance computed taking into account tree-level scatterings (blue curve), adding Sommerfeld corrections (solid red curve), and adding bound state formation (magenta). We consider DM as a fermion* $\mathrm{SU}(2)_L$ *triplet (left panel) and as a fermion quintuplet (right panel). In the first case the* $\mathrm{SU}(2)_L$*-invariant approximation is not good, but it's enough to show that bound states have a negligible impact. In the latter case the* $\mathrm{SU}(2)_L$*-invariant approximation (dashed red curve) is reasonably good, and adding bound states has a sizeable effect.*

is present at $M_\chi = 2.7\,\mathrm{TeV}$, in agreement with the component computation of the energy level carried out numerically. Thereby, we will consider only such $1s_1$ state (where the pedix denotes isospin). Fig. 1.4a shows its binding energy as function of the temperature for $M_\chi = 2.7\,\mathrm{TeV}$. The fact that the binding energy is small suggests that the Sommerfeld enhancement can be sizeable, and that bound-state formation gives a small correction to the effective annihilation cross section.

The only existing bound state has $\ell = S = 0$ and, in dipole approximation, can only be produced from an initial state with $\ell = 1$ and $S = 0$. No such state exists in the case of DM annihilations relevant for indirect DM detection, where the initial state is $\chi_0\chi_0$, that only exist with even $(-1)^{\ell+S}$ due to Pauli statistics [67]. In the case of DM annihilations relevant for thermal freeze-out, the bound state can be produced by $\chi_+\chi_-$ co-annihilations. In the $\mathrm{SU}(2)_L$-invariant computation this difference arises because we have isospin as an extra quantum number: the bound state with $\ell = 0$ and $I = 1$ can be produced from an initial state with $\ell = 1$, $I = 3$. As discussed above, the $\mathrm{SU}(2)_L$-invariant approximation is not accurate; nevertheless it suffices to estimate that the bound-state contribution is negligible.

Fig. 1.4a compares the approximated binding energy with the one computed numerically from the full potential of eq. (1.80). In $\mathrm{SU}(2)_L$-invariant approximation the annihilation width is $\Gamma_{\mathrm{ann}} = 8\alpha_2^5 M_\chi$, and the production cross section $\chi\chi \to B_{1s_1}\gamma$ is given by eq. (1.51) (with $C_{\mathcal{J}} = C_{\mathcal{T}} = \sqrt{2}$) times $\alpha_{\mathrm{em}}/3\alpha_2$ to take into account that only the photon can be emitted (thermal masses do not kinematically block the process), given that the non-thermal masses

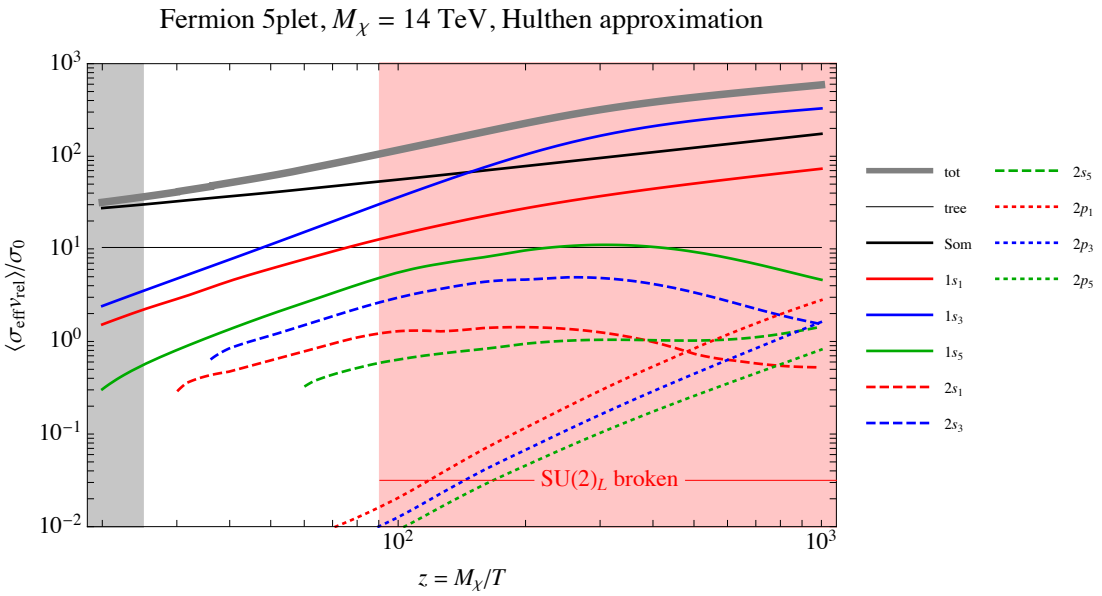


Figure 1.6: *Assuming that DM is a fermionic* $\mathrm{SU}(2)_L$ *quintuplet, we show its thermally-averaged effective annihilation cross section at tree level in s-wave (horizontal line), adding Sommerfeld corrections (black curve), and the contributions from bound state formation for the bound states listed in eq. (3.2.1).*

$M_{W,Z}$ are much bigger than the binding energy. Even with this rough (over)estimate, bound-state formation affects the DM relic density by a negligible amount, at the % level. Its effect is not visible in Fig. 1.5 where we show the DM thermal abundance as function of the DM mass.

### 1.6.2 Minimal Dark Matter fermion quintuplet

We next consider the Minimal DM fermionic quintuplet [69]. The DM-DM states formed by two quintuplets of $\mathrm{SU}(2)_L$ decompose into the following isospin channels

$$5 \otimes 5 = 1_S \oplus 3_A \oplus 5_S \oplus 7_A \oplus 9_S. \tag{1.87}$$

In the limit of unbroken $\mathrm{SU}(2)_L$ the $s$-wave annihilation cross-section reads [62][6]

$$\sigma_{\rm ann} v_{\rm rel} = \frac{207}{20}\frac{\pi\alpha_2^2}{M_\chi^2}\left[\frac{16}{69}S_6 + \frac{25}{69}S_5 + \frac{28}{69}S_3\right] \tag{1.89}$$

where the tree-level cross section of eq. (1.15) has been decomposed into channels with $I = \{1, 3, 5\}$ (higher $I$ do not annihilate into SM particles), and the appropriate Sommerfeld factor inserted for each channel. The cosmological DM abundance is reproduced for $M_\chi \approx 9.3\,\mathrm{TeV}$ [62,23]. Fig. 1.5b shows that the $\mathrm{SU}(2)_L$ invariant approximation can be reasonably good. The approximation is exact at $T > T_{\rm cr}$, which includes the freeze-out temperature. The approximations remains good below the critical temperature because electroweak vector masses are smaller than $\alpha_{\rm eff} M_\chi$, and badly fails only at $T \gtrsim \Delta M$, when the temperature gets smaller than the mass splittings $\Delta M \sim \alpha_{\rm em} M_W$ between neutral and charged DM components and co-annihilations become Bolztmann-suppressed. In this temperature range $T \gtrsim M_W^2/M_\chi$, such that the Sommerfeld correction is well approximated by its Coulombian limit.

## Bound states

In view of the selection rules discussed in the previous section, the allowed configurations are

| $I$ | $V$ i.e. | $\lambda$ | allowed $\ell$ |
|---|---|---|---|
| 1 | $-6\alpha_2/r$ | 6 | even if $S=0$, odd if $S=1$ |
| 3 | $-5\alpha_2/r$ | 5 | even if $S=1$, odd if $S=0$ |
| 5 | $-3\alpha_2/r$ | 3 | even if $S=0$, odd if $S=1$ |
| 7 | 0 | 0 | no bound state |
| 9 | $4\alpha_2/r$ | $-4$ | no bound state |

(1.90)

where we have computed the non-abelian effective potential in each isospin channel. Eq. (1.86) shows that various bound states exist for $M_\chi \sim 10\,\mathrm{TeV}$. Taking thermal masses and the small dependence on $\ell$ into account, Fig. 1.4b show the binding energies as function of the temperature for $M_\chi = 14\,\mathrm{TeV}$. We consider formation of the $1s_I$, $2s_I$ and $2p_I$ 'quintonium' bound states in each isospin channel $I$:

[6] Ref. [69] performed a computation of Sommerfeld effects taking into account the breaking of $\mathrm{SU}(2)_L$. In order to reproduce the correct $\mathrm{SU}(2)_L$-invariant limit, the non-abelian part of the potential in the sector with total electric charge $Q = 1$ and spin $S = 1$ must be changed by a sign that makes it different from the sector with $Q = 1$, $S = 0$. Eq. (18) of [69] must be changed into

$$V_{Q=1}^{S=0} = \begin{matrix} \\ - \\ 0 \end{matrix}\begin{matrix} \begin{matrix} ++ & + \end{matrix} \\ \begin{pmatrix} 5\Delta M - 2A & -\sqrt{6}B \\ -\sqrt{6}B & \Delta M + 3B \end{pmatrix} \end{matrix}, \qquad V_{Q=1}^{S=1} = \begin{matrix} \\ - \\ 0 \end{matrix}\begin{matrix} \begin{matrix} ++ & + \end{matrix} \\ \begin{pmatrix} 5\Delta M - 2A & -\sqrt{6}B \\ -\sqrt{6}B & \Delta M - 3B \end{pmatrix} \end{matrix}. \tag{1.88}$$

where $A = \alpha_{\rm em}/r + \alpha_2 c_{\rm W}^2 e^{-M_Z r}/r$ and $B = \alpha_2 e^{-M_W r}/r$ and $\Delta M$ is the mass splitting produced by electroweak symmetry breaking. Namely, the sign of the non-abelian Coulomb potential depends on spin, unlike what assumed in earlier works.

| Name | $I$ | $S$ | $n$ | $\ell$ | $\lambda$ | $\Gamma_{\rm ann}/M_\chi$ | $\Gamma_{\rm dec}/M_\chi$ | Produced from |
|---|---|---|---|---|---|---|---|---|
| $1s_1$ | 1 | 0 | 1 | 0 | 6 | $3240\ \alpha_2^5$ | 0 | $p_3$ |
| $1s_3$ | 3 | 1 | 1 | 0 | 5 | $15625\ \alpha_2^5/48$ | 0 | $p_1,\ p_5$ |
| $1s_5$ | 5 | 0 | 1 | 0 | 3 | $567\alpha_2^5/4$ | 0 | $p_3,\ p_7$ |
| $2s_1$ | 1 | 0 | 2 | 0 | 6 | $405\ \alpha_2^5$ | $\mathcal{O}(\alpha_2^4\alpha_{\rm em}^2)$ | $p_3$ |
| $2s_3$ | 3 | 1 | 2 | 0 | 5 | $15625\alpha_2^5/384$ | $\mathcal{O}(\alpha_2^4\alpha_{\rm em}^2)$ | $p_1, p_5$ |
| $2s_5$ | 5 | 0 | 2 | 0 | 3 | $567\alpha_2^5/32$ | $\mathcal{O}(\alpha_2^4\alpha_{\rm em}^2)$ | $p_3, p_7$ |
| $2p_1$ | 1 | 1 | 2 | 1 | 6 | $\mathcal{O}(\alpha_2^7)$ | $\approx 0.8\,\alpha_2^4\alpha_{\rm em}$ | $s_3$ |
| $2p_3$ | 3 | 0 | 2 | 1 | 5 | $\mathcal{O}(\alpha_2^7)$ | $\approx 0.5\,\alpha_2^4\alpha_{\rm em}$ | $s_1, s_5$ |
| $2p_5$ | 5 | 1 | 2 | 1 | 3 | $\mathcal{O}(\alpha_2^7)$ | $\approx 0.2\,\alpha_2^4\alpha_{\rm em}$ | $s_3, s_7$ |

(1.91)

The possibile initial states that can form each bound state are selected as follows. In dipole approximation the value of the spin quantum number $S$ is conserved and the angular momentum $\ell$ is changed by one unity. Furthermore a vector boson is emitted, such that the initial isospin $I_{\rm in}$ must be $I \pm 2$. This leaves the possible initial states listed in the last column of the above table.

Each contribution to bound state formation is given by the generic formulæ in section 1.3 inserting the group theory factors appropriate for the given $\mathrm{SU}(2)_L$ representations, as explicitly given in Table 1.1. For example, let us consider the formation of the $1s_1$ bound state. The cross-section is given by eq. (1.51) and (1.50) with $T_R = 10$, $d_R = 5$, $S = 0$. Once a bound state is formed, we need to determine its branching ratio into SM particles. For $1s_I$ and $2s_I$ states, they are well approximated by eq. (1.7). For $2p_I$ states they are given by eq. (1.8) and well approximated by $\mathrm{BR}(2p_I \to 1s_I) \times \mathrm{BR}(1s_I \to \mathrm{SM})$.

Fig. 1.5b shows the DM cosmological abundance as function of its mass $M_\chi$. We summed the Sommerfeld-enhanced cross section (computed in $\mathrm{SU}(2)_L$ components) with the bound-state cross section computed in $\mathrm{SU}(2)_L$-invariant approximation. As discussed above, the $\mathrm{SU}(2)_L$ invariant approximation only holds at $T \gtrsim \Delta M$, such that we switch-off the bound-state contribution to the effective annihilation cross section at $T < M_\chi/10^3$ (upper border of the magenta band in Fig. 1.5b) or at $T < M_\chi/10^4$ (lower magenta band). We adopted the couplings from [87] and normalized them at $M_\chi$ when computing annihilation rates, and at the inverse Bohr-radius $\alpha_2 M_\chi$ when computing potentials.

We find that bound state formation increase by $\sim 40\%$ the effective annihilation cross section defined in eq. (1.6), leading to a $\sim 20\%$ increase in the value of $M_\chi$ that reproduces the cosmological DM abundance. After including bound state formation, the cosmological DM abundance is reproduced for $M_\chi \approx 14\,\mathrm{TeV}$.

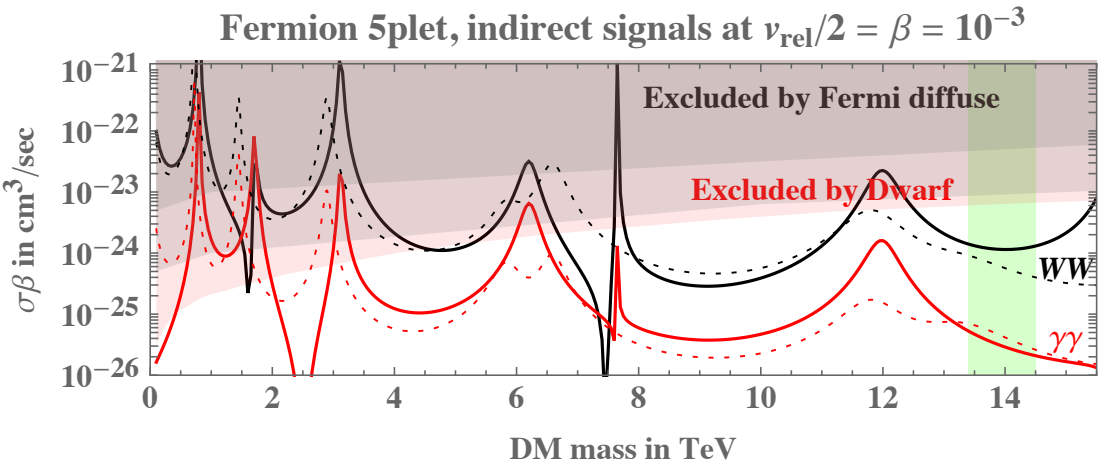


Figure 1.7: *Sommerfeld-enhanced cross section for indirect detection of a fermion 5-plet at* $\beta = 10^{-3}$. *The grey areas are excluded by the Fermi diffuse bound (computed in a conservative way, and in a more aggressive way); the red area is excluded by bound on dwarfs. The dotted curves are the analytic* $\mathrm{SU}(2)_L$*-invariant approximation of eq.* (1.92). *The green band shows the quintuplet mass for which the observed DM relic density is reproduced.*

## Indirect detection

We now investigate the indirect detection prospects of the quintuplet dark matter model. A study of the direct annihilation of quintuplet dark matter leading to $W^+W^-$, $ZZ$, $\gamma\gamma$ has been performed in [69, 68, 23, 89, 90], finding that the Sommerfeld enhancement plays a crucial role. Photons resulting from $W, Z$ decays give a continuum photon spectrum, which imply strong constraints if there is a large DM density around the Galactic Center, see Fig. 6 of [69]. However the DM density profile is unknown. In Fig. 1.7 we compare the signal with the trustable bound from the diffuse photon spectrum measured by Fermi. We show two bounds: a weaker safe bound obtained by demanding that the DM signal (computed assuming a Burkert density profile) never exceeds the measured spectrum, and a bound stronger by a factor $\approx 10$ obtained by subtracting the putative astrophysical background [23]. The continuous curves is the prediction from a component computation [69], and the dotted curves are obtained from the $\mathrm{SU}(2)_L$-symmetric approximation

$$(\sigma v_{\rm rel})_{WW} \approx \frac{2\pi\alpha_2^2}{M_\chi^2}(2\sqrt{S_6} + \sqrt{S_3})^2, \qquad (\sigma v_{\rm rel})_{\gamma\gamma} = \frac{4\pi\alpha_{\rm em}^2}{M_\chi^2}(\sqrt{S_6} - \sqrt{S_3})^2 \tag{1.92}$$

as well as $\sigma_{ZZ} = \sigma_{\gamma\gamma}/\tan^4\theta_{\rm W}$, $\sigma_{\gamma Z} = 2\sigma_{\gamma\gamma}/\tan^2\theta_{\rm W}$. Here $S_6$ ($S_3$) are the Sommerfeld factors for the $I = 1$ and ($I = 5$) channel: around $M \approx 12\,\mathrm{TeV}$ they are enhanced by a zero-energy bound state with $n = 4$ ($n = 3$). The formulæ above correctly reproduce the peaks of the cross-section associated to zero energy bound states while they miss the dips due to less important Ramsauer-Townsend effect, see [91].

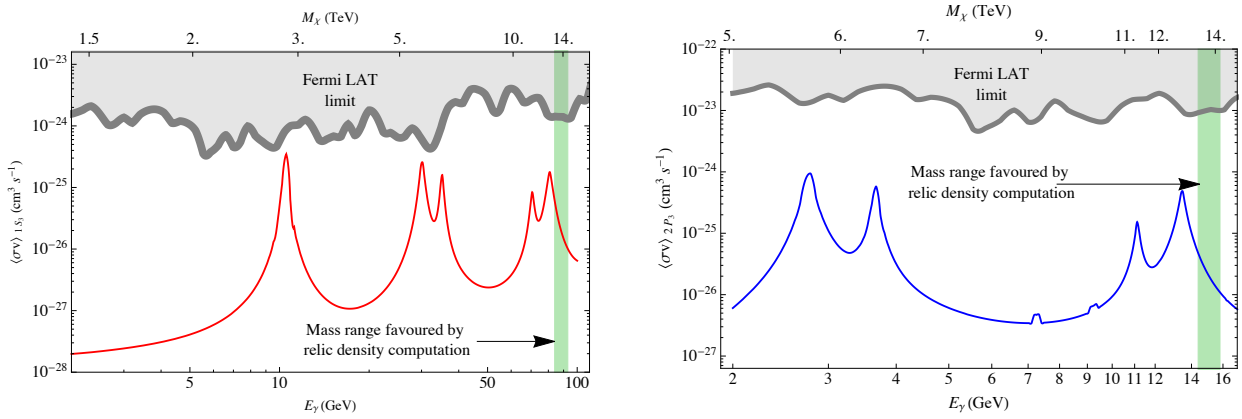


Figure 1.8: *Cross sections for producing a monochromatic photon after bound-state annihilation in the quintuplet model. We consider the contribution of the* $1s_3$ *(left) and* $2p_3$ *(right) bound state. This signal cross section is compared with the bounds from Fermi-LAT, assuming a contracted NFW DM density profile and a* $3^\circ$ *aperture around the galactic center ('R3' region) [88]. The Fermi-LAT limits on the* $\gamma$*-line cross sections have been appropriately rescaled taking into account that one photon with energy smaller that the DM mass is emitted.*

Eq. (1.92) is obtained by writing the neutral component of the $\chi_0\chi_0$ state as linear combination of states with given total isospin:

$$|\chi_0\chi_0\rangle = \frac{1}{\sqrt{5}}|I=1, I_3=0\rangle - \sqrt{\frac{2}{7}}|I=5, I_3=0\rangle + \sqrt{\frac{18}{35}}|I=9, I_3=0\rangle. \tag{1.93}$$

The continuum spectrum of photons resulting from $W, Z$ decays and fragmentations is not the most clean experimental signal, given that astrophysics produce a largely unknown continuum background. A monochromatic gamma line would give a clean signature, but a visible gamma line is not a generic feature of dark matter models [92, 93]. We discuss here the possibility to search for quintuplet dark matter by looking for monochromatic photons emitted in the bound state formation processes $\chi_0\chi_0 \to B\gamma$.

The $\chi_0\chi_0$ DM state of eq. (1.93) can only exist with even $\ell + S$ due to Pauli statistics. In the dipole approximation $\mathrm{SU}(2)_L$ conservation implies that only $I = 3$ bound states can be formed either from the $I = 1$ or the $I = 5$ component of $\chi_0\chi_0$: the deepest such bound state is $1s_3$, with binding energy $E_B \approx 60\,\mathrm{GeV}(M_\chi/10\,\mathrm{TeV})$. Therefore only the photon can be emitted in its formation, and consequently only the neutral component of the bound state can be produced from $\chi_0\chi_0$. The $M_{W,Z}$ masses cannot be neglected when computing the potentials. Then, the cross section for bound state formation is obtained by applying eq. (1.49) to the desired single component, rather than summing over all possible components. The final result is

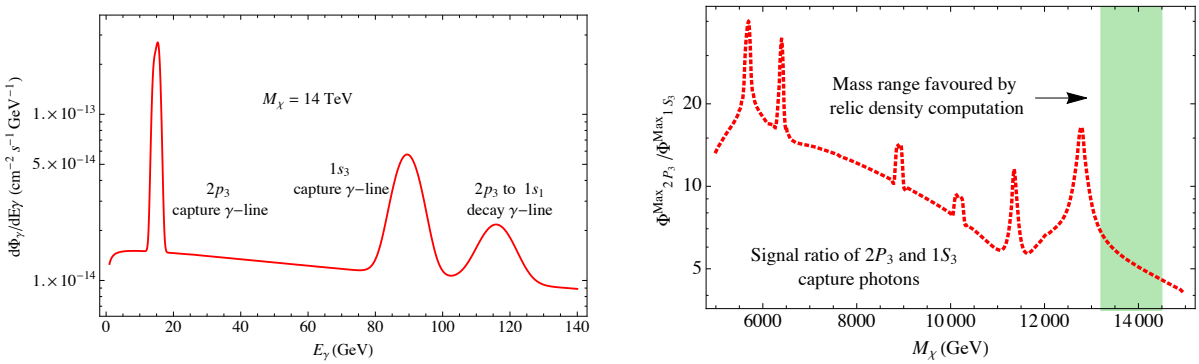


Figure 1.9: *In the left panel we show the $\gamma$-line spectrum predicted by the quintuplet model for the $1s_3$ and $2p_3$ capture processes, computed in $\mathrm{SU}(2)_L$-invariant approximation. A 10% energy resolution of the detector is assumed. We choose a benchmark DM mass of $M_\chi = 14\,\mathrm{TeV}$. In the right panel we show the ratio of the two $\gamma$-line signal strength as a function of the DM mass.*

$$\sigma v_{\rm rel}(\chi_0\chi_0 \to B_{3n\ell}\gamma) = 25\frac{\alpha_{\rm em}}{\alpha_2}\left[\sqrt{\frac{1}{5}(\sigma v_{\rm rel})^{n\ell}_{\rm bsf}\big|^{C_{\mathcal{J}}=\sqrt{2},C_{\mathcal{T}}=-\sqrt{2}}_{\lambda_i=6,\lambda_f=5}} \pm \sqrt{\frac{2}{7}(\sigma v_{\rm rel})^{n\ell}_{\rm bsf}\big|^{C_{\mathcal{J}}=\sqrt{7/5},C_{\mathcal{T}}=+\sqrt{28/5}}_{\lambda_i=3,\lambda_f=5}}\right]^2 \tag{1.94}$$

where the first (second) term corresponds to the $1 \to 3$ ($5 \to 3$) contribution, and the $I = 3$ bound state $B$ is further identified by its $n, \ell$ quantum numbers, and its spin is $S = 1$ (0) for $\ell$ even (odd). In this approximation we neglect the splitting between the various components of the multiplet. The above cross section is 2-3 orders of magnitude below $(\sigma v_{\rm rel})_{WW}$, with a similar pattern of Sommerfeld enhancements: thereby the annihilation of the bound state into $WW$ or similar states do nor produce relevant extra effects. The interesting new feature is the monochromatic photon.

We average the cross section assuming that the DM velocity distribution in the galactic rest frame is a Maxwell-Boltzmann with root mean square velocity $220\,\mathrm{km/s} < v_0 < 270\,\mathrm{km/s}$, cut off by a finite escape velocity $450\,\mathrm{km/s} < v_{\rm esc} < 650\,\mathrm{km/s}$:

$$f(v) = N \times e^{-v^2/v_0^2}\,\theta(v_{\rm esc} - v). \tag{1.95}$$

The normalisation constant $N$ is fixed such that $\int d^3v\ f(v) = 1$. Furthermore we assume that all DM is made of 5plets. We show the velocity-averaged photon capture cross sections in Fig. 1.8. The signal is below experimental bounds, and in some mass range it is close to the current sensitivity of the Fermi-LAT satellite. Both lines from the $1s_3$ and the $2p_3$ capture processes appear to be in principle detectable in the future. Additionally, the $2p_3$ bound state decays into the $1s_1$ and $1s_5$ states through emission of a photon, leading to extra gamma lines. In the

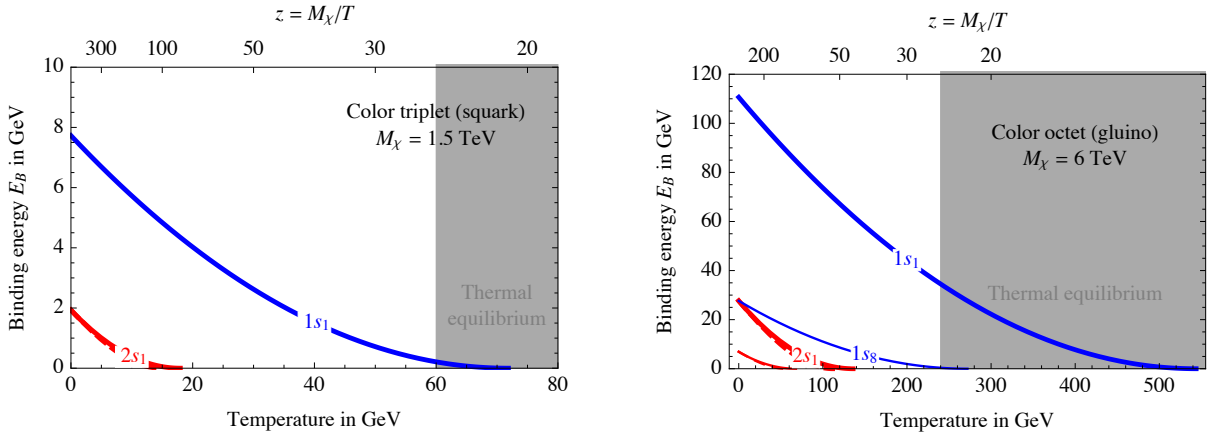


Figure 1.10: *Energies of bound states made of two squarks (left) or of two gluinos (right) as color singlets (tick), color octets (thin), $n = 1$ (blue), $n = 2$ (red), $\ell = 0$ (continuous), $\ell = 1$ (dashed).*

Coulomb limit their energies are

$$E_\gamma = \frac{\alpha_2^2}{4}\left(\lambda_f^2 - \frac{\lambda_i^2}{4}\right) M_\chi \,, \tag{1.96}$$

where $\lambda_i = 5$ and $\lambda_f = (6, 3)$ for $1s_1$ and $1s_5$ respectively and $\Gamma_{2p_3 \to 1s_1+\gamma}/\Gamma_{2p_3 \to 1s_5+\gamma} = 0.38$. This provides us with a window of opportunity to obtain spectroscopic data about the dark matter in the universe and learn about its gauge interactions. Fig. 1.9a shows that the extra peaks emerge over the continuum spectrum of photons from DM annihilations. Fig. 1.9b shows the ratio of the line signal intensities provides information about the dark matter mass. This information can then be confronted with searches for less specific emission of continuum photons at high energies stemming from direct dark matter annihilation.

### 1.6.3 Neutralino DM co-annihilating with a squark

We next consider neutralino Dark Matter with mass close enough to a squark $\chi' = \tilde{q}$ such that co-annihilations determine the relic abundance through the effective cross section of eq. (1.16) as discussed in section 1.2.1. The QCD process $\tilde{q}\tilde{q}^* \to gg$ dominates over weak processes such as $\tilde{q}\tilde{q} \to qq$, that we neglect. A squark $\tilde{q}$ is a scalar colour triplet, and a $\tilde{q}\tilde{q}^*$ state decomposes as $3 \otimes \overline{3} = 1 \oplus 8$. The QCD potential $V = -\lambda_i \alpha_3 / r$ is attractive with $\lambda_1 = 4/3$ in the singlet channel, and repulsive with $\lambda_8 = -1/6$ in the octet channel. Squarks annihilate into gluons at tree-level in $s$-wave, and the cross section of eq. (1.17) gets Sommerfeld-enhanced as [71]

$$\sigma v_{\rm rel} = \frac{7}{27}\frac{\pi\alpha_3^2}{M_{\tilde{q}}^2}\left[\frac{2}{7}S_{4/3} + \frac{5}{7}S_{-1/6}\right]. \tag{1.97}$$

| $R \rightleftarrows R'$ | $\sum_{aMM'} \lvert C_{\mathcal{J}}^{aMM'} + \gamma C_{\mathcal{T}}^{aMM'} \rvert^2$ |
|---|---|
| $1 \rightleftarrows 8$ | $\frac{4}{3}\lvert 1 \mp \frac{3}{2}\gamma \rvert^2$ |
| $3 \rightleftarrows \overline{6}$ | $3\lvert 1 \mp \gamma \rvert^2$ |

| $R \rightleftarrows R'$ | $\sum_{aMM'} \lvert C_{\mathcal{J}}^{aMM'} + \gamma C_{\mathcal{T}}^{aMM'} \rvert^2$ |
|---|---|
| $1_S \rightleftarrows 8_A$ | $3\left\lvert 1 \mp \frac{3}{2}\gamma \right\rvert^2$ |
| $8_A \rightleftarrows 8_S$ | 6 |
| $8_S \rightleftarrows 10_A \oplus \overline{10}_A$ | $3\left\lvert 2 \mp 3\gamma \right\rvert^2$ |
| $8_A \rightleftarrows 27_S$ | $9\left\lvert 1 \mp \frac{5}{2}\gamma \right\rvert^2$ |

Table 1.2: *Formation of a bound state made of two squarks (left) or two gluinos (right). We show the group theory factors for formation of a bound state in the representation $R'$ made from an initial state in the representation $R$ and viceversa.*

Bound states can exist in the color singlet channel with $S = 0$ and any $\ell$, given that they are made of distinguishable scalars. The lowest lying $\tilde{q}\tilde{q}^*$ bound states (we neglect $\tilde{q}\tilde{q}$ bound states, which can only annihilate through weak processes) are

| Name | $R$ | $n$ | $\ell$ | $\lambda$ | $\Gamma_{\rm ann}/M_{\chi'}$ | $\Gamma_{\rm dec}/M_{\chi'}$ | Produced from |
|---|---|---|---|---|---|---|---|
| $1s_1$ | 1 | 1 | 0 | 4/3 | $32\alpha_3^5/81$ | 0 | $p_8$ |
| $2s_1$ | 1 | 2 | 0 | 4/3 | $4\alpha_3^5/81$ | $\mathcal{O}(\alpha_3^6)$ | $p_8$ |
| $2p_1$ | 1 | 2 | 1 | 4/3 | $\mathcal{O}(\alpha_3^7)$ | $O(\alpha_3^6)$ | $s_8$ |

(1.98)

Taking into account the gluon thermal mass, and renormalizing the strong coupling at the inverse Bohr radius, we find that the $1s_1$ bound state exists around the freeze-out temperature, see eq. (1.73). All other states only form at much lower temperatures, as shown in the left panel of Fig. 1.10. Even the binding energy of the $1s_1$ state gets significantly reduced by the gluon thermal mass,indicating that the Coulomb approximation is not accurate. We used the approximation described in section 1.3.5. The Clebsh-Gordon factors for bound-state formation are listed in Table 1.2a while the left panel of Fig. 1.11 shows the contribution of bound states to the total co-annihilation rate. The impact of bound states on the DM relic density is shown in Fig. 1.12 where, for small mass splittings, we have included post confinement effects that will be discussed in the next chapter.

Furthermore, so far we have ignored the possibility that $\tilde{q}$ can decay, implicitly assuming that its life-time is long enough. To conclude, we discuss what 'long enough' means and whether this assumption is plausible. A squark can decay into a neutralino DM and a quark, with rate

$$\Gamma(\tilde{q} \to q\chi) \sim \frac{g^2}{8\pi} \frac{\sqrt{(M_{\tilde{q}}^2 - M_\chi^2)^2 - 2m_q^2(M_\chi^2 + M_{\tilde{q}}^2) + m_q^4}}{M_{\tilde{q}}} \tag{1.99}$$

This new effect can be taken into account by the density-matrix formalism of eq. (1.75), which

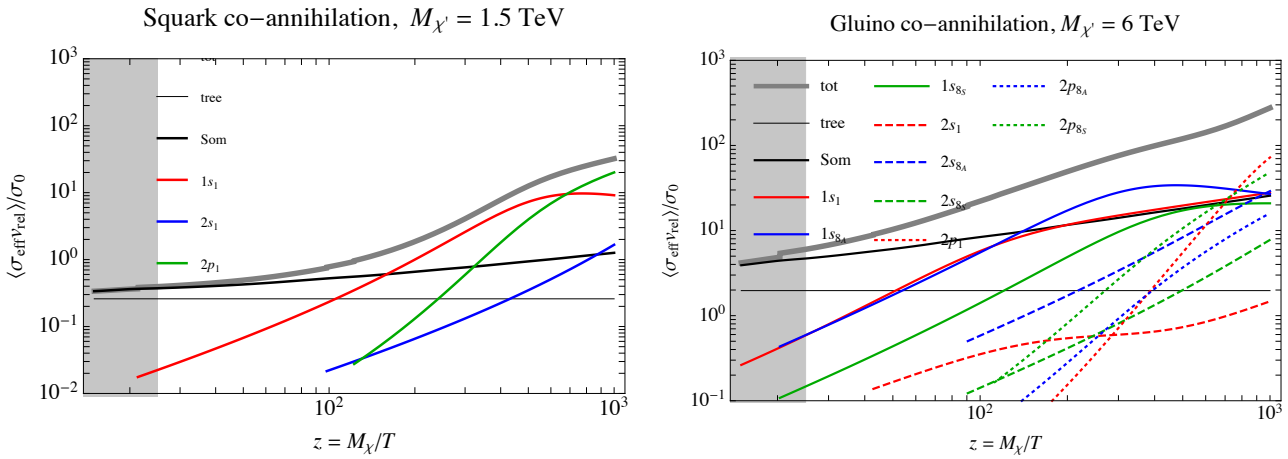


Figure 1.11: *Thermally-averaged effective co-annihilation cross section at tree level in s-wave (horizontal line), adding Sommerfeld corrections (black curve), and the contributions from bound state formation for the bound states listed in eq. (1.104).*

can be conveniently approximated by adding a stochastic term to the Schroedinger equation (1.22), represented by a non-unitary $\Gamma$ term in the Hamiltonian [80, 94], such that

$$-\frac{\nabla^2\psi}{M_\chi} + V\psi = (E + i\Gamma)\psi. \tag{1.100}$$

As it can be understood also from the uncertainty relation $\Delta E\,\Delta t > 1$, bound states only exist if the decay width $\Gamma$ is smaller than the binding energy $E_B \sim \alpha_3^2 M_{\chi'}$. This is satisfied only if the squark decay width of eq. (1.99) is strongly suppressed by the phase space. Such kinematical suppression can reasonably happen if the squark is a stop $\tilde{t}$ [95], such that its tree-level decays into a top quark is kinematically blocked if $M_{\tilde{t}} - M_\chi < M_t$, allowing for a $\sim 5\%$ non-degeneration around $M_\chi \sim 3\,\text{TeV}$. Furthermore, at finite temperature this degeneracy gets broken by thermal corrections to the Higgs vev and to the squark mass $\Delta M_T \sim g_3^2 T^2/M_\chi$, which effectively account for scatterings such as $g\tilde{q} \to \chi q$ that never get kinematically blocked, giving rise to a thermal $\tilde{q}$ width $\Gamma \sim \alpha_3\alpha_1 T^3/M_\chi^2$. Such effects can be neglected at the decoupling temperature $T_{\rm dec} \sim M_\chi/25$.

### 1.6.4 Neutralino DM co-annihilating with a gluino

We next consider neutralino Dark Matter with mass close enough to a gluino $\tilde{g}$ such that co-annihilations determine the relic abundance through the effective cross section of eq. (1.16). The product of two color octets decomposes as

$$8 \otimes 8 = 1_S \oplus 8_A \oplus 8_S \oplus 10_A \oplus \overline{10}_A \oplus 27_S. \tag{1.101}$$

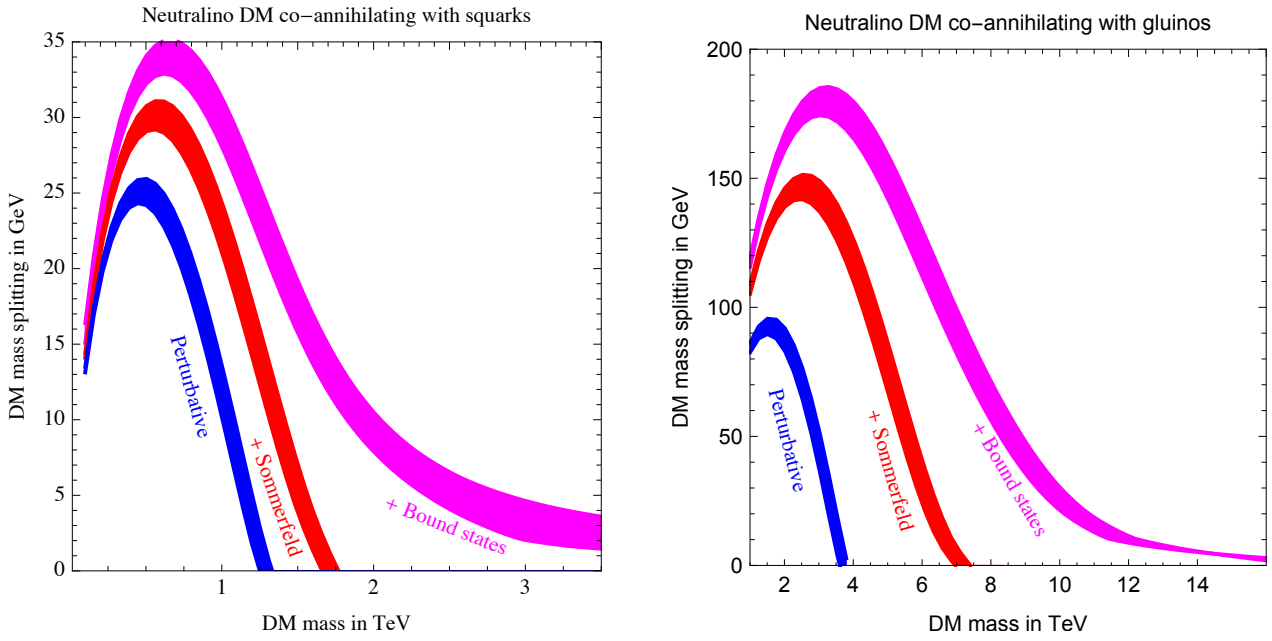


Figure 1.12: *The colored bands represent the regions in the plane of mass splitting between the colored partnter (gluino/squark) and the dark matter (neutralino) in which the correct relic abundance is reproduced within three standard deviations. The computation has been performed at tree-level (blue), taking into account Sommerfeld enhancement (red) and bound state formation (magenta). In the latter case, the tail at large $M$ and small $\Delta M \sim \Lambda_{\rm QCD}$ is due to QCD confinement effects that will be discussed in Chapter 2.*

Each channel experiences the following potentials

| Color | $V$ i.e. | $\lambda$ | allowed $\ell$ |
|---|---|---|---|
| $1_S$ | $-3\alpha_3/r$ | 3 | even if $S=0$, odd if $S=1$ |
| $8_A$ | $-\frac{3}{2}\alpha_3/r$ | 3/2 | even if $S=1$, odd if $S=0$ |
| $8_S$ | $-\frac{3}{2}\alpha_3/r$ | 3/2 | even if $S=0$, odd if $S=1$ |
| $10_A \oplus \overline{10}_A$ | 0 | 0 | no bound state |
| $27_S$ | $\alpha_3/r$ | $-1$ | no bound state |

(1.102)

where on the last column we listed the bound states supported in the attractive channels. The symmetric channels can annihilate into two gluons at tree level, and the $8_A$ channel can annihilate into quarks: the Sommerfeld-corrected $s$-wave annihilation cross-section is [71]

$$\sigma v_{\rm rel} = \frac{27}{32}\sigma_0\left[\frac{1}{6}S_3 + \frac{1}{3}S_{3/2} + \frac{1}{2}S_{-1}\right] + \frac{9}{8}\sigma_0 S_{3/2}, \qquad \sigma_0 = \frac{\pi\alpha_3^2}{M_{\tilde g}^2} \tag{1.103}$$

where the first (second) term comes from annihilations into gluons (quarks).

Furthermore, around the freeze-out temperature two (one) bound states in the singlet (octet)

channel exist, as illustrated in Fig. 1.10b, which takes the gluon thermal mass into account. We assume that gluino decay is slow enough, $\Gamma_{\tilde{g}} \ll E_B$, that gluino bound states can form. Furthermore, we assume that the gluino and DM are kept in relative equilibrium. If DM is a bino, these assumptions are satisfied by having relatively heavy squarks. Gluino bound states have been considered in [96,97] where the gluon thermal mass was neglected and only the singlet bound states with $n = 1$ was included. Furthermore, we include the non-abelian contribution to bound-state formation (latter diagram in Fig. 1.2), whose effect is described by the $C_{\mathcal{T}}$ contribution in Table 1.2b, and our $C_{\mathcal{J}}$ differs by a factor $1/\sqrt{2}$.

At zero temperature the lowest lying bound states are:

| Name | $R$ | $S$ | $n$ | $\ell$ | $\lambda$ | $\Gamma_{\text{ann}}/M_\chi$ | $\Gamma_{\text{dec}}/M_\chi$ | Produced from |
|---|---|---|---|---|---|---|---|---|
| $1s_1$ | $1_S$ | 0 | 1 | 0 | 3 | $243\alpha_3^5/4$ | 0 | $p_{8_A}$ |
| $1s_{8_A}$ | $8_A$ | 1 | 1 | 0 | 3/2 | $81\alpha_3^5/32$ | 0 | $p_1$, $p_{8_S}$, $p_{27_S}$ |
| $1s_{8_S}$ | $8_S$ | 0 | 1 | 0 | 3/2 | $243\alpha_3^5/128$ | 0 | $p_{8_A}$, $p_{10_A}$ |
| $2s_1$ | $1_S$ | 0 | 2 | 0 | 3 | $243\alpha_3^5/32$ | $\mathcal{O}(\alpha_3^6)$ | $p_{8_A}$ |
| $2s_{8_A}$ | $8_A$ | 1 | 2 | 0 | 3/2 | $81\alpha_3^5/256$ | $\mathcal{O}(\alpha_3^6)$ | $p_1, p_{8_S}, p_{27_S}$ |
| $2s_{8_S}$ | $8_S$ | 0 | 2 | 0 | 3/2 | $243\alpha_3^5/1024$ | $\mathcal{O}(\alpha_3^6)$ | $p_{8_A}, p_{10_A}$ |
| $2p_1$ | $1_S$ | 1 | 2 | 1 | 3 | $\mathcal{O}(\alpha_3^7)$ | $\approx \alpha_3^6$ | $s_{8_A}$ |
| $2p_{8_A}$ | $8_A$ | 0 | 2 | 1 | 3/2 | $\mathcal{O}(\alpha_3^7)$ | $\approx 0.1\alpha_3^5$ | $s_1$, $s_{8_S}$, $s_{27_S}$ |
| $2p_{8_S}$ | $8_S$ | 1 | 2 | 1 | 3/2 | $\mathcal{O}(\alpha_3^7)$ | $\approx 0.1\alpha_3^5$ | $s_{8_A}$, $s_{10_A}$ |

(1.104)

Fig. 1.11b shows how each bound state contributes to the effective annihilation cross section, and Fig. 1.12b shows how the resulting DM abundance gets affected. We find a moderate shift of the regions where the thermal abundance reproduces the cosmological DM abundance. The largest effect arises when $M_{\tilde{g}} - M_\chi$ is small, such that formation of $2p$ bound states from $s$-wave free states become sizeable at low temperatures. At even smaller temperatures post-confinement effects has to be taken into account as describe in the next chapter.

## 1.7 Summary

In the first part of the chapter we presented generic expressions and tools for computing non-abelian bound state formation. We specialised these formulæ to an unbroken gauge group, such that a significant simplification over a component computation is obtained by making use of group algebra. We applied these results to study how formation of bound states of two Dark Matter particles decreases their thermal abundance, in various concrete DM models.

1. In section 1.6.1 we assumed that Dark Matter is a fermionic 3plet of $\text{SU}(2)_L$ with zero hypercharge, for example a supersymmetric wino. We find that the $\text{SU}(2)_L$-invariant approximation is only qualitatively accurate. Nevertheless it is enough to establish that bound states have a negligible impact, at the % level, on the thermal relic DM abundance.

Furthermore, it shows that the non-abelian Coulomb energy depends on total spin, unlike what assumed in previous computations: we thereby repeated a component computation with the correct signs, and including thermal corrections to the weak mass splitting between charged and neutral components of the DM multiplet; finding again no sizable effects due to bound state formation.

2. In section 1.6.2 we assumed that Dark Matter is an accidentally stable fermionic 5plet of $\mathrm{SU}(2)_L$ with zero hypercharge. We found that 'quintonium' bound states reduce the DM thermal abundance by about 30%, increasing the DM mass that reproduces the cosmological abundance to about 14 TeV. We also considered bound-state corrections to DM indirect detection, finding that the 5-plet predicts a characteristic spectrum of mono-chromatic $\gamma$ lines around $E_\gamma \sim (10 - 80)\,\mathrm{GeV}$, with rates of experimental interest.

3. In section 1.6.3 we have considered Dark Matter co-annihilating with a scalar color triplet, a squark in supersymmetric models, finding that bound states give a mild shift ($\mathcal{O}(20\%)$ for neutralino masses around 1 TeV) in the thermal relic density.

4. In section 1.6.4 we have considered Dark Matter co-annihilating with a fermionic color octet, a gluino in supersymmetric models, improving the results of [96] by taking into account thermal masses and bound-state formation with gluon emission forms gluons, as depicted in the last diagram of Fig. 1.2. Bound state formation gives a significant correction ($\mathcal{O}(200\%)$ for neutralino masses in the range $2 \div 6\,\mathrm{TeV}$) to the thermal relic DM density.

We think that our results should be improved along two lines. First, concerning the weak 5plet, a computation in components will be needed to take into account the breaking of $\mathrm{SU}(2)_L$ and precisely determine the DM mass. Second, we included the effect of thermal masses, and assumed that they do not kinematically block bound-state formation for the reasons discussed in section 1.5.2. While we expect this to be a reasonable approximation, a careful study of thermal effects, possibly along the lines of [83], will be needed to achieve a more precise result.

# Chapter 2

## A closer look to the strongly coupled case

Extensions of the Standard Model (SM) sometimes predict (quasi)stable colored particles whose cosmological abundance is severely constrained because of their strong interactions with baryonic matter. When it comes to compute their relic density, the analysis carried out in the previous chapter is not the end of the story since it does not include non-perturbative effects that can take place after QCD confinement. In this chapter we show that these effects can significantly reduce the relic density of colored relics.

In particular we study the case of Split SuperSymmetry [98,99] where the new supersymmetric fermions are much lighter than the new supersymmetric scalars, and gauginos can become long-lived giving peculiar signatures at colliders and potential cosmological problems. These problems were explored in [100], where the relic gluino abundance (before late gluino decay in neutralino and colored SM particles) was computed including perturbative gluino annihilations and arguing that one can neglect non-perturbative effects arising after confinement at $T \sim \Lambda_{\rm QCD}$. We show that such effects cannot be ignored and, including them, we find that the relic gluino abundance is reduced by a few orders of magnitude, thereby weakening cosmological bounds on the model.[1]

Non-perturbative QCD effect are relevant not only for colored relics but also in the case of particles co-annihilating with a colored partner. We will briefly discuss the case of a neutralino co-annihilating with a gluino or a squark.

The chapter is organized as follows. In section 2.1 we compute the thermal relic abundance of (quasi)stable gluinos and in section 2.2 we reconsider the cosmological bounds and discuss the associated phenomenology. Conclusions are given in section 2.3.

[1] The relevance of confinement effects has been estimated in [101] in the case of colored particles charged under $U(1)_{\rm em}$. This scenario differs from the one we are considering (where the colored particle is electromagnetically neutral) because QCD bound states of electromagnetically charged particles can be formed or broken by emitting or absorbing photons.

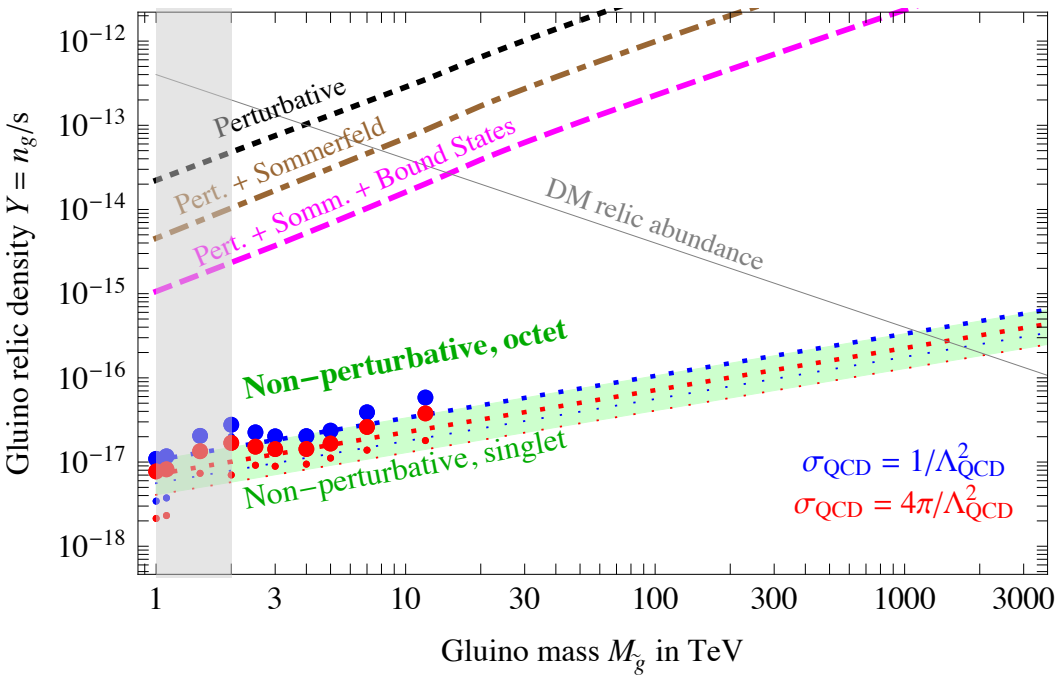


Figure 2.1: *Predicted gluino abundance. Relic stable gluinos exceed the DM density if* $M_{\tilde{g}} \gtrsim$ PeV. *The bands show the non-perturbative analytic result for* $\sigma_{\rm QCD} = 1/\Lambda^2_{QCD}$ *(blue) and* $\sigma_{\rm QCD} = 4\pi/\Lambda^2_{QCD}$ *(red). The thin (thick) lines assume that only singlet bound states (octet bound states too) can form with QCD size; similarly, the small (large) dots show our numerical computation for some values of the gluino mass.*

## 2.1 Relic gluinos

We consider a Majorana fermion in the adjoint of SU(3). In supersymmetric models this is known as gluino and denoted as $\tilde{g}$. The gluino can be stable if it is the lightest supersymmetric particle. Otherwise it can decay via squark exchange into a quark, an antiquark and a neutralino or chargino, or radiatively to a gluon and a neutralino, with quarks and squarks in the loop. The resulting lifetime is long if sfermions have a much heavier mass $m_{\rm SUSY}$ [102, 103]:

$$\tau_{\tilde{g}} = \frac{4\ \text{sec}}{N} \left(\frac{m_{\rm SUSY}}{10^9\ \text{GeV}}\right)^4 \left(\frac{\text{TeV}}{M_{\tilde{g}}}\right)^5 , \tag{2.1}$$

where $N$ is an order-one function [103]. A stable or long lived gluino is probed and constrained by cosmology.

### 2.1.1 Computing the relic gluino abundance

Fig. 2.1 shows our result for the gluino relic abundance, before their possible slow decays. This is computed as follows. The upper curves show the relic abundance after a first decoupling at $T \sim M_{\tilde{g}}/25$, as computed in various approximations:

1. at tree level in the perturbative expansion,
2. taking into account Sommerfeld corrections, *i.e.* using the annihilation cross section given in eq. (1.103),
3. taking into account also formation of bound states as discussed in the previous chapter.

These effects reduce by about 1 order of magnitude the gluino abundance, controlled by the Boltzmann equation

$$\frac{Hz}{s}\frac{dY_{\tilde{g}}}{dz} = -\langle \sigma_{\rm ann} v_{\rm rel}\rangle (Y_{\tilde{g}}^2 - Y_{\tilde{g}}^{\rm eq2}) \tag{2.2}$$

where $z = M_{\tilde{g}}/T$, $Y_{\tilde{g}} = n_{\tilde{g}}/s$, $s$ is the entropy density at temperature $T$; $H(T)$ is the Hubble constant.

If $\tau_{\tilde{g}} < M_{\rm Pl}/\Lambda_{\rm QCD}^2 \sim \mu$sec gluinos decay before the QCD phase transition leaving no cosmological effects. Otherwise gluinos recouple as the temperature approaches the QCD scale, and their relic abundance is determined by a re-decoupling at temperatures mildly below the QCD phase transition. At this point gluinos have formed $\tilde{g}g$ and/or $\tilde{g}q\bar{q}'$ hadrons which scatter with large cross sections $\sigma_{\rm QCD} = c/\Lambda_{\rm QCD}^2$ where $c \sim 1$, making about $M_{\rm Pl}/\Lambda_{\rm QCD} \sim 10^{19}$ scatterings in a Hubble time. For comparison, the proton-proton elastic scattering cross section at low energy is known to be $\sigma_{\rm el} \approx 100\,{\rm mb}$, corresponding to $c \approx 23$.

Although gluinos are much rarer than gluons and quarks, occasionally, two gluino hadrons meet forming a $\tilde{g}\tilde{g}$ bound state plus $n$ pions through the processes:

$$\tilde{g}g + \tilde{g}g \to \tilde{g}\tilde{g} + n\pi \qquad \text{or} \qquad \tilde{g}q\bar{q}' + \tilde{g}q\bar{q}' \to \tilde{g}\tilde{g} + n\pi\,. \tag{2.3}$$

Classically such state has angular momentum $\ell \approx \mu v_{\rm rel} b$ where $b \approx 1/\Lambda_{\rm QCD}$ is the impact parameter; $\mu \simeq M_{\tilde{g}}/2$ is the reduced mass; $v_{\rm rel} \sim (T/M_{\tilde{g}})^{1/2}$ is the relative velocity. Thereby $\ell \sim (M_{\tilde{g}}T)^{1/2}/\Lambda_{\rm QCD}$, is large for $M_{\tilde{g}} \gg \Lambda_{\rm QCD} \gtrsim T$. The quantum-mechanical total QCD cross section for forming $\tilde{g}\tilde{g}$ bound states is large because many partial waves contribute. This can be parameterized defining the maximal angular momentum as $\ell_{\rm max} \equiv \sqrt{c/2\pi} M_{\tilde{g}} v_{\rm rel}/\Lambda_{\rm QCD}$ obtaining (see e.g. [104])

$$\sigma_{\rm QCD} = \sum_{\ell=0}^{\ell_{\rm max}} \sigma_\ell \simeq \frac{c}{\Lambda_{\rm QCD}^2}, \qquad \sigma_\ell = 4\pi \frac{2\ell+1}{M_{\tilde{g}}^2 v_{\rm rel}^2} \sin^2\delta_\ell. \tag{2.4}$$

where the phase shifts average to $\langle \sin^2\delta_\ell\rangle \simeq 1/2$, and $c$ is a dimensionless parameter which, as discussed above, parametrizes the strength of the gluino hadrons self scatterings. This expectation is consistent with numerical results in toy calculable models [105].

The cross section relevant for reducing the gluino abundance is not $\sigma_{\rm QCD}$, but the smaller cross section $\sigma_{\rm ann}$ for forming $\tilde{g}\tilde{g}$ states which annihilate into SM particles before being broken by interactions with the plasma. Assuming that a $\tilde{g}\tilde{g}$ with angular momentum $\ell$ and energy $\sim T$ annihilates before being broken with probability $\wp_\ell(T)$, one has[2]

$$\sigma_{\rm ann} = \sum_{\ell=0}^{\ell_{\rm max}} \sigma_\ell \wp_\ell. \tag{2.6}$$

A large cross section needs large $\ell$, but $\wp_\ell$ can be small at large $\ell$. We compute $\wp_\ell$ as the probability that the $\tilde{g}\tilde{g}$ bound state radiates an energy large enough to become unbreakable (bigger than $\approx T$) before the next collision, after a time $\Delta t \sim 1/n_\pi v_\pi \sigma_{\rm QCD}$. In such a case it becomes unbreakable and keeps radiating until $\tilde{g}\tilde{g}$ annihilate.

The key quantity to be computed is thereby the power radiated by the relevant bound states which have $n, \ell \gg 1$. In the abelian case, this is well approximated by its classical limit: Larmor radiation. Having assumed neutral constituents, we can neglect photon radiation. Similarly, gravitational radiation has cosmologically negligible rates $\Gamma_{\rm grav} \sim E_B^3/M_{\rm Pl}^2$. The dominant radiation mechanism is gluon radiation, which differs from abelian radiation because gluons are charged under QCD. This makes a difference when (as in our case) particles are accelerated because of the strong force itself. While a photon can be soft and its emission leaves the bound state roughly unchanged, an emitted gluon has its own QCD potential energy, and its emission changes the QCD potential among gluinos by an order one amount (in particular, a singlet bound state becomes octet). As the classical limit of gluon emission is not known, we apply the quantum formulæ.

We need to compute the power radiated by highly excited $\tilde{g}\tilde{g}$ bound states, with sizes of order $1/\Lambda_{\rm QCD}$. Smaller bound states can be approximated by the Coulomb-like non-relativistic limit of the QCD potential, and can have various color configurations, in particular singlets and octets. At large distances, they appear as color singlets because they are surrounded by a soft gluon cloud at distance of order $1/\Lambda_{\rm QCD}$, which (since the typical momenta of the $\tilde{g}$ is much larger than $\Lambda_{\rm QCD}$) acts as a spectator when computing their inner behaviour. In the opposite

[2]This intuitive picture can be formally justified writing a network of Boltzmann equations, one for each bound state $I$ with different $\ell$ and $n$. Such equations contain the formation rates $\gamma_I$, the thermally averaged breaking rates $\Gamma_I^{\rm break}$, the annihilation rates $\Gamma_I^{\rm ann}$, the decay rates among the states $\Gamma_{IJ}$. This is unpractical, given that hundreds of states play a relevant role. To get some understanding, we consider a toy system with three states. Of these three states, only state 1 can be produced, and only state 3 can annihilate. The state 1 can decay to state 2, which can decay to state 3. Assuming that the rates are faster than the Hubble rate, we showed in the previous chapter that one can reduce the network of Boltzmann equations to the single Boltzmann equation eq. (2.2) for the total gluino density, controlled by an effective annihilation rate equal to $\wp\gamma_1$ where

$$\wp = {\rm BR}_{12}{\rm BR}_{23}, \qquad {\rm BR}_{12} = \frac{\Gamma_{12}}{\Gamma_{12} + \Gamma_1^{\rm break}}, \qquad {\rm BR}_{23} = \frac{\Gamma_{23}}{\Gamma_{23} + \Gamma_2^{\rm break} + {\rm BR}_{12}\Gamma_1^{\rm break}} \tag{2.5}$$

where the last term takes into account that 2 can upscatter to 1. We see that $\wp$ does not depend on $\Gamma_3^{\rm ann}$ and has the expected physical meaning. In view of QCD uncertainties we cannot compute all order unity factors, such that it is appropriate to employ the simpler intuitive picture.

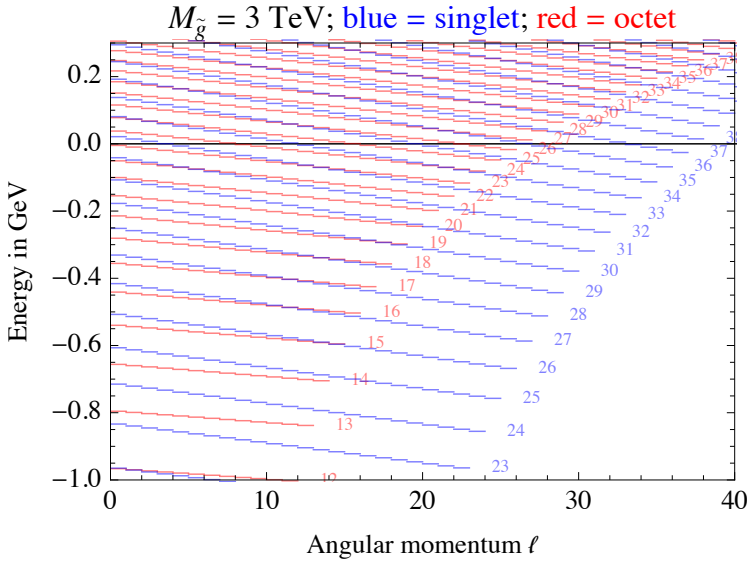


Figure 2.2: *Quantum energy levels of a $\tilde{g}\tilde{g}$ bound state which have energy close to 0. Values of $n$ are shown.*

limit, states larger than $1/\Lambda_{\rm QCD}$ can only be color-singlet hadrons. For our purpose what is needed are QCD-size bound states which are the most challenging, as confinement effects are starting to be relevant. We will estimate their effect into two opposite limits:

8) assuming that color octet $\tilde{g}\tilde{g}$ bound states are relevant, such that radiation is dominated by single-gluon emission (pion emission after hadronization) into singlet states. This is computed in section 2.1.2.

1) assuming that only color singlets $\tilde{g}\tilde{g}$ exist, such that radiation is dominated by color-singlet double-gluon emission (pion emission after hadronization) among singlets. This is computed in section 2.1.3.

While the two cases are analytically very different (e.g. different powers of the strong coupling), QCD is relatively strongly coupled so that the numerical final results in the two limiting cases will be similar.

Before starting the computations, we summarize generic results for QCD bound states.

### The bound states

We compute the energy levels of the $\tilde{g}\tilde{g}$ bound states assuming the non-relativistic QCD potential

$$V(r) = \lambda \begin{cases} -\dfrac{\alpha_3(\bar{\mu})}{r}\left[1 + \dfrac{\alpha_3}{4\pi}\left(\dfrac{11}{7} + 14(\gamma_E + \ln \bar{\mu} r)\right)\right] & r \ll 1/\Lambda_{\rm QCD} \quad [106] \\ -\dfrac{\alpha_{3\rm lattice}}{r} + \sigma r & r \sim 1/\Lambda_{\rm QCD} \quad [107] \end{cases} \tag{2.7}$$

where $\lambda = (C_R + C_{R'} - C_Q)/2$ for the potential among representation $R$ and $R'$ in the $Q$ configuration with $C_1 = 0$, $C_3 = 4/3$, $C_8 = 3$ being the Casimirs. So $\lambda = 3$ (3/2) for the potential among octets in the singlet (octet) configuration. Lattice simulations indicate $\alpha_{3\text{lattice}} \approx 0.3$ and $\sigma \approx (0.4\,\text{GeV})^2$. The one-loop correction to the perturbative term means that the QCD potential is roughly given by the tree level potential with the strong coupling renormalised at the RGE scale $\bar{\mu} \approx 1/r$. At finite temperature $\sigma(T) \approx \sigma(0)\sqrt{1 - T^2/T_{\text{QCD}}^2}$ with $T_{\text{QCD}} \approx 170\,\text{MeV}$ [107].

The product of two color octets decomposes as

$$8 \otimes 8 = 1_S \oplus 8_A \oplus 8_S \oplus 10_A \oplus \overline{10}_A \oplus 27_S. \tag{2.8}$$

such that there are three attractive channels and the gluino bound states exist in the following configurations

| Color | $V$ i.e. | $\lambda$ | allowed $\ell$ |
|---|---|---|---|
| $1_S$ | $-3\alpha_3/r$ | 3 | even if $S = 0$, odd if $S = 1$ |
| $8_A$ | $-\frac{3}{2}\alpha_3/r$ | 3/2 | even if $S = 1$, odd if $S = 0$ |
| $8_S$ | $-\frac{3}{2}\alpha_3/r$ | 3/2 | even if $S = 0$, odd if $S = 1$ |

. (2.9)

The energy eigenvalues in a potential $V = -\alpha_{\text{eff}}/r + \sigma_{\text{eff}} r$ are [108]

$$E_{n\ell} \approx \frac{\mu\alpha_{\text{eff}}^2}{2}\left[-\frac{1}{n^2 t} + 12tn\varepsilon x\right] \simeq \begin{cases} -\mu\alpha_{\text{eff}}^2/2n^2 & \text{Coulomb limit} \\ 3(x\sigma_{\text{eff}})^{2/3}/2\mu^{1/3} & \text{string limit} \end{cases} \tag{2.10}$$

where $\mu \approx M_{\tilde{g}}/2$ is the reduced mass, $\ell = \{0, 1, \ldots\}$ is angular momentum, $n \geqslant 1 + \ell$, $x = 1.79(n - \ell) + \ell - 0.42$, $\varepsilon = \sigma_{\text{eff}}/4\alpha_{\text{eff}}^3\mu^2$ is a dimension-less number and $t$ is the positive solution to $t = 1 - 4n^3\varepsilon x t^3$. In the limit where the Coulomb force dominates one has $t \simeq 1$ and $\varepsilon \simeq 0$; bound states have size $n^2 a_0$ where $a_0 = 1/\mu\alpha_{\text{eff}}$ is the Bohr radius. The linear force dominates when $n^2 a_0 \gg \sqrt{\alpha_{\text{eff}}/\sigma} \sim 1/\Lambda_{\text{QCD}}$.

Fig. 2.2 shows the levels with nearly zero energy for $M_{\tilde{g}} = 3\,\text{TeV}$.

### The breaking rate

Once formed $\tilde{g}\tilde{g}$ states can be broken by interactions with pions in the plasma:

$$\tilde{g}\tilde{g} + \pi \to g\tilde{g} + g\tilde{g} + \pi\,. \tag{2.11}$$

The probabilities $\wp_\ell$ that a given state radiates enough energy before being broken can be computed in two different ways.

Based on classical intuition, one can simply compare its energy loss rate with the breaking rate. While this simplification holds in the abelian case, we have to deal with a non-abelian dynamics, where gluon emission changes singlet to octet states, and vice versa. This is relevant, as singlet and octet decay rates are significantly different (especially for some singlet states which only decay through higher-order effects, as discussed below). It's not clear what is the classical

limit of this system in the limit of large quantum numbers $n, \ell$.

We then perform a quantum computation, determining the $\wp_\ell$ by simulating transitions among the many different states. This is feasible up to masses $M_{\tilde{g}} \sim 10\,\text{TeV}$, because it involves a growing number of states at larger $M_{\tilde{g}}$.

We then need the breaking rate of the individual bound states. Thermal equilibrium between direct and inverse process (also known as Milne relation) does not allow one to infer the breaking rates from the total creation rate, because the latter is cumulative over all bound states. We assume that the breaking rate is given by the thermal average of the pion scattering cross section, assumed to be equal to $1/\Lambda_{\text{QCD}}^2$, and perform the thermal average $\langle \sigma_{\text{break}} v_{\text{rel}} \rangle$ over the distribution of pions with energies large enough to break the bound states. The number density of pions with enough energy to break a bound state with binding energy $E_B$ is[3]

$$n_\pi^{\text{eq}}(E_\pi > E_{B_I}) \approx \frac{3\,(T\,(E_B + m_\pi))^{3/2}}{2\sqrt{2}\pi^{3/2}} \exp\left(-\frac{E_B + m_\pi}{T}\right). \tag{2.12}$$

such that $\langle \Gamma_{\text{break}} \rangle \approx \langle \sigma_{\text{break}} v_{\text{rel}} \rangle n_\pi^{\text{eq}}(E_\pi > E_B)$.

### 2.1.2 Color octet states and single gluon emission

In this section we compute $\sigma_{\text{ann}}$, assuming that two colliding $\tilde{g}$ can form a $\tilde{g}\tilde{g}$ system with all 64 possible color configurations of eq. (2.8), and with relative weights determined by combinatorics rather than by energetics. Then the effective annihilation cross section is determined by summing over attractive channels as

$$\sigma_{\text{ann}} \propto \frac{1}{64}\sigma_{\text{ann}}^1 + \frac{1}{8}(\sigma_{\text{ann}}^{8_S} + \sigma_{\text{ann}}^{8_A}). \tag{2.13}$$

We fix the proportionality factor to $\approx 4$ such that the total cross section is $\sigma_{\text{QCD}} = c/\Lambda_{\text{QCD}}^2$, where $c \sim 1$ parameterizes our ignorance of the overall QCD cross section. The annihilation cross section is dominated by $\sigma_{\text{ann}}^{8_A}$ because the state $8_A$ radiates much more than 1 or $8_S$. Indeed, because of selection rules, single-gluon emission allows the following decays with $\Delta\ell = \pm 1$:

$$1 \to 8_A, \qquad 8_A \to 1, 8_S \qquad 8_S \to 8_A. \tag{2.14}$$

Taking hadronization into account two pions are emitted, such that the binding energy of the final state $E_B'$ must be larger than $E_B + 2m_\pi$, otherwise the decay is kinematically blocked. If the energy gap is somehow bigger than $\Lambda_{\text{QCD}}$, inclusive decay rates can be reliably computed by treating the gluon as a parton.

Since the 1 state is more attractive than $8_{S,A}$, the above conditions are easily satisfied for the $8_A \to 1$ decay, while $1 \to 8_A$ decays are kinematically blocked at larger $\ell$ and allowed at small enough $\ell$ (elliptic enough classical orbit), but suppressed with respect to the abelian result.

[3] In the energy balance used to derive this equation, non-perturbative contributions to the binding energies (of both the $\tilde{g}\tilde{g}$ and $\tilde{g}g$ states) have been neglected.

In our numerical results we sum over all possible final states using wave-functions computed in WKB approximation using the Langer transformation. We also provide a simple approximated analytic result obtained assuming Coulombian wave-functions (which is valid for deep final states, but not for the QCD-size initial states)[4]

$$\Gamma_{n\ell}(8_A \to 1_S) \approx \frac{2}{n^2}\alpha_3^5\mu, \qquad W_{n\ell}(8_A \to 1_S) = \frac{8\alpha_3^7\mu^2}{n^3\ell}\,. \tag{2.15}$$

The decay rate must be compared with the thermal breaking rate, which is given by pion scatterings such as $(\tilde{g}\tilde{g}) + \pi \to (\tilde{g}g) + (\tilde{g}g) + \pi$. Since we considered bound states made of neutral gluinos, they are not broken by photon scatterings to leading order. The result is very simple: the $8_A$ decay rate is so fast that its actual value is irrelevant: all $8_A$ allowed states have $\wp_\ell = 1$ at the relevant temperatures $T \lesssim \Lambda_{\rm QCD}$. On the other hand, $8_S$ and 1 states contribute negligibly. Then, the annihilation rate is controlled by a much simpler condition: $8_A$ bound states with binding energy $E_B \sim T$ only exist up to some maximal $\ell \leqslant \ell_{\rm max8}$, which can be easily computed. For $M_{\tilde{g}} = 3\,\text{TeV}$ Fig. 2.2 shows that $\ell_{\rm max8} \approx 25$. For generic $M_{\tilde{g}} \gg T$, $\ell_{\rm max8}$ is well approximated by imposing the vanishing of $E_{n\ell}$ in eq. (2.10), finding

$$\ell_{\rm max8} = (12\epsilon t^2)^{-1/4} \approx \left(\frac{3M_{\tilde{g}}^2\alpha_3^3}{16\sigma}\right)^{1/4} \tag{2.16}$$

having approximated $t \approx 1$ in the last expression. Using eq. (2.10), the deepest available singlet state has energy gap $\Delta E = \frac{9}{4}\sqrt{3\alpha_3\sigma} \approx 0.9\,\text{GeV}$ (see also Fig. 2.2) and can only decay via higher order processes.

The effective annihilation cross section is

$$\sigma_{\rm ann} \approx \frac{\sigma_{\rm ann}^{8_A}}{2} \approx \frac{1}{2}\sum_{\ell=0}^{\ell_{\rm cr}}\sigma_\ell \approx \frac{1}{2}\frac{2\pi}{M_{\tilde{g}}^2 v_{\rm rel}^2}\ell_{\rm cr}^2, \qquad \ell_{\rm cr} = \min(\ell_{\rm max}, \ell_{\rm max8}). \tag{2.17}$$

At low (high) temperatures one has $\ell_{\rm cr} \simeq \ell_{\rm max} \propto v_{\rm rel}$ ($\ell_{\rm cr} \simeq \ell_{\rm max8} \propto v_{\rm rel}^0$) such that the thermal average for $\ell \gg 1$ is $\langle\sigma_{\rm ann}v_{\rm rel}\rangle \simeq 2\sigma_{\rm QCD}\sqrt{T/\pi M_{\tilde{g}}}$ ($\langle\sigma_{\rm ann}v_{\rm rel}\rangle \simeq \sqrt{3\pi\alpha_3^3/16 M_{\tilde{g}}T\sigma}$). Taking the minimum of these two limits (which are equal at $T = T_{\rm cr} = \pi\sqrt{3\alpha_3^3/\sigma}/8\sigma_{\rm QCD}$ with $\sigma_{\rm QCD} = c/\Lambda_{\rm DC}^2$), we obtain an approximation valid at a generic intermediate $T$:

$$\langle\sigma_{\rm ann}v_{\rm rel}\rangle = \sigma_{\rm QCD}\sqrt{\frac{4T}{\pi M_{\tilde{g}}}}\begin{cases} 0 & \text{for} \quad T > T_{\rm QCD}\,, \\ T_{\rm cr}/T & \text{for} \quad T_{\rm cr} < T < T_{\rm QCD}, \\ 1 & \text{for} \quad T < T_{\rm cr} \end{cases} \tag{2.18}$$

The Boltzmann equation of eq. (2.2) is approximatively solved by

[4] In the same approximation, the smaller energy radiated into $8_S$ is given by a Larmor-like formula, given that the initial and final state are equally attractive.

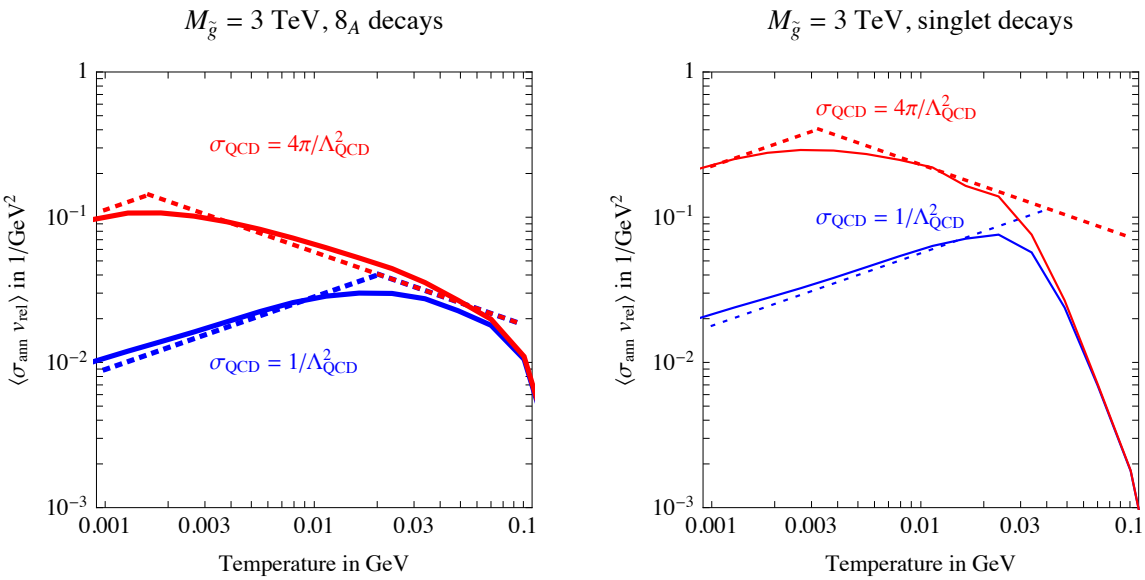


Figure 2.3: *The effective annihilation cross section of gluino $\tilde{g}\tilde{g}$ bound states, assuming that they form color-octet $8_A$ states (left) or only color-singlet states (right). The solid curves are the numerical computation the dashed lines are the maximal geometrical cross sections given by the analytic approximation.*

$$Y_{\tilde{g}}(\infty) \approx \sqrt{\frac{45}{g_{SM}\pi}}\frac{1}{M_{\tilde{g}}M_{Pl}}\left[\int_{M_{\tilde{g}}/T_{QCD}}^{\infty} dz \frac{\langle\sigma_{ann}v_{rel}\rangle}{z^2}\right]^{-1} \approx \frac{9\sqrt{5M_{\tilde{g}}/g_{SM}}}{4\sigma_{QCD}T_{cr}^{3/2}M_{Pl}(3\sqrt{T_{QCD}/T_{cr}}-2)} \quad (2.19)$$

where the $dz$ integral is dominated by $T \sim T_{QCD}$: for $T_{cr} \ll T_{QCD}$ the abundance simplifies to

$$Y_{\tilde{g}}(\infty) \approx \frac{1}{\pi M_{Pl}}\sqrt{\frac{60 M_{\tilde{g}}\sigma}{g_{SM}T_{QCD}\alpha_3^3}} \approx 0.6\ 10^{-17}\sqrt{\frac{M_{\tilde{g}}}{3\,\text{TeV}}\frac{170\,\text{MeV}}{T_{QCD}}}. \quad (2.20)$$

The final relic abundance does not have a strong dependence on $\sigma_{QCD}$, as it is only relevant at relatively low temperatures. The DM critical density is exceeded if $M_{\tilde{g}} \gtrsim$ PeV. Fig. 2.3a shows the full numerical result for $\langle\sigma_{ann}v_{rel}\rangle$, which agrees with the analytic maximal value (apart from some smoothing at $T \sim T_{cr}$) up to about 50 MeV: thereby the numerical abundance is better reproduced lowering $T_{QCD}$ down to 50 MeV in eq. (2.20). This is done in the analytic estimate plotted in Fig. 2.1.

### 2.1.3 Color-singlet states and two gluon emission

Single-gluon emission switches the color of the bound state as $1 \leftrightarrow 8$ and its angular momentum $\ell$ by $\pm 1$: as a consequence kinematics blocks single-gluon decays of various color-singlet bound states, roughly all the ones in Fig. 2.2 which don't have nearby octet states. In particular, decays

of singlet states with maximal $\ell$ are blocked, and octet states with maximal $\ell$ can (but need not) decay to singlets with blocked decays.

We thereby take into account two-gluon emission, which allows for $1 \to 1$ decays with $\Delta\ell = \{0, \pm 2\}$. The rates of $2g$ transitions are mildly suppressed by $\mathcal{O}(\alpha_3^3)$ compared with the $1g$ decay rates. If the energy difference $\Delta E$ is much bigger than $\Lambda_{\rm QCD}$, gluon hadronization proceeds with unit probability and the $2g$ decay widths can be computed using 2nd order non-relativistic perturbation theory [109]:

$$\Gamma^{2g}_{n,\ell\to n',\ell'} \approx \frac{3\alpha_3^2}{16\pi}\int_0^{\Delta E} dk\, k^3\,(\Delta E - k)^3 \times \\ \times \sum_{m,m'}\left|\langle\psi_{n,\ell,m}|r_i\left\{\frac{1}{-E_{n',\ell'}+H_8-k}+\frac{1}{-E_{n',\ell'}+H_8-(\Delta E-k)}\right\}r_i|\psi_{n',\ell',m'}\rangle\right|^2 \tag{2.21}$$

where $r_i = \{x, y, z\}$ is the relative distance between the two $\tilde{g}$; $k$ is the momentum of the hadron produced in the hadronization of the two outgoing gluons, $\Delta E = E_{n',\ell'} - E_{n,\ell}$ and $H_8$ the free Hamiltonian of the virtual intermediate octet state. The angular part of the matrix elements, already carried out in eq. (2.21), imposes the selection rule $|\ell' - \ell| = 0, 2$. The two-gluon $1 \leftrightarrow 1$ rates are given by an abelian-like expression, unlike the one-gluon $1 \leftrightarrow 8$ transitions. The rates for $8 \to 8$ two-gluon transitions are given by a similar expression, with $H_8$ replaced by $H_1$.

Hadronization is possible down to the kinematical limit $\Delta E \approx 2m_\pi$. However the energy difference between two singlet states with maximal $\ell$, $|\Delta\ell| = 2$ and nearby $n$ is $\sim \sigma^{3/4}\alpha_3^{-1/4}M_{\tilde{g}}^{-1/2}$, which, in view of the $M_{\tilde{g}}$ suppression, can be smaller than $2m_\pi$. In such a case the decay can still proceed through off-shell pions, which produce photons and leptons. How to estimate these suppressed decays is discussed in section 4.4.6 of Chapter 4. We neglect multi-gluon emission, which allows bigger jumps in $\ell$.

The $2g$ rates are included in numerical computations which assume that QCD-scale color octets exist. The result was discussed in the previous sub-section, as $2g$ decays give a relatively minor correction.

We consider the opposite extreme possibility that octet states with QCD-size do not exist, and that only color singlets exist. We can again obtain an analytic lower bound on the final $\tilde{g}$ abundance by assuming that all singlet levels fall fast. Then the cross section $\sigma_{\rm ann} \approx \sigma^1_{\rm ann}$ is only limited by $\ell_{\rm max1} = \sqrt{2}\ell_{\rm max8}$ such that

$$\langle\sigma_{\rm ann}v_{\rm rel}\rangle = \sigma_{\rm QCD}\sqrt{\frac{16T}{\pi M_{\tilde{g}}}}\begin{cases} 0 & \text{for} \quad T > T_{\rm QCD}\,, \\ T_{\rm cr}/T & \text{for} \quad T_{\rm cr} < T < T_{\rm QCD}, \\ 1 & \text{for} \quad T < T_{\rm cr} \end{cases} \tag{2.22}$$

where now $T_{\rm cr} = \pi\sqrt{3\alpha_3^3/\sigma}/4\sigma_{\rm QCD}$. The resulting relic gluino abundance is 2 times lower than in eq. (2.19), and with the new value of $T_{\rm cr}$. Fig. 2.3b shows that this limit only holds at $T \lesssim 20\,$MeV, such that the analytic expression reproduces the numerical value for $Y_{\tilde{g}}$ by reducing $T_{\rm QCD}$ down

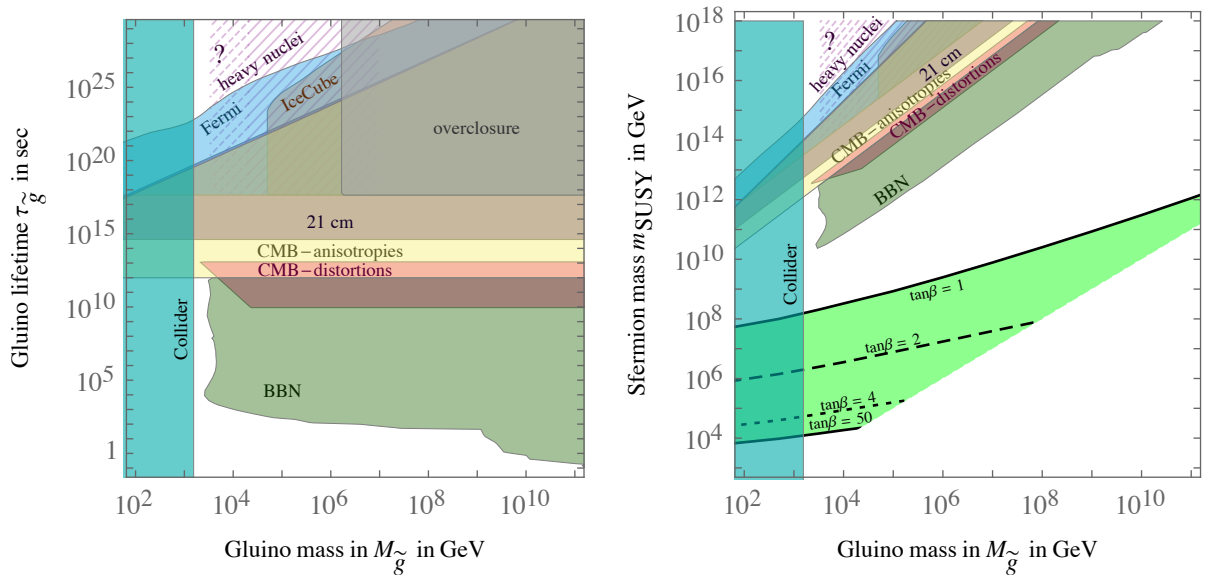


Figure 2.4: *Cosmological constraints on long-lived gluinos.* **Left***: As a function of the gluino lifetime.* **Right***: As a function of the sfermion mass scale* $m_{\rm SUSY}$*, which in Split SuperSymmetry determines the gluino lifetime.*

to $\sim 20\,\text{MeV}$.

## 2.2 Phenomenology

### 2.2.1 Cosmological bounds and signatures

Bounds on quasi-stable relics depend on their lifetime $\tau_{\tilde{g}}$; on their mass $M_{\tilde{g}}$; on their relic abundance, that for gluinos we computed in terms of $M_{\tilde{g}}$, and on their decay modes. As mentioned above, we assume that gluinos decay to neutralinos (assumed to be the Lightest Super-symmetric Particle, LSP) plus either a gluon or a quark and an antiquark. Here we assume that half of gluino energy is carried away by the LSP; if the LSP is not much lighter than the gluino, even less energy goes into SM states and one would obtain weaker bounds.

Our final result is plotted in Fig. 2.4, using the thick red dashed line of Fig. 2.1: even using updated experimental bounds (discussed below), our bounds on a (quasi)stable gluino are significantly weaker than those derived in [100]. The reason is that our relic density takes into account non-perturbative gluino annihilations, and is much smaller than the 'perturbative' gluino relic density assumed in [100], see Fig. 2.1. In particular, we find that a (quasi)stable gluino just above present collider bounds is still allowed provided that its lifetime is smaller than about $10^{12}\,\text{s}$ or larger than about $10^{22}\,\text{s}$.

In the rest of this section we summarize the various bounds on decaying relics plotted in

Fig. 2.4, moving from smaller to larger lifetimes.

### Big Bang Nucleosynthesis

A gluino that decays during BBN can disturb the successful BBN predictions of light element abundances, which get affected in different ways, depending on the gluino lifetime (for more details see [110, 111]):[5]

- For $0.1\,\mathrm{s} \lesssim \tau_{\tilde{g}} \lesssim 10^2\,\mathrm{s}$ the mesons and nucleons produced by gluino decays quickly reach kinetic equilibrium with the thermal bath of background photons and $e^{\pm}$ and thus do not have enough energy to destroy light nuclei. However, the extra pions, kaons and nucleons present in the thermal bath increase the $p \leftrightarrow n$ conversion rate, thus increasing the $n/p$ ratio and as a consequence the primordial $^4$He mass fraction $Y_p$.

- For $\tau_{\tilde{g}} \gtrsim 10^2\,\mathrm{s}$ the gluino decay products do not thermalize before interacting with nuclei, due to the lower temperature of the plasma at these times. The still energetic nucleons (the mesons decay before they can interact) can thus hadrodissociate $^4$He which in turn also increases the D abundance (e.g. via $p + {}^4\mathrm{He} \to \mathrm{D} + {}^3\mathrm{He}$).

- For $\tau_{\tilde{g}} \gtrsim 10^7\,\mathrm{s}$ photodissociation of $^4$He, which induces increased $^3$He and D abundances, becomes relevant. Photodissociation is not relevant at earlier times because the $\gamma$-spectrum is cut off at the threshold energy $E^{\gamma}_{\mathrm{th}} \approx m_e^2/(22\,T)$ [114] for $e^+e^-$ pair production from energetic $\gamma$'s with thermal $\gamma$'s, so that photons are not energetic enough to break up nuclei.

The resulting constraints have been computed in [110] and updated and improved in [111]. The constraints are given in the $(\tau_X, \xi_X)$ plane for different main decay modes of $X$, where $X$ is the unstable relic (the gluino in our case) and $\xi_X = E_{\mathrm{vis}} Y_X$ is its destructive power. Since we assume that half of gluinos' energy is carried away by the LSP we have $E_{\mathrm{vis}} \approx M_{\tilde{g}}/2$. The bounds for the various hadronic decay modes are similar since in all cases they induce hadronic showers, and our bounds are based on the plot for the $t\bar{t}$ mode.

The effects from photodissociation depend only on the total injected energy and not from the details of the decay channels, so that for $\tau_{\tilde{g}} \gtrsim 10^7\,\mathrm{s}$ the bounds do not explicitly depend on $M_{\tilde{g}}$ to a good approximation. At earlier times, the effects depend on the number of hadrons produced in the hadronization process, which scales with a power of $M_{\tilde{g}}$. Thus we fit the bounds, given in [111] for $M_X = 1\,\mathrm{TeV}, 10\,\mathrm{TeV}, 10^2\,\mathrm{TeV}, 10^3\,\mathrm{TeV}$, to a power-law function of $M_{\tilde{g}}$.

The left-handed panel of Fig. 2.4 shows the resulting bounds in green. In the right-hand panel we show the same bounds with the gluino lifetime computed as function of the SUSY breaking scale $m_{\mathrm{SUSY}}$.

[5] In addition, gluinos could also disturb the BBN predictions if they participate themselves in the nuclear reactions occurring during BBN [112, 113]. This would be the case if the gluino $R$-hadrons bind into nuclei which are relevant during BBN. Since we do not know whether this is the case or not, we ignore such effects here.

### Distortion of the CMB blackbody spectrum

Gluinos with lifetimes between $\sim 10^7\,\mathrm{s}$ and $\sim 10^{13}\,\mathrm{s}$ (the latter corresponds to recombination) can lead to deviations of the CMB spectrum from a blackbody form. When the Universe is $10^7\,\mathrm{s}$ old, photon number changing processes such as double Compton scattering are not efficient any more, so that photons injected into the plasma can induce a chemical potential $\mu \simeq 1.41\,\delta\epsilon/\epsilon$ [115] in the Bose-Einstein distribution of the CMB radiation, where [116]

$$\frac{\delta\epsilon}{\epsilon} \simeq 4\times 10^{-3}\sqrt{\frac{\tau_{\tilde{g}}}{10^6\,\mathrm{s}}}\frac{M_{\tilde{g}}Y_{\tilde{g}}B_\gamma}{10^{-9}\,\mathrm{GeV}}\exp\left[-\left(\frac{6.1\times 10^6\,\mathrm{s}}{\tau_{\tilde{g}}}\right)^{5/4}\right]. \tag{2.23}$$

After $\sim 4\times 10^{11}\Omega_b h^2\,\mathrm{s}$ [116], elastic Compton scatterings do not maintain thermal equilibrium anymore. An injection of photons 'Comptonizes' the spectrum, i.e. it leads to a mixture of blackbody spectra of different temperatures. This is described by the Compton $y$-parameter, given by $y = \delta\epsilon/4\epsilon$ [115].

The 95% CL limits from the FIRAS instrument on the COBE satellite are $|\mu| < 9\times 10^{-5}$ and $|y| < 1.5\times 10^{-5}$ [117, 118]. The resulting constraints on the gluino lifetime are shown in pink in Fig. 2.4. Here we assumed that $\sim 45\%$ (see e.g. [119]) of the energy that is not carried away by the LSP goes into photons. The resulting bounds are less constraining than the BBN bounds. However future bounds from PIXIE [120] will be stronger by 2 to 3 orders of magnitude.

### CMB anisotropies

The electromagnetic energy ejected into the gas at or after recombination by decaying relics modifies the fraction of free electrons and heats the intergalactic medium. This leads to modifications of the CMB angular power spectrum, measured by Planck. The maximally allowed density of a long-lived relic as a function of its lifetime has been computed assuming decay products with fixed energies in the range from 10 KeV up to 10 TeV [121] respectively 1 TeV [122]. The $e^+, e^-, \gamma$ from hadronic decays do not have fixed energies, and moreover we do not know the energy spectrum of the decay products of relics with a mass significantly larger than 10 TeV. For very large gluino masses the bounds we show are therefore only indicative. We consider the middle of the band in [122] and obtain bounds by assuming that half of gluinos energy goes into SM states and that 60% (see e.g. [119]) of the latter goes into $e^+, e^-, \gamma$. In Fig. 2.4 we show the resulting constraints for a gluino with a lifetime $\gtrsim 10^{12}\,\mathrm{s}$ in yellow.

### 21-cm line

If confirmed, the observation of an absorption feature in the low energy tail of the CMB spectrum [16] allows us to put an upper bound on the temperature of the intergalactic medium (IGM) at redshift $z \approx 17$. Decays of relic particles during the dark ages are constrained, mainly because they inject energy in the IGM heating it, erasing the absorption feature. Bounds on decaying DM particles, with masses up to 10 TeV, have been computed in [17, 18, 13]. We rescale these

bounds to a generic abundance, still assuming that half of gluino energy goes into SM states and that 60% (see e.g. [119]) of the latter goes into $e^+, e^-, \gamma$. The result is shown in Fig. 2.4. Similarly to the case of the CMB bounds in the previous section, the 21 cm bounds for very large gluino masses are only indicative and subject to significant uncertainty.

### Constraints from gamma-ray telescopes and neutrino detectors

Decaying gluinos with larger lifetimes are constrained by the measurement of cosmic ray spectra, in particular of photons or neutrinos. We adopt the results of [123] who computed limits on the lifetime of DM decaying to $b\bar{b}$, from data from the FERMI gamma ray telescope and the neutrino detector ICECUBE, up to a DM mass of $10^{12}$ GeV. We rescale the bounds of [123] taking into account that the density of our relics differs from the DM density. Ref. [123] derives bounds assuming a relic that decays to $b\bar{b}$. We assume that 50% of the gluino's energy goes to the LSP and the rest goes into hadronic decay channels, which lead to similar spectra as $b\bar{b}$. Fig. 2.4 shows the resulting constraints on a long-lived gluino from FERMI (in blue) and ICECUBE (in orange). The ICECUBE limits exceed the bounds from FERMI data for $M_{\tilde{g}} \gtrsim 10^7$ GeV.

### Searches for super-massive nuclei

Coming finally to stable gluinos, lattice simulations indicate that they would form neutral $\tilde{g}g$ hadrons [124], as well as a minor component of baryonic states such as $\tilde{g}uud$ (according to [125] the lightest gluino baryon could be $\tilde{g}uds$). They behave as strongly interacting Dark Matter. This is allowed by direct detection experiments performed in the upper atmosphere and by searches for super-massive nuclei in the Earth and in meteorites if their relic abundance is a few orders of magnitude smaller than the cosmological DM abundance, although the precise bound is subject to considerable uncertainties (a more detailed discussion can be found in section 3.3 of the next chapter). In Fig. 2.4 we indicate the tentative constraints that arise from the search for supermassive nuclei in meteorites by Rutherford backscattering of $^{238}$U, $N_{\rm SIMP}/N_n|_{\rm meteorites} \lesssim 2 \times 10^{-12}$ [126], assuming a heavy nuclei capture cross section of $\sigma_{\rm capture} = 10^{-2}/\Lambda^2_{\rm QCD}$. Presumably, there is still an open window, from TeV masses above the LHC [101] up to about 10 TeV.

### Higgs mass

In the right panel of Fig. 2.4 we considered Split SuperSymmetry, such that the gluino lifetime is computed as function of the sfermion mass $m_{\rm SUSY}$, see eq. (2.1). This scale is further constrained within the split MSSM by the observed Higgs mass, which is reproduced within the green region (for different values of $\tan\beta$) in the $(M_3, m_{\rm SUSY})$ plane. We computed $M_h$ as in [127], assuming that gauginos and Higgsinos are degenerate at the gluino mass $M_3$ and that all scalars are degenerate at $m_{\rm SUSY}$. Allowing the masses to vary and taking into account uncertainties on $M_t$ and $\alpha_3$ slightly expands the region. Within the Higgs-allowed region the gluino decays promptly on cosmological time-scales, evading all cosmological bounds.

No prediction for the Higgs mass arises in extensions of the MSSM. However, roughly the same region is obtained by imposing the meta-stability bound on Higgs vacuum decay, which implies that the Higgs quartic $\lambda_H$ cannot be too negative, $\lambda_H \gtrsim -0.05$. A substantially larger $m_{\rm SUSY}$, such that the gluino is long-lived, is obtained assuming that Higgsinos are heavy (possibly with masses of order $m_{\rm SUSY}$: in such a case the RGE for the Higgs quartic are those of the SM (with slightly different values of $g_{2,3}$ due to the light gluino and wino), and the Higgs quartic can remain positive up to $m_{\rm SUSY} \sim M_{\rm Pl}$ within the uncertainty range for the top quark mass.

### 2.2.2 Collider signals

Next, we discuss some aspects of the phenomenology of long-lived gluinos at hadron colliders, in particular the LHC. Long-lived gluinos can be pair produced and after hadronization form long-lived hybrid states with SM quarks and gluons, known as '$R$-hadrons'. We conservatively assume that the signal at the LHC is just energy deposit in the calorimeter, rather than charged particles in the tracker. It is difficult to trigger on these event and so an initial state jet is required. The LHC places the limit $M_{\tilde{g}} > 1.55$ TeV on a Majorana gluino [128].

The other possibility is the production of a $\tilde{g}\tilde{g}$ bound state. Assuming that states with $\ell = 0$ dominate the rates, they are color $8_A$ with spin $S = 1$ and color singlets or $8_S$ with $S = 0$ (see eq. 2.9). They are produced through gluon and quark fusion respectively; and, in the narrow width approximation (see eq. (5.41) for more details), their production cross section is given by:

$$\sigma_0 = \sum_{n=1}^{\infty} \frac{C_{gg}}{2M_{\tilde{g}}\, s\, n^3} \left(\Gamma^1_{gg} + 8\Gamma^{8_S}_{gg}\right) = \frac{\zeta(3)\, C_{gg}}{2M_{\tilde{g}}\, s} \left(\Gamma^1_{gg} + 8\Gamma^{8_S}_{gg}\right) , \tag{2.24}$$

$$\sigma_1 = 2\sum_{n=1}^{\infty} \frac{C_{uu}\Gamma^{8_A}_{uu} + C_{dd}\Gamma^{8_A}_{dd}}{M_{\tilde{g}}\, s\, n^3} = \frac{2\,\zeta(3)}{M_{\tilde{g}}\, s} \left(C_{uu}\Gamma^{8_A}_{uu} + C_{dd}\Gamma^{8_A}_{dd}\right) , \tag{2.25}$$

where $C_{ij}$ is the luminosity of partons $ij$, and $\Gamma_{ij}$ are the decay rates for $n = 1$ bound states into partons $ij$. The decay rates are given by

$$\frac{\Gamma^1_{gg}}{M_{\tilde{g}}} = \frac{9\alpha_3^5\lambda_1^3}{2\,F} , \qquad \frac{\Gamma^{8_S}_{gg}}{M_{\tilde{g}}} = \frac{9\alpha_3^5\lambda_8^3}{8\,F}, \qquad \frac{\Gamma^{8_A}_{qq}}{M_{\tilde{g}}} = \frac{3\alpha_3^5\lambda_8^3}{2\,F} , \tag{2.26}$$

with $F = 2$ for the Majorana gluino and $F = 1$ for a Dirac particle, and with the channel strength $\lambda_1 = 3$ and $\lambda_8 = 3/2$.

Since the resonances annihilate to two gluons or two quarks, we assume a 100% branching ratio to two jets and apply the LHC di-jet bounds [129] to the sum of the cross sections. In Fig. 2.5 we compare the bounds on the resonances to the slightly stronger $R$-hadron bound.

Concerning future colliders, the expected reach of a 100 TeV hadron collider with 1000 fb$^{-1}$ is 7 (9)TeV for a Majorana (Dirac) gluino, having used [130] to perform an approximate rescaling. The $R$-hadron search would then reach 10 TeV and 14.5 TeV respectively. Thus a 100 TeV collider would reach the benchmark mass of a thermally produced Dirac gluino, which - as will

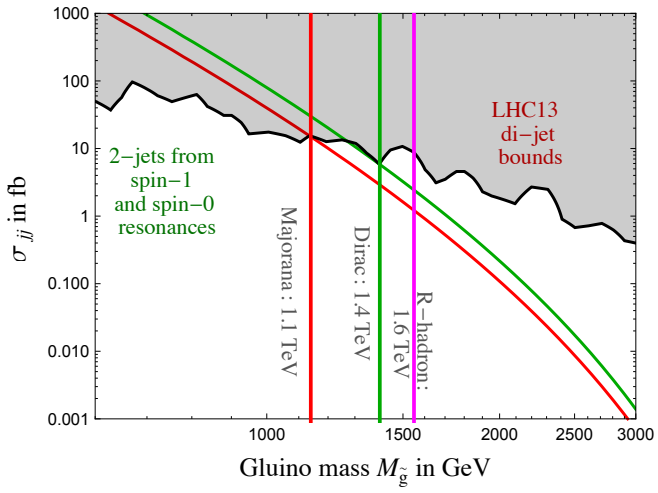


Figure 2.5: *The black curve is the di-jet upper bound on the cross section for production of spin-1 and spin-0 bound states from LHC data at* 13 TeV*; the red (green) curve is the theoretical prediction assuming a Majorana (Dirac) gluino. From this we derive the experimental bounds (vertical lines). The thin vertical line shows the bound from R-hadron searches.*

be discussed in the next chapter is a viable dark matter candidate.

### 2.2.3 Implications for Dark Matter co-annihilations

The thermal relic abundance of a particle is affected by co-annihilations with particles of similar mass. One example is co-annihilations of neutralino DM with heavier colored particles, for example gluinos. As discussed in sections 1.6.4, co-annihilations can be enhanced by Sommerfeld corrections and bound-state formation. We point out here that a much bigger effect is produced by the non-perturbative QCD effects discussed in the previous sections, if the mass splitting $\Delta M$ between the co-annihilating species is comparable or smaller than $\Lambda_{\rm QCD}$. [6] This is shown in Fig. 2.6a in the neutralino/gluino co-annihilation case, assuming that squarks mediate fast neutralino/gluino conversions. We see that the neutralino mass which reproduces the observed DM density gets much higher at $\Delta M \lesssim$ GeV. In the limit $\Delta M \ll$ GeV the relic abundance is dominantly set by the new QCD annihilations. As a result, the neutralino mass can reach up to a PeV, heavier than the maximal relic DM mass allowed if DM annihilations are dominated by partial waves with low $\ell$ [104].

### 2.2.4 Quasi-stable squark

In the previous sections we considered a Majorana gluino. A real scalar in the octet of $\mathrm{SU}(3)_c$ would behave similarly to the Majorana gluino. On the other hand, a (quasi)stable particle in

[6] Such a near-degeneracy is unnatural.

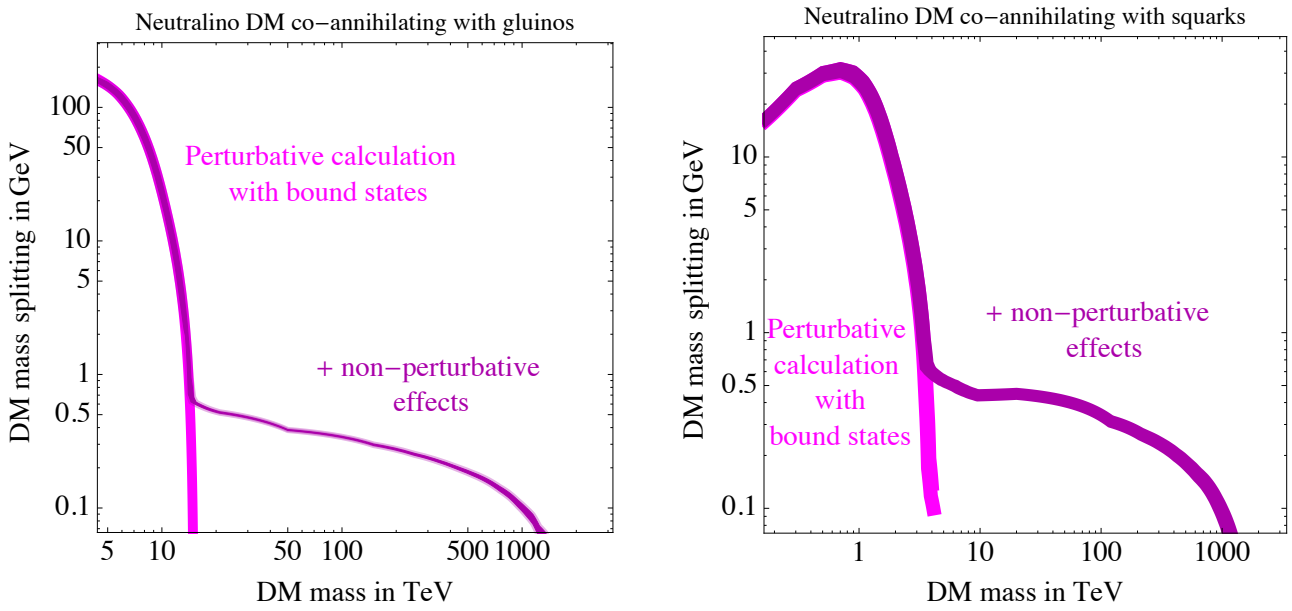


Figure 2.6: *The pink (purple) line in the plots indicates the region of the parameter space in which the neutralino relic density matches the one of the DM if non-perturbative effects are ignored (included). Because of co-annihilations with gluinos (left panel) or stops (right panel), non-perturbative QCD annihilations that take place at $T \lesssim \Lambda_{QCD}$ significantly increase the DM neutralino mass reproducing the observed DM abundance, if the mass difference between the neutralino and the colored partner is smaller than a few* GeV*. In the case of stops (right panel), the big effect is only estimated and only present if stop baryons decay to SM particles before decaying to neutralinos; otherwise confinement only gives a $\mathcal{O}(1)$ effect.*

the fundamental 3 of color $\mathrm{SU}(3)_c$ can behave in a qualitatively different way. Since the 3 is a complex representation, the particle must be a complex scalar or a Dirac fermion, which can carry a conserved charge.

For definiteness, we consider the possibility of a (quasi)stable squark, and more specifically a stop $\tilde{t}$, as RGE effects tend to make $\tilde{t}$ lighter than other squarks. A stable stop arises if $\tilde{t}$ is the lightest SUSY particle (LSP) and $R$-parity is conserved. A quasi-stable stop arises if $R$-parity is almost conserved, or if the stop decays slowly into the LSP: this can happen e.g. when the LSP is a gravitino. Collider bounds on stops [132] tend to ignore the possibility that the lighter stop $\tilde{t}$ is the (quasi)stable LSP, because it is usually considered to be already excluded by cosmology.

In cosmology, perturbative QCD $\tilde{t}\tilde{t}^* \to gg$ annihilations dominate over $\tilde{t}\tilde{t} \to tt$ annihilations and leave a roughly equal amount of relic $\tilde{t}$ and $\tilde{t}^*$. Perturbative QCD annihilations are enhanced by Sommerfeld and bound-state effects discussed in the previous chapter. The relic $\tilde{t}$ abundance after perturbative annihilations is plotted in Fig. 2.7 and approximated by

$$\frac{n_{\tilde{t}}}{s} \approx \frac{M_{\tilde{t}}}{M_{\rm Pl}\alpha_3^2}. \tag{2.27}$$

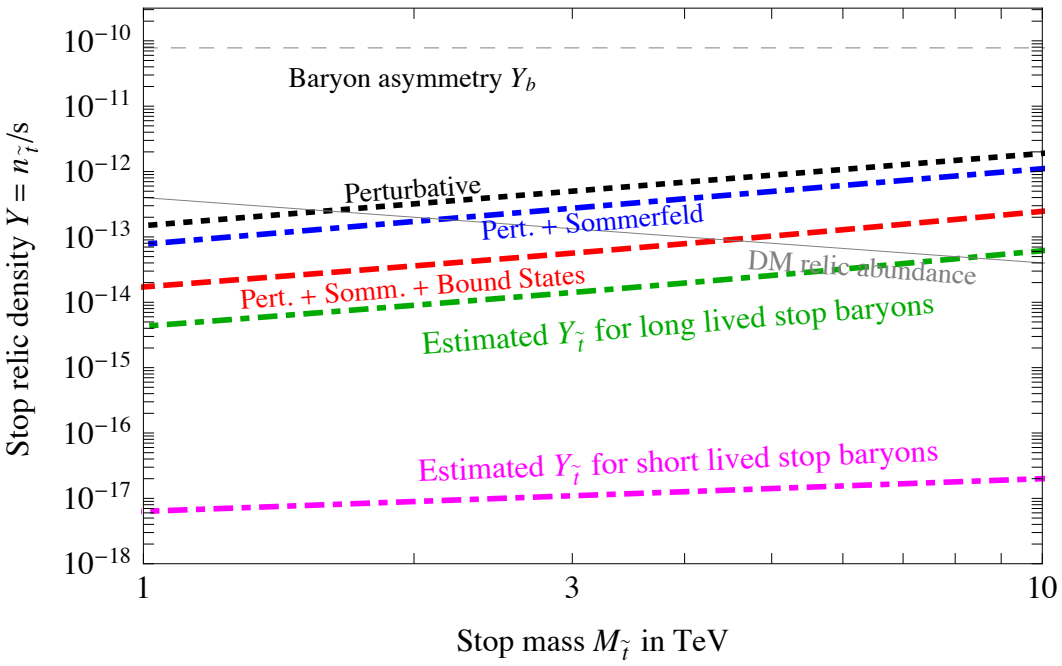


Figure 2.7: *Stop relic abundances. The $\tilde{t}\tilde{t}\tilde{t}$ baryons could be relatively long lived and have an abundance not suppressed by QCD confinement effects*

For $M_{\tilde{t}} <$ PeV this is smaller than the baryon asymmetry $n_b/s \sim 10^{-10}$, that we neglect given that its effect is model dependent. Indeed, we do not know how the baryon asymmetry is generated: it might be generated at the weak scale such that it would not affect heavier stops. Even if a baryon asymmetry is present at stop decoupling, $\tilde{t}\bar{t} \leftrightarrow \tilde{t}^* t$ scatterings could easily concentrate the baryon asymmetry to lighter baryons fast enough that the asymmetry is irrelevant for stops. If instead the baryon asymmetry enhances the relic stop abundance, bounds would become stronger.

After the QCD phase transition, stops form hadrons. In view of the large QCD cross sections, the stop hadrons with dominant abundance are deeply-bounded states which contain stops only. They are $\tilde{t}\tilde{t}^*$ and the charged baryons $\tilde{t}\tilde{t}\tilde{t}$. Both fall to the ground state and decay through annihilations of the constituents. In particular, a bound state containing two or more stops decays, in its ground state, with a life-time $\Gamma_{\tilde{t}\tilde{t}} \sim \alpha_3^3 M_t^3 \sigma_{\tilde{t}\tilde{t}} v_{\rm rel}$ where the cross section for $\tilde{t}\tilde{t} \to tt$ can be roughly estimated as $\sigma_{\tilde{t}\tilde{t}} v_{\rm rel} \sim \sum_{i=\{1,2,3\}} \alpha_i^2/M_i^2$, ignoring possible extra velocity suppressions. Then, $\Gamma_{\tilde{t}\tilde{t}}$ is cosmologically fast unless gauginos (with masses $M_i$) are heavier than $\sim 10^{10}\,$GeV.

We expect a roughly equal number of $\tilde{t}\tilde{t}^*$ annihilations for each produced $\tilde{t}\tilde{t}\tilde{t}$ given that QCD group algebra implies that both $\tilde{t}\tilde{t}^*$ and $\tilde{t}\tilde{t}$ feel an attractive Coulombian QCD force, such that they can form deep, unbreakable, Coulombian bound states. Assuming that a $\tilde{t}$ binds with probability $\wp$ to a $\tilde{t}$ and with probability $1-\wp$ to a $\tilde{t}^*$ and thereby that a deep $\tilde{t}\tilde{t}$ binds with probability $1-\wp$ to $\tilde{t}$ and with probability $\wp$ to a $\tilde{t}^*$, the average number of $\tilde{t}\tilde{t}^*$ per produced

baryon is

$$\frac{\langle N_{\tilde{t}\tilde{t}^*}\rangle}{\langle N_{\tilde{t}\tilde{t}\tilde{t}} + N_{\tilde{t}^*\tilde{t}^*\tilde{t}^*}\rangle} = \frac{1/\wp + 1/(1-\wp) - 1}{r + 1/r - 1}. \tag{2.28}$$

This equals 3 assuming no baryon asymmetry $r \equiv N_{\tilde{t}}/N_{\tilde{t}}^*$ and $\wp = 1/2$, namely neglecting that $\tilde{t}\tilde{t}^*$ is more attractive than $\tilde{t}\tilde{t}$. Extra hadrons and mesons that contain quarks have a much smaller abundance, that is not relevant here. If the charge 2 states $\tilde{t}\tilde{t}\tilde{t}$ decay fast on cosmological scales, final abundances and bounds are similar to the gluino case. If (quasi)stable, they are instead subject to strong cosmological constraints. In particular during BBN $\tilde{t}^*\tilde{t}^*\tilde{t}^*$ can bind to $^4$He reducing its charge and thereby the Coulomb suppression of nuclear reactions, opening up a new channel for $^6$Li production,

$$(\tilde{t}^*\tilde{t}^*\tilde{t}^*\ {}^4\mathrm{He}) + D \to {}^6\mathrm{Li} + \tilde{t}^*\tilde{t}^*\tilde{t}^*\,, \tag{2.29}$$

which can strongly alter Lithium abundances (see [135] for a brief review). Charge $-1$ states with lifetime $\gtrsim 10^5$ are subject to the BBN bound $Y \lesssim 2.5 \times 10^{-17}$ [112]. A study of analogous constraints on relics with charge $-2$ is beyond the scope of this work.

Next, we study the scenario where a quasi-stable stop co-annihilates with a slightly lighter DM neutralino. Post-confinement effects are relevant if $\Delta M \lesssim$ GeV. Roughly half of the stops form $\tilde{t}\tilde{t}^*$ mesons, and the others form $\tilde{t}\tilde{t}\tilde{t}$ baryons. The impact on the DM abundance is very different, depending on which process dominates $\tilde{t}\tilde{t}\tilde{t}$ decays. If it is dominated by stop annihilations into SM particles, post-confinement effects strongly suppress the DM abundance, similarly to the gluino/neutralino co-annihilation scenario. A much smaller order one effect is obtained if instead stops decay to DM neutralinos and SM particles with rate $\Gamma_{\tilde{t}} \gtrsim \Gamma_{\tilde{t}\tilde{t}}$. The region where the DM abundance is reproduced is estimated in Fig. 2.6b in the two extreme possibilities, having assumed $\sigma_{\mathrm{QCD}} = 1/\Lambda_{\mathrm{DC}}^2$.

## 2.3 Summary

We have reconsidered the relic abundance of neutral colored relics, finding that hadron collisions at temperatures below the QCD scale reduce it by a few orders of magnitude. In particular we considered a quasi-stable gluino: Fig. 2.1 shows its relic abundance, and Fig. 2.4 the cosmological constraints, taking into account the new effect and new data.

Co-annihilations between gluinos and neutralino DM are similarly strongly affected by confinement, provided that their mass difference is smaller than a few GeV, as shown in Fig. 2.6a.

In section 2.2.4 we considered charged colored relics, in particular the case of a quasi-stable stop. In this case, confinement gives a big contribution to co-annihilations with neutralinos only if $\tilde{t}\tilde{t}\tilde{t}$ baryons decay into SM particles via $\tilde{t}\tilde{t} \to tt$ before stop decays to neutralinos.

# Part II

# Dark Matter from confining sectors

So far our focus has been on scenarios where the DM is an elementary particle. In this context we have studied how formation of *unstable* bound states of DM particles can affect the cosmological history, and give peculiar indirect detection signals. In this second part of the work we move to the study of models where the DM is in the form of *stable* bound states. We start (Chapter 3) with the case where the force keeping these bound states glued together is already present in the SM, then we move to the case (Chapters 4 and 5) where a new confining dark force provides the binding interaction.

# Chapter 3

# Colored DM

The first model we propose challenges one of the common feature of DM models: the DM is an uncolored particle. Indeed we suggest that the DM could be a composite state of new heavy colored particle, $\mathcal{Q}$, for simplicity electrically neutral. $\mathcal{Q}$ could be a heavy quark in the $3 \oplus \bar{3}$ representation of $\mathrm{SU}(3)_c$, or a 'Dirac gluino' in the $8 \oplus 8$ representation, such that $\mathcal{Q}$ annihilates with $\bar{\mathcal{Q}}$, but not with itself. We dub this neutral quark as *quorn*. Perturbative annihilations between $\mathcal{Q}$ and $\bar{\mathcal{Q}}$ (together with effects induced by unstable $\mathcal{Q}\bar{\mathcal{Q}}$ bound states) leave a thermal relic density of order $\Omega_{\mathcal{Q}} h^2 \sim 0.1\, M_{\mathcal{Q}}/7\,\mathrm{TeV}$. After the quantum chromo-dynamics (QCD) phase transition at temperature $T \lesssim \Lambda_{\mathrm{QCD}} \approx 0.27\,\mathrm{GeV}$ colored particles bind into hadrons. Subsequent annihilations among hadrons reduce their relic abundance, increasing the value of $M_{\mathcal{Q}}$ needed to reproduce the observed cosmological abundance, $\Omega_{\mathrm{DM}} h^2 \sim 0.1$ for $M_{\mathcal{Q}} \approx 12\,\mathrm{TeV}$.

The *quorn-onlyum* hadrons made of $\mathcal{Q}$ only ($\mathcal{Q}\mathcal{Q}$ if $\mathcal{Q} \sim 8$, and $\mathcal{Q}\mathcal{Q}\mathcal{Q}$ if $\mathcal{Q} \sim 3$) are acceptable DM candidates, as they have a small Bohr-like radius $a \sim 1/\alpha_3 M_{\mathcal{Q}}$. This scenario is believed to be excluded because it predicts other hybrid hadrons where $\mathcal{Q}$ binds with SM quarks $q$ or gluons $g$. Such hybrids, $\mathcal{Q}qq$, $\mathcal{Q}\mathcal{Q}q$, $\mathcal{Q}\bar{q}$ (if $\mathcal{Q} \sim 3$) and $\mathcal{Q}g$, $\mathcal{Q}q\bar{q}'$ (if $\mathcal{Q} \sim 8$), have size of order $1/\Lambda_{\mathrm{QCD}}$ and thereby cross sections of order $\sigma_{\mathrm{QCD}} \sim 1/\Lambda^2_{\mathrm{QCD}}$ for interactions with baryonic matter. Their cosmological abundance must be orders of magnitude smaller than the DM abundance $\Omega_{\mathrm{DM}} \approx 0.1$, while naively one might expect that cosmological evolution results into $\Omega_{\mathrm{hybrid}} \gg \Omega_{\mathrm{DM}}$, given that quarks and gluons are much more abundant than quorns $\mathcal{Q}$.

We will show that cosmological evolution gives $\Omega_{\mathrm{hybrid}} \sim 10^{-4}\Omega_{\mathrm{DM}}$, such that this scenario is allowed. This is not surprising, taking into account that quorn-onlyum has a binding energy $E_B \sim \alpha_3^2 M_{\mathcal{Q}} \sim 200\,\mathrm{GeV}$ much larger than hybrids, $E_B \sim \Lambda_{\mathrm{QCD}}$. Quorn-onlyum thereby is the ground state, reached by the universe if it has enough time to thermalise. This depends on two main factors:

i) quorns are much rarer than quarks and gluons: $n_{\mathcal{Q}} \sim 10^{-14} n_{q,g}$ when the DM abundance is reproduced;

ii) QCD interactions are much faster than the Hubble rate $H \sim T^2/M_{\mathrm{Pl}}$: a loose bound state with a $\sigma_{\mathrm{QCD}}$ cross section recombines $N \sim n_{q,g}\sigma_{\mathrm{QCD}}/H \sim M_{\mathrm{Pl}}/\Lambda_{\mathrm{QCD}} \sim 10^{19}$ times in a

Hubble time at temperature $T \sim \Lambda_{\rm QCD}$.

Since $10^{19}$ is much bigger than $10^{14}$, *chromodark-synthesis* cosmologically results into quorn-onlyum plus traces of hybrids. This is analogous to Big Bang Nucleo-synthesis, that leads to the formation of deeply bounded Helium plus traces of deuterium and tritium.

The chapter is organised as follows. In section 3.1 we define the model, and summarize the main features of its QCD interactions. In section 3.2 we discuss how cosmology leads to dominant formation of $\mathcal{Q}$-onlyum hadrons. In section 3.3 we show that the abundance of hybrids is small enough to be compatible with bounds. In section 3.4 we show that $\mathcal{Q}$-onlyum DM is compatible with bounds. A summary of our results is given in the conclusions in section 3.5.

## 3.1 The model

We consider the following extension of the SM:[1]

$$\mathscr{L} = \mathscr{L}_{\rm SM} + \bar{\mathcal{Q}}(i\not{D} - M_{\mathcal{Q}})\mathcal{Q}. \tag{3.1}$$

The only new ingredient is $\mathcal{Q}$: a Dirac fermion with quantum numbers $(8,1)_0$ under $\mathrm{SU}(3)_c \otimes \mathrm{SU}(2)_L \otimes \mathrm{U}(1)_Y$ i.e. a neutral color octet. The only free parameter is its mass $M_{\mathcal{Q}}$. Like in Minimal Dark Matter models [139] $\mathcal{Q}$ is automatically stable, as no renormalizable interaction with SM particles allows its decay, which can first arise due to dimension-6 effective operators such as $\mathcal{Q}DDU$ and $\mathcal{Q}LDQ$ where $Q$ ($L$) is the SM quark (lepton) doublet, and $U$ ($D$) is the right-handed SM up-type (down-type) quark. The decay rate is cosmologically negligible if such operators are suppressed by the Planck scale.

After confinement $\mathcal{Q}$ forms bound states. For $M_{\mathcal{Q}} \gg \Lambda_{\rm DC}/\alpha_3$ states made by $\mathcal{Q}$-only are Coulombian. The $\mathcal{Q}\bar{\mathcal{Q}}$ bound states are unstable: $\mathcal{Q}$ and $\bar{\mathcal{Q}}$ annihilate into gluons and quarks. No such annihilation arises in $\mathcal{Q}\mathcal{Q}$ bound states as we assumed that $\mathcal{Q}$ carries an unbroken U(1) dark baryon number that enforces the Dirac structure such that $\mathcal{Q}\mathcal{Q}$ is stable. The DM candidate is the quorn-onlyum $\mathcal{Q}\mathcal{Q}$ ground state, neutral, color-less and with spin-0.[2] As we will see, if $\mathcal{Q}\mathcal{Q}$ is a thermal relic, the observed cosmological DM abundance is reproduced for $M_{\mathcal{Q}} \sim 12.5\,\mathrm{TeV}$. This mass is large enough that $\mathcal{Q}$ does not form QCD condensates. The $\mathcal{Q}\mathcal{Q}$ potential in the color-

[1] Within the SM, QCD could give rise to Dark Matter as 'strangelets' made of many *uds* quarks [137] or as 'sexaquark' *uuddss* [138]. However there is no experimental nor lattice evidence that such objects exist. We thereby extend the SM.

[2] Other assignments of quantum numbers of $\mathcal{Q}$ are possible. A scalar would give similar physics. A fermionic $\mathcal{Q} \sim (3 \oplus \bar{3}, 1)_0$ under $\mathrm{SU}(3)_c \otimes \mathrm{SU}(2)_L \otimes \mathrm{U}(1)_Y$ would give the $\mathcal{Q}\mathcal{Q}\mathcal{Q}$ baryon as a viable DM candidate. As the gauge quantum numbers of a neutral color triplet are exotic, the $\mathcal{Q}\mathcal{Q}q$, $\mathcal{Q}qq$ and $\mathcal{Q}\bar{q}$ hadrons containing light quarks would have fractional charges. Fractionally charged hadrons are subject to stronger experimental bounds [136]. A $\mathcal{Q} \sim (3,2,1/6) = (\mathcal{Q}_u, \mathcal{Q}_d)$, with the same quantum numbers of SM left-handed quarks $Q$, would give as lightest state the neutral DM candidate $\mathcal{Q}_u\mathcal{Q}_d\mathcal{Q}_d$. This is excluded by direct detection mediated at tree level by a $Z$, being a weak doublet with hypercharge $Y \neq 0$. Allowing for an additional confining group, a $\mathcal{Q} \sim 8$ can be build out of $\mathcal{Q} \sim 3$ obtaining double composite Dark Matter.

singlet channel is $V(r) = -3\alpha_3/r$, so the binding energy is $E_B = 9\alpha_3^2 M_{\mathcal{Q}}/4n^2 \approx 200\,\text{GeV}/n^2$, which is bigger than $\Lambda_{\text{QCD}}$ up to $n \sim 20$. We adopt the value $\Lambda_{\text{QCD}} \approx 0.27\,\text{GeV}$.

The quantum numbers of the hybrid hadrons, $\mathcal{Q}g$ and $\mathcal{Q}q\bar{q}'$, are not exotic. We expect that the isospin singlet $\mathcal{Q}g$ is lighter than $\mathcal{Q}q\bar{q}'$ (isospin $3 \oplus 1$) by an amount of order $\Lambda_{\text{QCD}}$, which accounts for the relative motion of $q$ and $\bar{q}'$, where $q, q' = \{u, d\}$. A lattice computation is needed to safely establish who is lighter. Assuming that $\mathcal{Q}q\bar{q}'$ is heavier, then its neutral component $\mathcal{Q}q\bar{q}$ decays to $\mathcal{Q}g$ with a lifetime of order $1/\Lambda_{\text{QCD}}$. The slightly heavier components $\mathcal{Q}u\bar{d}$ and $\mathcal{Q}d\bar{u}$ with electric charges $\pm 1$ have a lifetime of order $v^4/\Lambda_{\text{QCD}}^5$.

The above DM model has possible extra motivations. The fermion $\mathcal{Q}$ appears as a 'Dirac gluino' in some $N = 2$ supersymmetric models [140], where sfermions can mediate its decay, if $R$-parity is broken. Alternatively, the heavy quarks $\mathcal{Q}$ could be identified with those introduced in KSVZ axion models [141]. In such a case our U(1) symmetry gets related to the Peccei-Quinn symmetry. Corrections to the Higgs mass squared proportional to $M_{\mathcal{Q}}^2$ arise at 3 loops and are comparable to its measured value for $M_{\mathcal{Q}} \approx 12\,\text{TeV}$ [142].

### 3.1.1 Confinement

QCD confinement happens in cosmology through a smooth crossover. In Cornell parametrisation [143] the QCD potential between two quarks in the $F$undamental representation at temperature $T$ in the singlet configuration is approximated as $V_{q\bar{q}}(r) \approx -\alpha_{F\text{eff}}/r + \sigma_F r$. In the perturbative limit one has $\alpha_{F\text{eff}} = C_F\alpha_3$ where $C_F = (N_c^2 - 1)/2N_c = 4/3$ is the quadratic Casimir and $\alpha_3$ is renormalized around $1/r$. At $r \sim 1/\Lambda_{\text{QCD}}$ lattice simulations find $\alpha_{F\text{eff}} = 0.4$ and $\sigma_F \approx (0.45\,\text{GeV})^2$ [107]. The potential between two adjoints is similarly approximated by a Coulombian term plus a flux tube:

$$V_{\mathcal{Q}\mathcal{Q}}(r) \approx -\frac{\alpha_{\text{eff}}}{r} + \sigma r. \tag{3.2}$$

Perturbation theory implies $V_{\mathcal{Q}\mathcal{Q}}/C_A \approx V_{q\bar{q}}/C_F$ [144] where $C_A = N_c = 3$. Thereby $\alpha_{\text{eff}} \approx 3\alpha_3$ and $\sigma(0) \approx 9\sigma_F(0)/4 \approx (0.67\,\text{GeV})^2$, as verified on the lattice [145]. At finite temperature the Coulombian force gets screened by the Debye mass and the string appears only below the critical temperature $T_c \approx 170\,\text{MeV}$ as $\sigma(T) \approx \sigma(0)\sqrt{1 - T^2/T_c^2}$ [107].

### 3.1.2 Eigenvalues in a linear plus Coulombian potential

We will need the binding energies of a non-relativistic $\mathcal{Q}\mathcal{Q}$ hadron. We thereby consider the Hamiltonian $H = \vec{p}^{\,2}/2\mu + V(r)$ in 3 dimensions that describes its motion around the center of mass, with reduced mass $2\mu \simeq M_{\mathcal{Q}}$. The potential is given by eq. (3.2). As usual, wave-functions are decomposed in partial waves as $\psi(r, \theta, \phi) = \sum_{\tilde{n},\ell,m} R_{\tilde{n}\ell}(r) Y_{\ell m}(\theta, \phi)$ where $\tilde{n}$ is the principal quantum number. For each $\ell = 0, 1, 2, \ldots$ we define as $\tilde{n} = 1$ the state with lowest energy, so that $\tilde{n} = 1, 2, 3, \ldots$. The radial wave function $R_{\tilde{n}\ell}(r)$ has $\tilde{n} - 1$ nodes. Unlike in the hydrogen atom there are no free states: angular momentum $\ell$ is not restricted to $\ell < \tilde{n}$. In order to match

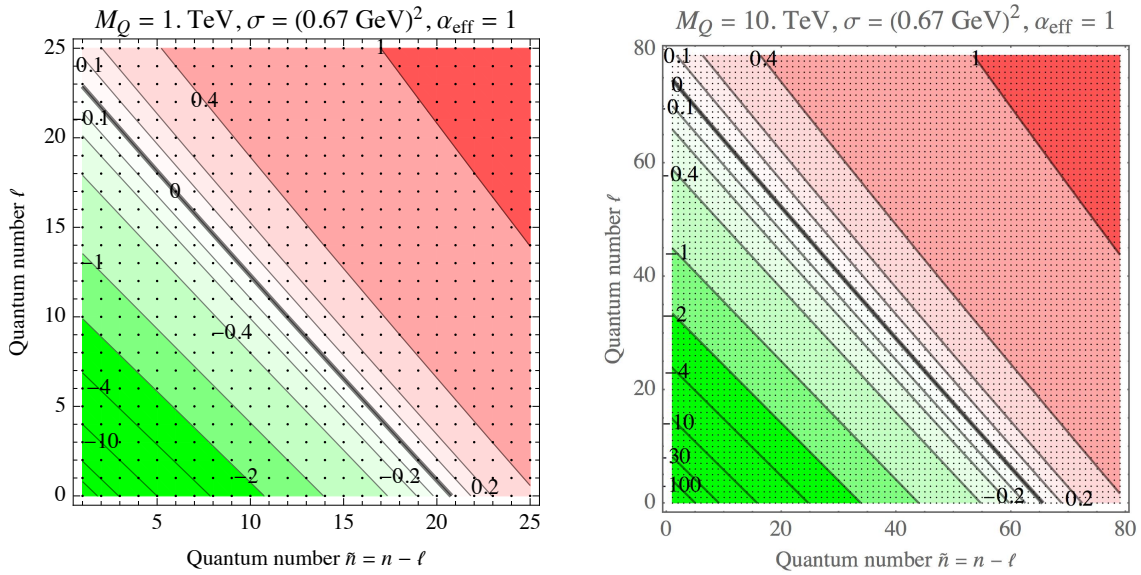


Figure 3.1: *Binding energies $E_{\tilde{n}\ell}$ in* GeV *for a $\mathcal{Q}\mathcal{Q}$ in the singlet configuration. States with $E_{\tilde{n}\ell} < -0.2\,\text{GeV}$ (in green) are well approximated by the Coulombian limit. Increasing $M_\mathcal{Q}$ leads to a larger number of Coulombian states and to a deeper ground state. $\mathcal{Q}\mathcal{Q}$ states are cosmologically mostly produced in the region with larger $\ell$ of the band $E \sim \Lambda_{QCD}$.*

with the Coloumbian limit in its usual notation we define $n \equiv \tilde{n} + \ell$ such that, at given $\ell$, only $n \geqslant \ell + 1$ is allowed.

The reduced wave function $u_{\tilde{n}\ell}(r) = rR_{\tilde{n}\ell}(r)$ obeys the Schroedinger equation in one dimension in the effective potential $V_{\rm eff} = V + \ell(\ell+1)\hbar^2/2\mu r^2$. Dimensional analysis implies that energy eigenvalues have the form

$$E_{\tilde{n}\ell} = \alpha_{\rm eff}^2 \mu \times f(\varepsilon, \tilde{n}, \ell), \qquad \text{where} \qquad \varepsilon \equiv \frac{\sigma}{4\alpha_{\rm eff}^3 \mu^2} = 10^{-8} \frac{\sigma}{\text{GeV}^2} \left(\frac{10\,\text{TeV}}{M_\mathcal{Q}}\right)^2 \left(\frac{1}{\alpha_{\rm eff}}\right)^3. \quad (3.3)$$

From [108][3] we extract the approximation valid at leading order in $\varepsilon \ll 1$

$$E_{\tilde{n}\ell} = \frac{\alpha_{\rm eff}^2 \mu}{2}\left[ -\frac{1}{n^2} + \varepsilon n(14.3n - 6.3\ell - 3.34) + \cdots \right]. \quad (3.4)$$

The first term is Coulombian. The second term accounts for the linear potential, and becomes relevant at large $n, \ell$. In particular, assuming $\ell \simeq n \gg 1$, Coulombian states with negative binding energy exist up to $\ell, n \lesssim 0.5\varepsilon^{-1/4}$. The ground state has binding energy $E_B = -E_{10} \sim 200\,\text{GeV}$ for $M_\mathcal{Q} \sim 10\,\text{TeV}$.

In the opposite limit where the linear force dominates and the Coulomb-like force can be

[3] We thank C. Gross for having pointed out a typo in [108].

neglected, all energy levels are positive and states with higher $\ell$ have higher energy [108]

$$E_{\tilde{n}\ell} \approx \frac{3\sigma^{2/3}}{(2\mu)^{1/3}} \left(0.897\tilde{n} + \frac{\ell}{2} - 0.209\right)^{2/3} \tag{3.5}$$

such that thermalisation lowers $\ell$. The dependence on $\sigma, \mu$ and the ground state energy can also be computed variationally, assuming a trial wave-function $\psi(r) = e^{-r/r_c}/r_c^{3/2}$, such that the typical size is $r_c \sim (\mu\sigma)^{-1/3}$. Fig. 3.1 shows the binding energies for relevant values of the parameters.

We next discuss bound states $B_{\mathcal{Q}}$ made of one heavy $\mathcal{Q}$ plus a gluon. It cannot be described by non-relativistic quantum mechanics. Nevertheless, its binding energy can roughly be obtained by eq. (3.5) taking a small reduced mass $\mu \sim \sqrt{\sigma}$. One then expects that such states are in their ground states at $T \lesssim \Lambda_{\rm QCD}$, and that their mass is $M_{B_{\mathcal{Q}}} = M_{\mathcal{Q}} + \mathcal{O}(\Lambda_{\rm QCD})$.

### 3.1.3 Decay rates of excited bound states

Energy losses due to quantum decay of a $\mathcal{Q}\mathcal{Q}$ state with $n, \ell \gg 1$ into deeper states can be approximated with classical Larmor radiation. This holds in dipole approximation, where a state can only decay to $\ell' = \ell \pm 1$.

To see this, we consider a hydrogen-like system with $V = -\alpha/r$ and reduced mass $\mu$. Assuming a circular orbit as in [101] one gets the emitted power

$$W^{\rm circ}_{\rm Larmor} = \frac{2\alpha a^2}{3} = \frac{2\mu^2\alpha^7}{3n^8} \tag{3.6}$$

having inserted the acceleration $a = \alpha/\mu r^2$ and converted the orbital radius into $n^2$ times the Bohr radius as $r = r_n = n^2/\alpha\mu$. Similarly, the binding energy is $E = -\alpha/2r = -\alpha^2\mu/2n^2$.

At the quantum level, a circular orbit corresponds to a state with maximal $\ell = \ell_{\rm circ} = n$. In dipole approximation such a state decays only to $n' = \ell' = n - 1$, emitting a soft photon with energy $\Delta E_{\rm Larmor} = |E_n - E_{n-1}| \simeq \alpha^2\mu/n^3$, such that the decay rate is

$$\Gamma^{\rm circ}_{\rm Larmor} = \frac{W^{\rm circ}_{\rm Larmor}}{|\Delta E_{\rm Larmor}|} = \frac{2}{3}\left(\frac{\alpha}{n}\right)^5 \mu. \tag{3.7}$$

This matches the quantum decay rate.

Let us now consider a generic state. Classically, a generic elliptic orbit is parameterized by its energy $E$ and by its angular momentum $\ell \leqslant \ell_{\rm circ}$, where $\ell_{\rm circ} = \sqrt{\alpha^2\mu/2E}$ is the value corresponding to a circular orbit. The Larmor radiation power, averaged over the orbit, is

$$\langle W_{\rm Larmor}\rangle = W^{\rm circ}_{\rm Larmor} \frac{3 - (\ell/\ell_{\rm circ})^2}{2(\ell/\ell_{\rm circ})^5}. \tag{3.8}$$

Due to the larger acceleration at the point of minimal distance, the radiated energy for $\ell \ll \ell_{\rm circ}$

is much larger than in the circular case: this is why $e\bar{e}$ colliders are built circular.

This classical result for non-circular orbits agrees with the quantum results for $n, \ell \gg 1$, summarized in Appendix C for the hydrogen atom, which can be approximated as

$$\Gamma_{n\ell} \simeq \frac{2\alpha^5\mu}{3n^3\ell^2}, \qquad W_{n\ell} \simeq \frac{2\alpha^7\mu^2}{3n^8}\frac{3-(\ell/n)^2}{2(\ell/n)^5}. \tag{3.9}$$

In the quantum computation the enhancement at small $\ell < n$ appears after summing over the available final states with small $n' \geqslant \ell - 1$ which allows for energy jumps $|E_n - E_{n'}|$ larger than in the circular case.

In the opposite limit where the linear part of the potential dominates over the Coulombian part, energy losses of highly excited states are again well approximated by classical Larmor radiation, which does not depend on the shape of the orbit, given that the force does not depend on the radius: $W_{\rm Larmor} = 8\alpha_{\rm eff}\sigma^2/3M_{\mathcal{Q}}^2$ is negligibly small. This is confirmed by numerical quantum computations.

### 3.1.4 Cross section for formation of a loose $\mathcal{Q}\mathcal{Q}$ bound state

We here estimate the cross section $\sigma_{\rm tot}(B_{\mathcal{Q}} + B_{\mathcal{Q}} \to B_{\mathcal{Q}\mathcal{Q}} + X)$ for formation of a *loose* bound state containing two heavy quarks $\mathcal{Q}$, starting from two bound states $B_{\mathcal{Q}}$ containing one $\mathcal{Q}$.

Assuming that $B_{\mathcal{Q}} = \mathcal{Q}g$ can be approximated as a $\mathcal{Q}$ and a gluon kept together by a flux tube with length $\ell \sim 1/\Lambda_{\rm QCD}$, the following geometrical picture emerges. The cross section is $\sigma_{\rm tot} \approx \pi\ell^2\wp$ at energies $E \sim M_{\mathcal{Q}}v^2 \lesssim \Lambda_{\rm QCD}$ such that there is not enough energy for breaking the QCD flux tubes, and the recombination probability of two flux tubes is $\wp \sim 1$, like in string models. Independently from the above geometric picture, the size of the bound state is of order $1/\Lambda_{\rm QCD}$, and thereby one expects a cross section $\sigma_{\rm QCD} = c/\Lambda_{\rm QCD}^2$, with $c \approx \pi$ in the geometric picture. In the following we will consider $c = \{1, \pi, 4\pi\}$. For example the measured $pp$ cross section corresponds to $c \approx 10$.

While this expectation is solid at energies of order $\Lambda_{\rm QCD}$, at lower temperatures the cross section might be drastically suppressed if the residual van der Waals-like force has a repulsive component, which prevents the particles to come close enough. We will ignore this possibility, which would result into a higher abundance of hybrid relics.

More in general, processes that only require a small energy exchange $E$ can have large cross sections of order $1/E^2$.[4]

### 3.1.5 Cross section to form an un-breakable $\mathcal{Q}\mathcal{Q}$ bound state

We can finally compute the quantity of interest for us: the thermally averaged cross section $\sigma_{\rm fall}(T)$ for collisions between two $\mathcal{Q}g$ states which produce an unbreakable $\mathcal{Q}\mathcal{Q}$ hadron. This

[4]The authors of [146] propose a quantum mechanical model where processes analogous to $\sigma(B_{\mathcal{Q}} + B_{\mathcal{Q}} \to B_{\mathcal{Q}\mathcal{Q}} + X)$ are computed in terms of cross sections suppressed by $1/M_{\mathcal{Q}}$. This large suppression seems to derive from their arbitrary assumption that the cross section should be dominated by an $s$-channel resonance.

is the same problem we faced in Chapter 2 when we wanted to compute $\sigma_{\rm fall}(T)$ for gluinos. However, given that we just need an order of magnitude estimate of the hybrid relic, we will not perform a brute force quantum mechanical computation. And, for the sake of computational simplicity, we will try to give an estimate of $\sigma_{\rm fall}(T)$ by following an analogy with Larmor radiation. Only for the value of $M_{\mathcal{Q}}$ that reproduces the observed DM relic density, we also perform the full quantum computation described in Chapter 2 to check our results.

An unbreakable $\mathcal{Q}\mathcal{Q}$ hadron is formed when the loose bound state discussed in the previous section radiates more energy (through pion emission) than $\sim T$ in the time $\Delta t$ before the next collision with a pion of the thermal bath, such that it becomes un-breakable and later falls down to its deep ground state. In view of the previous discussion, we proceed as follows. A large total cross section $\sigma_{\rm QCD} \sim \pi/\Lambda^2_{\rm QCD}$ needs a large impact parameter $b \sim 1/\Lambda_{\rm QCD}$, and thereby the $\mathcal{Q}\mathcal{Q}$ state is produced with large angular momentum $\ell \sim M_{\mathcal{Q}} v b$.

The issue is whether a bound state with large $\ell$ gets broken or radiates enough energy becoming un-breakable [101]. As discussed in section 3.1.3, abelian energy losses are well approximated by classical Larmor radiation, and it is crucial to take into account that non-circular orbits radiate much more than circular orbits. The $\mathcal{Q}\mathcal{Q}$ potential is given by eq. (3.2), with a large $\alpha_{\rm eff} \approx 3\alpha_3(\bar{\mu})$ renormalized at $\bar{\mu} \sim 1/r \sim \Lambda_{\rm QCD}$.

The cross section for falling into an un-breakable $\mathcal{Q}\mathcal{Q}$ bound state is computed as follows. We simulate classical collisions, averaging over the velocity distribution at temperature $T$ and over the impact parameter $b$. We numerically solve the classical equation of motion for the $\mathcal{Q}\mathcal{Q}$ system, starting from an initial relative distance $b$ and an orthogonal relative velocity $v$. From the solution $\vec{x}(t)$ we compute the radiated energy $\Delta E$ by integrating the radiated power $W_{\rm Larmor} \sim 2\alpha_{\rm eff}\ddot{\vec{x}}^2/3$ for a time $\Delta t$. We impose $\Delta E \gtrsim T$ where $\Delta t$ is the average time between two collisions at temperature $T$. We estimate it as $\Delta t \sim 1/n_\pi v_\pi \sigma_{\rm QCD}$ where $n_\pi$ is the pion number density and $\sigma_{\rm QCD} = c/\Lambda^2_{\rm QCD}$ such that $\Delta t \simeq \Lambda^2_{\rm QCD}/T^3$ at $T \gg m_\pi$, while the pion density is Boltzmann suppressed at lower $T$.

The resulting $\sigma_{\rm fall}(T)$ is plotted in Fig. 3.2, computed by varying the uncertain QCD parameters as $\alpha_{\rm eff} = \{0.3, 1, 3\}$, $c = \{1, \pi, 4\pi\}$. We see that even for $\alpha_{\rm eff} \sim 1$ the fall cross section $\sigma_{\rm fall}(T)$ equals to the total cross section $\sigma_{\rm QCD}$ at temperatures below $(0.1 - 0.3)\Lambda_{\rm QCD}$, and it is mildly smaller at $T \sim \Lambda_{\rm QCD}$. If instead $\alpha_{\rm eff} \sim 4\pi$ one would have $\sigma_{\rm fall} = \sigma_{\rm QCD}$ even at $T \sim \Lambda_{\rm QCD}$. The value $\alpha_{\rm eff} \sim 4\pi$ can account for non-perturbative QCD effects: it is not unreasonable to think that the bound state can quickly radiate the maximal binding energy $E_B \sim 200\,\text{GeV}$ by emitting in one shot a hundred of gluons with energy $E \sim 2\,\text{GeV}$ each.

A rough analytical estimate for $\sigma_{\rm fall}(T)$ can be obtained as follows. As discussed above, states that radiate fast enough arise only in the Coulombian part of the potential. In view of eq. (3.8), their energy loss rate is $W_{\rm Larmor} \sim \alpha^7_{\rm eff} M^2_{\mathcal{Q}}/\ell^8$, which can be big enough only for relatively small $\ell \sim M_{\mathcal{Q}} b v$. Imposing $\Delta E \gtrsim T$ for $v \sim \sqrt{T/M_{\mathcal{Q}}}$ gives

$$\sigma_{\rm fall} \sim \frac{c}{\Lambda^2_{\rm QCD}} \min(1, 0.3A) \qquad A = \frac{\alpha^{7/4}_{\rm eff}\Lambda^{5/2}_{\rm QCD}}{M^{1/2}_{\mathcal{Q}} T^2} \tag{3.10}$$

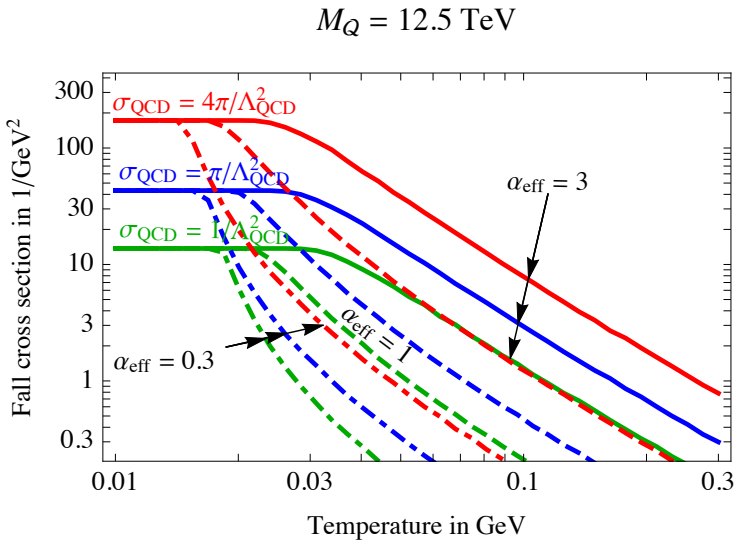


Figure 3.2: *Thermally averaged cross section for falling in an unbreakable bound state as computed numerically for* $M_{\mathcal{Q}} = 12.5\,\text{TeV}$ *and for different values of* $\alpha_{\rm eff} = 0.3$ *(dot-dashed)* 1 *(dashed),* 3 *(continuous) and for different values of the total QCD cross section,* $\sigma_{\rm QCD} = c/\Lambda^2_{QCD}$*,* $c = 1$ *(green),* $\pi$ *(blue),* $4\pi$ *(red). Eq.* (3.10) *approximates this numerical result.*

where the order one numerical value was added by roughly fitting to Fig. 3.2, for the values of the total QCD cross section there assumed. The fall cross section is only suppressed by a small power of $M_{\mathcal{Q}}$, explaining why we find a large $\sigma_{\rm fall} \sim \sigma_{\rm tot}$ for $M_{\mathcal{Q}} \sim 12.5\,\text{TeV}$. In the analytic estimate we neglected the fact that $m_\pi \sim \Lambda_{\rm QCD}$: this is taken into account by the relatively large ad hoc numerical factor added to eq. (3.10) such that it provides a better agreement with the numerical result in Fig. 3.2 for $M_{\mathcal{Q}} \sim 12.5\,\text{TeV}$.

## 3.2 Cosmological relic densities

We can now compute how strong QCD interactions lead to an abundance of the $\mathcal{Q}$-onlyum DM candidate $\mathcal{Q}\mathcal{Q}$ much larger than the severely constrained hybrid bound states $\mathcal{Q}g$. We describe what happens during the cosmological evolution, from the usual decoupling of free $\mathcal{Q}$ at $T \sim M_{\mathcal{Q}}/25$ (section 3.2.1), to recoupling (section 3.2.2) at $T \gtrsim \Lambda_{\rm QCD}$, to $T \sim \Lambda_{\rm QCD}$ (section 3.2.3), to redecoupling at $T \lesssim \Lambda_{\rm QCD}$ (section 3.2.4), to nucleosynthesis at $T \sim 0.1\,\text{MeV}$ (section 3.2.5).

### 3.2.1 $\mathcal{Q}$ decoupling at $T \sim M_{\mathcal{Q}}/25$

As usual, at $T \gtrsim M_{\mathcal{Q}}$ the free $\mathcal{Q}$ annihilate into SM particles much faster than the Hubble rate, remaining in thermal equilibrium until they decouple at $T = T_{\rm dec} \approx M_{\mathcal{Q}}/25$, leaving the usual relic abundance, determined by their annihilation cross-section in this decoupling phase. The

non-relativistic $s$-wave cross section reads

$$\sigma_{\rm ann} v_{\rm rel} = \frac{\sigma_{\mathcal{Q}\bar{\mathcal{Q}}} v_{\rm rel}}{2} = \frac{63}{64}\left(\frac{1}{14}S_3 + \frac{10}{14}S_{3/2} + \frac{3}{14}S_{-1}\right)\frac{\pi\alpha_3^2}{M_{\mathcal{Q}}^2} \tag{3.11}$$

where the strong coupling is renormalized around $M_{\mathcal{Q}}$, while it is renormalized around $\alpha_3 M_{\mathcal{Q}}$ in the Sommerfeld factors $S_n$ corresponding to the various color channels:

$$S_n = \frac{2\pi n \alpha_3/v_{\rm rel}}{1 - e^{-2\pi n\alpha_3/v_{\rm rel}}}. \tag{3.12}$$

We define $Y_{\mathcal{Q}} \equiv (n_{\mathcal{Q}} + n_{\bar{\mathcal{Q}}})/s$, where $s$ is the entropy density, and assume no dark baryon asymmetry, $n_{\mathcal{Q}} = n_{\bar{\mathcal{Q}}}$.

As shown in the previous chapter, perturbative formation of bound states gives an order one correction to the final relic and needs to be included in the cosmological evolution. The bound states made by our 'Dirac gluinos' can be divided into stable $\mathcal{Q}\mathcal{Q}$ or $\bar{\mathcal{Q}}\bar{\mathcal{Q}}$ states that carry two units of dark baryon number, and unstable $\mathcal{Q}\bar{\mathcal{Q}}$ states, where $\mathcal{Q}$ and $\bar{\mathcal{Q}}$ annihilate. The latter come into spin-0 and spin-1 combinations, while the stable states have only the spin allowed by Fermi statistics: in particular the singlet ground state has spin 0. Among the unstable bound states the most relevant for the relic abundance at $T \gg \Lambda_{\rm QCD}$ are the ones that decay faster and have larger binding energy. These are listed in Table 3.1. The corresponding effective rates are plotted in Fig. 3.3. We only estimated the annihilation widths of those states that exist only as $\mathcal{Q}\bar{\mathcal{Q}}$; they are suppressed by $\mathcal{O}(\alpha_3^2)$ making these states negligible (the formation cross section does not depend on spin) unless numerical factors compensate for the suppression.

These rates determine a network of Boltzmann equations for the abundance of free $\mathcal{Q}$ and for the abundances $Y_I = n_I/s$ of the various bound states $I$ as function of $z = M_{\mathcal{Q}}/T$. Such equations are

$$\begin{cases} sHz\dfrac{dY_Q}{dz} &= -2\gamma_{\rm ann}\left[\dfrac{Y_{\mathcal{Q}}^2}{Y_{\mathcal{Q}}^{\rm eq2}} - 1\right] - 2\displaystyle\sum_I \gamma_I\left[\frac{Y_{\mathcal{Q}}^2}{Y_{\mathcal{Q}}^{\rm eq2}} - \frac{Y_I}{Y_I^{\rm eq}}\right], \\ sHz\dfrac{dY_I}{dz} &= n_I^{\rm eq}\left\{\langle\Gamma_{I\rm break}\rangle\left[\dfrac{Y_{\mathcal{Q}}^2}{Y_{\mathcal{Q}}^{\rm eq2}} - \frac{Y_I}{Y_I^{\rm eq}}\right] + \langle\Gamma_{I\rm ann}\rangle\left[1 - \frac{Y_I}{Y_I^{\rm eq}}\right] + \displaystyle\sum_J \langle\Gamma_{I\to J}\rangle\left[\frac{Y_J}{Y_J^{\rm eq}} - \frac{Y_I}{Y_I^{\rm eq}}\right]\right\} \end{cases}. \tag{3.13}$$

Here $\gamma_I$ is the thermal-equilibrium space-time density of formations of bound state $I$, related to the thermal average $\langle\Gamma_{I\rm break}\rangle$ of the breaking rate $\Gamma_{I\rm break}$ as described in section 1.1. Furthermore $\Gamma_{I\rm ann}$ is the decay rate of bound state $I$ due to annihilations between its $\mathcal{Q}$ and $\bar{\mathcal{Q}}$ constituents: it vanishes for the $\mathcal{Q}\mathcal{Q}$ and $\bar{\mathcal{Q}}\bar{\mathcal{Q}}$ states. Finally, $\Gamma_{I\to J} = -\Gamma_{J\to I}$ is the decay rate from state $I$ to state $J$. To reduce the number of differential equations while including $\mathcal{Q}\mathcal{Q}$ and $\bar{\mathcal{Q}}\bar{\mathcal{Q}}$ states, we need to extend the strategy of section 1.1. The annihilation rates, $\Gamma_{\rm ann}$, for these states vanish, so we can now only reduce the network of Boltzmann equations to two equations: one for $Y_{\mathcal{Q}}$ (density of free $\mathcal{Q}$) and one for $Y_{\mathcal{Q}\mathcal{Q}} = \sum_{I\in\mathcal{Q}\mathcal{Q}} Y_I$ (total density of stable bound states,

| made of | color | $S$ | $n$ | $\ell$ | $E_B/M_{\mathcal{Q}}$ | $\Gamma_{\rm ann}/M_{\mathcal{Q}}$ | $\Gamma_{\rm dec}/M_{\mathcal{Q}}$ | Annihilation |
|---|---|---|---|---|---|---|---|---|
| $\mathcal{Q}\bar{\mathcal{Q}}$ | $1_S$ | 0 | 1 | 0 | $9\alpha_3^2/4$ | $243\alpha_3^5/2$ | 0 | $gg$ |
| $\mathcal{Q}\bar{\mathcal{Q}}$ | $1_S$ | 1 | 1 | 0 | $9\alpha_3^2/4$ | $\sim \alpha_3^7$ | $\sim \alpha_3^6$ | $gggg$ |
| $\mathcal{Q}\bar{\mathcal{Q}}$ | $8_A$ | 1 | 1 | 0 | $9\alpha_3^2/16$ | $81\alpha_3^5/16$ | $\sim \alpha_3^6$ | $q\bar{q}$ |
| $\mathcal{Q}\bar{\mathcal{Q}}$ | $8_A$ | 0 | 1 | 0 | $9\alpha_3^2/16$ | $\sim \alpha_3^6$ | $\sim \alpha_3^6$ | $ggg$ |
| $\mathcal{Q}\bar{\mathcal{Q}}$ | $8_S$ | 0 | 1 | 0 | $9\alpha_3^2/16$ | $243\alpha_3^5/64$ | $\sim \alpha_3^6$ | $gg$ |
| $\mathcal{Q}\bar{\mathcal{Q}}$ | $8_S$ | 1 | 1 | 0 | $9\alpha_3^2/16$ | $\sim \alpha_3^7$ | $\sim \alpha_3^6$ | $gggg$ |
| $\mathcal{Q}\bar{\mathcal{Q}}$ | $1_S$ | 0 | 2 | 0 | $9\alpha_3^2/16$ | $243\alpha_3^5/16$ | $\sim \alpha_3^6$ | $gg$ |
| $\mathcal{Q}\bar{\mathcal{Q}}$ | $1_S$ | 1 | 2 | 0 | $9\alpha_3^2/16$ | $\sim \alpha_3^7$ | $\sim \alpha_3^6$ | $gggg$ |
| $\mathcal{Q}\bar{\mathcal{Q}}$ | $8_A$ | 1 | 2 | 0 | $9\alpha_3^2/64$ | $81\alpha_3^5/128$ | $\sim \alpha_3^6$ | $q\bar{q}$ |
| $\mathcal{Q}\bar{\mathcal{Q}}$ | $8_A$ | 0 | 2 | 0 | $9\alpha_3^2/64$ | $\sim \alpha_3^6$ | $\sim \alpha_3^6$ | $ggg$ |
| $\mathcal{Q}\bar{\mathcal{Q}}$ | $8_S$ | 0 | 2 | 0 | $9\alpha_3^2/64$ | $243\alpha_3^5/512$ | $\sim \alpha_3^6$ | $gg$ |
| $\mathcal{Q}\bar{\mathcal{Q}}$ | $8_S$ | 1 | 2 | 0 | $9\alpha_3^2/64$ | $\sim \alpha_3^7$ | $\sim \alpha_3^6$ | $gggg$ |
| $\mathcal{Q}\bar{\mathcal{Q}}$ | $1_S$ | 0 | 2 | 1 | $9\alpha_3^2/16$ | $\sim 0$ | $\sim \alpha_3^6$ | |
| $\mathcal{Q}\bar{\mathcal{Q}}$ | $1_S$ | 1 | 2 | 1 | $9\alpha_3^2/16$ | $\sim \alpha_3^7$ | $\sim \alpha_3^6$ | $gg$ |
| $\mathcal{Q}\bar{\mathcal{Q}}$ | $8_A$ | 1 | 2 | 1 | $9\alpha_3^2/64$ | $\sim 0$ | $\approx 0.1\alpha_3^5$ | |
| $\mathcal{Q}\bar{\mathcal{Q}}$ | $8_A$ | 0 | 2 | 1 | $9\alpha_3^2/64$ | $\sim \alpha_3^7$ | $\approx 0.1\alpha_3^5$ | $q\bar{q}$ |
| $\mathcal{Q}\bar{\mathcal{Q}}$ | $8_S$ | 0 | 2 | 1 | $9\alpha_3^2/64$ | $\sim 0$ | $\approx 0.1\alpha_3^5$ | |
| $\mathcal{Q}\bar{\mathcal{Q}}$ | $8_S$ | 1 | 2 | 1 | $9\alpha_3^2/64$ | $\sim \alpha_3^7$ | $\approx 0.1\alpha_3^5$ | $gg$ |
| $\mathcal{Q}\mathcal{Q}$ | $1_S$ | 0 | 1 | 0 | $9\alpha_3^2/4$ | 0 | 0 | DM candidate |
| $\mathcal{Q}\mathcal{Q}$ | $8_A$ | 1 | 1 | 0 | $9\alpha_3^2/16$ | 0 | 0 | |
| $\mathcal{Q}\mathcal{Q}$ | $8_S$ | 0 | 1 | 0 | $9\alpha_3^2/16$ | 0 | 0 | |
| $\mathcal{Q}\mathcal{Q}$ | $1_S$ | 0 | 2 | 0 | $9\alpha_3^2/16$ | 0 | $\sim \alpha_3^6$ | |
| $\mathcal{Q}\mathcal{Q}$ | $8_A$ | 1 | 2 | 0 | $9\alpha_3^2/64$ | 0 | $\sim \alpha_3^6$ | |
| $\mathcal{Q}\mathcal{Q}$ | $8_S$ | 0 | 2 | 0 | $9\alpha_3^2/64$ | 0 | $\sim \alpha_3^6$ | |
| $\mathcal{Q}\mathcal{Q}$ | $1_S$ | 1 | 2 | 1 | $9\alpha_3^2/16$ | 0 | $\sim \alpha_3^6$ | |
| $\mathcal{Q}\mathcal{Q}$ | $8_A$ | 0 | 2 | 1 | $9\alpha_3^2/64$ | 0 | $\approx 0.1\alpha_3^5$ | |
| $\mathcal{Q}\mathcal{Q}$ | $8_S$ | 1 | 2 | 1 | $9\alpha_3^2/64$ | 0 | $\approx 0.1\alpha_3^5$ | |

Table 3.1: *Properties of lowest lying Coulombian bound states made of $\mathcal{Q}\bar{\mathcal{Q}}$ (upper) and $\mathcal{Q}\mathcal{Q}$ (lower). The subscript $S$ or $A$ denote if the state is obtained as a symmetric or antisymmetric combination in color space. Slower rates have only been estimated.*

that satisfies $Y_{\mathcal{QQ}}/Y^{\rm eq}_{\mathcal{QQ}} = Y_I/Y^{\rm eq}_I$ for all stable states $I$). The equations are

$$\begin{cases} sHz\dfrac{dY_{\mathcal{Q}}}{dz} &= -2\gamma^{\rm eff}_{\rm ann}\left[\dfrac{Y^2_{\mathcal{Q}}}{Y^{\rm eq2}_{\mathcal{Q}}}-1\right]-2\gamma_{\rm fall}\left[\dfrac{Y^2_{\mathcal{Q}}}{Y^{\rm eq2}_{\mathcal{Q}}}-\dfrac{Y_{\mathcal{QQ}}}{Y^{\rm eq}_{\mathcal{QQ}}}\right] \\ sHz\dfrac{dY_{\mathcal{QQ}}}{dz} &= n^{\rm eq}_{\mathcal{QQ}}\langle\Gamma_{\rm break}\rangle\left[\dfrac{Y^2_{\mathcal{Q}}}{Y^{\rm eq2}_{\mathcal{Q}}}-\dfrac{Y_{\mathcal{QQ}}}{Y^{\rm eq}_{\mathcal{QQ}}}\right] \end{cases} \tag{3.14}$$

where $\gamma^{\rm eff}_{\rm ann}$ includes the effects of $\mathcal{Q}\bar{\mathcal{Q}}$ bound states and is given by the same expression as in section 1.1. The total fall rate that accounts for the cumulative effect of all $\mathcal{QQ}$ and $\bar{\mathcal{Q}}\bar{\mathcal{Q}}$ bound states is given by the sum of the formation rates of all such states, $\gamma_{\rm fall} = \sum_{I\in\mathcal{QQ}}\gamma_I$, which equals $n^{\rm eq}_{\mathcal{QQ}}\langle\Gamma_{\rm break}\rangle \equiv \sum_{I\in\mathcal{QQ}}\langle\Gamma_{I\rm break}\rangle n^{\rm eq}_I$. Notice that $Y_{\mathcal{Q}} + 2Y_{\mathcal{QQ}}$ remains constant when a $\mathcal{QQ}$ bound state is formed.

We now derive an approximated analytic solution by computing the deviation from equilibrium of the stable bound states. First, we appreciate that at temperatures at which the quorn annihilation goes out of equilibrium the second of the above equations is still in equilibrium and thus the effect of stable bound states can be ignored in the solution for the first equation. The asymptotic solution in this phase is

$$\begin{cases} Y_{\mathcal{Q}}(z) &\approx \left[Y_{\mathcal{Q}}(z_{\rm dec})^{-1}+\lambda\displaystyle\int_{z_{\rm dec}}^{z}\frac{\langle\sigma^{\rm eff}_{\rm ann}v_{\rm rel}\rangle}{z'^2}\,dz'\right]^{-1} \\ Y_{\mathcal{QQ}}(z) &\approx Y^0_{\mathcal{QQ}}(z)+\dfrac{1}{\lambda}Y^1_{\mathcal{QQ}}(z) = Y_{\mathcal{Q}}(z)^2\dfrac{Y^{\rm eq}_{\mathcal{QQ}}}{Y^{\rm eq2}_{\mathcal{Q}}}+\dfrac{1}{\lambda}Y^1_{\mathcal{QQ}}(z) \end{cases} \tag{3.15}$$

where $z_{\rm dec}\approx 25$ and $1/\lambda = H/s|_{T=M_{\mathcal{Q}}}$. Expanding in small $1/\lambda$ one finds $Y^1_{\mathcal{QQ}}(z)$ and determines the temperature at which $Y^0_{\mathcal{QQ}}(z)\approx Y^1_{\mathcal{QQ}}(z)/\lambda$, finding

$$1 \approx \frac{\langle\Gamma_{\rm break}\rangle M_{\mathcal{Q}}}{E_B H(T) z} \approx \frac{\langle\Gamma_{\rm break}\rangle}{H\left(T\approx E_B\right)}\,. \tag{3.16}$$

This gives the asymptotic solution for $\Lambda_{\rm QCD}\ll T\ll M_{\mathcal{Q}}$:

$$\begin{cases} Y^{-1}_{\mathcal{Q}}(z) &\approx Y^{-1}_{\mathcal{Q}}(z_{\rm dec})+\lambda\displaystyle\int_{z_{\rm dec}}^{z}\frac{dz'}{z'^2}\left[\langle\sigma^{\rm eff}_{\rm ann}v_{\rm rel}\rangle+\langle\sigma_{\rm fall}v_{\rm rel}\rangle\left(1+\frac{\langle\Gamma_{\rm break}\rangle M_{\mathcal{Q}}}{E_B H(z')z'}\right)^{-1}\right] \\ Y_{\mathcal{QQ}}(z) &\approx \dfrac{1}{2}\left[\left(Y^{-1}_{\mathcal{Q}}(z_{\rm dec})+\lambda\displaystyle\int_{z_{\rm dec}}^{z}\frac{dz'}{z'^2}\langle\sigma^{\rm eff}_{\rm ann}v_{\rm rel}\rangle\right)^{-1}-Y_{\mathcal{Q}}(z)\right]. \end{cases} \tag{3.17}$$

Using the specific rates for the main perturbative bound states listed in Table 3.1 we obtain the values of $Y_{\mathcal{Q}}$ and of $Y_{\mathcal{QQ}}$ at temperatures $T\gg\Lambda_{\rm DC}$. The result is shown in Fig. 3.4b, where they are denoted as 'perturbative'. We see that such effect can be neglected. At confinement, non-perturbative QCD effects force all free $\mathcal{Q}$ to bind with SM quarks and gluons to form strongly interacting hadrons, as discussed in the following.

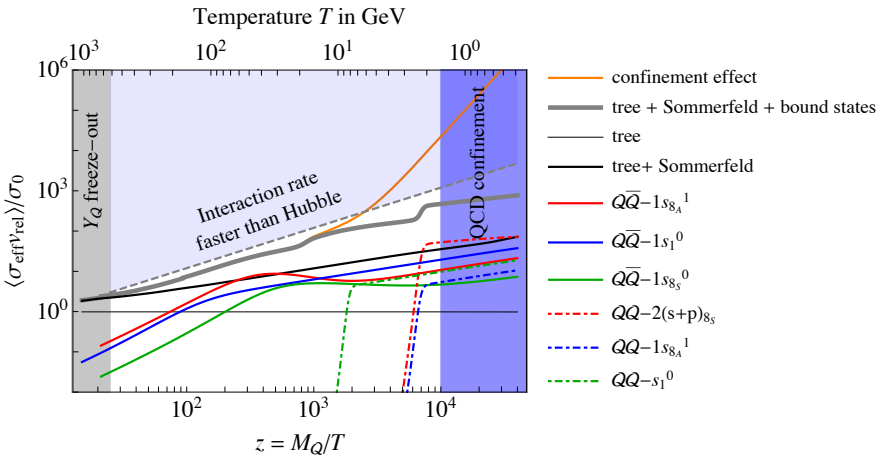


Figure 3.3: *Thermally-averaged effective annihilation cross section in units of* $\sigma_0 = \pi\alpha_3^2/M_{\mathcal{Q}}^2$ *for* $M_{\mathcal{Q}} = 12.5\,\text{TeV}$. *The horizontal line is the tree-level value in s-wave; the black curve is the result obtained adding Sommerfeld corrections; the thick gray curve is the result adding also* $\mathcal{Q}\bar{\mathcal{Q}}$ *bound-state corrections. The other curves show the contributions from the main bound states among those listed in Table 3.1. The orange curve is an estimate of confinement effects that lead to recoupling at low* $T \lesssim 10\,\text{GeV}$.

### 3.2.2 $\mathcal{Q}$ recoupling at $T \gtrsim \Lambda_{\rm QCD}$

DM annihilations recouple below the decoupling temperature $T_{\rm dec}$ if the thermally averaged DM annihilation cross section $\sigma_{\rm ann}(T)$ grows at low temperatures faster than $1/T^{3/2}$. In such a case DM recouples, and its abundance $n_{\rm DM}$ is further reduced. A tree-level cross section $\sigma_{\rm ann} \sim g^4/M_{\rm DM}^2$ does not recouple. A Sommerfeld enhancement $S \sim 1/v_{\rm rel} \propto 1/\sqrt{T}$ leads to order one effects, but not to recoupling (unless enhanced by some resonance). Formation of bound states with small quantum number $n \sim 1$ give other similar effects. In the previous section we included such order one corrections, adapting the results of Chapter 1. At this stage $\mathcal{Q}$ can form relatively deep bound states with heavy quarks, which eventually decay.

The QCD coupling grows non-perturbative at $T \gtrsim \Lambda_{\rm QCD}$ giving a more dramatic recoupling effect: bound states with size $r_{Bn} \sim (\alpha_3/n) M_{\mathcal{Q}}$ can be formed through a large cross section $\sigma_{\rm ann} \sim 1/r_{Bn}^2$, having omitted powers of the strong coupling. The increase of the cross section as $n \to \infty$ is tamed by a competing effect: only bound states with $E_{Bn} \gtrsim T$ are actually formed at temperature $T$ (as better discussed in Appendix D), leading to a re-coupling cross section that grows as $\sigma_{\rm ann} \sim 1/T^2$ for $T \gtrsim \Lambda_{\rm QCD}$.

### 3.2.3 Chromodark-synthesis at $T \sim \Lambda_{\rm QCD}$

This effect culminates after confinement. Cosmological effects of confinement begin when the Coulombian force $\alpha_{\rm eff}/r^2$ becomes weaker than the string tension $\sigma(T)$ at the typical distance $r \sim 1/T$. Given that gluons and quarks are much more abundant than $\mathcal{Q}$, the free $\mathcal{Q}$ form

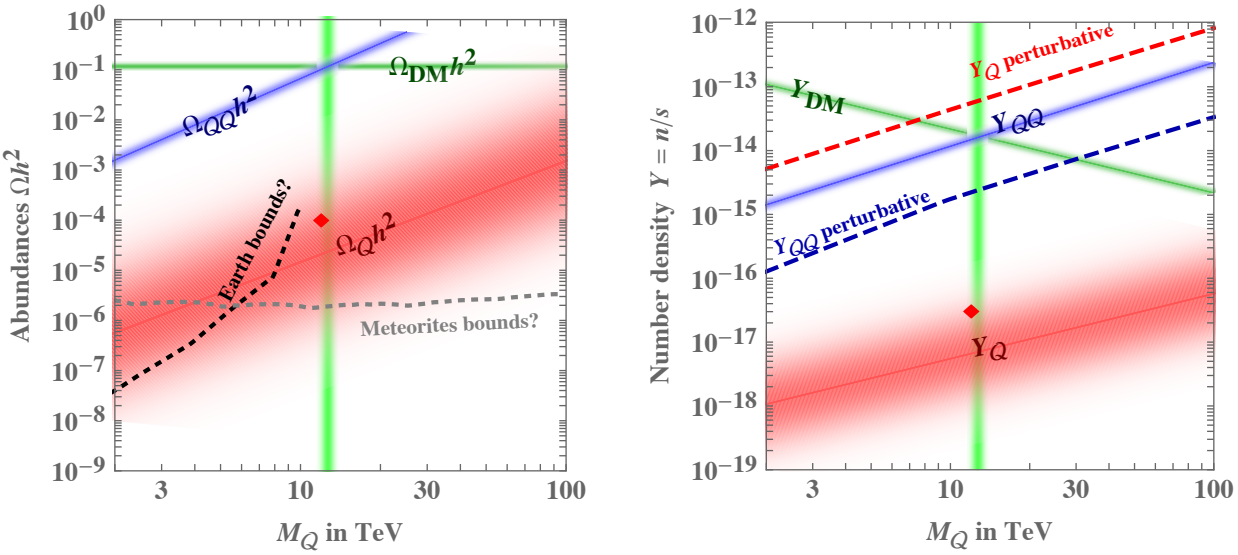


Figure 3.4: *Thermal relic abundances of the DM $\mathcal{Q}\mathcal{Q}$ hadron (blue band) and of hybrid $\mathcal{Q}g$ hadrons (red band, as obtained varying $\alpha_{\rm eff}$ and $\sigma_{\rm QCD}\Lambda^2_{QCD}$ between 1 and $4\pi$). The red diamonds show the relic of hybrids hadrons obtained with the more precise estimate of $\sigma_{\rm fall}$ given in Chapter 2.* **Left***: mass densities. The desired DM abundance is reproduced for $M_{\mathcal{Q}} \sim 12.5\,$TeV. The sub-dominant abundance of hybrid $\mathcal{Q}g$ hadrons and the relative experimental upper bounds are subject to large and undefined nuclear, cosmological and geological uncertainties, see section 3.3.* **Right***: number densities $Y = n/s$ of $\mathcal{Q}\mathcal{Q}$ DM states and of $\mathcal{Q}$ hybrids. We also show the abundance of $\mathcal{Q}\mathcal{Q}$ bound states before confinement (dashed curve).*

$\mathcal{Q}g$ and $\mathcal{Q}q\bar{q}'$ bound states, which have a binding energy of order $\Lambda_{\rm QCD}$ and scatter among themselves and with other hadrons with cross sections of typical QCD size, $\sigma_{\rm QCD} = c/\Lambda^2_{\rm QCD}$ with $c \sim 1$. In this stage $H \sim \Lambda^2_{\rm QCD}/M_{\rm Pl} \sim 10^{-20}\Lambda_{\rm QCD}$, such that a $\mathcal{Q}g$ hadron experiences $10^{20}$ QCD scatterings in a Hubble time. Given that the relative abundance of $\mathcal{Q}$ is $Y_{\mathcal{Q}} \sim 10^{-14}$, two $\mathcal{Q}g$ will meet, forming either deep $\mathcal{Q}\mathcal{Q}$ hadrons (which remain as DM) or $\mathcal{Q}\bar{\mathcal{Q}}$ hadrons (which annihilate into SM particles). The abundance of $\mathcal{Q}$-only hadrons gets dramatically suppressed, until they decouple.

While most DM particles form in this phase, a precise description is not needed to compute the final abundances, which are dominantly determined by what happens during the final redecoupling, where the dominant SM degrees of freedom are semi-relativistic pions, while the baryon abundance is negligible, in view of the Boltzmann factor $e^{-m_p/T}$ and of the small asymmetry.

### 3.2.4 $\mathcal{Q}$ redecoupling at $T \lesssim \Lambda_{\rm QCD}$

We need a precise description of the final redecoupling which occurs at temperatures of tens of MeV. One might think that the simplified Boltzmann equations for the density of free $\mathcal{Q}$ and of $\mathcal{Q}\mathcal{Q}$ bound states, eq. (3.14), can be replaced with corresponding equations for the total density

of $B_{\mathcal{Q}}$ bound states ($\mathcal{Q}g$ and $\mathcal{Q}q\bar{q}'$) and for the total density of $B_{\mathcal{Q}\mathcal{Q}}$ bound states.

A slightly different strategy is needed. Indeed, the simplification that allowed to reduce the network of Boltzmann equations (one for each bound state) to two is valid only if: *i*) all $B_{\mathcal{Q}}$ bound states are in thermal equilibrium among them; *ii*) all $B_{\mathcal{Q}\mathcal{Q}}$ bound states are in thermal equilibrium among them. Bound states are subject to QCD interactions, with large $\sigma_{\rm QCD}$ cross sections, such that the corresponding interaction rates are much faster than the Hubble rate. However, as discussed in section 3.1.3, non-perturbative QCD interactions now lead to the formation of a large variety of bound states, with large $n$ and $\ell$ quantum numbers which suppress the decay rates among them. Some decay rates can be slower than the Hubble rate. This issue was solved in section 3.1.5 where we computed an effective cross section for the formation of all unbreakable $\mathcal{Q}\mathcal{Q}$ bound states, that later fall to the $\mathcal{Q}\mathcal{Q}$ ground state. The same cross section, almost as large as the QCD cross section, holds for the formation of unbreakable $\mathcal{Q}\bar{\mathcal{Q}}$, that later annihilate:

$$\sigma_{\rm fall} = \sigma_{\rm ann} \lesssim \sigma_{\rm QCD}. \tag{3.18}$$

The equality of the classical non-perturbative total cross section for forming $\mathcal{Q}\bar{\mathcal{Q}}$ bound states with the total cross section for forming $\mathcal{Q}\mathcal{Q}$ bound states, is compatible with the perturbative quantum cross sections computed in section 3.2.1. Indeed, because of Fermi anti-symmetrisation in the $\mathcal{Q}\mathcal{Q}$ case cross sections are twice bigger, while the number of $\mathcal{Q}\bar{\mathcal{Q}}$ states is twice bigger (after restricting to colour-singlet bound states and averaging odd with even $\ell$).

One extra process can take place: annihilations between $\mathcal{Q}\mathcal{Q}$ and $\bar{\mathcal{Q}}\bar{\mathcal{Q}}$ in their ground states. In section 3.4.2 we will compute its cross section, finding that it can be neglected in our present cosmological context. Together with eq. (3.18) this implies a simple result: *half of the $\mathcal{Q}$ and $\bar{\mathcal{Q}}$ present before redecoupling annihilate, and half end up in our DM candidates*, the $\mathcal{Q}\mathcal{Q}$ and $\bar{\mathcal{Q}}\bar{\mathcal{Q}}$ ground states. Boltzmann equations are only needed to compute how small is the residual fraction of $\mathcal{Q}$ in loose hybrid hadrons, which are phenomenologically relevant in view of their large detection cross sections.

We thereby group bound states in two categories. We define $Y_{\mathcal{Q}\mathcal{Q}}$ as the density of all *unbreakable* $\mathcal{Q}\mathcal{Q}$ bound states, produced with cross section $\sigma_{\rm fall}$. We define $Y_{\mathcal{Q}}$ as the density of $\mathcal{Q}$ in loose bound states: the $\mathcal{Q}$ in bound states containing a single $\mathcal{Q}$ ($\mathcal{Q}g$, $\mathcal{Q}q\bar{q}'$), and those in loose $\mathcal{Q}\mathcal{Q}$ and $\mathcal{Q}\bar{\mathcal{Q}}$ bound states at relative distances $\sim 1/\Lambda_{\rm QCD}$, that get broken by QCD scatterings.

The relevant Boltzmann equation are:

$$sHz\frac{dY_{\mathcal{Q}}}{dz} = -2(\gamma^{\rm eff}_{\rm fall} + \gamma^{\rm eff}_{\rm ann})\left[\frac{Y^2_{\mathcal{Q}}}{Y^{\rm eq2}_{\mathcal{Q}}} - 1\right], \qquad sHz\frac{dY_{\mathcal{Q}\mathcal{Q}}}{dz} = \gamma^{\rm eff}_{\rm fall}\left[\frac{Y^2_{\mathcal{Q}}}{Y^{\rm eq2}_{\mathcal{Q}}} - 1\right]. \tag{3.19}$$

valid for $T \lesssim \Lambda_{\rm QCD}$ i.e. $z \gtrsim z_{\rm QCD} \equiv M_{\mathcal{Q}}/\Lambda_{\rm QCD}$. In the non-relativistic limit the space-time density of interactions is determined by the cross sections as $2\gamma \simeq (n^{\rm eq}_{B_{\mathcal{Q}}})^2 \langle \sigma v_{\rm rel} \rangle$. The asymptotic solutions

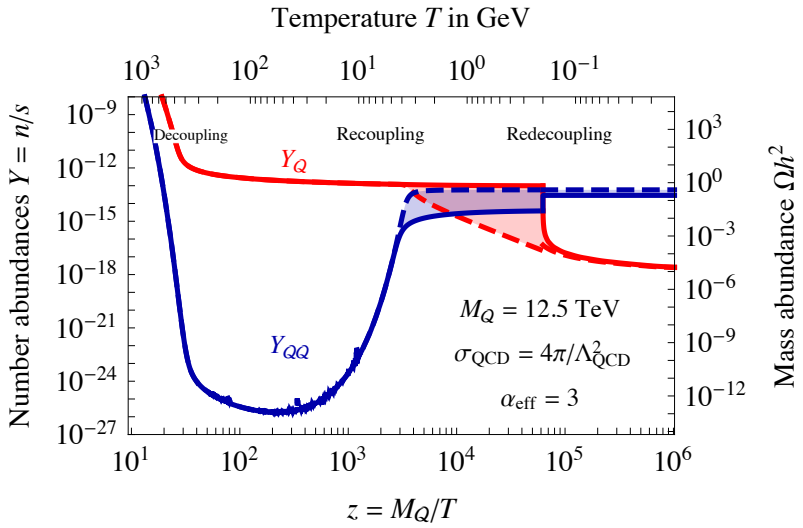


Figure 3.5: *Cosmological evolution of the abundances of $\mathcal{Q}$ states and of $\mathcal{QQ}$ DM states for $M_\mathcal{Q} = 12.5\,\text{TeV}$. The uncertain phase at $T \gtrsim \Lambda_{QCD}$ negligibly affects the final relic abundances: the dashed curves assume non-perturbative effects before confinement estimated as $\sigma = \sigma_{\rm QCD}(\Lambda_{QCD}/T)^2$; the solid curves neglect such effects. The mass abundance on the right axis is computed assuming $\mathcal{QQ}$ particles with mass $2M_\mathcal{Q}$.*

to this system of equations are

$$\begin{cases} Y_\mathcal{Q}^{-1}(\infty) \approx Y_\mathcal{Q}^{-1}(z_{\rm QCD}) + \lambda \displaystyle\int_{z_{\rm QCD}}^{\infty} \frac{\langle\sigma^{\rm eff}_{\rm fall} v_{\rm rel}\rangle + \langle\sigma^{\rm eff}_{\rm ann} v_{\rm rel}\rangle}{z'^2} dz' \,, \\ Y_{\mathcal{QQ}}(\infty) \approx Y_{\mathcal{QQ}}(z_{\rm QCD}) + \dfrac{1}{2} \dfrac{Y_\mathcal{Q}(z_{\rm QCD})\,\langle\sigma^{\rm eff}_{\rm fall} v_{\rm rel}\rangle}{\langle\sigma^{\rm eff}_{\rm fall} v_{\rm rel}\rangle + \langle\sigma^{\rm eff}_{\rm ann} v_{\rm rel}\rangle + z_{\rm QCD}/\lambda\, Y_\mathcal{Q}(z_{\rm QCD})} \end{cases} \tag{3.20}$$

with the last term roughly equals $Y_\mathcal{Q}(z_{\rm QCD})/4$. Fig. 3.4 shows our final result: the DM abundance and the hybrid abundance as function of the only free parameter, $M_\mathcal{Q}$. The left panel shows the mass abundances $\Omega = \rho/\rho_{\rm cr}$; the right panel shows the number abundances $Y = n/s$. The hybrid abundances are plotted as bands, given that they are affected by QCD uncertainties; smaller values are obtained for larger $c = \sigma_{\rm QCD}\Lambda^2_{\rm QCD}$ and for larger $\alpha_{\rm eff}$. Varying them between 1 and $4\pi$, the hybrid abundance changes by a factor 100. The DM abundance, less affected by QCD uncertainties, is plotted as a blue curve. The right panel shows that the DM $\mathcal{QQ}$ abundance is mostly made at the non-perturbative level; the perturbative bound states computed in section 3.2.1 only play a significant role in enhancing $\mathcal{Q}\bar{\mathcal{Q}}$ annihilations.

The observed DM abundance is reproduced for

$$M_\mathcal{Q} \approx (12.5 \pm 1)\,\text{TeV} \tag{3.21}$$

and the hybrid mass abundance is about $10^4$ smaller that the DM abundance (between $10^3$ and

$10^5$ within our assumed range of QCD parameters). For such mass, Fig. 3.5 shows the cosmological evolution of the abundances. It also shows how large uncertainties at $T \sim \Lambda_{\rm QCD}$ before redecoupling have a negligible impact on the final abundances, which is dominantly determined by redecoupling.

An analytic argument that shows that $\Omega_{\rm hybrid} \ll \Omega_{\rm DM}$ is unavoidable and that gives the dependence of the final abundances on $M_{\mathcal{Q}}, M_{\rm Pl}, \Lambda_{\rm QCD}$ (eq. (D.4)) is given in Appendix D.

### 3.2.5 Nucleodark-synthesis

Redecoupling is completed at temperatures $T \sim 10\,{\rm MeV}$. Later nucleons bind into light nuclei at the Big Bang Nucleosynthesis (BBN) temperature $T_{\rm BBN} \sim 0.1\,{\rm MeV}$. Various authors tried to compute what happens to SIMPs during BBN, and how SIMPs affect ordinary BBN [147–150][5]. Our predicted amount of Strongly Interacting Massive Particles, $Y_{\rm SIMP} \sim 10^{-18}$, has negligible effects on ordinary BBN, which constrains $Y_{\rm SIMP} \lesssim 10^{-12}$. Such studies however disagree on what happens to SIMPs during BBN. Do SIMPs bind with (some) nuclei? Does a significant fraction of SIMPs remain free?

We present our understanding, but we cannot provide a safe answer. Indeed, nuclear forces are not understood from first principles, not even for ordinary $p$ and $n$ [151]. Long-range nuclear properties are determined by couplings to pions, known thanks to chiral perturbation theory [152]. Heavier QCD states contribute to short-range nuclear forces: however QCD is here only used as inspiration to write phenomenological nuclear potentials to be fitted to $p, n$ data, see e.g. [153].

In our scenario there are two types of SIMPs with distinct properties. The $\mathcal{Q}g$ hybrids are isospin singlets and thereby do not couple to pions. The $\mathcal{Q}q\bar{q}$ hybrids form an isospin triplet (with charges $0, \pm 1$) coupled to pions.

Presumably $\mathcal{Q}q\bar{q}'$ are heavier and decay promptly to $\mathcal{Q}g$. Then, the $\mathcal{Q}g$ singlet states, which do not feel the pion force, are expected to behave similarly to the $\Lambda$ baryon, which does not bind to protons to form heavy deuterons [154]. Maybe such SIMPs do not bind with any nuclei, or maybe they find a way to form bound states with big enough nuclei. An attractive force can be provided by exchange of an isospin-singlet scalar meson, such as the $\sigma$ (mass $M \sim 0.6\,{\rm GeV}$) or glueballs (mass $M \sim 1.5\,{\rm GeV}$) provided that their effective Yukawa couplings $y_{\rm SIMP}$ and $y_N$ to the SIMP and to nucleons are large enough and have the same sign. In spherical well and Born approximation and for $M_{\mathcal{Q}} \gg M$, the hybrid can form a bound state in a nucleus with atomic number $A$ if [155]

$$y_{\rm SIMP} y_N > \frac{12\pi}{A^{5/3}} \frac{M^2}{{\rm GeV}^2}. \tag{3.22}$$

If SIMPs bind to light nuclei, after BBN they dominantly end up in Helium or free, with a relatively large amount in Beryllium, according to [148, 149].

The $\mathcal{Q}q\bar{q}'$ states, which feel the pion force, have an interaction potential with a range of ap-

[5]Here and in the following, by SIMP we mean particles that interact strongly with SM particles.

proximately 2 fm. If they are the lighter stable bound states, during BBN they get incorporated into nuclei with an efficiency close to 100% [150]. In the Milky Way, SIMPs in charged nuclei can loose a significant fraction of their energy by interactions with ambient matter.

No SIMP searches have yet been performed in galactic clouds, which would probe the SIMP primordial abundance. After BBN, SM matter forms stars and planets: primordial SIMPs sink to their center before these objects possibly solidify. Stars (rather than BBN) later produce the observed elements heavier than He. In the next section we estimate the present geological abundance of SIMPs.

## 3.3 Signals of relic hybrid hadrons

In our model $\mathcal{Q}$-onlyum DM is accompanied by hybrid hadrons, containing heavy colored $\mathcal{Q}$ bound together with SM quarks or gluons. In this section we discuss their signals. While SIMP DM has been excluded long ago, in our model SIMPs have a sub-dominant abundance, $f_{\rm SIMP} \equiv \rho_{\rm SIMP}/\rho_{\rm DM}$ below $10^{-3}$, possibly a few orders of magnitude smaller. Such small value of $\rho_{\rm SIMP}$ makes indirect SIMP detection signals negligible ($f^2_{\rm SIMP}\sigma_{\rm QCD} \lesssim 10^{-24}\,{\rm cm}^3/{\rm sec}$) despite that SIMPs interact with matter nucleons and with themselves through large cross sections of order $\sigma_{\rm QCD} \sim 1/\Lambda^2_{\rm QCD}$. See also [157]. In some models SIMPs can have electric charge (fractional in exotic models).

As discussed in section 3.3.1, galactic SIMPs are stopped by the upper atmosphere of the Earth and slowly sink. Thereby SIMPs are not visible in direct detection experiments performed underground. Their later behaviour depends on whether SIMPs bind with nuclei: if yes they indirectly feel atomic forces; otherwise they sink even within solid bodies, such as the present Earth. In section 3.3.2 we summarize bounds on the SIMP abundance, to be compared with their present abundance, estimated in sections 3.3.3 and 3.3.4.

### 3.3.1 Direct detection of hybrid hadrons

Despite their reduced abundance, SIMPs would be excluded by a dozen of orders of magnitude, if they reach the underground direct detection detectors with enough energy to trigger events. This is not the case. The energy loss of a neutral SIMP in matter is [158]

$$\frac{dE}{dx} = -E\sum_A n_A \sigma_A \frac{2m_A}{M_{\mathcal{Q}}} \qquad \text{for } m_A \ll M_{\mathcal{Q}} \tag{3.23}$$

where $n_A$ is the number density of nuclei with atomic number $A$ and mass $m_A \approx Am_p$; $2m_A/M_{\mathcal{Q}}$ is the fractional energy loss per collision and $\sigma_A \approx \sigma_p\, A^2(m_A/m_p)^2$ is the SIMP cross section on a nucleus [159], written in terms of the SIMP scattering cross section on protons, $\sigma_p \approx \pi/\Lambda^2_{\rm QCD} \approx 1.6\ 10^{-26}\,{\rm cm}^2$. The cross section $\sigma_A$ is coherently enhanced at the energies of interest for us, $E = M_{\mathcal{Q}}v^2/2 \sim$ MeV for $v \sim 10^{-3}$. The densities $n_A$ in the Earth crust can be written as

$n_A = f_A\rho/m_A$ where $\rho$ is the total mass density and $f_A$ is the mass fraction of material $A$, $\sum_A f_A = 1$. The energy loss following from eq. (3.23) is

$$E(x) = E_0 \exp\left[ -\int \rho\, dx\, \frac{\mathrm{m}^2}{70\,\mathrm{kg}} \frac{\langle A^4\rangle}{16.6^4} \frac{10\,\mathrm{TeV}}{M_{\mathcal{Q}}} \frac{\sigma_p}{\pi/\Lambda^2_{\mathrm{QCD}}}\right]. \tag{3.24}$$

Thereby SIMPs with $M_{\mathcal{Q}} \approx 10$ TeV thermalize in the Earth atmosphere, which has a column depth of $10^4\,\mathrm{kg/m}^2$ and $\langle A^4\rangle^{1/4} \approx 16.6$, before reaching the crust with $\langle A^4\rangle^{1/4} \approx 31$ and density $\rho \approx 3\,\mathrm{g/cm}^3$. SIMPs do not reach direct detection experiments, situated about a km underground.

Some direct detection searches have been performed by balloon experiments at high altitudes. The authors of [160] claim that it is questionable whether such experiments exclude a SIMP with density $\rho_{\mathrm{SIMP}} = \rho_\chi$. Our predicted abundance $\rho_{\mathrm{SIMP}} \sim 10^{-4}\rho_{\mathrm{DM}}$ is allowed.

After thermalisation, SIMPs diffuse with thermal velocity $v_{\mathrm{thermal}} \approx \sqrt{6T/M_{\mathcal{Q}}} \approx 40\,\mathrm{m/s}$ at temperature $T \approx 300$ K. In the Earth gravitational field $g = 9.8\,\mathrm{m/s}^2$, SIMPs not bound to nuclei sink with a small drift velocity that can be estimated as follows. Each collision randomises the SIMP velocity because $v_{\mathrm{drift}} \ll v_{\mathrm{thermal}}$. Thereby the drift velocity is the velocity $v_{\mathrm{drift}} \approx g\tau/2$ acquired during the time $\tau \approx d/v_{\mathrm{thermal}}$ between two scatterings, where $d = 1/(\sum_A n_A\sigma_A) \sim 0.1\,\mathrm{mm}$ in the Earth crust. Thereby the sinking velocity is

$$v_{\mathrm{drift}} \approx 0.1\,\mathrm{km/yr}. \tag{3.25}$$

Diffusion gives a non-uniform SIMP density on the length-scale $T/M_{\mathcal{Q}}g \approx 25\,\mathrm{m}$ dictated by the Boltzmann factor $e^{-M_{\mathcal{Q}}gh/T}$.

Finally, SIMP concentrate around the center of the Earth, where they annihilate heating of the Earth [160]. Bounds on such effect imply that the SIMP abundance must be sub-dominant with respect to the DM abundance, $\rho_{\mathrm{SIMP}} < 10^{-3}\rho_{\mathrm{DM}}$. This bound is satisfied in our model, where $\rho_{\mathrm{SIMP}} \sim 10^{-4}\rho_{\mathrm{DM}}$.

The situation is somehow different if SIMPs bind with (some) nuclei, either during BBN (mostly forming He), or by colliding with nuclei in the Earth atmosphere (possibly mostly forming N, O, He, H) or crust. A SIMP contained in a hybrid nucleus with charge $Z \sim 1$ has a much bigger energy loss in matter, as computed by Bethe

$$\frac{dE}{dx} \approx \frac{Kz^2}{\beta^2} \ln\frac{2m_e\beta^2}{I}, \qquad K = \frac{4\pi\alpha^2 n_e}{m_e}, \qquad I \sim Z\,10\,\mathrm{eV}. \tag{3.26}$$

The mean free path in Earth of a SIMP in a charged state is thereby $L_\pm \sim M_{\mathcal{Q}}\beta^4/K \sim 2\ 10^{-5}\,\mathrm{cm}\,(\beta/0.001)^4$. Again, SIMPs do not reach underground detectors. The main difference is that SIMPs bound in nuclei sink in the ocean and in the primordial Earth, but not in the solid crust, where electric atomic forces keep their positions fixed on geological time-scales.

| Element Studied | $N_{\rm SIMP}/N_N$ at $M_{\rm SIMP} = 10\,{\rm TeV}$ Bound | Expectation? | Formation Mechanism |
|---|---|---|---|
| He space | – | $10^{-10}$ | BBN |
| Be Earth | $7\,10^{-9}$ [156] | No | BBN |
| Oxygen water | $3\,10^{-14}$ [156] | No | accumulation |
| Enriched petro-$C^{14}$ | $10^{-16}$ [156] | $10^{-15}$? | accumulation |
| Iron Earth | $10^{-12}$ [162] | $10^{-15}$? | accumulation |
| Meteorites | $4\,10^{-14}$ [126] | $10^{-14}$? | capture |

Table 3.2: *Experimental bounds on the density of Strongly Interacting Massive Particles with non-exotic electric charges, compared to the expected abundance of our hybrid, roughly estimated assuming that it binds in nuclei (otherwise they sink), and assuming* $f_{\rm SIMP} \approx 10^{-5}$.

### 3.3.2 Searches for accumulated hybrid hadrons

Experimental searches for accumulated SIMPs consist in taking a sample of matter, and searching if some atom has an anomalous mass or charge, see [163] for a recent review. The results, detailed below, imply relative abundances smaller than $\mathcal{O}(1/N_A)$ (inverse of the Avogadro number) *in the selected samples.*

The searches often involve a first phase of sample enrichment in hybrids (for example centrifuge treatment of a sample of water, or use of radioactive materials), followed by a second phase of hybrid detection, with the most successful being the mass spectroscopy and Rutherford backscattering [126].

Limits on the SIMP fraction in the sample depend on the SIMP mass: in the range GeV to TeV, the best bounds are derived from mass spectroscopy of enriched sea water samples [164]. Here the hypothetical particle is a positively charged SIMP, which could form heavy water replacing a proton. The bounds on the relative abundance are of order $N_{\rm SIMP^+}/N_N < 10^{-27}$ where $N_N$ is the number of nuclei.

For heavier SIMPs, mass spectroscopy seems to provide weaker limits. Stringent limit stems from studies of material from meteorites. In [126] the Rutherford backscattering technique was used to set a limit on the SIMP-to-nucleon number density in the tested meteorites that covers the range $100\,{\rm GeV} < M_{\rm SIMP} < 10^7\,{\rm GeV}$. This technique does not depend on the SIMP charge and thus also applies to neutral SIMPs. For $M_{\rm SIMP} \sim 10\,{\rm TeV}$ the limit is [126]

$$\frac{N_{\rm SIMP}}{N_n} \lesssim 3\ 10^{-14} \frac{10\,{\rm TeV}}{M_{\rm SIMP}} \qquad \text{(meteorites)} \tag{3.27}$$

where $N_n$ is the number of nucleons.

These bounds should be compared with the predicted SIMP abundance in the selected sam-

ples. If the tested samples were representative of the average cosmological composition, our model would predict

$$\left.\frac{N_{\rm SIMP}}{N_n}\right|_{\rm cosmo} = \frac{m_N}{M_{\mathcal{Q}}}\frac{\Omega_{\rm SIMP}}{\Omega_b} = 5\ 10^{-9}\frac{10\,{\rm TeV}}{M_{\mathcal{Q}}}\frac{f_{\rm SIMP}}{10^{-5}} \tag{3.28}$$

having used the cosmological density of baryonic matter, $\Omega_b h^2 \approx 0.022$, and of DM, $\Omega_{\rm DM} h^2 \approx 0.12$. The predicted abundance in the selected samples is much lower than the cosmological average and depends on their geological history.

### 3.3.3 Abundance of hybrid hadrons in the Earth

Testing a sample of sea water does not lead to bounds, because the atoms that contain heavy hybrid hadrons sink to the bottom. Similarly, the Earth once was liquid, so that the primordial heavy hybrids sank to the core of the Earth.[6]

Objects made of normal matter accumulate SIMPs due to collisions with SIMP relics in the interstellar medium. Heavy hybrids accumulated in the Earth crust, if captured by nuclei, presumably stopped sinking after that the crust solidified. In order to set bounds, we thereby consider the SIMPs captured by the Earth in the time $\Delta t \sim 4\,{\rm Gyr}$ passed since it is geologically quasi-stable. We ignore convective geological motion. The Earth is big enough to stop all SIMPs, so that the total mass of accumulated SIMPs is

$$M \sim \rho_{\rm SIMP} v_{\rm rel} \pi R_E^2\, \Delta t \sim 2.5\ 10^{10}\,{\rm kg}\,\frac{f_{\rm SIMP}}{10^{-5}} \tag{3.29}$$

having inserted the escape velocity from the Galaxy $v \sim 10^{-3}$ and assumed that the SIMP galactic density follows the DM matter halo density $\rho_{\rm DM} \approx 0.3\,{\rm GeV/\,cm^3}$ as $n_{\rm SIMP} = f_{\rm SIMP}\rho_{\rm DM}/M_{\rm SIMP}$. The rate of $\mathcal{Q}\bar{\mathcal{Q}}$ annihilations of stopped SIMPs is negligible, because suppressed by $e^{-M_{\mathcal{Q}} r}$ where $r$ is the macroscopic distance between $\mathcal{Q}$ and $\bar{\mathcal{Q}}$.[7]

The number of SIMPs accumulated in the Earth is

$$\left.\frac{N_{\rm SIMP}}{N_n}\right|_{\rm Earth} = \frac{M}{M_{\mathcal{Q}}}\frac{m_N}{M_{\rm Earth}} \approx 4\ 10^{-19}\frac{10\,{\rm TeV}}{M_{\mathcal{Q}}}\frac{f_{\rm SIMP}}{10^{-5}}\frac{v_{\rm rel}}{10^{-3}}. \tag{3.30}$$

If SIMPs are not captured by nuclei and sink as in eq. (3.25), their present density in the crust is negligibly small, $N_{\rm SIMP}/N_n \sim 10^{-23}$. If SIMPs get captured in nuclei, a significant fraction of such SIMPs could be in the crust, with a local number density higher by some orders of magnitude. In Fig. 3.4 we plot the bound from Earth searches assuming that all SIMPs stop in the atmosphere and sink slowly through earth until captured by a nucleus, which might happen

[6] The Earth crust contains significant abundances of some heavier elements: those that preferentially form chemical bounds with light elements, reducing the average density. This possibility does not hold for too heavy hybrids with mass $\sim 10\,{\rm TeV}$.

[7] The SIMP thermonuclear energy content $Mc^2$ could be artificially released through $\mathcal{Q}\bar{\mathcal{Q}}$ annihilations, and is about $10^4$ times larger than the world fossil energy reserve, $10^{23}\,{\rm J}$.

in the upper 10 km. The capture cross section with nuclei is discussed below.

### 3.3.4 Abundance of hybrid hadrons in meteorites

Meteorites result from accumulation of interstellar dust and contain heavy elements. The tested meteorites consist mainly of carbon and/or iron. These elements have not been produced by Big-Bang-Nucleosynthesis, which produced H and He ($Z \leqslant 2$), nor by cosmic ray fission, which produced Li, Be, B ($Z \leqslant 5$). Heavier elements have been synthesized from nuclear burning in stars and have later been dispersed away through various explosive processes: core-collapse supernovæ, accretion supernovæ, merging neutron stars and $r$-process nucleosynthesis. Primordial SIMPs would have sunk to the center of stars, and would have presumably remained trapped there, undergoing $\mathcal{Q}\bar{\mathcal{Q}}$ annihilations.

Thereby, the SIMP relative abundance in meteorites made of heavy elements is expected to be significantly smaller than the average relative cosmological abundance.

In order to set bounds we compute the amount of SIMPs accumulated in meteorites. Meteorites are the oldest objects in the solar system and are so small that heavy hybrids do not sink in them. While the Earth is large enough that it captures all SIMPs intercepted by its surface, we consider meteorites small enough that the opposite limit applies: SIMPs are captured by all nuclei within the volume of the meteorite. Thus we need to estimate the probability $\wp$ that a nucleus captured a SIMP in a time $\Delta t$:

$$\left.\frac{N_{\rm SIMP}}{N_n}\right|_{\rm meteorite} = \wp = n_{\rm SIMP}\sigma_{\rm capture}v_{\rm rel}\Delta t \approx 7\ 10^{-12}\frac{\sigma_{\rm capture}}{1/\Lambda_{\rm QCD}^2}\frac{10\,{\rm TeV}}{M_{\rm SIMP}}\frac{f_{\rm SIMP}}{10^{-5}}\frac{\Delta t}{5\,{\rm Gyr}}\frac{v_{\rm rel}}{10^{-3}}. \tag{3.31}$$

This value is roughly two orders of magnitude above the meteorite bound in eq. (3.27).

However, the capture cross sections of SIMP by nuclei are very uncertain. Taking into account that they are not coherently enhanced, the maximal value is the area of the nucleus, $\sigma_{\rm capture} \sim A^{2/3}/\Lambda_{\rm QCD}^2$ [165]. The measured capture cross sections of neutrons by nuclei are smaller: in most cases $\sigma_{\rm capture} \sim 0.01/\Lambda_{\rm QCD}^2$ at MeV energies. Assuming this capture cross section we obtain the possible meteorite bound

$$f_{\rm SIMP} = \frac{\rho_{\rm SIMP}}{\rho_{\rm DM}} \lesssim 10^{-5}\frac{\sigma_{\rm capture}}{0.01/\Lambda_{\rm QCD}^2} \tag{3.32}$$

plotted in Fig. 3.4 and summarized in Table 3.2. Our SIMPs have MeV energies, but the long-distance attractive force mediated by pions (present for neutrons, where it is the only effect understood from first principles) is absent for $\mathcal{Q}g$ SIMPs, which are isospin singlets. Their capture cross section could be much smaller, and possibly our SIMPs do not form bound states with nuclei, such that meteorite bounds are not applicable.

### 3.3.5 Neutrinos from SIMP annihilations in the Sun

Annihilations of SIMPs accumulated in the center of the sun provide an extra neutrino signal. The capture rate does not depend on the SIMP cross section, given that it is so large that all SIMPs that hit the Sun get captured, such that

$$\Gamma_{\rm capt} = n_{\rm SIMP} v_{\rm rel} \pi R_{\rm sun}^2 \approx \frac{10^{20}}{\rm sec} \frac{f_{\rm SIMP}}{10^{-5}} \frac{12.5\,{\rm TeV}}{M_{\mathcal{Q}}} \tag{3.33}$$

where $R_{\rm sun} \approx 7\ 10^8\,{\rm m}$ is the solar radius. Around the relevant mass, IceCube provides the bound $\Gamma_{\rm ann} \lesssim 7\ 10^{20}\,{\rm sec}^{-1}$ on DM annihilating to $b\bar{b}$ [166]. Our $\mathcal{Q}$ dominantly annihilates to gluons and light quarks, providing a slightly smaller neutrino flux [167]. We thereby conclude that the IceCube bound is satisfied even assuming a SIMP annihilation rate in equilibrium with the capture rate, $\Gamma_{\rm ann} \approx \Gamma_{\rm capt}/2$.

Also DM accumulates in the center of the Sun and, by annihilating to neutrinos, gives a detectable signal in IceCube [166]. For typical parameters, equilibrium between capture and annihilation is achieved ($\Gamma_{\rm ann} \approx \Gamma_{\rm capt}/2$). Hence, given that the capture cross section depends on the DM-nucleon cross section and the DM mass, the neutrino flux expected by these annihilations depends on the cross section for DM direct detection. The IceCube bounds are weaker than those from direct detection experiments, and satisfied in our model [166].

## 3.4 Dark matter signals

In our model DM is a $\mathcal{Q}\mathcal{Q}$ hadron. In this section we discuss the DM signals: direct detection (section 3.4.1), indirect detection (section 3.4.2) and collider (section 3.4.3).

### 3.4.1 Direct detection of DM

Direct detection of DM is a low energy process, conveniently described through effective operators. Composite DM gives operators which can be unusual with respect to those characteristic of elementary DM with tree-level-mediated interactions to matter. For example, a fermionic bound state can have a magnetic dipole moment, which is strongly constrained. In our case DM is a non-relativistic scalar bound state $\mathcal{Q}\mathcal{Q}$ made of two colored neutral fermions $\mathcal{Q}$. Its dominant interaction with low-energy gluons is analogous to the Rayleigh scattering of photons from neutral hydrogen. Describing our $\mathcal{Q}\mathcal{Q}$ bound state as a relativistic field $B$ with canonical dimension one, we can write an effective Lagrangian valid up to energies of order $\mathcal{O}(\alpha_3^2 M_{\mathcal{Q}})$:

$$\mathscr{L}_{\rm eff} = C_S^g \mathcal{O}_S^g + C_{T_2}^g \mathcal{O}_{T_2}^g = M_{\rm DM} \bar{B} B [c_E \vec{E}^{a2} + c_B \vec{B}^{a2}]. \tag{3.34}$$

The first expression employs the conventional basis of operators

$$\mathcal{O}_S^g = \frac{\alpha_3}{\pi}\bar{B}B(G^a_{\mu\nu})^2\,, \qquad \mathcal{O}^g_{T_2} = -\frac{\bar{B}\partial^\mu\partial^\nu B}{M^2_{\rm DM}}\mathcal{O}^g_{\mu\nu} \overset{E\ll M_Q}{\simeq} -\frac{\bar{B}B}{2}[(G^a_{0i})^2 + (G^a_{ij})^2] \tag{3.35}$$

where $(G^a_{\mu\nu})^2 = 2(\vec{B}^{a2} - \vec{E}^{a2})$ and $\mathcal{O}^g_{\mu\nu} \equiv G^{a\rho}_\mu G^a_{\nu\rho} - \frac{1}{4}\eta_{\mu\nu}G^a_{\rho\sigma}G^{a\rho\sigma}$. In the second expression we rewrote them in terms of the chromo-electric $E^a_i = G^a_{0i}$ and chromo-magnetic $\vec{B}^a$ components, such that $c_E$ is $4\pi$ times the chromo-electric polarizability of the bound state, $c_E \sim 4\pi a^3$ where $a = 2/(3\alpha_3 M_\mathcal{Q})$ is its Bohr-like radius. Furthermore $c_B \ll c_E$ is suppressed by the velocity $v \sim \alpha_3$ of the $\mathcal{Q}$ in the bound state. Neglecting the chromo-magnetic interaction, the coefficients renormalized at the high scale (that we approximate with $M_Z$) are

$$C^g_{T_2}(M_Z) = -M_{\rm DM}c_E, \qquad C^g_S(M_Z) = \frac{C^g_{T_2}(M_Z)}{4}\frac{\pi}{\alpha_3}. \tag{3.36}$$

The low energy effective coupling of DM to nucleons is $f_N|B|^2\bar{N}N$ [168] with

$$\frac{f_N}{m_N} = -12C^g_S(M_Z)f_g - \frac{3}{4}C^g_{T_2}(M_Z)g(2,M_Z) \tag{3.37}$$

where $f_g = 0.064$ and $g(2, M_Z) = 0.464$. The spin-independent direct detection cross-section is

$$\sigma_{\rm SI} = \frac{f_N^2}{4\pi}\frac{m_N^2}{M^2_{\rm DM}} \approx 2.3\ 10^{-45}\,{\rm cm}^2 \times \left(\frac{20\,{\rm TeV}}{M_{\rm DM}}\right)^6\left(\frac{0.1}{\alpha_3}\right)^8\left(\frac{c_E}{1.5\pi a^3}\right)^2. \tag{3.38}$$

This is close to the XENON1T bound [169], $\sigma_{\rm SI} \lesssim 3\ 10^{-44}\,{\rm cm}^2 \times M_{\rm DM}/20\,{\rm TeV}$, that holds at $M_{\rm DM} \gg 100\,{\rm GeV}$ up to the standard assumptions about the DM galactic halo.

Thereby we perform a dedicated computation of the $c_E$ coefficient, which is possible in perturbative QCD. Adapting the techniques developed for the hydrogen atom and for bottomonium [170], the effective Lagrangian of eq. (3.34) also describes the shift in the $\mathcal{Q}\mathcal{Q}$ ground-state energy induced by external chromo-electric and chromo-magnetic fields:

$$H_{\rm eff} = -\frac{1}{2}[c_E\vec{E}^{a2} + c_B\vec{B}^{a2}]. \tag{3.39}$$

The external field $\vec{E}^a$ adds a chromo-dipole interaction to the non-relativistic Hamiltonian of the $\mathcal{Q}\mathcal{Q}$ bound state, as well as the associated non-abelian effects. Perturbation theory at second order then gives a shift in the ground state energy $E_{10}$, which allows one to reconstruct $c_E$ as

$$c_E = \frac{8\pi\alpha_3}{3}\frac{C}{N_c^2-1}\langle B|\vec{r}\frac{1}{H_8 - E_{10}}\vec{r}|B\rangle \tag{3.40}$$

where $|B\rangle$ is the $\mathcal{Q}\mathcal{Q}$ ground state, $N_c = 3$ and $C$ is the Casimir coefficient, defined by $C\delta_{ij} = (T^aT^a)_{ij}$ and equal to 3 for our assumed octet representation. Summing over all al-

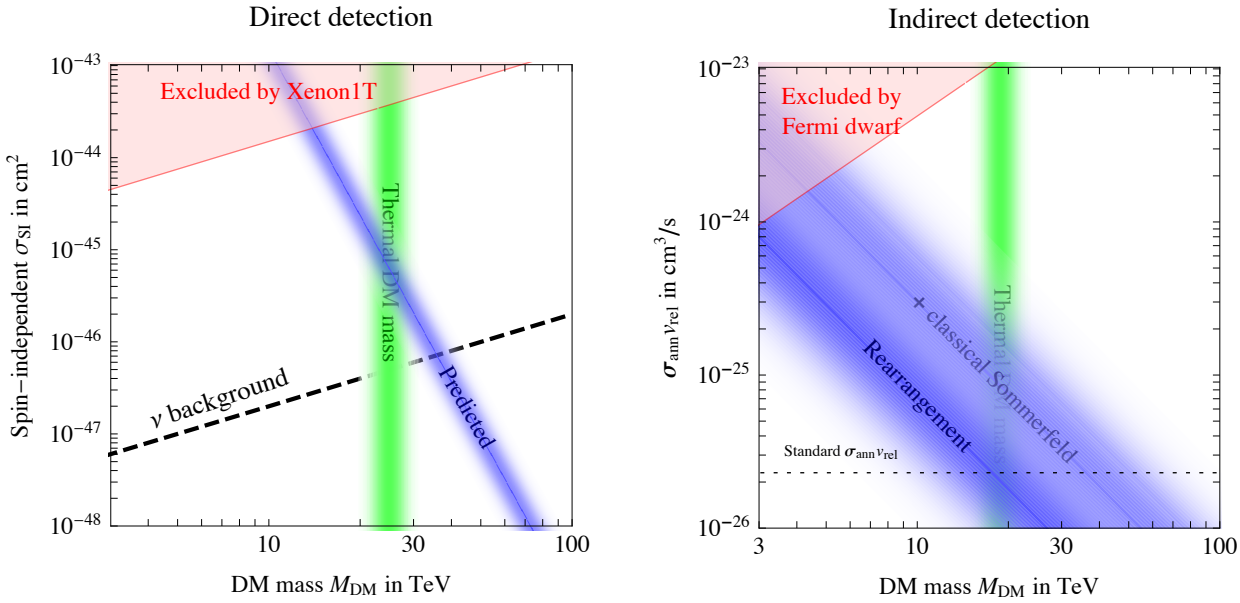


Figure 3.6: **Left**: *Direct detection signals of $\mathcal{QQ}$ dark matter, as computed in section 3.4.1. We also show the neutrino floor, which will eventually limit future direct searches.* **Right**: *Indirect detection signals as computed in section 3.4.2. We show the current dwarf galaxy constraints by FermiLAT, which have only a mild systematic uncertainty due to the dark matter J-factor, and the future sensitivity of the CTA [171] experiment to photons from dwarf galaxies.*

lowed intermediate states with free Hamiltonian $H_8$ in the octet channel we find (see Appendix E)

$$c_E|_{\rm DM} = (0.36 + 1.17)\pi a^3 \tag{3.41}$$

where the first (second) contribution arises from intermediate bound (free) states. The non-abelian nature of QCD manifests in the fact that the allowed intermediate states are $p$-wave color octets: they are less bound (relatively to the ground state) than in the hydrogen atom case, such that our $c_E$ coefficient is significantly smaller than what would be suggested by a naive rescaling of the abelian result.

Eq. (3.41) is the coefficient used as a reference value in the cross section of eq. (3.38). Higher order QCD interactions and relativistic effects conservatively amount up to a 50% uncertainty. As plotted in Fig. 3.6a our predicted DM mass $M_{\rm DM} \approx 25\,\text{TeV}$ is higher than the DM mass excluded by direct detection, $M_{\rm DM} \gtrsim 14\,\text{TeV}$.

### 3.4.2 Indirect detection of DM

Two DM particles in the galactic halo can annihilate into gluons and quarks giving rise to indirect detection signals. The energy spectra of the resulting final-state stable particles ($\bar{p}$, $\bar{e}$, $\gamma$, $\nu$) is well approximated by the general results of non-relativistic annhilations computed in [172]. We need to compute the annihilation cross section between the DM = $\mathcal{QQ}$ Coloumbian bound state

and $\overline{\mathrm{DM}} = \bar{\mathcal{Q}}\bar{\mathcal{Q}}$. It is enhanced and dominated by the recombination process

$$(\mathcal{Q}\mathcal{Q}) + (\bar{\mathcal{Q}}\bar{\mathcal{Q}}) \to (\mathcal{Q}\bar{\mathcal{Q}}) + (\mathcal{Q}\bar{\mathcal{Q}}) \tag{3.42}$$

followed by later $\mathcal{Q}\bar{\mathcal{Q}}$ annihilations to SM particles. This is similar to what happens for hydrogen/anti-hydrogen annihilation, which proceeds through recombination $(ep) + (\bar{e}\bar{p}) \to (e\bar{e}) + (p\bar{p})$ followed by later $e\bar{e}$ and $p\bar{p}$ annihilations, giving rise to a large $\sigma_{\rm ann} v_{\rm rel} \sim 1/\alpha m_e^2$, of atomic-physics size, rather than of particle-physics size, $\sigma_{\rm ann} v_{\rm rel} \sim \alpha^2/m_{e,p}^2$. Detailed quantum computations have been performed for $m_p \gg m_e$ [173]. This simplifying approximation is not valid in our case. Rather, the common mass $M_{\mathcal{Q}}$ implies that DM recombinations are not exotermic, such that the cross section should be constant for small $v_{\rm rel}$ (up to long distance effects). Since the scale associated to the bound state is the Bohr radius we estimate

$$\sigma_{\rm ann} \sim \pi a^2 \tag{3.43}$$

For indirect detection experiments $\sigma v_{\rm rel}$ is thus suppressed by the DM velocity: Fig. 3.6b shows the result for $v_{\rm rel} \sim 10^{-3}$.

Long distance Sommerfeld effects could enhance the DM recombination cross section at $v_{\rm rel} \ll \alpha_3$. Classically, this can be estimated as follows. The interaction between two neutral atoms at distance $r \gg a$ is given by the non-abelian Van der Waals electric attraction, $V_{\rm el} \approx -0.7 a^6/r^7$ [174, 170, 175], having used eq. (3.41) for the numerical coefficient. A 4-particle intermediate state forms if $K > \max_r V_{\rm eff}(r)$ where $V_{\rm eff} = V_{\rm el} + L^2/2M_{\mathcal{Q}} r^2$ is the usual effective potential. This determines the maximal impact parameter $b_{\rm max}$, and thereby the cross section[8]

$$\sigma_{\rm ann} v_{\rm rel} \sim \pi b_{\rm max}^2 v_{\rm rel} \sim \frac{v_{\rm rel}^{3/7}}{\alpha_3^{12/7} M_{\mathcal{Q}}^2} \qquad (\alpha_3^{5/2} \ll v_{\rm rel} \ll \alpha_3). \tag{3.44}$$

This estimate is also shown in Fig. 3.6b. At astrophysically low velocities $v_{\rm rel} \sim 10^{-3} \lesssim \alpha_3^{5/2}$ the magnetic dipole interaction $V_{\rm mag} \sim \alpha_3/r^3 M_{\mathcal{Q}}^2$ becomes as important as the electric interaction, giving $\sigma_{\rm ann} v_{\rm rel} \sim \alpha_3^{2/3}/M_{\mathcal{Q}}^2 v_{\rm rel}^{1/3}$. However, a quantum computation is needed even to get the correct parametric dependence.

In any case, indirect detection signals are below present bounds, as shown in Fig. 3.6b. We plotted bounds on gamma ray emission from dwarfs, given that searches in the galactic center region are subject to large astrophysical uncertainties, and other bounds are weaker.

[8] A more precise result can be obtained from a classical computation. Focusing on the color singlet channel, we numerically compute the classical motion of a $\mathcal{Q}\mathcal{Q}$ bound state in its ground state (circular orbit with radius $a$ in some plane) which collides with relative velocity $v_{\rm rel}$ and impact parameter $b$ with a similar $\bar{\mathcal{Q}}\bar{\mathcal{Q}}$ system. When the two bound states get closer and interact they can produce two $\mathcal{Q}\bar{\mathcal{Q}}$ bound states, which later annihilate. Confinement takes place at larger distances and plays a negligible role. By averaging over the relative orientations of the two systems and over the impact parameter gives the classical probability for this process, encoded into a velocity dependent cross section.

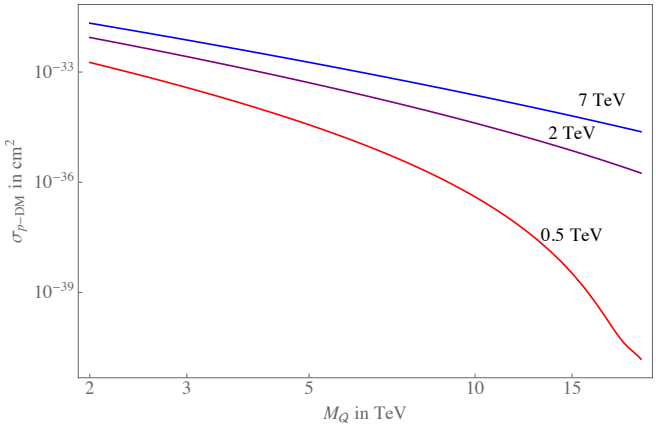


Figure 3.7: *Cross-section for excitation of the $\mathcal{QQ}$ DM ground state with a proton beam at* 0.5 *(red),* 2 *(purple),* 7 *(blue)* TeV*.*

### 3.4.3 Collider signals of DM

While DM usually gives missing-energy signals which are hardly detectable at hadron colliders, DM made of colored quorns $\mathcal{Q}$ gives very visible signals. Indeed, DM constituents $\mathcal{Q}$ are pair produced at colliders via QCD interactions. After hadronization they form hadrons. Presumably the neutral $\mathcal{Q}g$ is stable, and the charged $\mathcal{Q}q\bar{q}'$ are long-lived on collider time-scales, giving rise to tracks. Experiments at the LHC $pp$ collider at $\sqrt{s} = 13\,\mathrm{TeV}$ set the bound $M_{\mathcal{Q}} \gtrsim 2\,\mathrm{TeV}$ [176]. A larger $\sqrt{s} \sim 85\,\mathrm{TeV}$ is needed to discover the quorn with the mass expected from cosmology, $M_{\mathcal{Q}} \sim 12.5\,\mathrm{TeV}$. A $pp$ collider with $\sqrt{s} = 100\,\mathrm{TeV}$ would be sensitive up to $M_{\mathcal{Q}} \lesssim 15\,\mathrm{TeV}$ [177], as long as the detector can see the signal.

Furthermore, we explore the possibility of detecting collisions of protons in collider beams with ambient $\mathcal{QQ}$ DM. The $\mathcal{QQ}$ binding energy is $E_B \sim 200\,\mathrm{GeV}$. Protons with energies much larger than $E_B$ see the $\mathcal{QQ}$ system as two free $\mathcal{Q}$ and the QCD cross section is suppressed by the energy squared. Protons with energies comparable to $E_B$ see the system as a ball with Bohr radius $a = 2/3\alpha_3 M_{\mathcal{Q}}$. The cross-section for the excitation of the ground state through the absorption of a gluon can be estimated as the cross-section for ionization computed in [55, 66]

$$\sigma = 36\pi^2\alpha_3 a^2 \left(\frac{E_B}{E_g}\right)^4 \frac{1 + 9/4\zeta^2}{1 + 9\zeta^2} \frac{e^{-6\zeta \mathrm{arccot}(3\zeta)}}{1 - e^{-3\pi\zeta}} \tag{3.45}$$

where $E_g$ is the gluon energy and $\zeta = \alpha_3/v_{\mathrm{rel}} = 1/(3ap_{\mathrm{DM}})$ parametrises the momentum of $\mathcal{Q}$ in the final state. Energy conservation implies $E_g \approx E_B + M_{\mathrm{DM}} v_{\mathrm{rel}}^2/4$. Fig. 3.7 shows the proton-DM cross-section obtained convoluting with parton distribution functions. The event rate in a beam containing $N_p$ protons is small,

$$\frac{dN_p}{dt} = N_p \sigma \frac{\rho_{\mathrm{DM}}}{2M_{\mathcal{Q}}} = \frac{3}{\mathrm{year}} \frac{N_p}{10^{20}} \frac{\rho_{\mathrm{DM}}}{0.3\,\mathrm{GeV/cm^3}} \frac{20\,\mathrm{TeV}}{2M_{\mathcal{Q}}} \frac{\sigma}{10^{-33}\,\mathrm{cm}^2}. \tag{3.46}$$

$\mathcal{QQ}$ dark matter excitation by cosmic rays is negligible on cosmological time-scales.

## 3.5 Summary

We have shown that Dark Matter can be obtained from a colored neutral quark $\mathcal{Q}$ (dubbed *quorn*), that, after the QCD phase transition, forms deeply bound hadrons made of $\mathcal{Q}$ only (dubbed *quorn-onlyum*), plus traces of hybrid hadrons made of $\mathcal{Q}$ together with SM gluons or quarks (dubbed Strongly Interacting Massive Particles or SIMP). We explored the simplest model, where $\mathcal{Q}$ is a stable neutral Dirac fermion in the adjoint representation of $\mathrm{SU}(3)_c$. Such a state could be a Dirac gluino, or appear in natural axion models (see section 3.1).

Fig. 3.5 shows the cosmological evolution of the DM and hybrid abundances for the value of the quorn mass, $M_{\mathcal{Q}} \approx 12.5\,\mathrm{TeV}$, which reproduces the DM cosmological abundance as discussed in section 3.2. A first decoupling occurs, as usual, at $T \sim M_{\mathcal{Q}}/25$. Quorns recouple while the universe cools approaching the QCD phase transition at $T \sim \Lambda_{\mathrm{QCD}}$. This opens a phase of chromodark-synthesis: quorns fall into $\mathcal{QQ}$ singlet bound states, which have a binding energy $E_B \sim 200\,\mathrm{GeV}$. The cross sections grow large, up to $\sigma_{\mathrm{QCD}} \sim 1/\Lambda^2_{\mathrm{QCD}}$, because excited states with large angular momenta $\ell$ are formed. Such states efficiently cool falling to the ground state before being broken, as computed in section 3.1.5 where we show that quantum states with $n, \ell \gg 1$ are well approximated by classical physics. It is important to take into account that (non-abelian) Larmor radiation from elliptic orbits is much larger than for circular orbits.

Details of this uncertain phase are not much important for the final result: one half of free quorns annihilate, one half end up in $\mathcal{QQ}$ DM; the small residual abundance of $\mathcal{Q}g$ hybrids, $\rho_{\mathrm{SIMP}}/\rho_{\mathrm{DM}}$ between $10^{-3}$ and $10^{-6}$, is mostly determined at $T \sim 30\,\mathrm{MeV}$, when the states decouple again.

In section 3.4 we studied DM phenomenology. The quorn-onlyum DM state $\mathcal{QQ}$ with mass $M_{\mathrm{DM}} \approx 2M_{\mathcal{Q}} \approx 25\,\mathrm{TeV}$ has small residual interactions suppressed by powers of $1/M_{\mathcal{Q}}$. The cross section for direct DM detection is of Rayleigh type, suppressed by $1/M^6_{\mathcal{Q}}$. In section 3.4.1 we performed a non-trivial QCD bound-state computation, finding a cross section just below present bounds. The cross section for indirect DM detection is enhanced by recombination, $(\mathcal{QQ}) + (\bar{\mathcal{Q}}\bar{\mathcal{Q}}) \to (\mathcal{Q}\bar{\mathcal{Q}}) + (\mathcal{Q}\bar{\mathcal{Q}})$, and still compatible with bounds (section 3.4.2). At colliders quorns manifest as (quasi)stable charged tracks: LHC sets the bound $M_{\mathcal{Q}} \gtrsim 2\,\mathrm{TeV}$.

In section 3.3 we studied the SIMP hybrid states, which have large cross sections of order $1/\Lambda^2_{\mathrm{QCD}}$ and a relic abundance 3 or more orders of magnitude smaller than DM. In view of this, they seem still allowed by the experiments which excluded SIMP DM ($\rho_{\mathrm{SIMP}} = \rho_{\mathrm{DM}}$), although a dedicated project would be needed to predict their properties. Our model contains two kind of SIMPs: the isospin-singlet $\mathcal{Q}g$ with no interaction to pions; and the isospin triplet $\mathcal{Q}q\bar{q}'$. Presumably the latter are heavier and decay. We do not know whether $\mathcal{Q}g$ can bind with (large enough?) nuclei, and how they would bind during Big Bang Nucleosynthesis, given that there is no first-principle understanding of nuclear potentials. The following statements

are safe: our predicted SIMP abundance is so small that they negligibly affect ordinary BBN; SIMPs get stopped by the Earth atmosphere and are not visible in underground detectors; SIMP annihilations negligibly heat the Earth.

The interpretation of searches for rare hybrid heavy nuclei in samples of materials depends on the history of SIMPs and of the selected samples: from the Big Bang, to star burning, through Earth geology. The primordial abundance of SIMPs in the Earth and in stars sank down to their centres, undergoing $\mathcal{Q}\bar{\mathcal{Q}}$ annihilations. Thereby, in order to set bounds, we consider the smaller secondary abundance of SIMPs. Presumably most primordial SIMPs still are in galactic clouds, and the Earth is big enough to capture all SIMPs encountered along its trajectory. The total energy stored in captured SIMPs likely exceeds the energy of the world fossile fuel reserve by $10^4$. What happens after capture is unclear. If SIMPs do not bind in nuclei, they sink in the Earth ocean and crust with drift velocity $v \sim 0.1\,\mathrm{km/yr}$, such that their ground-level abundance is much below existing bounds. They can be searched for through dedicated enrichment processes and Rutherford backscattering experiments. If instead SIMPs bind within nuclei, electromagnetic interactions keep them in the crust since when the crust become geologically stable. Then, the local SIMP density can be comparable to present bounds, depending on the capture cross section by nuclei, which is highly uncertain.

SIMP searches have been also performed in meteorites, where SIMPs cannot sink. Despite this, meteorites are made of heavy elements synthesised by stars: primordial SIMPs sank to the center of stars, and never come back. The secondary abundance of SIMPs in meteorites depends on the SIMP capture cross section by individual nuclei, which is highly uncertain and possibly vanishing. Present bounds are satisfied assuming a SIMP capture cross sections comparable to the one of neutrons with similar MeV energy, $\sigma_{\mathrm{capture}} \sim 0.01/\Lambda^2_{\mathrm{QCD}}$.

In conclusion, colored DM seems still allowed, although close to various bounds. Direct detection seems to provide the strongest and more reliable probe.

We discussed the most promising model of colored DM: a neutral Dirac fermion $\mathcal{Q}$ in the adjoint representation of color. A scalar would give a similar phenomenology, and the DM abundance would be reproduced thermally for a similar $M_{\mathcal{Q}} \sim 12.5\,\mathrm{TeV}$. A smaller mass would be obtained for quorns in the fundamental of $\mathrm{SU}(3)_{\mathrm{c}}$, although the mass of the quorn-onlyum DM state $\mathcal{Q}\mathcal{Q}\mathcal{Q}$ would be $M_{\mathrm{DM}} \approx 3M_{\mathcal{Q}}$. In models where $\mathcal{Q}$ has an asymmetry, the DM abundance can be obtained for lower $M_{\mathcal{Q}}$ (though this would make more difficult to evade experimental bounds on hybrid states).

# Chapter 4

## Bound states from Dark Sectors: part I

From a modern point of view the SM is understood as an effective field theory with a very high ultraviolet cut-off, which appears renormalizable at energies currently probed in experiments. This feature notoriously gives rise to the SM hierarchy problem, but is also at the very origin of the attractive properties of the SM. In particular, global symmetries arise accidentally in the infrared and explain in the most economical way baryon and lepton number conservation, flavour and electroweak (EW) precision tests. These remarkable properties provide a compelling guidance to build possible extensions of the SM, even at the price of sacrificing the naturalness of the electroweak scale (as hinted anyway by experiments). In particular, the cosmological stability of DM can be elegantly explained in terms of accidental symmetries, in analogy with the stability of the proton following from baryon number conservation. This has to be contrasted with SM extensions where global symmetries are imposed ad hoc, like for example the case of $R$-parity in supersymmetry. A simple way to generate accidental symmetries is to extend the gauge theory structure of the SM by postulating a new confining dark color group. This idea was put forward in [178], where the role of the DM was played by an accidentally stable dark baryon made of dark quarks lighter than the confinement scale, $\Lambda_{\rm DC}$, of the dark-color group, see also [179–186]. In this chapter we explore the opposite regime, *i.e.* we take dark quarks with masses bigger than $\Lambda_{\rm DC}$, see also [187]. This leads to increased predictivity: in the presence of multiple dark-quarks, only the lightest one is typically relevant for DM physics, that is thereby determined in terms of two free parameters, $m_{\mathcal{Q}}$ and $\Lambda_{\rm DC}$.

Furthermore, it leads to novel characteristic signatures.

1. The cosmological history is not standard, and the relic DM abundance is determined in two stages: the dark-quark relic abundance freezes out at $T \sim m_{\mathcal{Q}}/25$ in the usual way, through weakly coupled annihilations with cross section $\sigma_{\mathcal{Q}\bar{\mathcal{Q}}} v_{\rm rel} \sim \pi\alpha_{\rm DC}^2/m_{\mathcal{Q}}^2$. This is followed at $T \sim \Lambda_{\rm DC}$ by a first-order dark phase transition [188], where a fraction of the dark quarks $\mathcal{Q}$ and $\bar{\mathcal{Q}}$ binds into mesons, that decay, and the remaining fraction forms stable dark-matter baryons $\mathcal{B}$ and $\bar{\mathcal{B}}$.

2. The $\mathcal{B}\bar{\mathcal{B}}$ annihilation cross section relevant for indirect DM detection is a few orders of

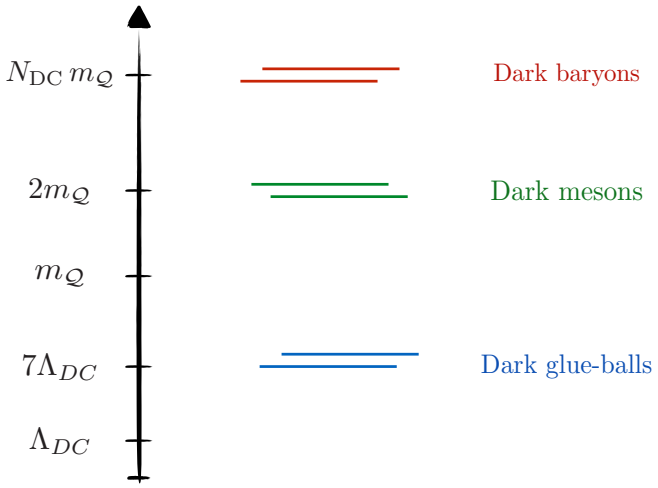


Figure 4.1: *Typical spectrum of the theory. We assume that the lightest dark quark is heavier than the dark confinement scale, $\Lambda_{DC}$. DM is dark baryon made of $N_{\rm DC}$ dark quarks. The lightest dark states are unstable dark glue-balls.*

magnitude larger than the usual $\mathcal{Q}\bar{\mathcal{Q}}$ annihilation cross section, being enhanced by dark-atomic $1/\alpha_{\rm DC}$ effects.

3. Fig. 4.1 illustrates the spectrum of the theory: the dark sector contains unstable dark-glue-balls with mass $M_\Phi \sim \Lambda_{\rm DC}$ which can be much lighter than DM with mass $\sim m_{\mathcal{Q}}$, and thereby potentially accessible to low-energy searches, such as high-luminosity fixed-target experiments. If $M_\Phi$ is larger than the binding energy, some dark quarks could have formed long-lived excited dark baryons, that de-excite emitting $\beta$ or $\gamma$ radio-activity.

The chapter is organized as follows. In section 4.1 we outline the scenario and the main options: SU($N_{\rm DC}$) and SO($N_{\rm DC}$) gauge theories, with dark quarks neutral or charged under the SM gauge group. In section 4.2 we study the bound states: lighter unstable dark glue-balls, dark mesons, stable dark baryons; we compute their binding energies by means of a variational method. In section 4.3 we study how baryon DM can form throughout the cosmological history. In section 4.4 we study signatures in cosmology, direct detection, indirect detection (enhanced by recombination), colliders, high-intensity experiments at lower energy, radioactive DM. Detailed computations in the main specific models are presented in section 4.5. In section 4.6 we conclude summarising the main novel results.

## 4.1 The scenario

We consider DM made of 'dark quarks', new fermions possibly charged under the SM gauge group and charged under a new confining gauge interaction $G_{\rm DC} = {\rm SU}(N_{\rm DC})$ or ${\rm SO}(N_{\rm DC})$. We will dub the new interaction Dark Color (DC). The dark-quarks are assumed to lie in the

fundamental representation of the DC group and to form a vectorial representation $R$ (in general reducible) of the SM

$$\mathcal{Q} \equiv (N_{\rm DC}, R) \oplus (\bar{N}_{\rm DC}, \overline{R}) \tag{4.1}$$

where $N_{\rm DC}$ and $\bar{N}_{\rm DC}$ indicate respectively the fundamental and anti-fundamental representation of the dark-color group, and $R$ is a representation of the SM groups. These theories are described by the renormalizable Lagrangian

$$\mathscr{L} = \mathscr{L}_{\rm SM} - \frac{1}{4g_{\rm DC}^2}\mathcal{G}^A_{\mu\nu}\mathcal{G}^{A\,\mu\nu} + \bar{\mathcal{Q}}_i(i\not{D} - m_{\mathcal{Q}_i})\mathcal{Q}_i + (y_{ij}H\mathcal{Q}_i\mathcal{Q}_j + \tilde{y}_{ij}H^*\mathcal{Q}_i\mathcal{Q}_j + \text{h.c.}) \tag{4.2}$$

where $\mathcal{G}^A_{\mu\nu}$ is the field-strength for the DC interactions. A topological term for the DC sector can be added, but it will not play an important role in the present work. When Yukawa couplings are allowed by the gauge quantum numbers, two independent couplings $y$ and $\tilde{y}$ exist for left and right chiralities of the vector-like fermions, breaking in general parity P and CP. The addition of new vector-like fermions charged under a dark gauge interaction maintains the successes of the SM for what concerns flavor and precision observables. As a consequence, the new physics can lie around the weak scale with no tension with experimental bounds, yet accessible to DM and collider experiments.

The renormalizable theories considered here enjoy accidental symmetries (dark baryon number, species number and generalisations of $G$-parity [189]) that lead to stability of particles that are therefore good DM candidates, if safe from decay by dimension five operators of the form $(\bar{\mathcal{Q}}_i\mathcal{Q}_j)(H^\dagger H)$. We focus on the simplest and more robust possibility: DM as the lightest dark-baryon, made of $\mathcal{Q}^{N_{\rm DC}}$. In fact, taking a GUT or a Planck scale as UV cut-off for our model, the approximate dark baryon number conservation is typically sufficient to guarantee stability over cosmological time scales.

Stability of the $\mathcal{Q}^{N_{\rm DC}}$ dark baryon can remain preserved up to dimension-6 operators in the presence of extra states charged under $G_{\rm DC}$, provided that they have quantum numbers different from $\mathcal{Q}$. Their thermal relic abundance would be sub-leading, if they are much lighter than $\mathcal{Q}$. For example, sticking to fundamentals of $G_{\rm DC}$, the $\mathcal{Q} \to -\mathcal{Q}$ symmetry remains preserved in the presence of a dark scalar $\mathcal{S}$, as long as fermion singlets $\nu_R$ and the consequent $\mathcal{Q}\mathcal{S}^*\nu_R$ operators are absent.

Choices of the gauge quantum numbers that lead to acceptable DM candidates have been presented in the literature [190]. We will adopt the simplest and most successful models.

The new point of our study is that we will study the phenomenology of such models assuming that the constituent dark quarks have masses $m_{\mathcal{Q}}$ larger than the confinement scale of the dark gauge interactions

$$\Lambda_{\rm DC} \approx m_{\mathcal{Q}} \exp\left[-\frac{6\pi}{11\, C_2(G)\, \alpha_{\rm DC}(m_{\mathcal{Q}})}\right] \tag{4.3}$$

where $C_2(\mathrm{SU}(N)) = N$, $C_2(\mathrm{SO}(N)) = 2(N-2)$[1] and $\alpha_{\rm DC}(m_{\mathcal{Q}})$ is the value of the coupling at the scale of the lightest dark quark. The temperature at which the dark confinement phase transition occurs roughly is $\Lambda_{\rm DC}$.

This scenario presents qualitatively novel aspects. Freeze-out of DM constituents $\mathcal{Q}$ occurs at the scale $m_{\mathcal{Q}}/25$ (or larger if there is a dark baryonic asymmetry [186]). At lower temperatures, $\mathcal{Q}$ forms an interacting fluid with dark gluons and possibly with some SM vectors. DM baryons only form in a second 'darkogenesys' stage at a lower temperature, around the dark confinement scale $\Lambda_{\rm DC}$ which could be as light as 100 MeV. For dark quark masses in the TeV range this translates into

$$\alpha_{\rm DC}(m_{\mathcal{Q}}) \approx \frac{6\pi}{11 C_2(G) \ln m_{\mathcal{Q}}/\Lambda_{\rm DC}} \approx 0.06 \frac{3/C_2(G)}{\ln m_{\mathcal{Q}}/(10^4 \Lambda_{\rm DC})}. \tag{4.4}$$

During a first order phase transition, a fraction of the dark quarks manage to form dark baryons, which remain as DM, and the remaining fraction annihilates into dark glue-balls, which later decay into SM particles.

### 4.1.1 Models

In the heavy quark regime, $m_{\mathcal{Q}} \gg \Lambda_{\rm DC}$, the dark baryon mass is roughly the sum of the constituent masses. Then, mixing between baryons made of different species is negligible as long as their mass splitting is larger than the binding energy

$$|m_{\mathcal{Q}_1} - m_{\mathcal{Q}_2}| > \max(\Lambda_{\rm DC}, \alpha_{\rm DC}^2 m_{\mathcal{Q}_1}). \tag{4.5}$$

We will assume that this is the case, such that DM is made of the lightest specie of dark quarks. Then, different gauge quantum numbers of $\mathcal{Q}$ give different models. They fall into two main categories: either $\mathcal{Q}$ is a neutral singlet $N$ under the SM gauge group, or it is charged. In the first case the DM candidate is $\mathcal{Q}^{N_{\rm DC}}$: a dark-baryon with spin $N_{\rm DC}/2$, singlet under the SM. In the second case DM has lower spin.

Let us discuss more in detail theories with charged $\mathcal{Q}$.

In theories with dark gauge group $G_{\rm DC} = \mathrm{SU}(N_{\rm DC})$ candidates with non-vanishing hypercharge are excluded by direct DM searches, so that a successful DM candidate is obtained if the lightest dark quark is a triplet $V$ under $\mathrm{SU}(2)_L$, neutral under $\mathrm{SU}(3)_c \otimes \mathrm{U}(1)_Y$[2]. Avoiding sub-Planckian Landau poles for $\mathrm{SU}(2)_L$ fixes $N_{\rm DC} = 3$.

The situation is different in theories with dark gauge group $G_{\rm DC} = \mathrm{SO}(N_{\rm DC})$: since its vectorial representation is real, the lightest dark baryon is a real particle, fermion or boson. Real particles cannot have a vector coupling to a spin-1 particle, so dark quarks with non-vanishing hypercharge are allowed as long as a small coupling with the Higgs splits the two degenerate real states. Acceptable DM candidates are obtained again for $\mathcal{Q} = V$, but also for

[1] This differs from [190] because we use a different convention for the normalization of $\alpha_{\rm DC}$, reflected by the different index $T = 2$ for the vector of $\mathrm{SO}(N)$, see Table 4.1. The present normalization satisfies $\alpha_{\mathrm{SO}(3)} = \alpha_{\mathrm{SU}(2)}$.

[2] An exception can be provided by models with degenerate dark quarks [191].

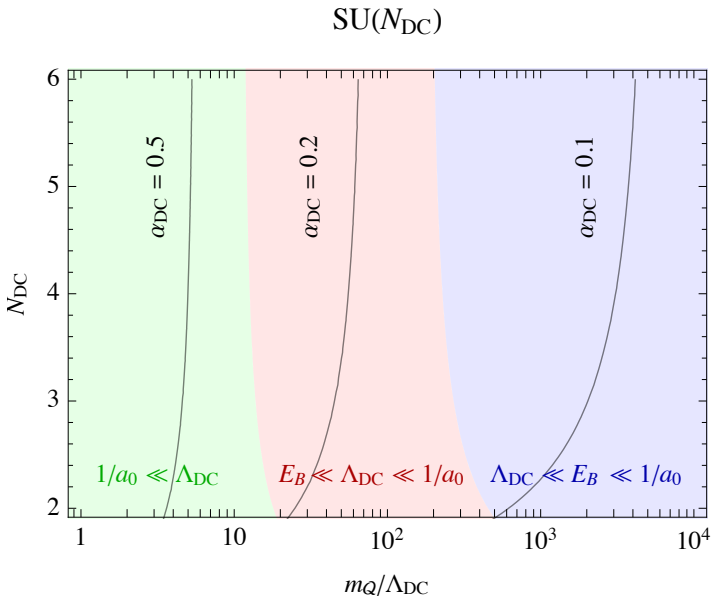


Figure 4.2: *Qualitatively different regions described in the text as function of the mass hierarchy* $m_{\mathcal{Q}}/\Lambda_{DC}$ *and of* $N_{\rm DC}$*, superimposed to a contour plot of* $\alpha_{DC}$ *renormalized at* $m_{\mathcal{Q}}$*. We assumed a* SU($N_{\rm DC}$) *gauge group; similar results hold for* SO($N_{\rm DC}$)*.*

$\mathcal{Q} = L \oplus N \oplus \dots$ or $\mathcal{Q} = L \oplus V \oplus \dots$ , where the lightest dark quark $L$ has the same gauge quantum numbers of a lepton doublet, such that Yukawa couplings to the Higgs are allowed. Such models can give rise to inelastic dark matter phenomenology [192].

## 4.2 The bound states

Dark gluons form dark glue-balls, $\Phi$, with mass $M_\Phi \approx 7\Lambda_{\rm DC}$. Dark quarks bind into dark mesons and dark baryons. In the Coulombic regime the size of dark quark bound states is set by the Bohr radius, $a_0 \sim 1/(\alpha_{\rm DC} m_{\mathcal{Q}})$ with binding energy $E_B \sim \alpha_{\rm DC}^2 m_{\mathcal{Q}}$. We can distinguish three different regimes, depending on the relative ordering of $1/a_0$, $E_B < 1/a_0$ and $\Lambda_{\rm DC}$:

A) If $\Lambda_{\rm DC} \ll E_B \ll 1/a_0$: confinement gives small corrections and bound states are well described by Coulombic potentials. This region roughly corresponds to $\alpha_{\rm DC} \lesssim 0.1$ and $m_{\mathcal{Q}} \gtrsim 10^3 \Lambda_{\rm DC}$ and is plotted in blue in Fig. 4.2 for a SU($N_{\rm DC}$) group.

B) If $E_B \lesssim \Lambda_{\rm DC} \lesssim 1/a_0$ dark baryons form at temperatures around the confinement scale in excited states, that later try to decay into lowest lying Coulombian bound states [187]. This region is plotted in red in Fig. 4.2 and roughy corresponds to $\alpha_{\rm DC} \sim 0.2$ and $m_{\mathcal{Q}} \sim 100\Lambda_{\rm DC}$.

C) If $1/a_0 \ll \Lambda_{\rm DC}$ bound states are similarly to quarkonium in QCD, dominated by confinement phenomena. This region is plotted in green in Fig. 4.2 and roughy corresponds to $\alpha_{\rm DC} \gtrsim 0.4$ and $m_{\mathcal{Q}} \lesssim 10\Lambda_{\rm DC}$.

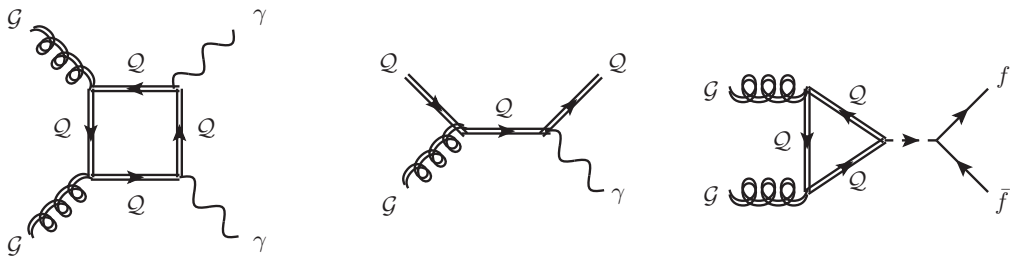


Figure 4.3: *Leading processes describing interactions between the SM and the dark gluons.*

### 4.2.1 Dark glue-balls

Under our assumptions, the lightest bound state in the dark sector are dark glue-balls ($\Phi$), with quantum numbers $J^{PC} = 0^{++}$ and mass $M_\Phi \approx 7\Lambda_{\rm DC}$ [193], which can be much lighter than the DM mass, $N_{\rm DC} m_{\mathcal{Q}}$. Interactions of dark gluons with the SM are induced by loops of dark quarks (possibly DM itself) charged under the SM sector as in Fig. 4.3. Assuming dark quarks with electro-weak charges we estimate the lifetime of the lightest $0^{++}$ glue-ball as (see section 4.4.5 and [194])

$$\tau_\Phi \sim \begin{cases} 10^{-8}\,\mathrm{s}\left(\frac{3}{N_{\rm DC}}\right)^2\left(\frac{500\,\mathrm{GeV}}{M_\Phi}\right)^9\left(\frac{m_{\mathcal{Q}}}{10\,\mathrm{TeV}}\right)^8 & \Phi \to \gamma\gamma \\ 10^{-6}\,\mathrm{s}\left(\frac{3}{N_{\rm DC}}\right)^2\left(\frac{0.1}{y_1 y_2}\right)^2\left(\frac{m_b}{m_q}\right)^2\left(\frac{50\,\mathrm{GeV}}{M_\Phi}\right)^7\left(\frac{\bar{m}_{\mathcal{Q}}}{10\,\mathrm{TeV}}\right)^4 & \Phi \to q\bar{q},\ \text{if } M_\Phi > 2m_q \\ 10^{-14}\,\mathrm{s}\left(\frac{3}{N_{\rm DC}}\right)^2\left(\frac{0.1}{y_1 y_2}\right)^2\left(\frac{500\,\mathrm{GeV}}{M_\Phi}\right)^5\left(\frac{\bar{m}_{\mathcal{Q}}}{10\,\mathrm{TeV}}\right)^4 & \Phi \to hh,\ \text{if } M_\Phi > 2M_h, \end{cases} \tag{4.6}$$

where $m_q$ is the mass of the SM quarks, $\bar{m}_{\mathcal{Q}} = (m_{\mathcal{Q}_1} m_{\mathcal{Q}_2})^{1/2}$, and $y_{1,2}$, $m_{\mathcal{Q}_{1,2}}$ are respectively the Yukawa couplings and masses of the dark quarks circulating in the loop. A smaller life-time arises in the presence of extra light states charged under $G_{\rm DC}$, for example a dark color scalar coupled to the SM through the Higgs portal. The glue-ball lifetime can vary from cosmological to microscopic values. As we will see, cosmological constraints generically imply[3]

$$\tau_\Phi + t_{\Lambda_{\rm DC}} \lesssim 1\,\mathrm{sec} \tag{4.7}$$

where $t_{\Lambda_{\rm DC}} \sim M_{\rm Pl}/g_*^{1/2}\Lambda_{\rm DC}^2$ is the cosmological time at which dark confinement occurs.

[3]We do not consider cosmologically stable glue-balls as DM candidates because their thermal abundance is generically too large if the dark sector was in thermal equilibrium with the SM.

| $G_{\rm DC}$ | Representation $R$ | Dimension $d$ | Index $T$ | Casimir $C$ |
|---|---|---|---|---|
| SU($N$) | fundamental | $N$ | $1/2$ | $(N^2-1)/2N$ |
| | adjoint | $N^2-1$ | $N$ | $N$ |
| SO($N$) | fundamental | $N$ | $2$ | $N-1$ |
| | adjoint | $N(N-1)/2$ | $2N-4$ | $2N-4$ |

Table 4.1: *The dimension, the index $T$ and the quadratic Casimir $C$ of fundamental and adjoint* SU($N$) *and* SO($N$) *representations.*

### 4.2.2 Dark mesons

Dark confinement implies that physical states at zero temperature are singlets of dark color: mesons and baryons. Assuming that dark quarks fill a representation $R = (R_{\rm DC}, R_{\rm SM})$ of the dark gauge group times the SM gauge group, the non-relativistic interaction between a $\mathcal{Q}$ and a $\bar{\mathcal{Q}}$ is a Coulomb/Yukawa potential mediated by dark vectors and by SM vectors. For a two-body state in the representation $J_{\rm DC} \in R_{\rm DC} \otimes \bar{R}_{\rm DC}$ of $G_{\rm DC}$ and $J_{\rm SM} \in R_{\rm SM} \otimes \bar{R}_{\rm SM}$ of $G_{\rm SM}$ the Coulombic potential is

$$V = -\frac{\alpha_{\rm DC}\lambda_{\rm DC} + \alpha_{\rm SM}\lambda_{\rm SM}}{r} \equiv -\frac{\alpha_{\rm eff}}{r}, \qquad \lambda_J = \frac{C_{R_J} + C_{\bar{R}_J} - C_J}{2}, \tag{4.8}$$

where $C_{R_J}$ are the quadratic Casimirs, see table 4.1. In the Coulombic regime the size of dark quark bound states is given by the Bohr radius, $a_0 \sim 2/(\alpha_{\rm eff} m_{\mathcal{Q}})$ while the energy is $E_B \sim \alpha_{\rm eff}^2 m_{\mathcal{Q}}/4$. For $\mathcal{Q}\bar{\mathcal{Q}}$ dark meson singlets one finds $\alpha_{\rm eff} = C_N \alpha_{\rm DC}$.

When $a_0 > \Lambda_{\rm DC}^{-1}$ the effects of confinement cannot be neglected. The effective potential can be approximated as $V \approx -\alpha_{\rm eff}/r + \Lambda_{\rm DC}^2 r$ so that the bound states are dominated by the Coulombian term when $\Lambda_{\rm DC}^2 a_0^2 < \alpha_{\rm eff}$ or equivalently $\Lambda_{\rm DC}/m_{\mathcal{Q}} \lesssim \alpha_{\rm DC}^{3/2}$: the Coulombic approximation does not hold in the green region of Fig. 4.2.

### 4.2.3 DM dark baryons

Under our assumptions DM is the neutral component of dark baryons made of the lightest dark-quark multiplet[4]. The lightest dark baryons are the $s$-wave bound states with minimal spin (altought extra spin gives a small extra mass, unlike in QCD).

If the lightest dark quark is a SM singlet, $\mathcal{Q} = N$, the lightest dark baryon has a symmetric spin wave-function, so that its spin is $N_{\rm DC}/2$. If instead $\mathcal{Q}$ has a multiplicity $N_F$ the lightest

[4]Electro-weak interactions split the neutral from the charged components of SU(2)$_L$ multiplets ($\Delta m_{\mathcal{Q}} = \alpha_2 M_W \sin^2(\theta_{\rm W}/2) \approx 165\,{\rm MeV}$ when hypercharge vanishes [139]). In our region of parameters $m_{\mathcal{Q}} \gg \Lambda_{\rm DC} \gtrsim$ GeV the mass splitting is always smaller than the binding energy of the baryons so that we can work in an approximate SU(2)$_L$ invariant formalism.

baryons fills the following representations, under both flavour and spin:

$$\text{lightest dark baryon} = \begin{cases} \ydiagram{2,1} & \text{for } N_{\rm DC} = 3 \\ \ydiagram{2,2} & \text{for } N_{\rm DC} = 4 \\ \ydiagram{3,2} & \text{for } N_{\rm DC} = 5 \end{cases} \tag{4.9}$$

so that their spin is either 0 (for $N_{\rm DC}$ even) or 1/2 ($N_{\rm DC}$ odd). For example in the model where $\mathcal{Q} = V$ (a $\mathrm{SU}(2)_L$ triplet) and $G_{\rm DC} = \mathrm{SU}(N_{\rm DC})$, the lighter dark baryons are triplets under $\mathrm{SU}(2)_L$ for $N_{\rm DC}$ odd and singlets for $N_{\rm DC}$ even.

The binding energy of dark baryons can be computed precisely using variational techniques. Let us consider a more general system made of $n \leqslant N_{\rm DC}$ SM singlets dark quarks $N$ in the anti-symmetric dark-color configuration. In the non-relativistic limit the Hamiltonian is

$$H = K + V, \qquad K = \sum_{i=1}^{n} \frac{p_i^2}{2m_{\mathcal{Q}}}, \qquad V = -\frac{C_N \alpha_{\rm DC}}{N_{\rm DC} - 1} \sum_{i<j}^{n} \frac{1}{r_{ij}} \tag{4.10}$$

where $\boldsymbol{r}_i$ is the position of dark-quark $i$ and $r_{ij} = |\boldsymbol{r}_i - \boldsymbol{r}_j|$. It is convenient to rewrite $H$ in terms of the center-of-mass coordinate $\boldsymbol{X} = \frac{1}{n}\sum_{i=1}^{n} \boldsymbol{r}_i$, of the associated canonical momentum $\boldsymbol{P} = \sum_{i=1}^{n} \boldsymbol{p}_i$, and of the distances $\boldsymbol{\delta}_i = \boldsymbol{r}_i - \boldsymbol{r}_n$ with associated canonical momenta $\boldsymbol{\pi}_i = \boldsymbol{p}_i - \boldsymbol{P}/n$ for $i = 1, \dots n-1$ The kinetic energy becomes

$$K = K_{\rm CM} + \frac{1}{m_{\mathcal{Q}}} \sum_{i \geqslant j}^{n-1} \boldsymbol{\pi}_i \cdot \boldsymbol{\pi}_j \tag{4.11}$$

where $K_{\rm CM} = P^2/2nm_{\mathcal{Q}}$. We compute the binding energy of the lightest baryons using the variational method with trial wave-functions for the dark-baryon state $|\mathcal{B}\rangle$ containing one parameter $k$ with dimensions of inverse length. Defining $\langle X \rangle = \langle \mathcal{B}|X|\mathcal{B}\rangle / \langle \mathcal{B}|\mathcal{B}\rangle$ we use $\boldsymbol{\pi}_i = -i\partial/\partial\boldsymbol{\delta}_i$ and parameterize $\langle 1/r_{ij} \rangle = C_V k$ and $\langle K - K_{\rm CM} \rangle = nC_K k^2/2m_{\mathcal{Q}}$ such that

$$\langle H - K_{\rm CM} \rangle = nC_K \frac{k^2}{2m_{\mathcal{Q}}} - C_V k \, \frac{n(n-1)}{2} \frac{C_N \alpha_{\rm DC}}{N_{\rm DC} - 1}. \tag{4.12}$$

Maximising with respect to $k$ gives the binding energy

$$E_B^{\mathcal{Q}^n} = C_E C_N^2 \alpha_{\rm DC}^2 m_{\mathcal{Q}} \times \frac{(n-1)^2}{(N_{\rm DC} - 1)^2} \qquad C_E = \frac{nC_V^2}{8C_K} \tag{4.13}$$

where the last factor equals 1 for dark baryons with $n = N_{\rm DC}$.

Table 4.2 shows the resulting coefficients for three different trial wave-functions. For $n = 2$ we reproduce the Coulombian binding energy. For $n = 3$ and gauge group SU(3) we reproduce the QCD result, $E_B^{\mathcal{QQQ}} \approx 0.46\alpha_{\rm DC}^2 m_{\mathcal{Q}}$ [133] (see also [134]). Numerical integration becomes increasingly difficult for higher $n$.

| | Trial dark-baryon wave-function $\psi_{\mathcal{B}}(\boldsymbol{r}_1, \dots \boldsymbol{r}_n)$ | | | | | | | | |
|---|---|---|---|---|---|---|---|---|---|
| | $\exp(-k\sum_{i<j}^{n} r_{ij})$ | | | $\sum_{i=1}^{n}\exp(-k\sum_{j=1}^{n} r_{ij})$ | | | $\exp(-k\sum_{i=1}^{n} r_i)$ | | |
| $n$ | $C_V$ | $C_K$ | $C_E$ | $C_V$ | $C_K$ | $C_E$ | $C_V$ | $C_K$ | $C_E$ |
| 2 | 1 | 1 | 0.25 | 1 | 1 | 0.25 | 5/8 | 1 | 0.10 |
| 3 | 1.43 | 2.8 | 0.27 | 0.92 | 1.22 | 0.26 | 5/8 | 1 | 0.14 |
| 4 | 1.7 | 5 | 0.28 | 0.88 | 1.3 | 0.29 | 5/8 | 1 | 0.19 |
| 5 | | | | 0.85 | 1.4 | 0.33 | 5/8 | 1 | 0.24 |
| 6 | | | | $\sim 0.8$ | $\sim 1.2$ | $\sim 0.4$ | 5/8 | 1 | 0.29 |

Table 4.2: *Binding energies of anti-symmetric bound states made of $n$ dark-quarks with mass $m_{\mathcal{Q}}$ with a non-abelian Coulombian potential. We use the variational method and assume three different trial wave functions. The coefficients $C_{V,K,E}$ are defined in eq. (4.13). In particular, for $n = N_{\rm DC}$ the bound states are dark baryons, and $E_B = C_E(C_N\alpha_{DC})^2 m_{\mathcal{Q}}$.*

The first two trial wave-functions depend only on relative distances $r_{ij}$ and give similar results for the binding energy (the biggest result is the best approximation). The third wave-function $\psi_{\mathcal{B}} = (k/\pi)^{n/2}\exp(-k\sum_{i=1}^{n} r_i)$, considered in [195] for $G = \mathrm{SU}(N_{\rm DC})$, depends on absolute coordinates $r_i$, such that the center-of-mass kinetic energy is not subtracted: it leads to $C_V = 5/8$ and $C_K = 1$ for any $n$ (we find order one factors that differ from the analogous computation in [195]), and the resulting binding energy can be a reasonable approximation at large $n$.

As the numerical computation becomes more difficult for large $N_{\rm DC}$, it useful to complement it with the following approximation. The binding energy of dark baryons can be semi-quantitatively understood by building them recursively adding dark quarks to a bound state. For $G_{\rm DC} = \mathrm{SU}(3)$ the baryon can be thought as a stable di-quark bound to a quark. Treating the di-quark as elementary we can construct a color singlet baryon adding the third quark. Summing up the binding energies of $\mathcal{Q}\mathcal{Q}$ and $\mathcal{Q}\mathcal{Q}+\mathcal{Q}$ one finds $E_B \sim 0.7\alpha_{\rm DC}^2 m_{\mathcal{Q}}$ not far from the correct value $E_B \sim 0.45\alpha_{\rm DC}^2 m_{\mathcal{Q}}$. Because the gauge wave-function of di-quarks is anti-symmetric, the spin of $s$-wave bound states is 1 for a symmetric flavor wave-function and 0 for an anti-symmetric wave-function. Generalising this argument to $N_{\rm DC}$ quarks one finds a Bohr radius $a_0^{-1} \approx \alpha_{\rm DC} N_{\rm DC} m_{\mathcal{Q}}$ and a binding energy $E_B \approx \alpha_{\rm DC}^2 N_{\rm DC}^3 m_{\mathcal{Q}}$ in agreement with [196].[5]

[5]The binding energy of $n-1$ antisymmetric dark quarks with an extra dark quarks is $E_B^{n-1,1} = \frac{1}{2}\lambda_{n-1,1,n}^2\alpha_{\rm DC}^2\mu_{n-1,1}$ where $\mu_{n_1,n_2} = n_1 n_2/(n_1+n_2)m_{\mathcal{Q}}$ is the reduced mass and $\lambda_{n_1,n_2,n_3} = (C_{n_1}+C_{n_2}-C_{n_3})/2$. The quadratic Casimir of the $n$-index antisymmetric tensor of $\mathrm{SU}(N_{\rm DC})$ is $C_n = \frac{1}{2}n(N_{\rm DC}-n)(1+1/N_{\rm DC})$. The total binding energy of a singlet made of the anti-symmetric combination of $n = N_{\rm DC}$ dark quarks is then

$$E_B^{\mathcal{Q}^n} \approx \sum_{n=2}^{N_{\rm DC}} E_B^{n-1,1} \approx \frac{N_{\rm DC}^2(N_{\rm DC}-1)}{24}\alpha_{\rm DC}^2 m_{\mathcal{Q}}. \tag{4.14}$$

### 4.2.4 Annihilations of DM dark baryons

Annihilations of DM dark baryons are relevant for computing their cosmological thermal abundance (section 4.3) and for indirect detection signals (section 4.4.2).

The cross section for annihilation of dark baryons $\mathcal{B}$ with dark anti-baryons $\bar{\mathcal{B}}$ receives a contribution of particle-physics size, due to perturbative annihilation of constituents, $\sigma_{\mathcal{B}\bar{\mathcal{B}}} v_{\rm rel} \sim \pi\alpha_{\rm DC}^2/m_{\mathcal{Q}}^2$. A bigger contribution arises at scattering energies smaller than the binding energy: the long-range Coulomb-like force inside baryons can distort the orbits of the constituent quarks such that two overlapping baryons can recombine into mesons. Despite the negligible energy transfer this rearrangement has a large effect, because the $\mathcal{Q}\bar{\mathcal{Q}}$ into mesons later annihilate, such that mesons decay.[6] Such recombination can take place efficiently only if $v_{\rm rel} \lesssim \alpha_{\rm DC}$: classically this corresponds to the condition that the relative velocity is not much larger than the orbital velocity; quantistically to the condition that the wave-length of the incoming particles is larger than the size of the bound states. At larger energy one has partonic scatterings among constituents, with the smaller cross section discussed above.

The dominant recombination, if allowed kinematically, arises when a dark baryon $\mathcal{Q}^{N_{\rm DC}}$ and a dark anti-baryon $\bar{\mathcal{Q}}^{N_{\rm DC}}$ emit one $\mathcal{Q}\bar{\mathcal{Q}}$ dark meson, leaving a dark baryonium bound state made of $N_{\rm DC}-1$ dark quarks $\mathcal{Q}$ and $N_{\rm DC}-1$ anti-quarks $\bar{\mathcal{Q}}$:

$$(\mathcal{Q}^{N_{\rm DC}}) + (\bar{\mathcal{Q}}^{N_{\rm DC}}) \to (\mathcal{Q}\bar{\mathcal{Q}}) + (\mathcal{Q}^{N_{\rm DC}-1})(\bar{\mathcal{Q}}^{N_{\rm DC}-1}). \tag{4.15}$$

Rearrangements into several mesons, such as $(\mathcal{Q}^{N_{\rm DC}}) + (\bar{\mathcal{Q}}^{N_{\rm DC}}) \to (\mathcal{Q}\bar{\mathcal{Q}})^{N_{\rm DC}}$, is suppressed at large $N_{\rm DC}$ [196].

Assuming an estimate similar to the hydrogen-anti-hydrogen result, the cross-section relevant for indirect detection and at late times during the freeze-out is

$$\sigma_{\mathcal{B}\bar{\mathcal{B}}} \sim \frac{\pi\, R_{\mathcal{B}}^2}{\sqrt{E_{\rm kin}/E_B}} \qquad \Rightarrow \qquad \sigma_{\mathcal{B}\bar{\mathcal{B}}} v_{\rm rel} \sim \frac{1}{\sqrt{N_{\rm DC}} C_N \alpha_{\rm DC}} \frac{\pi}{m_{\mathcal{Q}}^2} \tag{4.16}$$

which vastly exceeds the annihilation cross sections among dark-quark constituents, $\sigma_{\mathcal{Q}\bar{\mathcal{Q}}} v_{\rm rel} \sim \pi\alpha_{\rm DC}^2/m_{\mathcal{Q}}^2$. Heuristically the large cross-section can be understood as follows: when the baryon-anti-baryon overlap a quark anti-quark-pair becomes unbound and can form a meson. For low enough velocities this process happens with probability of order one leading to an almost geometric cross-section. Additionally we consider thermal correction to the Bohr radius, which can become important during the freeze-out process [187]. A more precise value of $\sigma_{\mathcal{B}\bar{\mathcal{B}}}$ needs a dedicated non-relativistic quantum mechanical computation.

Next, we can check which rearrangements are kinematically allowed. Considering, for example, $G_{\rm DC} = {\rm SU}(3)$ ($C_N = \frac{4}{3}$) or ${\rm SO}(3)$ ($C_N = 2$) we have the following binding energies:

[6] This phenomenon is somewhat analogous to the annihilation of hydrogen $(ep)$ with anti-hydrogen $(\bar{e}\bar{p})$, that can recombine as $(ep) + (\bar{e}\bar{p}) \to (e\bar{e}) + (p\bar{p})$ followed by the $e\bar{e}$ and $p\bar{p}$ annihilation processes. Recombination is energetically favourable because the two heavier protons can form a deep bound state. The rearrangement cross section is of atomic size, $\sigma v_{\rm rel} \sim \sqrt{m_e/m_H}\pi\alpha_{\rm em} a_0^2$ for $m_H v_{\rm rel}^2 < m_e \alpha_{\rm em}^2$ [197–200].

- The binding energy of a $\mathcal{Q}\bar{\mathcal{Q}}$ singlet meson is $E_B^{\mathcal{Q}\bar{\mathcal{Q}}} = \frac{1}{4} C_N^2 \alpha_{\rm DC}^2 m_{\mathcal{Q}}$, see the discussion around eq. (4.8).
- The binding energy of a $\mathcal{Q}\mathcal{Q}\mathcal{Q}$ baryon is $E_B^{\mathcal{Q}\mathcal{Q}\mathcal{Q}} \approx 0.26 C_N^2 \alpha_{\rm DC}^2 m_{\mathcal{Q}}$, see eq. (4.13).
- The binding energy of a $\mathcal{Q}\mathcal{Q}$ di-quark state is $E_B^{\mathcal{Q}\mathcal{Q}} = \frac{1}{4} E_B^{\mathcal{Q}\bar{\mathcal{Q}}}$, see eq. (4.13).

The rearrangement into 3 mesons is kinematically allowed, given that the energy difference is positive: $\Delta E_B = 3E_B^{\mathcal{Q}\bar{\mathcal{Q}}} - 2E_B^{\mathcal{Q}\mathcal{Q}\mathcal{Q}} \approx 0.23 C_N^2 \alpha_{\rm DC}^2 m_{\mathcal{Q}}$.

The dominant process in eq. (4.15) seems also allowed, in view of

$$\Delta E_B = E_B^{\mathcal{Q}\bar{\mathcal{Q}}} + E_B^{\mathcal{Q}\mathcal{Q}\bar{\mathcal{Q}}\bar{\mathcal{Q}}} - 2E_B^{\mathcal{Q}\mathcal{Q}\mathcal{Q}} \approx (1+2) E_B^{\mathcal{Q}\bar{\mathcal{Q}}} + 2E_B^{\mathcal{Q}\mathcal{Q}} - 2E_B^{\mathcal{Q}\mathcal{Q}\mathcal{Q}} = 0.35 C_N^2 \alpha_{\rm DC}^2 m_{\mathcal{Q}} > 0 \quad (4.17)$$

where we estimated the binding energy of $\mathcal{Q}\mathcal{Q}\bar{\mathcal{Q}}\bar{\mathcal{Q}}$ as the one of $\mathcal{Q}$-$\mathcal{Q}$ and of $\bar{\mathcal{Q}}$-$\bar{\mathcal{Q}}$, plus the $(\mathcal{Q}\mathcal{Q})$-$(\bar{\mathcal{Q}}\bar{\mathcal{Q}})$ binding energy approximated as $2E_B^{\mathcal{Q}\bar{\mathcal{Q}}}$, where the factor of 2 accounts for the reduced mass.

If the dark baryons $\mathcal{B}$ are not in the Coulombic regime, they can be approximated as heavy dark quarks kept together by flux tubes which give a confining linear potential $V \sim \Lambda_{\rm DC}^2 r$. The recombination cross section then is geometric, $\sigma_{\mathcal{B}\bar{\mathcal{B}}} \sim \pi R^2$, at any scattering energy [101,201,146]. Indeed this is the cross section for crossing of two flux tubes with length $\approx R$; lattice simulations suggest that the probability of reconnection is close to one (a similar process takes place in string theory, where the reconnection probability can be suppressed by the string coupling [202]).

## 4.3 DM relic abundance

We here study the thermal relic DM abundance, assuming a vanishing or negligible dark-baryon asymmetry. No such asymmetry can exist in $\mathrm{SO}(N_{\rm DC})$ models (because baryons are real particles), while generating an asymmetry in $\mathrm{SU}(N_{\rm DC})$ models requires substantially more complicated constructions [186]. We need to distinguish two qualitatively different scenarios:

- *Dark color confines before freeze out*, i.e. $\Lambda_{\rm DC} \gtrsim m_{\mathcal{Q}}/25$: dark baryons form before freeze-out, but their kinetic energy at freeze-out is large relative to their potential energy, so that the annihilation cross section is the one among constituents, $\sigma_{\mathcal{Q}\bar{\mathcal{Q}}} v_{\rm rel} \sim \pi \alpha_{\rm DC}^2 / m_{\mathcal{Q}}^2$, smaller than the cross section in the limit $\Lambda_{\rm DC} \gg m_{\mathcal{Q}}$ considered in previous works [190]. Thereby the DM mass suggested by the cosmological abundance is mildly smaller than $M_{\mathcal{B}} \sim 100\,\mathrm{TeV}$.
- We focus on the more radical possibility that *dark color confines after freeze out*, at $\Lambda_{\rm DC} \ll m_{\mathcal{Q}}/25$. Around freeze-out at $T \sim m_{\mathcal{Q}}/25$ the dark coupling $\alpha_{\rm DC}$ is perturbative and dark quarks $\mathcal{Q}$ are free. They later partially combine into DM baryons at $T \sim \Lambda_{\rm DC}$. The DM mass suggested by cosmology is smaller than in the previous case.

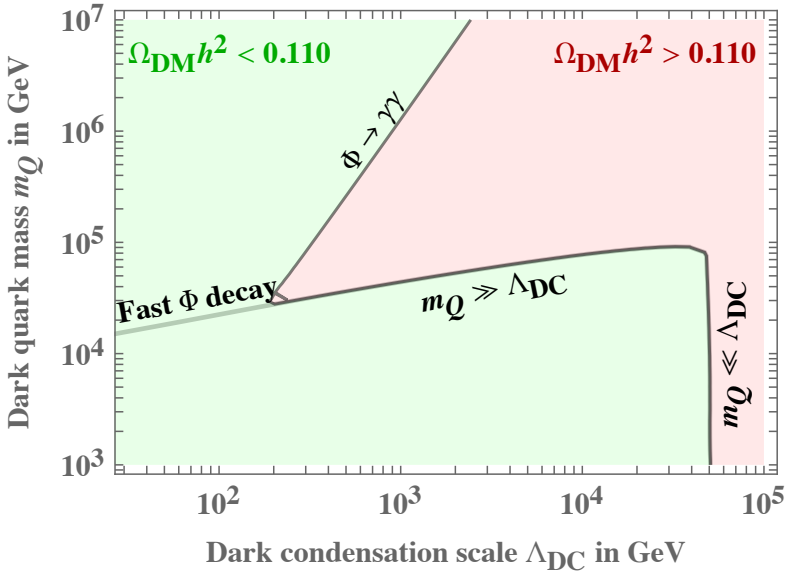


Figure 4.4: *Qualitative dependence of the DM relic abundance as function of $\Lambda_{DC}$ and of $m_{\mathcal{Q}}$: the cosmological value is reproduced along the boundary between the green and red regions. For $m_{\mathcal{Q}} \ll \Lambda_{DC} \approx 50\,\text{TeV}$ we recover the results of [190]. A lighter $m_{\mathcal{Q}}$ is allowed if instead $m_{\mathcal{Q}} \gg \Lambda_{DC}$, in view of the perturbative value of $\alpha_{DC}$ at freeze-out. However, if the glue-ball lifetime $\tau_\Phi$ is too long, glue-ball decays can wash-out the DM density. In the plot are showed 2 different scenarios: decay due to heavy states charged under the SM, and a shorter life-time, possible due to existence of a light scalar.*

The SM sector and the dark sector are in thermal contact during freeze-out if $\mathcal{Q}$ is charged under $G_{\rm SM}$ (for example $\mathcal{Q}$ could be a triplet under $\mathrm{SU}(2)_L$), or in the presence of a heavier dark quark $\mathcal{Q}'$ charged under the SM, provided that its mass is comparable to $\mathcal{Q}$. If instead $m_{\mathcal{Q}'} \gg m_{\mathcal{Q}}$ the two sectors decouple at $T \lesssim m_{\mathcal{Q}'}/25$; nevertheless they later evolve keeping equal temperatures as long as there are no entropy release takes place. Otherwise, if the numbers of degrees of freedom $g_{\rm SM}$ or $g_{\rm DC}$ depend on $T$ (this happens in the SM at $T \lesssim M_t$), the temperatures become mildly different, satisfying $g_{\rm SM}(T_{\rm SM})T_{\rm SM}^3/g_{\rm SM}(T_{\rm dec}) = g_{\rm DC}(T_{\rm DC})T_{\rm DC}^3/g_{\rm DC}(T_{\rm dec})$.

More importantly, the fraction of the dark energy density which does not contribute to forming DM dark baryons thermalizes into dark glue-balls which decay into SM particles. If the glue-balls are sufficiently long lived and dominate the energy density of the Universe at some stage of the cosmological evolution, the standard scaling $a \propto T^{-1}$ is modified into $a \propto T^{-8/3}$. During this early epoch of matter domination, the Universe expands faster than in the radiation-dominated era, leading to an enhanced dilution of the DM relic density. The situation is qualitatively illustrated in Fig. 4.4 and the precise computation of the effect is illustrated in section 5.2.2 of the next chapter.

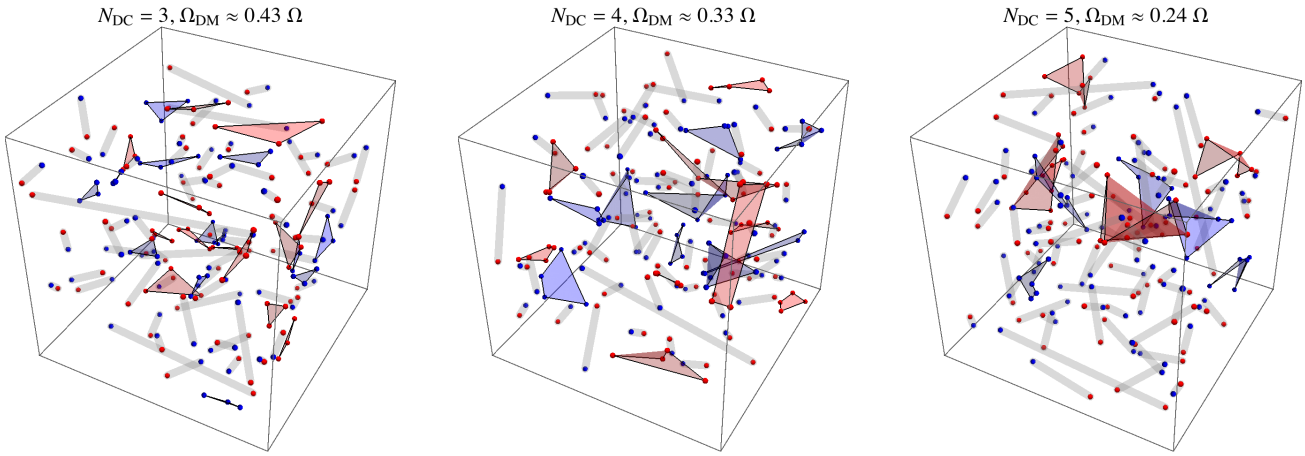


Figure 4.5: *Examples of dark condensation for* $N_{\rm DC} = 3$ *(left),* 4 *(middle) and* 5 *(right). Dark quarks* $\mathcal{Q}$ *(anti-quarks* $\bar{\mathcal{Q}}$*) are denoted as red (blue) dots, placed at random positions. We assume that each DM particle combines with its dark nearest neighbour, forming either unstable* $\mathcal{Q}\bar{\mathcal{Q}}$ *dark mesons (gray lines) or stable* $\mathcal{Q}^{N_{\rm DC}}$ *dark baryons (red regions) and* $\bar{\mathcal{Q}}^{N_{\rm DC}}$ *dark anti-baryons (blue regions).*

### 4.3.1 Freeze out of dark quarks and Dark Condensation

Let us discuss in detail the case where the confinement phase transition takes place after freeze-out, corresponding to a relatively small $\alpha_{\rm DC}(m_{\mathcal{Q}})$, see eq. (4.4).

The density of free quarks after freeze-out and before confinement can be computed by solving the coupled Boltzmann equations for the fermions and bound states, described in Appendix F. Formation of bound states from dark quarks is a negligible phenomenon until the dark gauge coupling is perturbative, given that only a small amount of dark quarks survived to their freeze-out, as demanded by the observed cosmological DM density. Formation of $N_{\rm DC} \otimes \bar{N}_{\rm DC}$ and $N_{\rm DC} \otimes N_{\rm DC}$ two-body bound states is further suppressed by the fact that it proceeds from a repulsive initial channel given that one dark-gluon must be emitted, in dipole approximation, to release the binding energy. In Appendix F we show that only a small fraction of dark quarks gets bound in stable $N_{\rm DC} \otimes N_{\rm DC}$ states.

Only when the temperature of the dark sector cools below the dark confinement scale, a dark phase transition happens (likely first order [203], leading to potentially observable gravity wave signals), and dark quarks must recombine to form either dark mesons or dark baryons. Dark mesons annihilate, heating the plasma of dark glue-balls, which later decay into SM particles. Only dark baryons survive as DM. Thereby we need to determine the fraction of DM that survives to this phase of dark condensation.

Unlike in QCD, dark quarks are much heavier than the confinement scale, so that we can neglect the possibility that $\mathcal{Q}\bar{\mathcal{Q}}$ pairs are created from the vacuum in order to favour the rear-

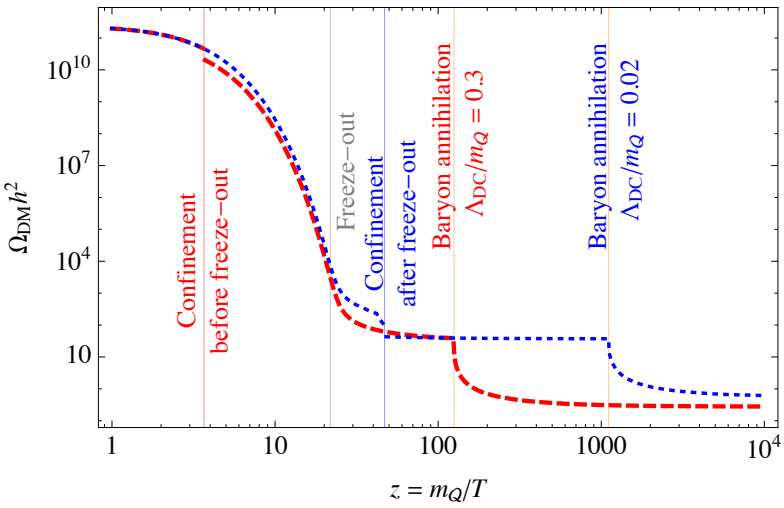


Figure 4.6: *The freeze-out history of two scenarios is displayed. The red line corresponds to confinement which takes place before freeze-out and the blue line shows the freeze-out which is followed by confinement and condensation. In both scenarios at late times, once the velocity drops below a critical value the constituent annihilation is replaced by a baryonic recombination, which leads to a late stage of dark matter annihilation and an additional depletion of the DM density.*

rangement of dark colors [204, 205]. Furthermore, dark quarks form a diluted gas, in the sense that the average distance $d(\Lambda_{\rm DC})$ between them is much larger than $1/\Lambda_{\rm DC}$,

$$d(T) \sim \frac{1}{n_{\mathcal{Q}}(T)^{1/3}} \sim \frac{1}{T}\left(\frac{2\pi T_f}{m_{\mathcal{Q}}}\right)^{\frac{1}{2}} e^{m_{\mathcal{Q}}/3T_f} \tag{4.18}$$

We are left with a classical combinatorics problem, a geometrical confinement. Each dark quark is connected to a string, and the sea of $\mathcal{Q}$ and $\bar{\mathcal{Q}}$ must recombine into color singlets. Assuming that a fraction $\wp_{\mathcal{B}}$ of dark quarks recombines into baryons the required abundance of DM is obtained for

$$\langle \sigma_{\mathcal{Q}\bar{\mathcal{Q}}} v_{\rm rel} \rangle \approx \frac{\wp_{\mathcal{B}}}{(23\,{\rm TeV})^2} \tag{4.19}$$

We assume in what follows that $\wp_{\mathcal{B}} \sim 1$ for small $N_{\rm DC} \sim 3$. A possible justification goes as follows. In three dimensions the distance of a dark quark to its nearest neighbour is 0.75 times smaller than the distance to its next to nearest neighbour, on average. This suggests that only the nearest neighbours are relevant to the recombination process. Assuming that each $\mathcal{Q}$ or $\bar{\mathcal{Q}}$ reconnects with probability one with its nearest neighbour, as illustrated in Fig. 4.5, the probability to form a dark baryon is roughly $(1/2)^{N_{\rm DC}-2}$ smaller than the probability of forming a dark meson. One than finds

$$\wp_{\mathcal{B}} \approx \frac{1}{1 + 2^{N_{\rm DC}-1}/N_{\rm DC}}. \tag{4.20}$$

At face value for $N_{\rm DC} = 3$ this gives a baryon fraction 0.4 in agreement with other estimates in the literature. One possible source of error arises from effects of crossing and rearrangement of flux tubes during the recombination process.

So far we assumed no dark-baryon asymmetry. In SU($N$) models dark baryon number is conserved and, in more complicated models, a dark-baryon asymmetry could be generated. Then one would get an extra contribution given by $\Omega_{\rm DM} = |\Omega_{\mathcal{Q}} - \Omega_{\bar{\mathcal{Q}}}|$.

The enhancement in $\sigma_{\mathcal{B}\bar{\mathcal{B}}}/\sigma_{\mathcal{Q}\bar{\mathcal{Q}}} \sim 1/\alpha_{\rm DC}^3$ due to recombination, discussed in section 4.2.4, leads to an extra dilution of the DM cosmological abundance, see Fig. 4.6. As the critical cross section relevant for cosmology scales as $\langle \sigma v_{\rm rel} \rangle \propto 1/T$, this effect can be relevant provided that $m_{\mathcal{Q}}/\Lambda_{\rm DC} \lesssim 10^3$.

A larger related effect can emerge in the intermediate region B) where $E_B \lesssim \Lambda_{\rm DC} \lesssim 1/a_0$ [187]. In this region the lowest lying bound states are Coulombian, but at temperature $T$ they get excited up to large distances where $V \simeq \sigma r$ ($\sigma \sim \Lambda_{\rm DC}^2$ is the flux tube tension) forming object with radius $R_{\mathcal{B}^*} \sim T/\Lambda_{\rm DC}^2$ much larger than the Bohr radius $a_0 = 2/(\alpha_{\rm DC} m_{\mathcal{Q}})$. Writing $V = -\alpha_{\rm DC}/r + \sigma r$, a thermal computation gives, for $T < \Lambda_{\rm DC}$

$$R_{\mathcal{B}^*}(T) \approx \left(a_0 + \frac{3 m_{\mathcal{Q}} T^5 \sqrt{m_{\mathcal{Q}} T}}{\sqrt{\pi}\sigma^4} e^{-E_B/T}\right)\left(1 + \frac{m_{\mathcal{Q}} T^4 \sqrt{m_{\mathcal{Q}} T}}{\sqrt{\pi}\sigma^3} e^{-E_B/T}\right)^{-1}. \tag{4.21}$$

The thermal radius reduces to $a_0$ for $T \ll E_B$, and to $3T/\Lambda_{\rm DC}^2$ for $T \sim \Lambda_{\rm DC}$. The critical temperature below which the dark baryons relax to the ground state is of order of $E_B$, and possibly somewhat lower in view of the entropy factor of the almost continuum states of excited states. At $T \sim \Lambda_{\rm DC}$ an excited baryon $\mathcal{B}^*$ can be approximated as $N_{\rm DC}$ dark quarks connected by flux tubes with length $R_{\mathcal{B}^*}$. When $\mathcal{B}^*$ scatters with $\bar{\mathcal{B}}^*$ two flux tubes can cross: lattice simulations suggest that the probability of reconnection is close to one; a similar process takes place in string theory, where the reconnection probability can be suppressed by the string coupling [202]. This results into a large geometric $\sigma_{\mathcal{B}^*\bar{\mathcal{B}}^*} \sim T^2/\Lambda_{\rm DC}^4$ for $T \lesssim \Lambda_{\rm DC}$, which enhances $\mathcal{Q}\bar{\mathcal{Q}}$ annihilations, as their rate inside thermally elongated hadrons is faster than the Hubble rate (except possibly for hadrons with large angular momenta). Depending on the precise unknown values of the phase transition temperature $T_c \sim \Lambda_{\rm DC}$ and of the string tension $\sigma \sim \Lambda_{\rm DC}^2$ such extra annihilations can be either subleading or substantially increase the value of the DM mass that reproduces the cosmological DM density [187]. In the rest of the chapter we do not consider this possibility.

## 4.4 Signatures

### 4.4.1 Cosmological constraints

We discuss the various cosmological bounds, that require $\Lambda_{\rm DC} \gtrsim 100$ MeV.

### Extra radiation

If $\Lambda_{\rm DC} \ll 1\,\text{MeV}$ (1 eV) dark gluons behave as extra relativistic degrees of freedom at the BBN (CMB) epoch. Their amount can be parametrised as a contribution to the effective number of neutrino species:

$$\Delta N_{\rm eff} = \frac{8}{7} d(G) \left(\frac{T_{\rm DC}}{T_{\rm SM}}\right)^4 \tag{4.22}$$

where $d(G)$ is the dimension of the dark color gauge group. Present bounds [206, 207] constrain $\Delta N_{\rm eff}(T \sim 1\,\text{MeV}) \lesssim 1$ and $\Delta N_{\rm eff}(T \sim 1\,\text{eV}) \lesssim 0.5$. This implies

$$\left(\frac{T_{\rm DC}}{T_\nu}\right)^4 = \left(\frac{2}{g_{\rm SM}(T_{\rm dec})}\right)^{4/3} \lesssim \frac{7}{16 d(G)} \tag{4.23}$$

This condition is marginally consistent with SU(3) and SO(3) theories if the dark sector decouples at temperature $T_{\rm dec} \gtrsim 1\,\text{GeV}$. Models with low confinement scale are however excluded by other cosmological constraints.

### Structure formation

Structures such as galaxies form because DM can freely cluster after matter/radiation equality, at $T \lesssim 0.74\,\text{eV}$. DM that interacts with lighter dark gluons would instead form a fluid [208, 209]: DM clustering is negligibly affected provided that either the confinement scale is large enough, $\Lambda_{\rm DC} \gtrsim 10\,\text{eV}$ or the dark gauge coupling is small enough, $\alpha_{\rm DC} \lesssim 10^{-8}$. We will follow the first option.

### Big Bang Nucleosynthesis

Dark-glue-balls with mass $M_\Phi \sim 7\Lambda_{\rm DC}$ decay into SM particles injecting non-thermal particles, which alter the cosmological abundances of light element or the CMB power spectrum. Barring a dark sector with $T_{\rm DC} \ll T_{\rm SM}$, avoiding this requires that injection from glue-ball decays is over at the BBN epoch, $T_{\rm SM} \sim$ MeV. This requires $\Lambda_{\rm DC} \gtrsim$ MeV and that the dark-glue-ball lifetime $\tau_\Phi$ is shorter than 1 sec [210].

### Cosmic Microwave Background

Dark matter that annihilates around at $T_{\rm dec} \sim 0.25\,\text{eV}$ injects particles which ionize hydrogen leaving an imprint on the Cosmic Microwave Background radiation (CMB). As the relevant quantity is the total injected power, the CMB bounds on the DM annihilation cross section are robust and do not depend on the details of the cascade process resulting from DM annihilation to SM final states. The bound is weaker than typical indirect detection bounds [22]

$$\frac{f_{\rm eff}\langle\sigma_{\rm ann} v_{\rm rel}\rangle}{M_\chi} < 4.1 \times 10^{-28} \frac{\text{cm}^3}{\text{sec GeV}} \tag{4.24}$$

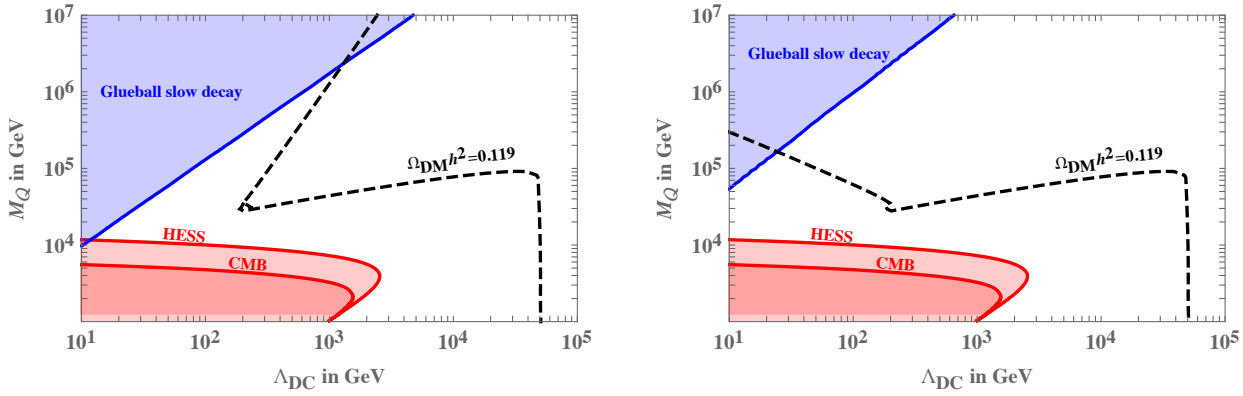


Figure 4.7: *Left (right) panel shows the region of the parameter space for the $V\ (N \oplus L)$ model which is ruled out by indirect constraints. The red region is ruled out by constraints on the DM annihilation cross section (the strongest are provided by HESS [25] and CMB observables [206]), which we estimate to be dominated by a recombination reaction of two dark baryons at low velocities. In the blue region the glueballs are either stable or have a lifetime bigger than 1 s. In the first case they overclose the Universe, in the second either they spoil BBN (if $1\,\mathrm{s} < \tau_\Phi < 10^{12}\,\mathrm{s}$) [210] or they are ruled out by diffuse gamma ray searches (if $10^{12}\,\mathrm{s} < \tau_\Phi < 10^{17}\,\mathrm{s}$) [213]. The black-dashed lines show the region where the DM relic density is reproduced.*

where $f_{\rm eff}$ is an efficiency parameter depending on the spectra of injected electrons and photons, given by

$$f_{\rm eff} = \frac{1}{2M_\chi}\int_0^{M_\chi} E\,dE\left[2f_{\rm eff}^{e^+e^-}\left(\frac{dN}{dE}\right)_{e^+} + f_{\rm eff}^{\gamma}\left(\frac{dN}{dE}\right)_{\gamma}\right] \tag{4.25}$$

where the ionization efficiencies for $e^\pm$ and $\gamma$ have been computed in [211, 212]. In our case $M_\chi$ is the mass of the composite dark baryon. The resulting bound is plotted in Fig. 4.7 and leads to a bound on the dark condensation scale $\Lambda_{\rm DC} \gtrsim 30$ MeV in the region where DM is a thermal relic.

### 4.4.2 Indirect detection

In the scenario where DM has no dark-asymmetry, dark baryons $\mathcal{B}$ can annihilate with dark anti-baryons $\bar{\mathcal{B}}$ producing indirect detection signals. The DM kinetic energy $M_{\mathcal{B}}v^2$ is typically much smaller than the energy of the excited states so that we can ignore higher resonances and consider only the ground state dark baryon. Given that after confinement DM is a DC singlet there is no Sommerfeld enhancement due to DC interactions. Still, the low-energy annihilation cross section can be large due the large size of the bound states, as discussed in section 4.2.4, see eq. (4.16).

DM annihilation leads to the production of dark glue-balls, which are the lightest particles in

the dark sector. The minimal number of produced glue-balls is $k \gtrsim 2N_{\rm DC}$, possibly enhanced up tp $k \approx M_\chi/M_\Phi$ from dark hadronization effects. The dark glue-balls later decay to SM particles (two photons if they are lighter than $M_W$ or — if $\mathcal{Q}$ is coupled to the higgs — into $f\bar{f}$, where $f$ is heaviest SM fermion lighter than $M_\Phi/2$). The strongest bounds coming from indirect detection experiments looking for these annihilation products are reported in Fig. 4.7.

### 4.4.3 Direct Detection

Direct detection experiments see DM dark-baryons as a particle and cannot resolve its constituents. Indeed, the maximal momentum transfer in elastic interactions with nuclei of mass $m_N$ is $\approx m_N v \lesssim 100\,\text{MeV}$ in view of the galactic DM velocity $v \sim 10^{-3}$. In the range of parameters allowed for our models the size of DM bound states is smaller than the corresponding wave-length so DM bound states scatter coherently with the nucleus.[7]

#### $\mathrm{SU}(N_{\rm DC})$ models

We first discuss $\mathrm{SU}(N_{\rm DC})$ models where DM is complex. In the simplest case the dark-baryon DM belongs to a single multiplet of the SM interacting as in minimal dark matter models [139]. Direct detection constraints on $Z$-mediated scatterings are satisfied if the DM candidate has no hyper-charge, which implies integer isospin. The loop-level $W$-mediated cross section [139, 62, 215] is independent of the dark matter mass and entirely dependent by its $\mathrm{SU}(2)_L$ quantum number, equal to about $\sigma_{\rm SI} \approx 1.0 \times 10^{-45}\,\text{cm}^2$ for a weak triplet, and to $\approx 9.4 \times 10^{-45}\,\text{cm}^2$ for a weak quintuplet. The predicted cross-sections are above the neutrino floor and will be observable in future experiments if $M_{\mathcal{B}} \lesssim 15\,\text{TeV}$.

This simple result can however be drastically modified in the presence of heavier dark fermions. In models where the DM fermion has Yukawa couplings ($y$ for the left-handed chirality and $\tilde{y}$ for the right-handed chirality) with the Higgs and with an heavier dark-quark with non vanishing hypercharge, the DM candidate can acquire a vector coupling to the $Z$. The heavier dark-quarks have a vectorial coupling to the $Z$ given by

$$g_Z \equiv \frac{g_2}{\cos\theta_{\rm W}} \left(T_3 - Q \sin^2\theta_{\rm W}\right). \tag{4.26}$$

After electro-weak symmetry, the dark-quarks that make up the DM mix with the heavier dark quarks, acquiring an effective vectorial coupling

$$g_Z^{\rm eff} = \frac{g_Z}{2}(s_L^2 + s_R^2) \tag{4.27}$$

where $s_L$ and $s_R$ are the mixing of left and right chiralities. Since the $Z$ is coupled to a conserved current, the coupling $g_Z^{\mathcal{B}}$ to dark baryons is given by the sum of the constituent charges. For

[7] Some fraction of dark baryons could form dark nuclei [214], affecting direct detection signals.

example $g_Z^{\mathcal{B}} = N_{\rm DC} g_Z^{\rm eff}$ when the dark-baryon is made of electroweak singlets. At low energies we obtain the effective interaction between $\mathcal{B}$, the DM dark baryon, and the SM quarks $q$

$$\mathscr{L}_{\rm eff} \supset \frac{g_Z^{\mathcal{B}} g_Z^q}{M_Z^2} (\bar{\mathcal{B}}\gamma^\mu \mathcal{B})(\bar{q}\gamma_\mu q). \tag{4.28}$$

From this Lagrangian one obtains the spin-independent DM cross section on nuclei $N$

$$\sigma_{\rm SI} = \frac{(\mu_n G_{\rm F} \cos\theta_{\rm W})^2}{4\pi} \left(\frac{g_Z^{\mathcal{B}}}{g_2}\right)^2 \tag{4.29}$$

where $\mu_n$ is the reduced mass of the DM-nucleon system. The direct detection bound implies $g_Z^{\mathcal{B}} \lesssim 7 \times 10^{-4} \sqrt{M_{\mathcal{B}}/\,\text{TeV}}$.

When Yukawa couplings exist, Higgs mediated scatterings are also generated. The Yukawa coupling to the lightest mass eigenstate is $y_{\rm eff} = y s_L c_R + \tilde{y} c_L s_R$. The Yukawa coupling of dark-baryons is given by the sum of the Yukawa of the constituent dark quarks. The resulting SI cross section is [216]:

$$\sigma_{\rm SI} = \frac{\sqrt{2} G_F f_n^2}{\pi} \frac{\mu_n^4}{M_h^4} y_{\mathcal{B}}^2 \tag{4.30}$$

where $f_n \approx 1/3$ is the relevant nuclear form factor [217, 218]. Direct detection bounds imply $y_{\mathcal{B}} \lesssim 4 \times 10^{-2} \sqrt{M_{\mathcal{B}}/\,\text{TeV}}$.

Furthermore, fermionic composite DM that contains electrically charged constituents has a magnetic moment $\mu \sim e\alpha_{\rm DC}/(4\pi) m_{\mathcal{Q}}$ that can lead to a potentially observable cross-section with characteristic dependence on the recoil energy $E_R$, $d\sigma/dE_E \approx e^2 Z^2 \mu^2 / 4\pi E_R$.

### $\mathrm{SO}(N_{\rm DC})$ models

Models based with dark quarks in the fundamental of $G_{\rm DC} = \mathrm{SO}(N)_{\rm DC}$ behave differently, because the lightest fermion is a real Majorana state that cannot have vectorial couplings to the $Z$. Mass eigenstates $\chi_M$ have only axial couplings to the $Z$

$$\tilde{g}_Z^{\rm eff}\, \bar{\chi}_M \gamma_\mu \gamma_5 \chi_M \qquad \text{with strength} \qquad \tilde{g}_Z^{\rm eff} = \frac{g_2}{2\cos\theta_{\rm W}} (s_L^2 - s_R^2). \tag{4.31}$$

This contributes to spin dependent cross-sections with nuclei, subject to much weaker bounds. For this reason DM candidates with non-zero hypercharge are possible in the presence of a small mixing with a real particle. For what concerns Higgs interactions these are as in $\mathrm{SU}(N_{\rm DC})$ and similar bounds apply.

Vector coupling to the $Z$ can be present between DM and heavier states. DM made of electro-weak doublets gives two almost degenerate Majorana fermions split by

$$\Delta m \sim \frac{y^2 v^2}{\Delta m_{\mathcal{Q}}} \tag{4.32}$$

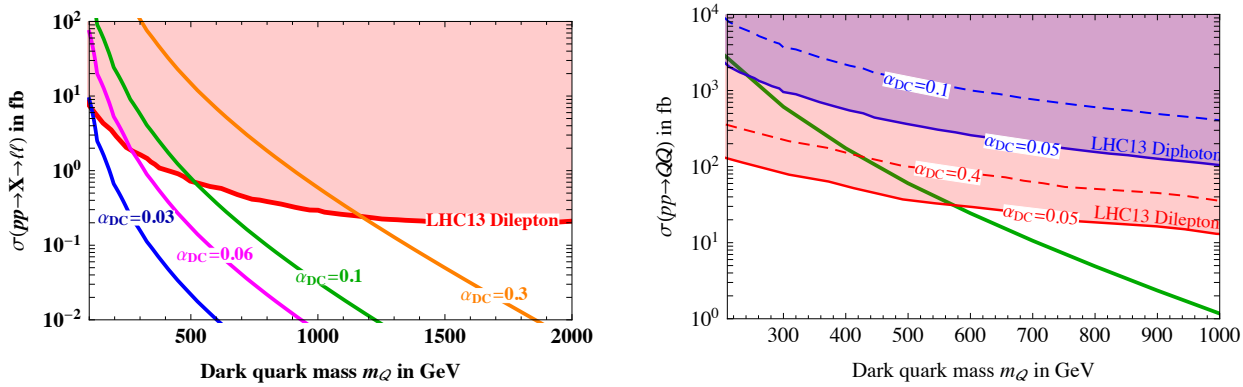


Figure 4.8: **Left:** *ATLAS bounds on the cross section for the direct production of a spin 1 resonance decaying into leptons ($\mu$ und e) [222].* **Right:** *ATLAS bounds on the dark quarks pair production cross section [222]. They are derived assuming that $\sim 1/3$ of the produced dark quarks form spin 1 bound states and the others spin 0 bound states.*

.

where $\Delta m_{\mathcal{Q}}$ is the mass splitting between the two dark quarks which get mixed. When the splitting is smaller than $\mathcal{O}(100\,\mathrm{KeV})$ inelastic transitions between the two states can take place giving rise to inelastic dark matter [192].

Finally, we comment on dipole moments. In models with $G_{\mathrm{DC}} = \mathrm{SU}(N_{\mathrm{DC}})$ and $m_{\mathcal{Q}} \ll \Lambda_{\mathrm{DC}}$, fermionic baryons acquire large magnetic dipole moments (which give characteristic signals in direct detection experiments [190]) thanks to non-perturbative effects. If instead $m_{\mathcal{Q}} \gg \Lambda_{\mathrm{DC}}$, neutral baryons have small magnetic moments given (at leading order) by the sum of the elementary moments. A similar result holds for electric dipoles, possibly generated by a $\theta_{\mathrm{DC}}$ angle by instantons, which are suppressed in the perturbative regime. Polarisability of weakly coupled dark matter bound states could also be of interest [219, 220].

### 4.4.4 Collider

If dark quarks are charged under the SM, bound states of the new sector can be produced singly or through the hadronization of the dark quarks produced in Drell-Yan processes.

Resonant single production does not depend on the details of the strong dynamics. In the narrow width approximation, the production cross-sections of a bound state $X$ of mass $M_X$ is given by

$$\sigma(pp \to X) = \frac{(2J_X+1)D_X}{M_X s} \sum_{\mathcal{P}} C_{\mathcal{P}\mathcal{P}} \Gamma(X \to \mathcal{P}\mathcal{P})\,, \tag{4.33}$$

where $D_X$ is the dimension of the representation, $J_X$ is its spin, $\mathcal{P}$ the parton producing the resonance and $C_{\mathcal{P}\mathcal{P}}$ are the dimension-less parton luminosities, see [221].

Bound states with spin-0 are produced from vector bosons fusion. For constituent dark quarks with $\mathrm{SU}(2)_L \times \mathrm{U}(1)_Y$ quantum numbers the decay width of singlet spin-0 bound states

is

$$\Gamma\left(X^{J=0}_{I=0}\to\gamma\gamma\right)=N_{\rm DC}\alpha^2\frac{|R_{n0}(0)|^2}{F^2m_{\mathcal{Q}}^2}\frac{(T_2+d_2Y^2)^2}{d_2} \tag{4.34}$$

where $T_2$ ($d_2$) is the index (dimension) of the $\mathrm{SU}(2)_L$ representation, $R_{n0}(0)$ is the value at the origin of the bound state wave-function and $F=1(2)$ for distinguishable (identical) dark quarks. The decay rates into $W$ and $Z$ bosons and into dark gluons $\mathcal{G}$ are

$$\begin{aligned}
\frac{\Gamma_{\gamma Z}}{\Gamma_{\gamma\gamma}} &\approx \frac{2(-T_2\cot\theta_{\rm W}+Y\tan\theta_{\rm W})^2}{(T_2+d_2Y^2)^2}\,, & \frac{\Gamma_{ZZ}}{\Gamma_{\gamma\gamma}} &\approx \frac{(T_2\cot\theta_W^2+Y\tan\theta_W^2)^2}{(T_2+d_2Y^2)^2}\,,\\
\frac{\Gamma_{WW}}{\Gamma_{\gamma\gamma}} &\approx 2\frac{T_2^2}{(T_2+d_2Y^2)^2\sin^4\theta_{\rm W}}\,, & \frac{\Gamma_{\mathcal{G}\mathcal{G}}}{\Gamma_{\gamma\gamma}} &\approx \frac{1}{16F}\frac{N_{\rm DC}^2-1}{N_{\rm DC}^2}\frac{d_2^2}{(T_2+d_2Y^2)^2}\frac{\alpha_{\rm DC}^2}{\alpha^2}\,.
\end{aligned} \tag{4.35}$$

Spin-1 bound states decay into fermions or scalars (and equivalent longitudinal gauge bosons $W,Z$), as their decays into massless gauge bosons is forbidden by the Landau-Yang theorem. For example, the decay width of an SU(2) triplet spin-1 bound state into a left-handed pair of SM fermions is

$$\Gamma^a\left(X^{J=1}_{I=1}\to f\bar f\right)=N_{\rm DC}\frac{\alpha_2^2}{12}\frac{|R_{n0}(0)|^2}{F^2m_{\mathcal{Q}}^2}T_2 \tag{4.36}$$

where we neglected possible hypercharge contributions. Singlet spin-1 bound states can also decay into three dark gluons with a rate:

$$\Gamma_{\mathcal{G}\mathcal{G}\mathcal{G}}=N_F\frac{\sum_{abc}d_{abc}^2}{36\,d_R}\frac{\pi^2-9}{\pi}\alpha_{\rm DC}^3\frac{|R_{n0}(0)|^2}{F^2m_{\mathcal{Q}}^2} \tag{4.37}$$

where $d_{abc}=2\,\mathrm{Tr}\left[T^a\{T^b,T^c\}\right]$ with $T^{a,b,c}$ generators of the dark-color group in the dark quarks representation.

For concreteness we focus on the model with $G_{\rm DC}=\mathrm{SU}(3)$ with a dark quark $\mathcal{Q}=V$. In the region of parameters relevant for DM, the dark coupling $\alpha_{\rm DC}$ is stronger than the electro-weak couplings, so that the bound states are dominantly shaped by the dark interactions. In the Coulomb limit, the radial wave function at the origin is then given by $|R_{n0}(0)|^2/m_{\mathcal{Q}}^2=(Fm_{\mathcal{Q}}\alpha_{\rm eff}^3)/(2n^3)$ with $\alpha_{\rm eff}$ defined as in (4.8). Spin-0 bound states are produced from photon fusion and decay mostly into dark gluons with the branching ratios given in eq. (4.35). In view of the small photon luminosity at LHC, no significant bound is obtained. Spin-1 resonances can be produced in electro-weak interactions from first generation quarks and decay into electrons and muons with a branching ratio of order 7%. In Fig. 4.8 we show the bound from current di-lepton searches that exclude dark quark masses up to 1 TeV. This is significantly stronger than typical collider bounds on electro-weak charged states.

Dark quarks with SM charges can be also pair produced in Drell-Yan processes. In the region of masses relevant for LHC, their kinetic energy is comparable to their mass. When dark quarks travel a distance $\ell\gg 1/\Lambda_{\rm DC}$ a flux tube develops between them carrying an energy $\Lambda_{\rm DC}^2\ell$, such

that they reach a maximal distance [223]

$$\ell_{\rm max} \sim \frac{m_{\mathcal{Q}}}{\Lambda_{\rm DC}^2} \sim 10^{-13}\,{\rm m}\left(\frac{m_{\mathcal{Q}}}{\rm TeV}\right)\left(\frac{\rm GeV}{\Lambda_{\rm DC}}\right)^2 \tag{4.38}$$

which is microscopic in the region relevant for DM phenomenology. The dark quarks will then oscillate and de-excite to the lowest lying bound states with the emission of dark glue-balls, until they eventually decay to SM states. It is difficult to determine the branching ratios into each SM channel. Assuming for simplicity that all dark quark pairs de-excite democratically to the lowest lying spin-0 and a spin-1 bound states, 2/3 of the events populate the spin-0 bound states (singlet and quintuplet) and 1/3 populate the spin-1 triplet. In Fig. 4.8 we show the bounds from di-photons and di-leptons on double productions of dark quarks. Especially in the region of large $\alpha_{\rm DC}$, these bounds are weaker than the bounds from single production.

### 4.4.5 Dark glue-balls at high-intensity experiments

Dark glue-balls can be produced either through the production and subsequent decay of dark mesons or through the effective operators [224–226]

$$\mathcal{O}_8 = \alpha_{\rm em}\alpha_{\rm DC}\mathcal{G}^A_{\mu\nu}\mathcal{G}^{\mu\nu A}F^{\rho\sigma}F_{\rho\sigma}\,, \qquad \mathcal{O}_6 = \frac{\alpha_{\rm DC}}{4\pi}H^\dagger H\mathcal{G}^A_{\mu\nu}\mathcal{G}^{\mu\nu A} \tag{4.39}$$

The diagrams in Fig. 4.3 generate $\mathcal{O}_{6,8}$ with coefficients

$$c_8(m_{\mathcal{Q}}) = \frac{T_{\rm DC}(T_2+d_2Y)}{60}\frac{1}{m_{\mathcal{Q}}^4}\,, \qquad c_6(m_{\mathcal{Q}}) = \frac{2T_{\rm DC}}{3}\frac{1}{h}\frac{\partial\ln(\det M_F(h))]}{\partial h}\bigg|_{h=0} \tag{4.40}$$

where $M_F(h)$ is Higgs-dependent dark quark mass matrix, $T_{\rm DC}$ the index of the dark quark, $T_2$ the isospin, and $Y$ its hypercharge.

After confinement, $\mathcal{O}_8$ gives rise to a coupling between $0^{++}$ glue-balls and the SM gauge bosons which allows the glue-balls to decay into photons. For the lightest $0^{++}$ glue-ball one finds [225]

$$\Gamma_{0^{++}\to\gamma\gamma} = \frac{\alpha_{\rm em}^2\alpha_{\rm DC}^2}{14400\pi}\frac{m_0^3 f_{0S}^2}{m_{\mathcal{Q}}^8}(T_2+d_2Y^2)^2 \tag{4.41}$$

where $f_{0S} \equiv \langle 0|{\rm Tr}\,\mathcal{G}_{\mu\nu}\mathcal{G}^{\mu\nu}|0^{++}\rangle$. Using the lattice result $4\pi\alpha_{\rm DC}f_{0S} \approx 3M_\Phi^3$ valid for SU(3) theories, one gets the dark-glue-ball lifetime in eq. (4.6) for models with electro-weak charges. The Yukawa couplings between the dark and the SM sector induce a mixing angle $\alpha$ between dark glue-balls and the SM Higgs

$$\sin\alpha \approx c_6\frac{\alpha_{\rm DC}}{4\pi}\frac{v f_{0S}}{M_h^2} \tag{4.42}$$

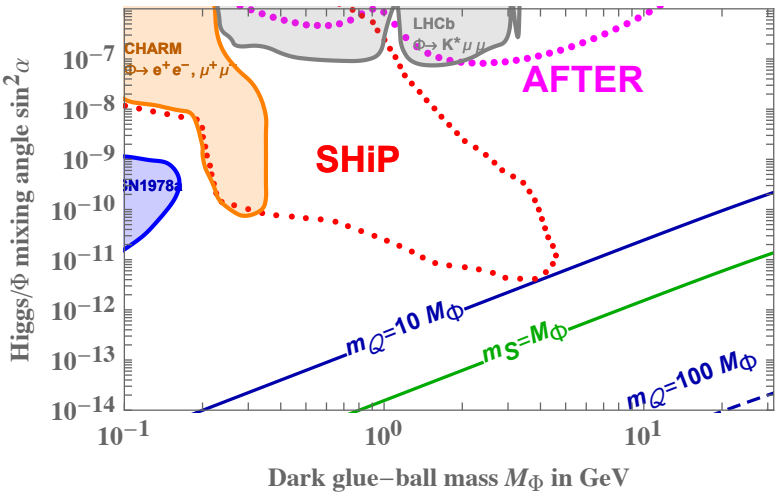


Figure 4.9: *Predicted values of the Higgs/dark gluon mixing angle $\alpha$, assuming dark quarks with Yukawa couplings $y = 1$ (blue lines) or adding a dark scalar with mass $m_S$ (green line) with a mixed quartic $\lambda_{HS} = 10^{-2}$, as function of the dark gluon mass $M_\Phi$. The shaded regions are excluded, the dotted curves can be probed by future SHiP [227] (red points) and AFTER [228] (magenta points) experimental proposals.*

giving rise to the dark glue-ball decay widths

$$\Gamma_{0^{++}\to f\bar{f}} = N_c \frac{M_\Phi}{16\pi} y_f^2 \sin^2\alpha\,, \qquad \Gamma_{0^{++}\to gg} = \frac{\alpha_s^2}{72\pi^3}\frac{M_\Phi^3}{v^2}\sin^2\alpha\,, \tag{4.43}$$

The cross-section for the production of dark glue-balls are negligible at LHC. Light dark glue-balls can be potentially produced in high luminosity experiments such as SHiP [227]. The SHiP experiment will operate at a center of mass energy $E_{\rm CM} \approx 27\,\text{GeV}$ and will produce approximately $10^{20}$ proton on target collisions. The distance from the target to the detector is approximately $L \sim 100\,\text{m}$ and the detector length is $S \sim 60\,\text{m}$. A detectable signal at SHiP arises if there are a few events in the detector

$$N_{\rm ev} \sim 10^{20}\frac{\sigma(pp\to\Phi)}{\sigma_{pp}} \times \left[e^{-L/\tau_\Phi}\left(1-e^{S/\tau_\Phi}\right)\right] \gtrsim \text{few} \tag{4.44}$$

where $\sigma_{pp} \sim 1/m_p^2$ is the proton-proton scattering cross section. This implies that the SHiP experiment will probe only a region of the parameter space which is already excluded by indirect detection bounds or electroweak precision tests (see next section). This conclusion is confirmed by the result of a more precise computation, shown in Fig. 4.9. In the same figure we also show the sensitivity of an hypothetical fixed target experiment (AFTER) operating with LHC beams at a center of mass energy $E_{\rm CM} \approx 115\,\text{GeV}$ and producing approximately $10^{15}$ proton on target [228].

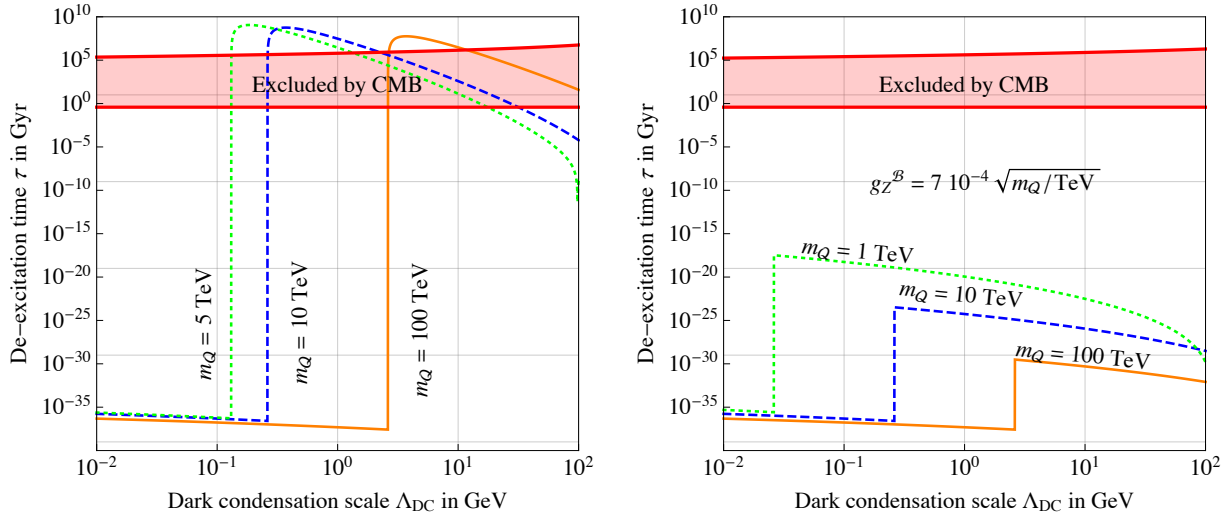


Figure 4.10: *De-excitation life-time of radio-active dark matter, that can be long when $M_\Phi \sim 7\Lambda_{DC}$ is larger than the binding energy. A very long $\tau$ is obtained when the life-time of dark glue-balls is so long that they dilute the DM density. In the left (right) panel glue-balls decay thanks to heavier dark quarks charged under $G_{\rm SM}$ (with a Yukawa coupling $y$ to the Higgs). Bounds from energy injection in the CMB spectrum are shown.*

The conclusion persists even if the theory is modified by adding an extra dark colored scalar neutral under $G_{\rm SM}$, coupled to the Higgs as $\lambda_{HS}|S|^2|H|^2$, which gives an extra contribution $c_6 = \lambda_{HS} T_{\rm DC}/(12 m_S^2)$, enhanced by its possibly small mass $m_S \ll M_h$. Imposing $|\lambda_{HS}| \lesssim 0.01$ in view of bounds on the Higgs invisible width, and $m_S \gtrsim \Lambda_{\rm DC}$ in order not to change the DM phenomenology, we find that dark glue-balls remain undetectable at SHiP.

### 4.4.6 Radioactive Dark Matter

As discussed in section 4.2 the parameter space allows for $E_B \lesssim \Lambda_{\rm DC} \lesssim 1/a_0$ (region B). This leads, in the primordial universe at temperatures $T \lesssim \Lambda_{\rm DC}$, to the production of excited DM bound states. These states can be long-lived if $\Delta E_B < M_\Phi$ such that decays to a dark glue-ball are kinematically forbidden. In models where $\mathcal{Q}$ is neutral under the SM, such excited bound states then can only decay to light SM states (such as $\gamma\gamma$ or $e^+e^-$) through an off-shell glue-ball-like state, giving rise to *radioactive dark-matter*. We can estimate the decay rate of such trapped excited bound states, by splitting the phase space in terms of the invariant mass $M$ of the off-shell virtual dark glue-ball $\Phi$ [221], obtaining

$$\Gamma(\mathcal{B}^* \to \mathcal{B}\,\text{SM}) \;=\; \frac{1}{\pi}\int_0^{\Delta E_B^2} M dM^2\, \frac{\Gamma(\mathcal{B}^* \to \mathcal{B}\,\Phi^*(M))\,\Gamma_{\Phi^*}(M)}{|M^2 - M_\Phi^2 + i\Gamma_\Phi M_\Phi|^2}\,. \tag{4.45}$$

where $\Gamma(\mathcal{B}^* \to \mathcal{B}\,\Phi^*)$ is the decay width into a virtual dark glue-ball with mass $M$, and $\Gamma_{\Phi^*}(M)$ is its decay width into SM states. We approximated the imaginary part of the propagator

$M\Gamma_{\Phi*}(M)$ with the value on-shell. If the dark glue-ball can be on shell, the integral around its peak gives $\Gamma(\mathcal{B}^* \to \mathcal{B}\,\mathrm{SM}) \simeq \Gamma(\mathcal{B}^* \to \mathcal{B}\,\Phi^*)$. We are interested in the opposite regime where the intermediate state is off-shell. For $M_\Phi \gg \Delta E_B$ the propagator is approximately constant and we estimate

$$\Gamma(\mathcal{B}^* \to \mathcal{B}\,\mathrm{SM}) \sim \frac{\Delta E_B^3}{\pi M_\Phi^4}\Gamma(\mathcal{B}^* \to \mathcal{B}\,\Phi^*(0))\Gamma_{\Phi*}(\Delta E_B)\,. \tag{4.46}$$

Taking into account that $\Phi^*$ is a dark glue-ball-like state that does not need to have spin 0, but can match the quantum numbers of two dark gluons, we estimate $\Gamma(\mathcal{B}^* \to \mathcal{B}\,\Phi^*(0)) \approx \alpha_{\rm DC}^4(m_\mathcal{Q})\alpha_{\rm DC}^2(\Lambda_{\rm DC})m_\mathcal{Q}$ as the decay rate into two massless dark gluons. The 4 powers of $\alpha_{\rm DC}(m_\mathcal{Q})$ arise from the bound-state wave function and binding energy, while the two powers of $\alpha_{\rm DC}(\Lambda_{\rm DC}) \sim 1$ arise from dark-gluon emission. $\Gamma_{\Phi*}(\Delta E_B)$ can be small, making excited $\mathcal{B}^*$ long lived, as shown in Fig. 4.10, where the large increase of the life-time corresponds to the transition from on-shell to off-shell decays. In models where Yukawa couplings exist excited DM can decay through $Z-$mediated processes giving a much shorter lifetime, see fig 4.10 right panel.

Bounds on radioactive DM can be inferred by rescaling bounds on decaying DM. An excessive reionization of CMB is roughly obtained for $t_{\rm CMB} \ll \tau < 1.1\,10^9\,\mathrm{Gyr} \times \Delta E_B/M_\mathcal{B}$ [229], where $t_{\rm CMB} \approx 380\,\mathrm{kyr}$ is the Universe age at photon decoupling and $M_\mathcal{B}$ is the DM mass. If DM is still $\gamma$-radioactive today, one must have $\tau > 10^{11}\,\mathrm{Gyr} \times \Delta E_B/M_\mathcal{B}$, for $0.1\,\mathrm{MeV} \lesssim \Delta E_B \lesssim 10\,\mathrm{GeV}$ [230]. If DM is still $\beta$-radioactive today, its de-excitation life-time(s) must be longer than $\tau > 10^7\,\mathrm{Gyr} \times \Delta E_B/M_\mathcal{B}$, for $\mathrm{MeV} \lesssim \Delta E_B \lesssim 10\,\mathrm{GeV}$ [230]. DM with $\tau \sim T_U$ can be borderline at MeV. In view of these bounds and of the model predictions, its seems unlikely that DM can be radioactive enough to heat solving the small-scale potential 'cusp/core' and 'missing satellite' problems of cold DM. In the parameter region without dark matter dilution by glue-ball decay the glue-ball lifetime has to be smaller than one second, as we discussed earlier. This leads to a half life of the radiative states of the order of a few hours. Thus they have no impact on the CMB spectrum.

### 4.4.7 Precision tests

Vector-like fermions do not give large corrections to electro-weak precision observables. The regime $m_\mathcal{Q} \ll \Lambda_{\rm DC}$ was discussed in [231, 232]. The result in the opposite regime is qualitatively similar. The corrections to the precision $S$ and $T$ parameters are

$$\Delta\hat{T} \sim N_{\rm DC}\frac{y^4}{16\pi^2}\frac{v^2}{m_\mathcal{Q}^2}, \qquad \Delta\hat{S} \sim N_{\rm DC}\frac{y^2}{16\pi^2}\frac{v^2}{m_\mathcal{Q}^2}\,. \tag{4.47}$$

Experimental bounds allow couplings $y \sim 1$ if $m_\mathcal{Q}$ is above a few hundred GeV.

Extra Yukawa coupling can give extra effects in flavour. For general Yukawa couplings, the theory contains CP violating phases $\mathrm{Im}[m_{\mathcal{Q}_1}m_{\mathcal{Q}_2}y^*\tilde{y}^*]$ which generate electric dipole moments of SM particles at two loops. Similar effects have been studied in supersymmetry [212]. In a

model with $\mathcal{Q} = L \oplus V$ we estimate

$$d_f \sim N_{\rm DC} e Q_f \frac{\alpha \,{\rm Im}\, y\tilde{y}}{16\pi^3} \frac{m_f}{m_L m_V} \ln \frac{m_L m_V}{M_h^2} \,. \tag{4.48}$$

For the electron this means

$$d_e \sim 10^{-27}\, e\,{\rm cm} \times {\rm Im}[y\tilde{y}] \times \frac{N_{\rm DC}}{3} \times \frac{{\rm TeV}^2}{m_L m_V} \tag{4.49}$$

to be compared with the experimental bound $d_e < 8.7 \times 10^{-29}\ e\,{\rm cm}$ [233]. A somewhat smaller effect is obtained in the $\mathcal{Q} = L \oplus N$ model.

## 4.5 Models

Finally, we analyse the microscopic structure of the simplest models with ${\rm SU}(N_{\rm DC})$ and ${\rm SO}(N_{\rm DC})$ dark gauge interactions. At energies greater than $\Lambda_{\rm DC}$ we have a set a fermions charged under $G_{\rm DC} \otimes G_{\rm SM}$. They annihilate into SM degrees of freedom or dark gluons. Moreover they can form bound states through the emission of dark gluons or SM gauge bosons.

At tree level, a dark quark with mass $m_{\mathcal{Q}}$ has the following $s$-wave annihilation cross section into massless gauge bosons

$$\langle \sigma v_{\rm rel} \rangle_{\rm ann} = \frac{A_1 + A_2}{16\pi g_\chi d_R} \frac{1}{M_\chi^2} \tag{4.50}$$

where

$$A_1 \equiv {\rm Tr}[T^a T^a T^b T^b] \,, \qquad A_2 \equiv {\rm Tr}[T^a T^b T^a T^b] \tag{4.51}$$

and $g_\chi = 4(2) d_R$ for Dirac or Majorana fermions. For dark quarks charged under both $G_{\rm DC}$ and $G_{\rm SM}$ the notation above stands for $T \equiv (g_{\rm DC} T_{\rm DC} \otimes 1) \oplus (1 \otimes g_{\rm SM} T_{\rm SM})$. For dark quarks in the irreducible representation $(N, R_{\rm SM})$ the formula above gives

$$\langle \sigma v_{\rm rel} \rangle_{\rm ann} = \frac{1}{d_{\rm SM}} \frac{K_1^{\rm DC} + K_2^{\rm DC}}{4(2) N_{\rm DC}^2} \frac{\pi \alpha_{\rm DC}^2}{M_\chi^2} + \frac{1}{N_{\rm DC}} \frac{K_1^{\rm SM} + K_2^{\rm SM}}{4(2) d_{\rm SM}^2} \frac{\pi \alpha_{\rm SM}^2}{M_\chi^2} + \frac{4 C_{\rm DC} C_{\rm SM}}{4(2) d_{\rm SM} N_{\rm DC}} \frac{\pi \alpha_{\rm DC} \alpha_{\rm SM}}{M_\chi^2} \,. \tag{4.52}$$

The group theory factors are listed in Table 4.1 using

$$K_1(R) = d(R) C(R)^2 \,, \qquad K_2(R) = K_1(R) - \frac{d(A) C(A) T(R)}{2} \,. \tag{4.53}$$

Furthermore, dark quarks charged under the SM undergo extra annihilations into SM fermions and into the Higgs.

Due to the attraction/repulsion of light mediators, the tree level cross-section is corrected by the Sommerfeld effect [234,62,235,236] as $\sigma \approx S \times \sigma_0$, where $S$ encodes the effect of long-distance interactions that deflect the incoming fermion wave-function. The effect of SM vectors is known

| $G_{\rm DC}$ | $R_i \rightleftarrows R_f$ | $I_{R_i \to R_f}$ |
|---|---|---|
| SU($N$) | $1 \rightleftarrows \text{adj}$ | $\frac{N^2-1}{2N}\left\lvert 1 \pm \frac{N}{2\lambda_f}\right\rvert^2$ |
| | $\begin{smallmatrix}\square\\\square\end{smallmatrix} \rightleftarrows \square\square$ | $\frac{N^3-N}{8}\left\lvert 1 \pm \frac{1}{\lambda_f}\right\rvert^2$ |
| SO($N$) | $1 \rightleftarrows \text{adj}$ | $(N-1)\left\lvert 1 \pm \frac{N-2}{\lambda_f}\right\rvert^2$ |
| | $\text{adj} \rightleftarrows \square\square$ | $\frac{N^3-N^2-4N+4}{4}\left\lvert 1 \pm \frac{2}{\lambda_f}\right\rvert^2$ |

Table 4.3: *Group-theory factors for formation of a bound state in the representation $R_f$ from an initial state in the representation $R_i$ and viceversa.*

from the literature. We focus here on the effect of dark gluons. For $s$-wave annihilation

$$S = \frac{2\pi\alpha_{\rm eff}/v_{\rm rel}}{1 - e^{-2\pi\alpha_{\rm eff}/v_{\rm rel}}} \tag{4.54}$$

where $\alpha_{\rm eff}$ is the effective coupling in each dark color channel as defined in eq. (4.8). The fermion bi-linears decompose in the representation of the dark-color group:

$$G_{\rm DC} = \text{SU}(N_{\rm DC}): \qquad N_{\rm DC} \otimes \bar{N}_{\rm DC} = \mathbb{1} \oplus \text{adj}, \qquad N_{\rm DC} \otimes N_{\rm DC} = \square\square \oplus \begin{smallmatrix}\square\\\square\end{smallmatrix} \tag{4.55}$$

$$G_{\rm DC} = \text{SO}(N_{\rm DC}): \qquad N_{\rm DC} \otimes N_{\rm DC} = \mathbb{1} \oplus \text{adj} \oplus \square\square. \tag{4.56}$$

The effective potential in each channel is given by eq. (4.8) with $\lambda_J = 0$ and $\lambda_I = \lambda_R$ where

$G_{\rm DC} = \text{SU}(N_{\rm DC})$

| $R$ | $\lambda_R \times (2N)$ | bound states |
|---|---|---|
| 1 | $N_{\rm DC}^2 - 1$ | yes |
| adj | $-1$ | no |
| $\square\square$ | $1 - N_{\rm DC}$ | no |
| $\begin{smallmatrix}\square\\\square\end{smallmatrix}$ | $N_{\rm DC} + 1$ | yes |

$G_{\rm DC} = \text{SO}(N_{\rm DC})$

| $R$ | $\lambda_R$ | bound states |
|---|---|---|
| 1 | $N_{\rm DC} - 1$ | yes |
| adj | 1 | yes |
| $\square\square$ | $-1$ | no |

(4.57)

Furthermore, two dark quarks can form a bound states emitting one vector. A pair of dark quarks in the fundamental representation feels an attractive force in the singlet and in the antisymmetric configuration. Using the results derived in the first chapter, the cross section for forming the ground state, with quantum numbers $n = 1$ and $\ell = 0$, is

$$(\sigma v_{\rm rel})_{\rm bsf} = \frac{1}{N_F}\sigma_0 \lambda_i (\lambda_f \zeta)^5 \frac{2S+1}{g_\chi^2} \frac{2^{11}\pi(1+\zeta^2\lambda_i^2)e^{-4\zeta\lambda_i \text{arccot}(\zeta\lambda_f)}}{3(1+\zeta^2\lambda_f^2)^3\,(1-e^{-2\pi\zeta\lambda_i})} \times I_{R_i \to R_f} \tag{4.58}$$

| Name | $I$ | $S$ | $n$ | $\ell$ | $\Gamma_{\rm ann}/M_\chi$ | $N_{\rm DC}=3$ | $N_{\rm DC}=4$ | $N_{\rm DC}=5$ | $\Gamma_{\rm dec}/M_\chi$ | Prod. from |
|---|---|---|---|---|---|---|---|---|---|---|
| $1s_1^-$ | 1 | 0 | 1 | 0 | | $(8/6)^3\alpha_{\rm DC}^5$ | $(15/8)^4\alpha_{\rm DC}^5$ | $3(24/10)^3\alpha_{\rm DC}^5$ | 0 | $p_{\rm adj}$ |
| $1s_1^+$ | 1 | 1 | 1 | 0 | $\frac{5(\pi^2-9)}{\pi}\times$ | $2^6\alpha_{\rm DC}^6/3^7$ | $15^3\alpha_{\rm DC}^6/2^{14}$ | $3^3(2/5)^6\alpha_{\rm DC}^6/7$ | 0 | $p_{\rm adj}$ |
| $1s_{\boxplus}$ | $\boxplus$ | 1 | 1 | 0 | | 0 | 0 | 0 | 0 | $p_{\square\square}$ |
| $2s_1^-$ | 1 | 0 | 2 | 0 | | $(8/12)^3\alpha_{\rm DC}^5$ | $15^4\alpha_{\rm DC}^5/8^5$ | $3(24/20)^3\alpha_{\rm DC}^5$ | $\mathcal{O}(\alpha_{\rm DC}^6)$ | $p_{\rm adj}$ |
| $2s_1^+$ | 1 | 1 | 2 | 0 | $\frac{5(\pi^2-9)}{\pi}\times$ | $2^3\alpha_{\rm DC}^6/3^7$ | $15^3\alpha_{\rm DC}^6/2^{17}$ | $6^3/7(\alpha_{\rm DC}/5)^6$ | $\mathcal{O}(\alpha_{\rm DC}^6)$ | $p_{\rm adj}$ |
| $2s_{\boxplus}$ | $\boxplus$ | 1 | 2 | 0 | | $\mathcal{O}(\alpha_{\rm DC}^6)$ | $\mathcal{O}(\alpha_{\rm DC}^6)$ | $\mathcal{O}(\alpha_{\rm DC}^6)$ | $\mathcal{O}(\alpha_{\rm DC}^6)$ | $p_{\square\square}$ |
| $2p_1^-$ | 1 | 0 | 2 | 1 | | $\mathcal{O}(\alpha_{\rm DC}^7)$ | $\mathcal{O}(\alpha_{\rm DC}^7)$ | $\mathcal{O}(\alpha_{\rm DC}^7)$ | $\mathcal{O}(\alpha_{\rm DC}^6)$ | $s_{\rm adj}$ |
| $2p_1^+$ | 1 | 1 | 2 | 1 | | $\mathcal{O}(\alpha_{\rm DC}^7)$ | $\mathcal{O}(\alpha_{\rm DC}^7)$ | $\mathcal{O}(\alpha_{\rm DC}^7)$ | $\mathcal{O}(\alpha_{\rm DC}^6)$ | $s_{\rm adj}$ |
| $2p_{\boxplus}$ | $\boxplus$ | 0 | 2 | 1 | | $\mathcal{O}(\alpha_{\rm DC}^7)$ | $\mathcal{O}(\alpha_{\rm DC}^7)$ | $\mathcal{O}(\alpha_{\rm DC}^7)$ | $\mathcal{O}(\alpha_{\rm DC}^6)$ | $s_{\square\square}$ |

Table 4.4: *Summary of perturbative di-quark bound states in* SU($N$) *models.*

where $\sigma_0 \equiv \pi\alpha_{\rm DC}^2/M_\chi^2$, $\zeta \equiv \alpha_{\rm DC}/v_{\rm rel}$ and $\lambda_{i,f}$ are the effective strength of the coupling $\alpha_{\rm eff} \equiv \lambda_I \alpha_{\rm DC}$ of the initial and final state channels respectively, in two-body representation $R_i$ and $R_f$. And similarly for the other excited levels. The $I_{R_i\to R_f}$ factors encode the group theory structure and are listed in Table 4.3.

### 4.5.1 Model with $G_{\rm DC} = {\rm SU}(3)$ and singlet dark quark

We first consider the model where the dark quark $\mathcal{Q}$ in the fundamental of SU($N_{\rm DC}$) is a singlet under the SM. We assume that extra unspecified heavier dark quarks with SM charges couple the dark sector with the SM sector, such that glue-balls decay into SM particles. The $s$-wave $\mathcal{Q}\bar{\mathcal{Q}}$ annihilation cross-section into dark gluons is

$$\langle\sigma v_{\rm rel}\rangle = \frac{N_{\rm DC}^4 - 3N_{\rm DC}^2 + 2}{16N_{\rm DC}^3}\left(\frac{2}{N_{\rm DC}^2-2}S_1 + \frac{N_{\rm DC}^2-4}{N_{\rm DC}^2-2}S_{\rm adj}\right)\times\frac{\pi\alpha_{\rm DC}^2}{M_\chi^2} \tag{4.59}$$

where $S_1$ and $S_{\rm adj}$ are the Sommerfeld factors for the singlet (attractive) and adjoint (repulsive) channels.

Let us consider the bound states. The SU($N_{\rm DC}$) interactions give two attractive configurations that can support bound states: the singlet contained in $\mathcal{Q}\otimes\bar{\mathcal{Q}}$ and the anti-symmetric configuration in $\mathcal{Q}\otimes\mathcal{Q}$. The former is unstable and gives a contribution to the effective annihilation cross section, see Appendix; the latter is stable and could give rise to dark-recombination at low temperatures ($T \lesssim \alpha_{\rm DC}^2 M_\chi$). The unstable bound state is made of Dirac particles so it exists for any choice of quantum numbers $n, \ell, s$. The stable bound state is made of identical particles, so that a fully anti-symmetric wave-function implies that it must have spin 1 in $s$-wave and spin-0 in $p$-wave. Moreover it can only be produced from an initial state in the symmetric configuration. The main bound states together with their key properties are summarized in Table 4.4.

If dark confinement happens after freeze-out, the thermal relic abundance of DM is obtained

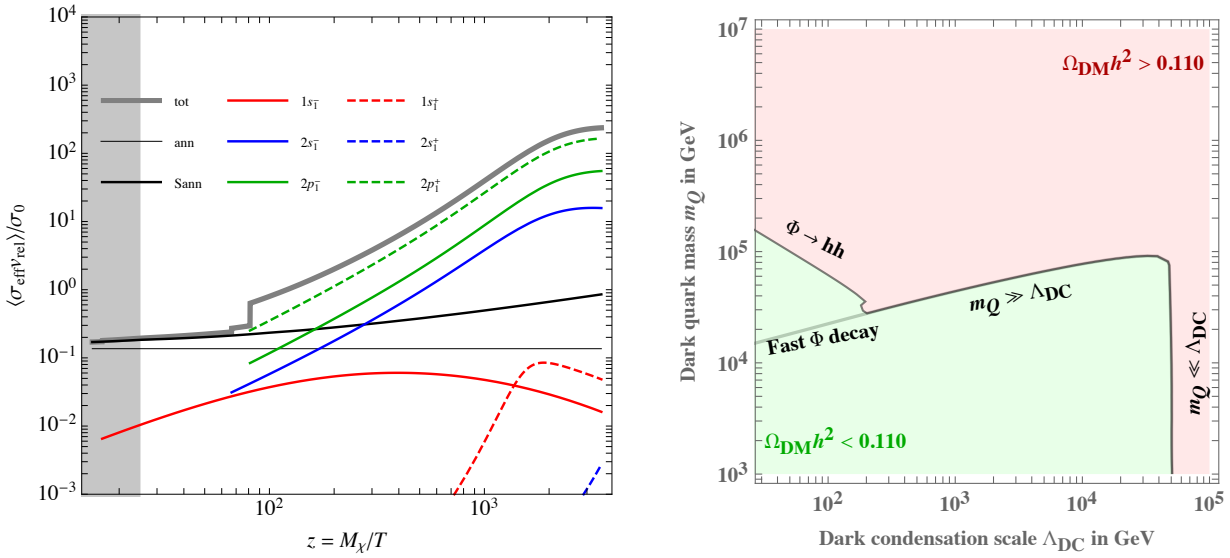


Figure 4.11: *Model with $G_{\rm DC} = {\rm SU}(3)$ and a dark quark neutral under $G_{\rm SM}$.* **Left***: thermally averaged cross sections for annihilation and for bound states formation, assuming $m_{\mathcal{Q}} = 10\,{\rm TeV}$ and $\alpha_{DC} = 0.1$ ($\Lambda_{DC} \approx 30\,{\rm GeV}$).* **Right***: region where dark baryons reproduce the DM cosmological abundance. A recombination fraction $\wp_{\mathcal{B}} = 0.4$ is assumed.*

by first solving the Boltzmann equations for the elementary dark quarks and their perturbative bound states. Table 4.4 implies that the bound states are produced from a repulsive initial state. This suppresses the production of stable and unstable di-quark bound states at late times, where the kinetic energy is insufficient to overcome the repulsion. As a consequence, we find that the thermal relic abundance is mostly due to perturbative annihilations boosted by the Sommerfeld enhancement, and by di-quark bound state production at earlier times. At $T \sim \Lambda_{\rm DC}$ confinement occurs in the dark sector, and a fraction of the dark quarks is converted into dark baryons. The dark baryons can undergo recombination annihilations, which have large cross sections, leading to a late-time dark matter depletion.

When dark confinement takes place before freeze-out, annihilations are still governed by the constituent cross section, provided that the typical velocities at freeze-out are large enough. At lower velocities, the larger recombination cross section produces a late-time dark matter depletion.

Taking all these effects into account, Fig. 4.11 shows an estimate of the parameter region where the thermal relic abundance of dark baryons matches the cosmological DM abundance.

A dark quark $\mathcal{Q}$ singlet under the SM can interact with the SM sector through heavier mediators. The most interesting possibility is realised adding a vector-like dark quark $L$, allowing to write Yukawa couplings with the SM Higgs

$$-\mathscr{L} = m_L L L^c + m_N N N^c + y\, L H N^c + \tilde{y}\, L^c H^\dagger N + \text{h.c.} \tag{4.60}$$

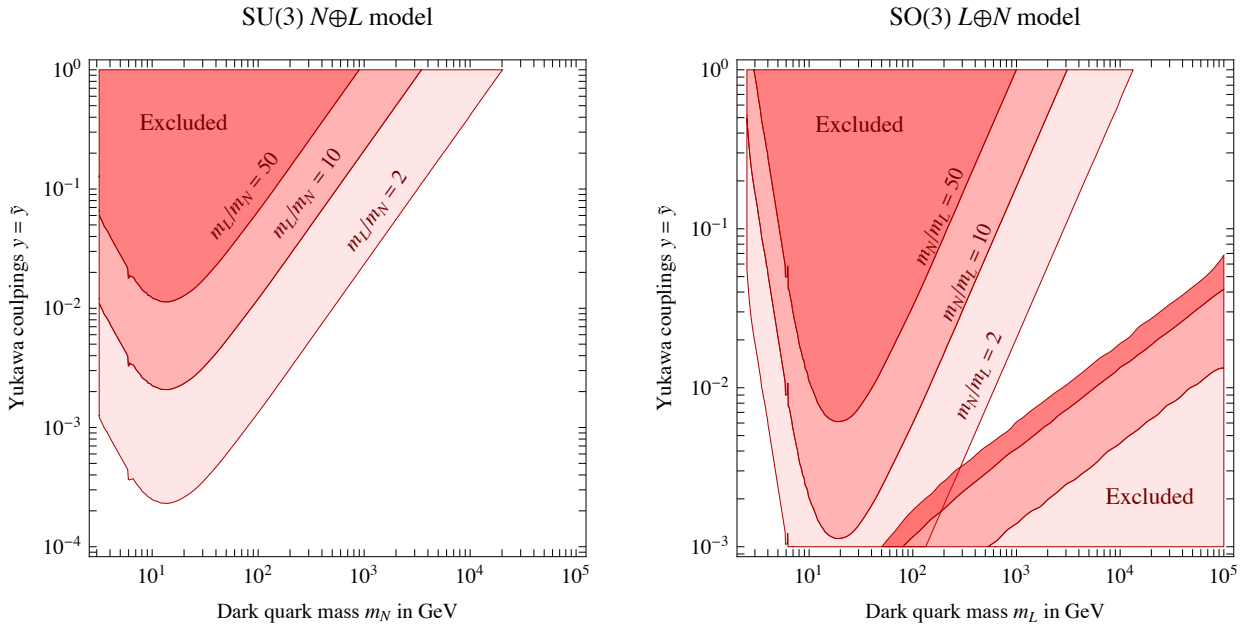


Figure 4.12: *Direct detection bounds, assuming dark quarks $\mathcal{Q} = N\oplus L$ with Yukawa couplings to the Higgs.* **Left:** *we consider the* SU(3) *model with $m_N < m_L$.* **Right:** *we consider the* SO(3) *model with $m_L < m_N$, such that a large enough Yukawa coupling is needed in order to suppress $Z$-mediated inelastic scatterings.*

As explained in section 4.4.3, after electro-weak symmetry breaking the singlets mix with the neutral component of the doublet generating an effective coupling to the $Z$ and to the Higgs. Denoting with $U_L$ and $U_R$ the rotation matrices to the mass eigenstate basis, the coupling to $Z$ is

$$\frac{g_2}{2\cos\theta_W} Z_\mu \left( \bar{N}_i (U_L^\dagger)_{2i} \bar{\sigma}^\mu (U_L)_{2j} N_j - \bar{N}_i^c (U_R^\dagger)_{2i} \bar{\sigma}^\mu (U_R)_{2j} N_j^c \right) . \tag{4.61}$$

For real Yukawa couplings (no CP violation) the $U_{L,R}$ are SO(2) matrices with rotation angle

$$\tan 2\theta_L = \frac{2\sqrt{2}v\,(m_L\tilde{y} + m_N y)}{2m_L^2 - 2m_N^2 + (yv)^2 - (\tilde{y}v)^2} \tag{4.62}$$

for $U_L$ and similarly for $U_R$. The light singlet dark quark $N$ acquires the coupling

$$\frac{g}{2\cos\theta_W} Z_\mu \left( (s_L^2 + s_R^2) \bar{N}\gamma_\mu N - (s_L^2 - s_R^2) \bar{N}\gamma_\mu\gamma_5 N \right) . \tag{4.63}$$

Bounds from Higgs-mediated interactions are typically weaker and have a different dependence on the mixings, namely

$$\frac{h}{\sqrt{2}} \left( \tilde{y}\, c_L s_R + y\, c_R s_L \right) \bar{N} N \, . \tag{4.64}$$

Fig.4.12 shows the bounds on the Yukawa coupling $y$, once we combine Higgs-mediated and

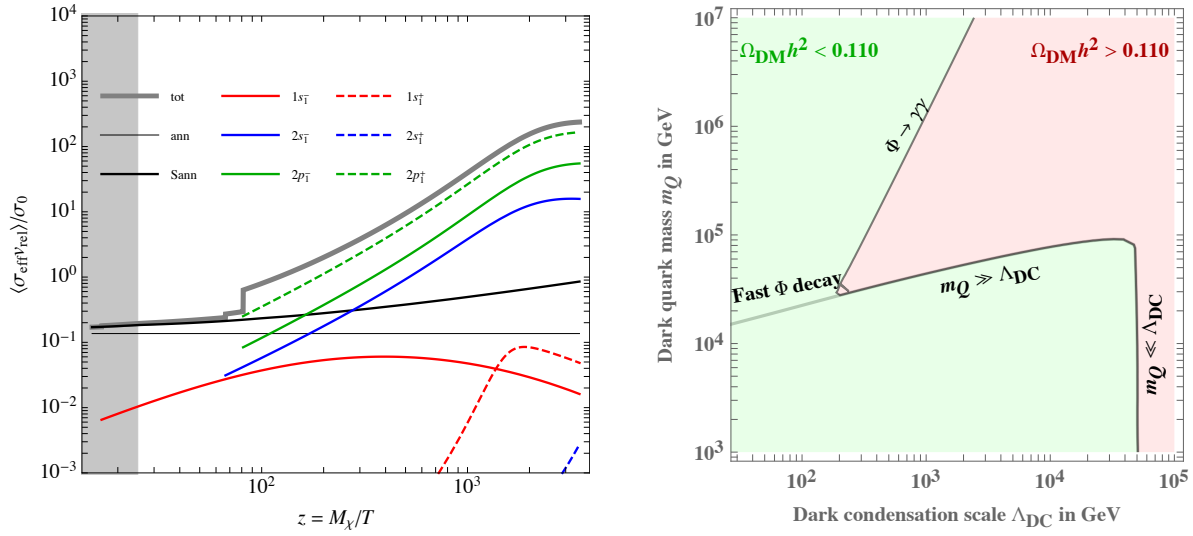


Figure 4.13: *Model with* $G_{\rm DC} = {\rm SU}(3)$ *and with a dark quark tripled under* ${\rm SU}(2)_L$. **Left:** *thermally averaged cross sections for annihilation and for bound states formation, assuming* $m_{\mathcal{Q}} = 10\,{\rm TeV}$ *and* $\alpha_{DC} = 0.07$ *(*$\Lambda_{DC} \approx 3$ *GeV).* **Right:** *region where dark baryons reproduce the DM cosmological abundance.*

$Z$-mediated effects. Experiments are sensitive even to heavy and weakly mixed fermions.

### 4.5.2 Model with $G_{\rm DC} = {\rm SU}(3)$ and dark quark triplet under ${\rm SU}(2)_L$

We next consider the $G_{\rm TC} = {\rm SU}(N_{\rm DC})$ model with dark quarks in a triplet ($V$) of ${\rm SU}(2)_L$. Requiring no sub-Planckian Landau poles selects $N_{\rm DC} = 3$. We compute in terms of ${\rm SU}(2)_L$ multiplets, neglecting the 165 MeV electro-weak splitting between charged and neutral components. SM gauge interactions keep the dark sector in thermal equilibrium with the SM sector. Pairs of dark quarks decompose as

$$\mathcal{Q}\otimes\overline{\mathcal{Q}} = (1\oplus 8, 1\oplus 3\oplus 5), \qquad \mathcal{Q}\otimes\mathcal{Q} = (\overline{3}\oplus 6, 1\oplus 3\oplus 5). \tag{4.65}$$

The annihilation cross-section among dark quarks is

$$\langle\sigma v_{\rm rel}\rangle = \left(\frac{7}{162}\frac{\pi\alpha_{\rm DC}^2}{M_\chi^2} + \frac{8}{27}\frac{\pi\alpha_{\rm DC}\alpha_2}{M_\chi^2} + \frac{37}{72}\frac{\pi\alpha_2^2}{M_\chi^2}\right)\left(\frac{2}{7}S_1 + \frac{5}{7}S_8\right). \tag{4.66}$$

where $\lambda_1 = 4/3$ and $\lambda_8 = -1/6$ are the effective strengths of the Sommerfeld factors for the singlet and octet channels. For $\alpha_{\rm DC} < 3\alpha_2$ the annihilation cross-section is dominated by the SM interactions.

In the absence of confinement the desired DM relic abundance is obtained for $m_{\mathcal{Q}} \approx 2.5{\rm TeV}/\sqrt{2N_{\rm DC}}$; such a model is however only allowed for $\alpha_{\rm DC} \lesssim 10^{-8}$ [208]. We assume that dark interactions

dominate or are comparable with the SM ones.

Neglecting SM interactions, the meson bound states are listed in Table 4.4. Each bound state has 9 components and decomposes as $1 \oplus 3 \oplus 5$ under $\mathrm{SU}(2)_L$. The singlet and quintuplet are symmetric under $\mathrm{SU}(2)_L$, so they have the same spin as in the previous case $\mathcal{Q} = N$ listed in Table 4.4. The triplet have the opposite spin, being anti-symmetric under $\mathrm{SU}(2)_L$.

The lightest baryons have spin 1/2 and lie in the adjoint representation of flavour $\mathrm{SU}(3)_F$, and split as $8 = 3 \oplus 5$ taking $\mathrm{SU}(2)_L$ gauge interactions into account, such that the triplet is lighter than the quintuplet.

Predictions for direct detection are then the same as for any fermion weak triplet (such as wino [237]): $\sigma_{\rm SI}$ lies above the the neutrino background for $m_{\mathcal{B}} \lesssim 15$ TeV. Constraints on Yukawa couplings with heavier dark quarks are similar to those discussed in the $N \oplus L$ model.

The annihilation cross-section relevant for indirect detection a few orders of magnitude above the canonical thermal value $3\ 10^{-26}\,\mathrm{cm}^3/\mathrm{sec}$, being dominated by long-range rearrangement processes as discussed around eq. (4.16); presumably without extra Sommerfeld enhancement. Present bounds are shown in Fig. 4.7, as a function of the dark glue-ball mass which controls the energy spectrum of final-state particles. We combine searches for diffuse gamma rays from the FermiLAT satellite and from the ground based H.E.S.S. observatory The FermiLAT limits are more relevant in the case of light glue-balls decaying into photons; the H.E.S.S. limits are sensitive to the cascade photons resulting from $W$ boson decays in case of heavy glue-balls. The sensitivity of the photon searches strongly depends on the number of steps in the dark hadronization cascade and is thus rather uncertain. The limits coming from annihilation into $WW$ are more robust. We also show the limits from CMB energy injection are shown, which have smaller astrophysical and theoretical uncertainties.

### 4.5.3 Models with $G_{\rm DC} = \mathrm{SO}(N_{\rm DC})$

As discussed in section 4.1.1, models with dark gauge group $\mathrm{SO}(N_{\rm DC})$ give rise to Majorana DM, allowing for lightest dark quakrs in more general representations under $G_{\rm SM}$. The annihilation cross-section of fermions in the fundamental of $\mathrm{SO}(N_{\rm DC})$ into dark gluons is

$$\langle \sigma v_{\rm rel} \rangle = \frac{N_{\rm DC}^2(N_{\rm DC}-1)}{2} \left( \frac{4}{N_{\rm DC}^2} S_{\mathbf{1}} + \frac{N_{\rm DC}^2 - 4}{N_{\rm DC}^2} S_{\square\square} \right) \times \frac{\pi \alpha_{\rm DC}^2}{M_\chi^2} \tag{4.67}$$

where $S_{\mathbf{1}}$ and $S_{\rm adj}$ are the Sommerfeld factors for the singlet and adjoint channel respectively. As a simple example we consider the model with a singlet $N$ and a doublet $L$,

$$-\mathscr{L} = m_L L L^c + \frac{m_N}{2} N^2 + y\, L H N + \tilde{y}\, L^c H^\dagger N + \text{h.c.} \tag{4.68}$$

Differently from the singlet model in section 4.5.1, $N$ and $N^c$ are the same particle. The mass matrix of the neutral states is

$$\mathscr{L} \supset \frac{1}{2}\,(N_1, N_2, N_3) \begin{pmatrix} 0 & m_L & vy/\sqrt{2} \\ m_L & 0 & v\tilde{y}/\sqrt{2} \\ vy/\sqrt{2} & v\tilde{y}/\sqrt{2} & m_N \end{pmatrix} \begin{pmatrix} N_1 \\ N_2 \\ N_3 \end{pmatrix} + \text{h.c.} \tag{4.69}$$

where the Weyl fermions $N_1$ and $N_2$ are the neutral components of $L$ and $L^c$ and $N_3 \equiv N$. The mass matrix can be diagonalised as $M_{\text{diag}} = U^T M U$, where, at leading order in the Yukawa couplings

$$U = \begin{pmatrix} \frac{1}{\sqrt{2}} & \frac{i}{\sqrt{2}} & -\frac{\tilde{y}v}{\sqrt{2}(m_L - m_N)} \\ \frac{1}{\sqrt{2}} & -\frac{i}{\sqrt{2}} & -\frac{yv}{\sqrt{2}(m_L - m_N)} \\ \frac{v(y+\tilde{y})}{2(m_L - m_N)} & \frac{i(y-\tilde{y})v}{2(m_L - m_N)} & 1 \end{pmatrix}. \tag{4.70}$$

The gauge coupling to the $Z$ in the flavor basis are $Q_Z = \text{diag}(1/2, -1/2, 0)$. Rotating to the mass basis we obtain the couplings of the mass eigenstates to the $Z$,

$$g_{ij} \equiv \left(U^\dagger Q_Z U\right)_{ij} = \begin{pmatrix} 0 & \frac{i}{2} & \frac{(y-\tilde{y})v}{4(m_L - m_N)} \\ -\frac{i}{2} & 0 & i\frac{(y+\tilde{y})v}{4(m_L - m_N)} \\ \frac{(y^* - \tilde{y}^*)v}{4(m_L - m_N)} & -i\frac{(y^* + \tilde{y}^*)v}{4(m_L - m_N)} & \frac{-(|y|^2 + |\tilde{y}|^2)v^2}{4(m_L - m_N)^2} \end{pmatrix}_{ij}. \tag{4.71}$$

Because the mass eigenstates are Weyl fermions, the diagonal couplings of DM to the $Z$ are purely axial. This can be made manifest converting to Majorana notation $\Psi_M \equiv (N, \bar{N})/\sqrt{2}$ such that $\bar{\Psi}^i_M \gamma^\mu \Psi^i_M$ vanishes identically. In this basis one finds

$$\frac{g_2}{\cos\theta_{\text{W}}} Z_\mu \left[a_{ij} \bar{\Psi}^i_M \gamma^\mu \gamma^5 \Psi^j_M + i v_{ij} \bar{\Psi}^i_M \gamma^\mu \Psi^j_M\right] \tag{4.72}$$

where $a_{ij} = -\text{Re}\, g_{ij}$ and $v_{ij} = \text{Im}\, g_{ij}$. From eq. (4.71) we see that the only non vanishing terms are of the form $\bar{\Psi}^i_M \gamma^\mu \gamma^5 \Psi^i_M$ and $\bar{\Psi}^i_M \gamma^\mu \Psi^j_M$ with $i \neq j$. The first interaction gives rise to spin-dependent interactions suppressed by the mixing with the heavier states, which are below the sensitivity of present experiments. The second interaction produces inelastic scattering between states with a mass splitting of order $\Delta m \sim y^2 v^2/(m_N - m_L)$.

The Higgs-mediated contribution to direct detection is similar to $\text{SU}(N_{\text{DC}})$ models. Writing $\mathscr{L}_H = y_{ij} h N^i N^j/\sqrt{2} + \text{h.c.}$ one finds

$$y_{ij} \equiv \left(U^T \frac{\partial M(h)}{\partial h} U\right)_{ij} = \begin{pmatrix} \frac{(y+\tilde{y})^2 v}{2(m_L - m_N)} & \frac{i(y^2 - \tilde{y}^2)v}{2(m_L - m_N)} & \frac{(y+\tilde{y})}{2} \\ \frac{i(y^2 - \tilde{y}^2)v}{2(m_L - m_N)} & -\frac{(y-\tilde{y})^2 v}{2(m_L - m_N)} & \frac{i(y-\tilde{y})}{2} \\ \frac{(y+\tilde{y})}{2} & \frac{i(y-\tilde{y})}{2} & -\frac{2y\tilde{y}v}{m_L - m_N} \end{pmatrix}_{ij}. \tag{4.73}$$

Fig. 4.12 illustrates the present bounds on the Yukawa couplings.

## 4.6 Summary

We studied fundamental theories of Dark Matter as baryons made of a dark quark $\mathcal{Q}$ with mass $m_{\mathcal{Q}}$, charged under a dark gauge group $\mathrm{SU}(N_{\rm DC})$ or $\mathrm{SO}(N_{\rm DC})$ that becomes strong at a scale $\Lambda_{\rm DC}$. The main options for the gauge quantum numbers of $\mathcal{Q}$ are: either neutral or charged under the SM gauge group. DM is stable because dark baryon number is accidentally conserved, analogously to the proton in the SM.

In past works the possibility that $\mathcal{Q}$ is lighter than the dark condensation scale $\Lambda_{\rm DC}$ has been studied, finding that the DM cosmological abundance is reproduced as a thermal relic for $\Lambda_{\rm DC} \sim 100\,\mathrm{TeV}$, which saturates the perturbative unitarity bound on DM annihilations. In this chapter we explored the opposite situation: this simple generalization leads to unusual and non-trivial DM phenomenology.

The dark confinement scale $\Lambda_{\rm DC}$ can be as low as 10 GeV, giving rise to unstable dark glue-balls with mass $M_\Phi \sim 7\Lambda_{\rm DC}$ as lightest dark particles. Dark glue-balls decay into lighter SM particles, and can be searched for in low-energy experiments.

In cosmology, dark quarks freeze-out as usual at $T \sim m_{\mathcal{Q}}/25$. DM can be lighter than 100 TeV because the dark gauge coupling $\alpha_{\rm DC}$ is perturbative, when renormalized at this energy. However, a second stage of cosmological history contributes to determining the DM relic abundance: after a first-order phase transition at $T \sim \Lambda_{\rm DC}$ (that can lead to gravitational waves) the dark quarks must bind into objects neutral under dark color: a fraction of dark quarks forms dark mesons, that decay, the rest binds into stable dark baryons $\mathcal{B}$ that survive as DM. We estimated this fraction in a geometric model of dark hadronization, that takes into account that dark strings do not break. As a consequence the annihilation cross section among dark quarks, $\sigma_{\mathcal{Q}\bar{\mathcal{Q}}} v_{\rm rel} \sim \pi\alpha_{\rm DC}^2/m_{\mathcal{Q}}^2$ can be smaller than the standard cosmological value, $3\ 10^{-26}\,\mathrm{cm}^3/\mathrm{sec}$.

More importantly, the annihilation cross section among dark baryons, $\sigma_{\mathcal{B}\bar{\mathcal{B}}} v_{\rm rel} \sim 1/\alpha_{\rm DC} m_{\mathcal{Q}}^2$, is typically much larger than $\sigma_{\mathcal{Q}\bar{\mathcal{Q}}}$, being enhanced by a negative power of $\alpha_{\rm DC}$. This happens because annihilation can proceed through an atomic-physics process, recombination: at low enough energy a dark quark $\mathcal{Q}$ in a dark baryon $\mathcal{B}$ can recombine forming a meson with a $\bar{\mathcal{Q}}$ in a $\bar{B}$; afterwards the meson decays through the usual particle-physics $\mathcal{Q}\bar{\mathcal{Q}}$ annihilation. If $m_{\mathcal{Q}} \gg \Lambda_{\rm DC}$ the bound state $\mathcal{B}$ is dominated by the Coulombian part of the potential, and this is similar to recombination occurring in hydrogen anti-hydrogen scattering. We computed the binding energies of dark baryons and mesons by means of a variational method, finding that recombination is kinematically allowed. If instead $m_{\mathcal{Q}} \gtrsim \Lambda_{\rm DC}$ the confining part of the potential is relevant, and the process can be seen as the crossing of dark strings (flux tubes of the dark color interaction). In cosmology, the large $\sigma_{\mathcal{B}\bar{\mathcal{B}}} \gg \sigma_{\mathcal{Q}\bar{\mathcal{Q}}}$ leads to extra dilution of the DM density. In astrophysics, it leads to large signals for indirect DM detection. Dark mesons decay into dark glue-balls: depending on the model their decays might be dominated by gauge couplings (producing photons) or by Yukawa couplings (producing leptons, which can provide a DM interpretation of the $e^+$ excess observed by PAMELA and AMS [238])).

Cosmological evolution leads to the formation of excited dark baryons, which quickly decay

into glue-balls provided that their excitation energy $\Delta E_B \sim \alpha_{\rm DC}^2 m_{\mathcal{Q}}$ is larger than $M_\Phi \sim 7\Lambda_{\rm DC}$. Otherwise, de-excitation can be slow, proceeding through off-shell dark glue-balls, giving rise to a novel phenomenon: dark matter that emits either $\beta$ or $\gamma$ radioactivity (again depending on whether gauge couplings of Yukawa couplings dominate). It would be interesting to explore whether radio-active DM can alleviate the core/cusp and missing-satellite issue of cold DM.

Finally, we studied the direct-detection and collider phenomenology of models where DM is made of heavy baryons. Heavy dark quarks can be produced at colliders, manifesting as narrow spin-0 or spin-1 resonances and producing effects in SM precision observables. Current bounds are consistent with a lightest dark quark charged under the SM heavier than 1-2 TeV.

# Chapter 5

# Bound states from Dark Sectors: part II

Here we continue our analysis of accidental composite DM models considering a new kind of candidate, the *gluequark*, which has properties different from those of dark baryons and mesons in several respects. Gluequarks are bound states made of one dark quark and a cloud of dark gluons in theories where the new fermions transform in the adjoint representation of dark color. They are accidentally stable due to dark parity, an anomaly free subgroup of dark fermion number, which is exact at the level of the renormalizable Lagrangian. Depending on the SM quantum numbers of the new fermions, violation of dark parity can arise from UV-suppressed dimension-6 operators thus ensuring cosmologically stable gluequarks for sufficiently large cut-off scales. Contrary to baryons and mesons, the physical size of the gluequark is determined by the confinement scale independently of its mass. In the regime of heavy quark masses, $M_{\mathcal{Q}} > \Lambda_{\rm DC}$, this implies a physical size larger than its Compton wavelength, see Fig. 5.1. The annihilation cross section for such a large and heavy bound state can be geometric, much larger than the perturbative unitarity bound of elementary particles. This in turn modifies the thermal relic abundance and can lead to significant effects in indirect detection experiments (similarly to what we already saw in Chapter 2 and 3). Also, the resulting cosmological history is non-standard and different from that of theories with baryon or meson DM candidates.

Bound states made of one dark fermion and dark gluons were considered in Ref. [239], where they couple to the SM sector through the neutrino portal. Similar DM candidates were also studied in Refs. [240, 241], in the context of supersymmetric gauge theories. There, bound states of one fermion (the dark gluino) and dark gluons arise as the partners of glueballs after confinement and were consequently called glueballinos. Ref. [240] showed that the observed DM abundance can be reproduced by a mixture of glueballs and glueballinos provided that the dark and SM sectors are decoupled very early on in their thermal history. In such scenario the two sectors interact only gravitationally, the dark gluino being neutral under the SM gauge group. Notice that the stability of glueballs in this case does not follow from an accidental symmetry but is a consequence of the feeble interaction between the SM and dark sectors. In this chapter we will focus on the possibility that dark fermions are charged under the SM gauge group, so that the lightest states of the dark sector may be accessible through non-gravitational probes. In this

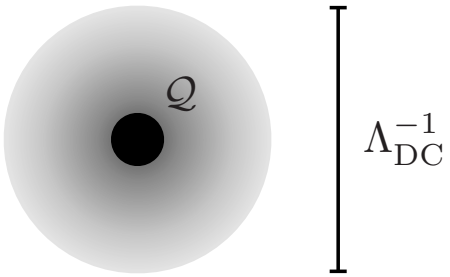


Figure 5.1: *Cartoon of the gluequark DM candidate. A heavy fermion in the adjoint of color gives rise to color singlet state surrounded by a gluon cloud of size* $1/\Lambda_{DC} \gg 1/M_{\mathcal{Q}}$.

case the dark and visible sectors stay in thermal equilibrium until relatively low temperatures, of the order of 1 GeV, and the thermal history of the Universe is rather different than that described in Refs. [240, 241]. In particular, we will argue that in our scenario dark glueballs cannot account for a sizeable fraction of DM because of BBN and CMB constraints.

Composite DM candidates from theories with adjoint fermions were also considered in the context of Technicolor models, see for example Refs. [242, 243]. Those constructions differ from ours in that technicolor quarks are assumed to transform as complex representations under the SM, but they can share common features with some of the models described in this chapter [1].

The chapter is organized as follows. Section 5.1 provides a classification of models with adjoint fermions that can lead to a realistic DM candidate. We outline the cosmological history of the gluequark in section 5.2 and present our estimate for the thermal relic abundance in section 5.3. Section 5.4 discusses a variety of bounds stemming from cosmological and astrophysical data, DM searches at colliders, direct and indirect detection experiments. We summarize and give our outlook in section 5.5. A discussion of the relevant cross sections can be found in the Appendices.

## 5.1 The models

We consider the scenario in which the SM is extended by a new confining gauge group $G_{\rm DC}$ (*dark colour*), and by a multiplet of Weyl fermions $\mathcal{Q}$ (*dark quarks*) transforming in the adjoint representation of $G_{\rm DC}$ and as a (possibly reducible) representation $R$ under the SM group $G_{\rm SM}$:

$$\mathcal{Q} \equiv (\text{adj}, R)\,. \tag{5.1}$$

In particular, we consider models where the dark quarks have quantum numbers under $\text{SU}(2)_L \times \text{U}(1)_Y$ but are singlets of $\text{SU}(3)_c$ color. We assume $R$ to be a real or vector-like representation,

[1] Reference [243] for example considered gluequark DM in the context of the so-called Minimal Walking Technicolor model, but its estimate of the thermal relic abundance focuses on the perturbative freeze-out and does not include any of the non-perturbative effects described in this work.

so that the cancellation of $G_{\rm SM}$ anomalies is automatic and mass terms for the dark quarks are allowed.

We performed a classification of the minimal models, *i.e.* those with the smallest representations and minimal amount of fields, which give a consistent theory of DM. We refer to them as 'minimal blocks'. Each block is characterised by two parameters: the dark quark mass $M_{\mathcal{Q}}$ and the value of the dark gauge coupling $g_{\rm DC}$ at $M_{\mathcal{Q}}$. A $CP$-violating $\theta$ term can also be included but does not play an important role in what follows. The renormalizable lagrangian thus reads

$$\mathcal{L} = \mathcal{L}_{\rm SM} - \frac{1}{4g_{\rm DC}^2}\mathcal{G}_{\mu\nu}^2 + \mathcal{Q}^\dagger i\bar{\sigma}^\mu D_\mu \mathcal{Q} - \frac{M_{\mathcal{Q}}}{2}\left(\mathcal{Q}\mathcal{Q} + \mathcal{Q}^\dagger\mathcal{Q}^\dagger\right). \tag{5.2}$$

It is possible to combine more than one minimal block; in this case the number of parameters increases: each module can have a different mass and, depending on the SM quantum numbers, Yukawa couplings with the Higgs boson may be allowed.

As long as all dark quarks are massive, the theory described by (5.2) confines in the infrared forming bound states. The symmetry $\mathcal{Q} \to -\mathcal{Q}$, *dark parity*, is an accidental invariance of the renormalizable Lagrangian. The physical spectrum is characterized by states that are either even or odd under dark parity. The gluequark, denoted by $\chi$ in the following, is the lightest odd state and has the same SM quantum numbers of its constituent dark quark, thus transforming as an electroweak multiplet. Radiative corrections will induce a mass splitting among different components, with the lightest state being accidentally stable at the renormalizable level thanks to its odd dark parity. The mass difference computed in Ref. [244] shows that the lightest component is always the electromagnetically neutral one, which therefore can be a DM candidate provided it has the correct relic density.

We select models with a suitable gluequark DM candidate by requiring them to be free of Landau poles below $10^{15}$ GeV. This is a minimal assumption considering that, as discussed below, astrophysical and cosmological bounds on the gluequark lifetime can be generically satisfied only for a sufficiently large cut-off scale. It is also compatible with Grand Unification of SM gauge forces. The ultraviolet behaviour of each model is dictated by the number of dark colors $N_{\rm DC}$ and by the dimension of the SM representation $R$, i.e. by the number of Weyl flavors $N_f$. Models with too large $N_f$ or $N_{\rm DC}$ imply too low Landau poles for $G_{\rm SM}$, and are thus excluded from our analysis. The list of minimal blocks that satisfy our requirements is reported in Table 5.1 for $\mathrm{SU}(N_{\rm DC})$, $\mathrm{SO}(N_{\rm DC})$ and $\mathrm{Sp}(N_{\rm DC})$ dark color groups. Each block is characterized by its accidental symmetry (that can be larger than the dark parity) and by the dimensionality of the lowest-lying operator $\mathcal{O}_{\rm dec}$ which violates it. The latter has the form

$$\mathcal{O}_{\rm dec} = \mathcal{O}_{\rm SM}\mathcal{G}^a_{\mu\nu}\sigma^{\mu\nu}\mathcal{Q}^a, \tag{5.3}$$

where $\mathcal{O}_{\rm SM}$ is a SM composite operator matching the $\mathrm{SU}(2)_L \times \mathrm{U}(1)_Y$ quantum numbers of the dark quark $\mathcal{Q}$. The operator (5.3) can in general induce the mixing of the gluequark with SM leptons, providing an example of partial compositeness. As long as the theory is not in the

| $N_f$ | Quantum numbers SU(2) × U(1) | $N_{\rm DC}$ SU | SO | Sp | Accidental Symmetry | $\mathcal{O}_{\rm dec}$ | Classical $[\mathcal{O}_{\rm dec}]$ |
|---|---|---|---|---|---|---|---|
| 1 | $N \equiv 1_0$ | All | All | All | $\mathbb{Z}_2$ | $\ell H \mathcal{G}_{\mu\nu}\sigma^{\mu\nu} N$ | 6 |
| 3 | $V \equiv 3_0$ | $\leqslant 3$ | $\leqslant 4$ | 1 | $\mathbb{Z}_2$ | $\ell H \mathcal{G}_{\mu\nu}\sigma^{\mu\nu} V$ | 6 |
| 4 | $L \equiv 2_{1/2} \oplus \bar{L} \equiv 2_{-1/2}$ | $\leqslant 4$ | $\leqslant 6$ | $\leqslant 2$ | U(1) | $\ell \mathcal{G}_{\mu\nu}\sigma^{\mu\nu} L$ | 5 |
| 6 | $T \equiv 3_1 \oplus \bar{T} \equiv 3_{-1}$ | 2 | 3 | 1 | U(1) | $\ell H^c \mathcal{G}_{\mu\nu}\sigma^{\mu\nu} T$ | 6 |

Table 5.1: *Minimal building blocks for models of gluequark DM. We require that a multiplet contains an electromagnetic neutral component and that the gauge couplings do not have Landau poles below* $10^{15}$ GeV*, assuming a representative mass of* 100 TeV *for the dark quarks. We denote with* $\ell$ *the SM lepton doublets.*

vicinity of a strongly-coupled IR fixed point at energies $E \gg M_{\mathcal{Q}}, \Lambda_{\rm DC}$, the dimension of $\mathcal{O}_{\rm dec}$ is simply given by $[\mathcal{O}_{\rm dec}] = 7/2 + [\mathcal{O}_{\rm SM}]$, as reported in the sixth column of Table 5.1. Among the minimal blocks, the $L\bar{L}$ model has $[\mathcal{O}_{\rm dec}] = 5$ classically. In this case the naive suppression of the gluequark decay rate is not enough to guarantee cosmological stability, although a stable DM candidate can still be obtained through additional dynamics, see the discussion in Appendix I. In the remaining minimal blocks the classical dimension of $\mathcal{O}_{\rm dec}$ is 6 and the gluequark can be sufficiently long lived. Indirect detection experiments and data from CMB and 21 cm line observations set important constraints on these models which will be discussed in section 5.4.

The behaviour of the theory at energies above the confinement scale depends largely on the number of dark flavors $N_f$ and on the value of the dark coupling $g_{\rm DC}$ at the scale $M_{\mathcal{Q}}$. One can identify two regimes. In the first, $g_{\rm DC}(M_{\mathcal{Q}})$ is perturbative and this necessarily implies a confinement scale smaller than the quark mass, $\Lambda_{\rm DC} < M_{\mathcal{Q}}$; we will call this the 'heavy quark' regime. In this case, depending on the value of $N_f$, there are three possible behaviours. For $N_f \geqslant N_f^{\rm AF} = 11/2$ the theory is not asymptotically free, hence starting from the UV the coupling gets weaker at lower scales until one reaches the quark mass threshold below which the dynamics becomes strong and confines. [2] For $N_f^c \leqslant N_f < N_f^{\rm AF}$, where $N_f^c$ is the non-perturbative edge of the conformal window, the theory flows towards an IR fixed point at low energies until the quark mass threshold is passed, below which one has confinement. Finally, if $N_f < N_f^c$ the coupling grows strong quickly in the infrared and confinement is triggered without delay. Only for this latter range of values of $N_f$ the confinement scale can be larger than the quark mass, $M_{\mathcal{Q}} < \Lambda_{\rm DC}$; we will refer to this as the 'light quark' regime. The physical spectrum, the phenomenology and the thermal history are rather different in the two regimes.

The infrared behaviour of $\mathrm{SU}(N_{\rm DC})$ gauge theories with fermions in the adjoint representation was extensively studied through lattice simulations, see for example [245–254] and references therein. There seems to be sufficient evidence for an infrared conformal phase of theories with $N_{\rm DC} = 2$ colors and $N_f = 4, 3$ massless Weyl flavors, while results with $N_f = 2$ are more uncertain though still compatible with a conformal regime. Theories with $N_f = 1$ are supersymmetric and have been shown to be in the confining phase. The case with $N_{\rm DC} = 3$ colors is much less studied

[2] Notice that the value of $N_f^{\rm AF}$, in the case of adjoint fermions, does not depend on the gauge group.

and no firm conclusion can be drawn on the conformal window. Notice that, independently of the number of colors, asymptotic freedom is lost for $N_f \geqslant 6$, while the existence of a weakly-coupled infrared fixed point can be established for $N_f = 5$ by means of perturbation theory. Besides determining which phase the massless theory is in, simulations give also information on the spectrum of bound states. In particular, information on the gluequark mass in the limit of heavy quark masses ($M_{\mathcal{Q}} \gg \Lambda_{\rm DC}$) can be obtained from lattice simulations with adjoint static sources, see for example Refs. [124, 255].

**Heavy quark regime:** In the heavy quark regime, the lightest states in the spectrum are glueballs, while those made of quarks are parametrically heavier. The value of the glueball mass is close to the one of pure gauge theories. Lattice results for pure glue SU(3) theories show that the $0^{++}$ state is the lightest with mass $m_{0^{++}} \sim 7\Lambda_{\rm DC}$, see for example [256]. Similar values are found for SU($N_{\rm DC}$) with different number of colors. The gluequark is expected to be the lightest state made of quarks, with a mass $M_\chi \sim M_{\mathcal{Q}}$. Other states made of more dark quarks (collectively denoted as mesons) quickly decay to final states comprising glueballs and gluequarks, depending on their dark parity.

The gluequark lifetime can be accurately estimated by computing the decay of its constituent heavy quark, similarly to spectator calculations for heavy mesons in QCD. In the minimal blocks where the dark parity-violating operator has dimension 6 the main decay channel for the lightest gluequark $\chi^0$ is $\chi^0 \to h\nu + n\Phi$ (where $\Phi$ indicates a glueball and $n \geqslant 1$). In the $V$ model of Table 5.1 with three dark flavors transforming as an EW triplet, the dim-6 operator

$$\frac{g_{UV}^2}{\Lambda_{UV}^2}\left(H^{c\dagger}\sigma^i \ell\, \mathcal{G}_{\mu\nu}\sigma^{\mu\nu}\mathcal{Q}^i + h.c.\right)$$

induces the decay of the gluequark with inverse lifetime

$$\frac{1}{\tau(\chi_0)} \simeq \frac{g_{UV}^4}{4096\pi^3}\frac{M_{\mathcal{Q}}^5}{\Lambda_{UV}^4} \simeq 10^{-28} g_{UV}^4 \left(\frac{M_{\mathcal{Q}}}{100\,\text{TeV}}\right)^5 \left(\frac{10^{18}\,\text{GeV}}{\Lambda_{UV}}\right)^4 \text{s}^{-1}\,. \tag{5.4}$$

Similar results apply for the $N$ and $T \oplus \bar{T}$ minimal blocks.

Glueballs can decay to SM particles through loops of dark quarks. In particular, since the latter are assumed to have electroweak charges, glueballs can always decay to photons through dimension-8 operators of the form $\mathcal{G}_{\mu\nu}\mathcal{G}^{\mu\nu}W_{\alpha\beta}W^{\alpha\beta}$ generated at the scale $M_{\mathcal{Q}}$. For all the minimal models in Table 5.1 this is the lowest-dimensional operator which induces glueball decay. The partial width into photons is determined to be [257, 225] [3]

$$\Gamma(\Phi \to \gamma\gamma) \simeq 0.7\,\text{s}^{-1}\left(\frac{N_{\rm DC}}{3}\right)^2 \left(\frac{M_\Phi}{500\,\text{GeV}}\right)^9 \left(\frac{100\,\text{TeV}}{M_{\mathcal{Q}}}\right)^8. \tag{5.5}$$

[3] To derive this and the following decay rates we used the value of the matrix element $\langle 0|\mathcal{G}_{\mu\nu}\mathcal{G}^{\mu\nu}|\Phi\rangle$ computed on the lattice for $SU(3)$, see Ref. *e.g.* [258].

When phase space allows, the decay channels $Z\gamma$, $W^+W^-$ and $ZZ$ open up producing one order-of-magnitude smaller lifetime. Relatively long-lived glueballs, as implied by the estimate (5.5), are subject to cosmological and astrophysical constraints as discussed in section 5.4.

Models with Yukawa couplings to the Higgs doublet can be obtained combining minimal blocks. In this case 1-loop radiative effects at the scale $M_{\mathcal{Q}}$ generate the dimension-6 effective operator $|H|^2\mathcal{G}^2_{\mu\nu}$, inducing a much shorter lifetime. If their mass is high enough, $M_\Phi > 2m_h$, glueballs predominantly decay to two Higgs bosons with a decay width

$$\Gamma(\Phi \to hh) \simeq 10^{12}\,\mathrm{s}^{-1} \left(\frac{N_{\rm DC}}{3}\right)^2 \left(\frac{y_1 y_2}{0.1}\right)^2 \left(\frac{M_\Phi}{500\,\mathrm{GeV}}\right)^5 \left(\frac{100\,\mathrm{TeV}}{\bar{M}_{\mathcal{Q}}}\right)^4 , \tag{5.6}$$

where $\bar{M}_{\mathcal{Q}} = (M_{\mathcal{Q}_1} M_{\mathcal{Q}_2})^{1/2}$, and $y_{1,2}$, $M_{\mathcal{Q}_{1,2}}$ are respectively the Yukawa couplings and masses of the dark quarks circulating in the loop. Lighter glueballs can decay through the mixing with the Higgs boson; as for the Higgs, the dominant channel for $M_\Phi < 150\,\mathrm{GeV}$ is that into bottom quarks, with a corresponding partial width [4]

$$\Gamma(\Phi \to b\bar{b}) \simeq 3 \cdot 10^{7}\,\mathrm{s}^{-1} \left(\frac{N_{\rm DC}}{3}\right)^2 \left(\frac{y_1 y_2}{0.1}\right)^2 \left(\frac{M_\Phi}{50\,\mathrm{GeV}}\right)^7 \left(\frac{10\,\mathrm{TeV}}{\bar{M}_{\mathcal{Q}}}\right)^4 . \tag{5.7}$$

**Light quark regime:** If dark quarks are lighter than $\Lambda_{\rm DC}$, the physical spectrum is radically different and one expects spontaneous breaking of the global $SU(N_f)$ symmetry down to $\mathrm{SO}(N_f)$. The lightest states are thus the (pseudo) Nambu-Goldstone bosons $\varphi$, while the DM candidate is the gluequark, accidentally stable and with a mass of the order of the confinement scale $\Lambda_{\rm DC}$. As discussed in section 5.3, and similarly to the baryonic DM theories of Ref. [178], reproducing the correct DM relic density in this regime fixes $\Lambda_{\rm DC} \sim 50\,\mathrm{TeV}$. The NGBs with SM quantum numbers get a mass from 1-loop electroweak corrections, which is predicted to be $\mathcal{O}(10\,\mathrm{TeV})$ for the value of $\Lambda_{\rm DC}$ of interest. Besides such a radiative correction, the quark mass term breaks explicitly the $\mathrm{SU}(N_f)$ global symmetry and gives an additional contribution. Including both effects, the NGB mass squared is given by

$$m^2_\varphi = c_0 M_{\mathcal{Q}} \Lambda_{\rm DC} + c_1 \frac{3\alpha_2}{4\pi} I(I+1)\Lambda^2_{\rm DC} , \tag{5.8}$$

where $I$ is the weak isospin of the NGB and $c_{0,1}$ are $\mathcal{O}(1)$ coefficients.

For fermions in the adjoint representations, only models with $N_f < 5$ light quarks can be in the regime $M_{\mathcal{Q}} < \Lambda_{\rm DC}$, since those with more fermions are either IR conformal or IR free. Therefore, among the minimal blocks of Table 5.1 only two are compatible with the light quark regime, *i.e.* the $V$ model and the $L \oplus \bar{L}$ model. The $V$ model has a global symmetry breaking $\mathrm{SU}(3) \to \mathrm{SO}(3)$ which leads to five NGBs transforming as an electroweak quintuplet. In the $L\oplus\bar{L}$ model one has $\mathrm{SU}(4) \to \mathrm{SO}(4)$ and nine NGBs transforming as $3_\pm, 3_0$ of $\mathrm{SU}(2)_{\rm EW} \times \mathrm{U}(1)_Y$.

[4] The scaling $\Gamma(\Phi \to b\bar{b}) \sim M^7_\Phi$ is approximately correct for $M_\Phi \ll m_h$, though eq. (5.7) is a good numerical estimate for $m_h \sim M_\Phi < 150\,\mathrm{GeV}$ as well.

The limit of very small quark masses, $M_{\mathcal{Q}}\Lambda_{\rm DC} \ll m_\varphi^2$, is experimentally interesting, since NGBs have predictable masses. In general, the lightest NGBs decay to SM final states through anomalies or Yukawa couplings, as in the case of the $V$ model. In some cases, however, some of the NGBs are accidentally stable due to unbroken symmetries of the renormalizable Lagrangian. An explicit violation of such accidental symmetries is expected to arise from higher-dimensional operators, possibly resulting into long-lived particles. An example of this kind is given by the $L \oplus \bar{L}$ model, where NGBs made of $LL$ or $\bar{L}\bar{L}$ constituents have $U(1)$ number $\pm 2$ and are stable at the renormalizable level, see Appendix I.

Since we assumed the dark quarks to transform as real or vectorlike representations under the SM gauge group, the fermion condensate responsible for the global symmetry breaking in the dark sector can be aligned along an $(SU(2)_L \times U(1)_Y)$-preserving direction (in non-minimal models, Yukawa interactions can generate a vacuum misalignment leading to Higgs partial compositeness, see [259,231]). As the strong dynamics preserves the EW gauge symmetry of the SM, it also affects electroweak precision observables through suppressed corrections which are easily compatible with current constraints for sufficiently high values of $\Lambda_{\rm DC}$, as required to reproduce the DM relic abundance [260, 58, 261].

Besides the NGBs, the physical spectrum comprises additional bound states with mass of order $\Lambda_{\rm DC}$. These include the gluequarks, which are expected to be the lightest states with odd dark parity, and mesons (i.e. bound states made of more than one dark quark) [5]. Except for the lightest gluequark, which is cosmologically stable, all the other states promptly decay to final states comprising NGBs and gluequarks, depending on their dark parity. In the minimal blocks where dark parity is broken by the dimension-6 operator $\ell H \mathcal{G}_{\mu\nu}\sigma^{\mu\nu}\mathcal{Q}$, the most important decay channels of the gluequark are $\chi^0 \to h\nu$ and $\chi^0 \to h\nu + \varphi$. The two-body decay dominates at large-$N_{\rm DC}$ and gives a lifetime of order

$$\frac{1}{\tau(\chi_0)} \sim \frac{g_{UV}^4}{8\pi}\frac{M_\chi^3 f_\chi^2}{\Lambda_{UV}^4} = 4\times 10^{-26} g_{UV}^4 \left[\frac{M_\chi}{100\,\text{TeV}}\right]^3 \left[\frac{f_\chi}{25\,\text{TeV}}\right]^2 \left[\frac{10^{18}\,\text{GeV}}{\Lambda_{UV}}\right]^4 \text{s}^{-1} \tag{5.9}$$

where $f_\chi$ is the decay constant of the gluequark [6].

To summarize our discussion on models, Table 5.1 reports the minimal blocks which have a potentially viable DM candidate and a sufficiently high cut-off, above $10^{15}$ GeV, as required for SM Grand Unification and to suppress the DM decay rate. In particular, the requirement on the absence of Landau poles restricts the list of possible models to a few candidates. As mentioned before, the case of the singlet was studied already in the literature [240, 241], and

[5] The existence of stable baryons in theories with adjoint fermions was investigated in Refs. [262, 263], where stable skyrmion solutions were identified and conjectured to correspond to composite states with mass of $O(N_{\rm DC}^2)$, interpolated from the vacuum by non-local operators. We will not include these hypothetical states in our analysis. In the light quark regime they are expected to annihilate with a geometric cross section and contribute a fraction of DM relic density comparable to that of the gluequarks.

[6] This has been defined by $\langle 0|\mathcal{G}_{\mu\nu}\sigma^{\mu\nu}\mathcal{Q}|\chi(p,r)\rangle = f_\chi M_\chi u_r(p)$, and scales as $f_\chi \sim M_\chi(N_{\rm DC}/4\pi)$ in the large-$N_{\rm DC}$ limit.

it will not be considered further in our study. We find that in all the other minimal blocks of Table 5.1 the $SU(3)_c \times SU(2)_L \times U(1)_Y$ gauge couplings unify with much lower precision than in the SM. Making the dark sector quantitatively compatible with SM Grand Unification thus requires extending these minimal blocks by including additional matter fields. Also, it would be interesting to explore the possibility of unifying both the visible and dark gauge couplings. We leave this study to a future work.

In the next sections we will discuss the thermal history of the Universe and try to estimate the DM relic density: section 3 explains the general mechanisms at work and is largely independent of the details of the models; section 4 gives a concrete example, adopting as a benchmark the $V$ model of Table 5.1, i.e. the minimal block with an $SU(2)_L$ triplet. For a discussion of the $L \oplus \bar{L}$ model see Appendix I.

## 5.2 Cosmological History

The Universe undergoes different thermal histories in the light and heavy quark regimes. We first give a brief overview of such evolution, followed by a more detailed discussion with quantitative estimates.

In the light quark regime the thermal history is relatively simple and similar to that described for baryonic DM in Ref. [178]. Dark color confines when dark quarks are relativistic and in thermal equilibrium. After confinement the gluequarks annihilate into NGBs with a non-perturbative cross section $\sigma v_{\rm rel} \sim \pi/\Lambda_{\rm DC}^2$, while glueballs are heavy and unstable. At temperatures $T \sim M_\chi/25$ the annihilation processes freeze out and the gluequarks start behaving as ordinary thermal relics.

In the heavy quark regime the thermal history is more complex and characterized by three different stages. Before confinement ($T \gtrsim \Lambda_{\rm DC}$), free dark quarks annihilate into dark gluons and undergo perturbative freeze-out at $T \sim M_{\mathcal{Q}}/25$ (see section 5.2.1). At confinement ($T \sim \Lambda_{\rm DC}$), the vast majority of the remaining dark quarks hadronizes into gluequarks, while the plasma of dark gluons is converted into a thermal bath of non-relativistic glueballs. The formation of mesons is suppressed by the low density of dark quarks compared to the ambient dark gluons. Glueballs overclose the Universe if they are cosmologically stable, therefore we consider the region of the parameter space where their lifetime is sufficiently short. As first pointed out in [264–266], and recently reconsidered in [267–269], decays of non-relativistic particles with a large and non-thermal energy density – like the glueballs – can modify the standard relation between the scale factor and the temperature during the cosmological evolution. If the glueballs are sufficiently long lived and dominate the energy density of the Universe at some stage of the cosmological evolution, the standard scaling $a \propto T^{-1}$ is modified into $a \propto T^{-8/3}$. During this early epoch of matter domination, the Universe expands faster than in the radiation-dominated era, leading to an enhanced dilution of the DM relic density (see section 5.2.2). Finally, interactions among

gluequarks can lead to a second stage of DM annihilation through the process

$$\begin{aligned} \chi + \chi &\to \mathcal{Q}\mathcal{Q}^* + \Phi/V \\ &\hookrightarrow \mathcal{Q}\mathcal{Q} \to \text{SM} \end{aligned} \tag{5.10}$$

where $\mathcal{Q}\mathcal{Q}^*$ is an excited bound state of dark quarks and $V$ stands for a SM vector boson or possibly a Higgs boson in models with Yukawa interactions. An analogous mechanism was first discussed in Ref. [98, 101, 201] and more recently by Ref. [187, 57, 105]. The process (5.10) proceeds in two steps. Initially, an excited bound state $\mathcal{Q}\mathcal{Q}^*$ with size $\mathcal{O}(1/\Lambda_{\rm DC})$ is formed by a collision of two $\chi$'s through a recombination of the constituent heavy quarks. This is similar to what happens for example in hydrogen anti-hydrogen scattering [197]. As a consequence of the large size of the gluequark (see the discussion in section 5.2.3), the corresponding recombination cross section is expected to be large $\sigma_{\rm rec} \approx \pi/\Lambda_{\rm DC}^2$. Once formed, the $\mathcal{Q}\mathcal{Q}^*$ can either decay ($\mathcal{Q}\mathcal{Q}^* \to \mathcal{Q}\mathcal{Q} + V \to$ SM) or be dissociated back into two gluequarks by interactions with the SM and glueball baths ($\Phi/V + \mathcal{Q}\mathcal{Q} \to \chi + \chi$). A naive estimate shows that the latter process typically dominates. This is because the largest contribution to the total cross section comes from scatterings with large impact parameters, $b \sim 1/\Lambda_{\rm DC}$, in which the $\mathcal{Q}\mathcal{Q}^*$ is produced with a large angular momentum, $\ell \sim M_{\mathcal{Q}} v b$. Bound states with $\ell \gg 1$ take more time to de-excite to lower states, and dissociation can happen before they reach the ground state. The annihilation of gluequarks through recombination is therefore inefficient as long as the glueball bath is present. Only when the glueballs decay away, a second stage of DM annihilation can take place through the process (5.10).

### 5.2.1 Thermal freeze-out

Thermal freeze-out is the first (only) phase of the cosmological evolution in the regime with heavy (light) quarks. In this stage the number density of free dark quarks (for $M_{\mathcal{Q}} > \Lambda_{\rm DC}$) or of gluequarks (for $M_{\mathcal{Q}} < \Lambda_{\rm DC}$) is reduced until it becomes so low that chemical equilibrium is no longer attained and freeze-out takes place. The number density at freeze-out is approximately given by

$$n(T_{\rm f.o.}) \simeq \frac{H(T_{\rm f.o.})}{\langle \sigma_{\rm ann} v_{\rm rel} \rangle}\,, \tag{5.11}$$

where $H$ is the Hubble parameter, and afterwards it is diluted by the Universe expansion.

In the heavy quark regime, free dark quarks annihilate with a perturbative cross section into dark gluons and into pairs of SM particles (vector bosons, Higgs bosons and fermions). The freeze-out temperature is of order $T_{\rm f.o.} \approx M_{\mathcal{Q}}/25$. A general expression for the annihilation cross section is reported in Appendix G, see eq. (G.2). For the $V$ model with $N_{DC} = 3$ analysed in the next section, the annihilation cross section into dark gluons and SM fields is

$$\langle \sigma_{\rm ann} v_{\rm rel} \rangle = \frac{\pi \alpha_{\rm DC}^2}{M_{\mathcal{Q}}^2} \left( \frac{27}{96} + \frac{1}{8} \left( 1 + \frac{25}{12} \right) \frac{\alpha_2^2}{\alpha_{\rm DC}^2} + \frac{1}{2} \frac{\alpha_2}{\alpha_{\rm DC}} \right) \left( \frac{1}{6} S_3 + \frac{1}{3} S_{3/2} + \frac{1}{2} S_{-1} \right)\,, \tag{5.12}$$

neglecting the mass of final states. The term from annihilation into SM particles separately shows the contribution of vectors and fermions plus longitudinal gauge bosons.

Terms in the second parenthesis encode the Sommerfeld enhancement from dark gluon exchange: $S_3$, $S_{3/2}$, $S_{-1}$ refer respectively to the 1, 8 and 27 color channels and are given by [71,55]

$$S_n = \frac{\alpha_{\rm DC}}{v_{\rm rel}} \frac{2\pi n}{1 - e^{-2\pi n \alpha_{\rm DC}/v_{\rm rel}}} \,. \tag{5.13}$$

In the light quark regime gluequarks annihilate into NGBs with a cross section that is expected to scale naively as

$$\langle \sigma_{\rm ann} v_{\rm rel} \rangle \sim \frac{\pi}{\Lambda_{\rm DC}^2} \,, \tag{5.14}$$

in analogy with nucleon-nucleon scattering in QCD [270]. Nambu-Goldstone bosons are unstable and later decay into SM particles.

### 5.2.2 Dilution

As well known, the number density of DM particles today is related to the number density at freeze-out by

$$n_{\rm DM}(T_0) = n_{\rm DM}(T_{\rm f.o}) \left( \frac{a_{\rm f.o.}}{a_0} \right)^3 . \tag{5.15}$$

This relation is usually rewritten in terms of temperatures assuming that between freeze-out and today the standard scaling $a \propto T^{-1}$ holds. However, the validity of the standard scaling relies upon the assumption that entropy is conserved in the SM sector, i.e. that no energy is injected into the SM plasma. In presence of large entropy injection one can have an epoch during which $a$ grows faster than $a \propto T^{-1}$. In this case the relation between $n_{\rm DM}(T_0)$ and $n_{\rm DM}(T_{\rm f.o})$ is given by:

$$n_{\rm DM}(T_0) = n_{\rm DM}(T_{\rm f.o}) \left( \frac{T_0}{T_{\rm f.o.}} \right)^3 \left( \frac{a\,(T_i)}{a\,(T_f)} \frac{T_i}{T_f} \right)^3 , \tag{5.16}$$

where $T_i$ and $T_f$ defines the temperature interval during which the non-standard scaling holds (see Fig. 5.2). The last term in parenthesis accounts for the suppression with respect to the naive relict density which would be obtained using the standard scaling. In the following we will show that late-time decays of dark glueballs can give rise to a non-standard scaling of the form $a \propto T^{-\alpha}$ with $\alpha > 1$. The corresponding suppression factor thus reads:

$$\mathcal{F} \equiv \left( \frac{a\,(T_i)}{a\,(T_f)} \frac{T_i}{T_f} \right)^3 = \left( \frac{T_f}{T_i} \right)^{3\alpha - 3} . \tag{5.17}$$

After dark color confinement, the energy density of the Universe can be divided into a relativistic component, $\rho_R$, containing all the SM relativistic particles, and a non-relativistic one, $\rho_M$, containing all the dark-sector long-lived degrees of freedom (i.e. dark glueballs and gluequarks). In particular, the energy density of glueballs at confinement is much larger than

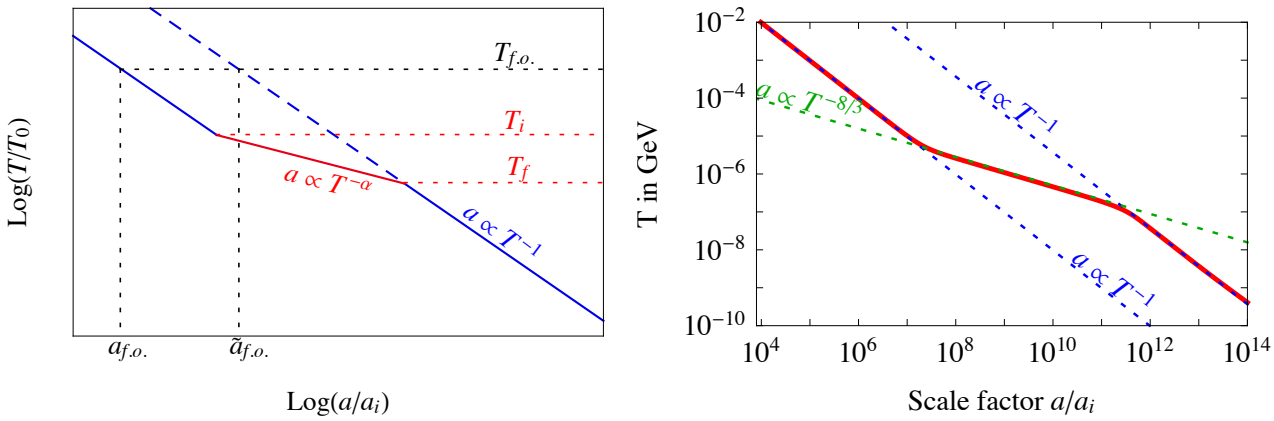


Figure 5.2: **Left:** *Sketch of the non-standard $a(T)$ scaling. Values of $\alpha > 1$ in eq.(5.17) imply a scale factor at freeze-out, $a_{f.o.}$, smaller than the one obtained from a standard cosmology, $\tilde{a}_{f.o.}$. This in turn leads to a suppression of the relic density by a factor $(a_{f.o.}/\tilde{a}_{f.o.})^3 = (T_f/T_i)^{3\alpha-3}$.* **Right:** *Scaling obtained by solving numerically (5.18) and (5.19) for $M_{\mathcal{Q}} = 100\,\text{TeV}$ and $T_{dc} = \Lambda_{DC} = 10\,\text{GeV}$. There exists an epoch during which the $a(T)$ scaling is very well approximated by a power law $a \propto T^{-\alpha}$ with $\alpha = 8/3$.*

the corresponding thermal energy density for a non-relativistic species, and this can lead to an early epoch of matter domination. Neglecting the subleading contribution of gluequarks to $\rho_M$, the evolution of $\rho_{M,R}$ is governed by [7]

$$\begin{cases} \dot{\rho}_M = -3H\rho_M - \Gamma_\Phi\,\rho_M \\ \dot{\rho}_R = -4H\rho_R + \Gamma_\Phi\,\rho_M \end{cases} \tag{5.18}$$

where $\Gamma_\Phi$ is the glueball decay rate and the Hubble parameter $H$ is given by the Friedmann equation:

$$H^2 = \frac{8\pi G}{3}\,(\rho_R + \rho_M)\ . \tag{5.19}$$

Since in the relevant region of the parameter space the dark and SM sectors are in thermal equilibrium at dark confinement, the initial conditions at $T = T_{dc} \approx \Lambda_{\rm DC}$ are given by

$$\rho_M(T_{dc}) = \xi\,\rho_R(T_{dc}) \qquad \text{with} \qquad \xi \equiv \frac{g_D(T_{dc})}{g_*(T_{dc})}\,, \tag{5.20}$$

where $g_D(T)$ and $g_*(T)$ count the number of relativistic degrees of freedom in the dark and SM sector respectively. Furthermore, assuming that the decay products thermalize fast enough, the

[7] Here we omit the contribution of glueball annihilations into SM vector bosons to the evolution of $\rho_{M,R}$. This contribution is negligible in the region of the parameter space where dilution is sizeable. Both the rate of glueball annihilation at temperatures of order $\Lambda_{\rm DC}$ and the glueball decay rate scale as $\Lambda_{\rm DC}^9/M_{\mathcal{Q}}^8$, so that the former, similarly to the latter, is expected to be smaller than Hubble when dilution is relevant. We have checked this naive expectation by verifying that after confinement the estimated annihilation rate is smaller than Hubble on branch 1 of Fig. 5.4.

temperature of the Universe below $T_{dc}$ is related to the relativistic energy density by:

$$\rho_R \equiv \frac{\pi^2}{30} g_* T^4 \qquad (T < T_{dc})\,. \tag{5.21}$$

The evolution during the early matter-dominated epoch, if the latter exists, can be described by solving analytically eq. (5.18) at leading order in $\rho_R/\rho_M$ for cosmic times $t \ll 1/\Gamma_\Phi$ [268]:

$$\rho_M = \bar{\rho}_M \left(\frac{\bar{a}}{a}\right)^3 e^{-\Gamma_\Phi (t-\bar{t})} \tag{5.22a}$$

$$\rho_R \simeq \bar{\rho}_R \left(\frac{\bar{a}}{a}\right)^4 + \frac{2}{5}\sqrt{\frac{3}{8\pi}}\Gamma_\Phi\, M_{\rm Pl}\, \bar{\rho}_M^{1/2} \left[\left(\frac{\bar{a}}{a}\right)^{3/2} - \left(\frac{\bar{a}}{a}\right)^4\right]. \tag{5.22b}$$

Here $\bar{\rho}_{M,R}$ and $\bar{a}$ denote the initial conditions at some time $\bar{t}$ much after the beginning of the matter-dominated epoch. The relativistic energy density is given by the sum of $\bar{\rho}_R$ (first term in eq.(5.22b)), diluted as $a^{-4}$, and the energy injected by glueball decays (second term in eq.(5.22b)), diluted as $\sim a^{-3/2}$. Initially the first term dominates and the standard scaling $a \propto T^{-1}$ is obtained; as long as the glueball lifetime is long enough, the second term will start to dominate at some temperature $T_i$, implying a non-standard scaling $a \propto T^{-8/3}$ (see Fig. 5.2). The value of $T_i$ can be found by equating the first and second terms of eq.(5.22b) and by using eqs.(5.19),(5.20):

$$T_i \simeq T_{dc}\,\xi \times \left[\frac{\Gamma_\Phi M_{\rm Pl}}{4.15\sqrt{g_*}\,T_{dc}^2\,\xi^2 + \Gamma_\Phi M_{\rm Pl}}\right]^{2/5}. \tag{5.23}$$

The non-standard scaling ends when almost all the glueballs are decayed, *i.e.* around $(t - t_{dc}) \sim \Gamma_\Phi^{-1}$, where $t_{dc}$ is the time at dark confinement. Using eqs. (5.19) and (5.20), one can translate this condition in terms of a temperature finding:

$$T_f \simeq \sqrt{M_{\rm Pl}\Gamma_\Phi}\,. \tag{5.24}$$

From eq.(5.17) it follows that late-time decays of glueballs dilute the naive relic density by a factor

$$\mathcal{F} = \left(\frac{T_f}{T_i}\right)^5 = \frac{0.28}{g_*^{5/4}}\,\frac{M_{\rm Pl}^{5/2}\Gamma_\Phi^{5/2}}{T_{dc}^5\,\xi^5}\left(\frac{4.15\sqrt{g_*}\,T_{dc}^2\,\xi^2 + \Gamma_\Phi M_{\rm Pl}}{\Gamma_\Phi M_{\rm Pl}}\right)^2, \tag{5.25}$$

where $\mathcal{O}(1)$ numerical factors omitted in eq.(5.24) have been included. When the glueballs are sufficiently long lived to give a sizeable dilution, the second term in the numerator inside the parenthesis of eq.(5.25) can be neglected and $\mathcal{F}$ is very well approximated by:

$$\mathcal{F} \simeq \frac{4.82}{g_*^{1/4}}\,\frac{\sqrt{M_{\rm Pl}\Gamma_\Phi}}{T_{dc}\,\xi}\,. \tag{5.26}$$

While the analytic formulas (5.22b)-(5.26) turn out to be quite accurate, in our estimate of the relic density performed in section 5.3 we will solve eq. (5.18) numerically without making any

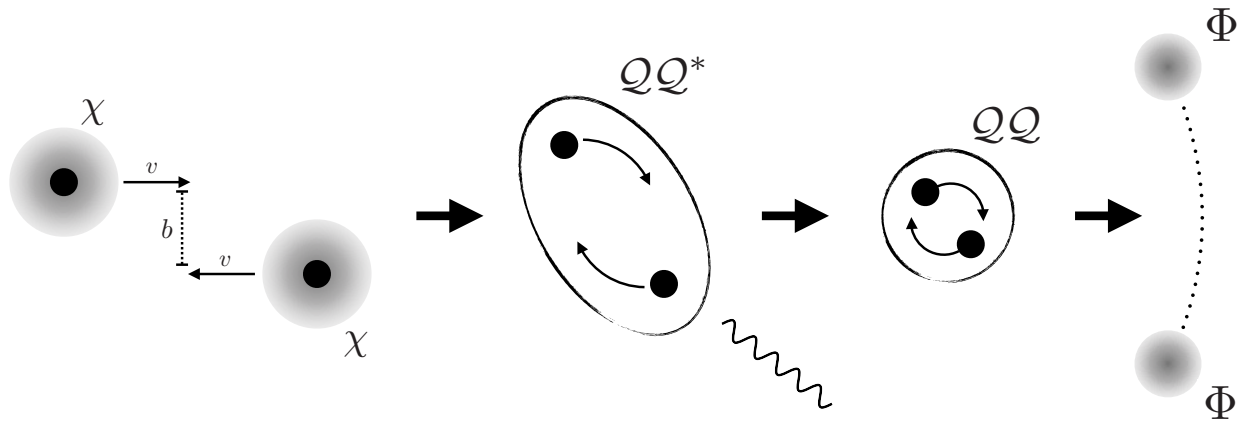


Figure 5.3: *Cartoon of the re-annihilation processes occurring after dark confinement. First, free quarks combine into color singlets gluequarks. Next, fast collisions form excited $\mathcal{Q}\mathcal{Q}^*$ states that at sufficiently low temperatures fall into the ground state and decay.*

approximation.

### 5.2.3 Reannihilation

At $T = T_{dc} \sim \Lambda_{\rm DC}$ the theory confines and the dark degrees of freedom reorganize into singlets of dark color. In the heavy quark regime, the number density of gluons is much larger than the one of fermions and the vast majority of free quarks $\mathcal{Q}$ hadronize into gluequarks. These can then collide and recombine in excited $\mathcal{Q}\mathcal{Q}^*$ states by emitting an electroweak gauge boson (or a Higgs boson in theories with Yukawa couplings) or a glueball when kinematically allowed, see eq. (5.10). The process goes through a recombination of the constituent heavy quarks, while the direct annihilation of these latter has a small and perturbative rate. Given that gluequarks have a size of order $1/\Lambda_{\rm DC}$, one expects naively a recombination cross section of order $\sigma_{\rm rec} \sim 1/\Lambda_{\rm DC}^2$. This value can in fact be reduced by kinematic constraints and the actual total cross section depends ultimately on the temperature at which the process takes place. A detailed discussion and estimates for the recombination cross section are given in Appendix H.

Once formed, $\mathcal{Q}\mathcal{Q}^*$ states with mass $M(QQ^*) > 2M_{\mathcal{Q}}$ will promptly decay back to two gluequarks. Lighter states, on the other hand, can either de-excite and thus decay into SM particles through the emission of a SM vector boson or a glueball ($\mathcal{Q}\mathcal{Q}^* \to \mathcal{Q}\mathcal{Q} + V/\Phi \to$ SM), or be dissociated by interactions with the glueball and SM plasmas ($\Phi/V + \mathcal{Q}\mathcal{Q}^* \to \chi + \chi$), see Fig. 5.3.

If de-excitation occurs faster than dissociation, a second era of efficient DM annihilation can take place, reducing the gluequark number density. While re-annihilation processes can be active over a long cosmological time interval, it is the last stage during which the re-annihilation cross section gets its largest value $\sigma_{\rm rea}$ that is most important to determine the final gluequark density. This last stage happens relatively quickly and can be characterized by a re-annihilation temperature $T_R$. The exact value of $T_R$ depends on the rate of dissociation and is difficult to

estimate. The largest uncertainties arise from the calculation of the de-excitation rate, which can vary over several orders of magnitude. We performed a thorough analysis taking into account the many dynamical ingredients which play a role in determining both the re-annihilation cross section and temperature. A detailed account is reported in Appendix H. We find that, under the most reasonable assumptions, dissociation of the most excited $QQ^*$ states occurs faster than de-excitation, as long as the glueball bath originating from dark gluons confinement is present; therefore, the re-annihilation temperature is approximately equal to the one at which glueballs decay ($T_R \approx T_D$). Besides this most probable scenario, in the following we will also consider the other extreme possibility where re-annihilation occurs right after confinement ($T_R = \Lambda_{\rm DC}$). The comparison between these two opposite scenarios will account for the theoretical uncertainties intrinsic to the determination of the non-perturbative dynamics characterizing our DM candidate.

In both benchmark scenarios considered above the last stage of the re-annihilation epoch occurs while entropy is conserved in the Universe and can thus be described by a set of standard Boltzmann equations given in eq. (H.1). They reduce to a single equation for sufficiently large de-excitation or glueball decay rates. This reads

$$\frac{dY_\chi}{dz} = -\frac{s\langle\sigma_{\rm rea} v\rangle}{Hz} Y_\chi^2 \,, \tag{5.27}$$

where $z = M_{\mathcal{Q}}/T$, $Y_\chi \equiv n_\chi/s$ and $s$ is the entropy density of the Universe. The equilibrium term can be neglected since $T_R \leqslant \Lambda_{\rm DC} \ll M_{\mathcal{Q}}$. Assuming a re-annihilation cross section which is constant and velocity independent [8], eq. (5.27) can be easily integrated analytically; one obtains (for $T < T_R$)

$$Y_\chi(T)^{-1} = Y_\chi(T_R)^{-1} + \frac{2}{3}\left(\frac{s\sigma_{\rm rea} v}{H}\right)_{T_R}\left[1 - \left(\frac{T}{T_R}\right)^{3/2}\right] . \tag{5.28}$$

Late-time annihilation significantly affects the gluequark relic density when the second term in the above equation dominates, *i.e.* roughly when

$$n_\chi \sigma_{\rm rea} v \gg H \qquad \text{at } T = T_R \,, \tag{5.29}$$

in agreement with a naive expectation. When condition (5.29) is met, any dependence from the previous stages of cosmological evolution, encoded in $Y_\chi(T_R)$, is washed out and the asymptotic value of the relic density is set only by re-annihilation. For temperatures $T$ sufficiently smaller than $T_R$ (but higher than a possible subsequent period of dilution, in the case $T_R \sim \Lambda_{\rm DC}$), eq.(5.28) can be recast in terms of the gluequark relic density as follows:

$$n_\chi(T) \simeq 1.4\, \frac{(M_{\mathcal{Q}} T_R)^{3/2}}{M_{\mathcal{Q}} M_{\rm Pl}} \frac{g_{\rm SM}(T)^{1/2}}{\sigma_{\rm rea}} \left(\frac{T}{T_R}\right)^3 \qquad \text{for } \; T \ll T_R \,. \tag{5.30}$$

[8] As explained in Appendix H, the last stage of re-annihilation can be effectively described by a constant cross section; the latter turns out to be also velocity independent in the relevant region of the parameter space of our theories.

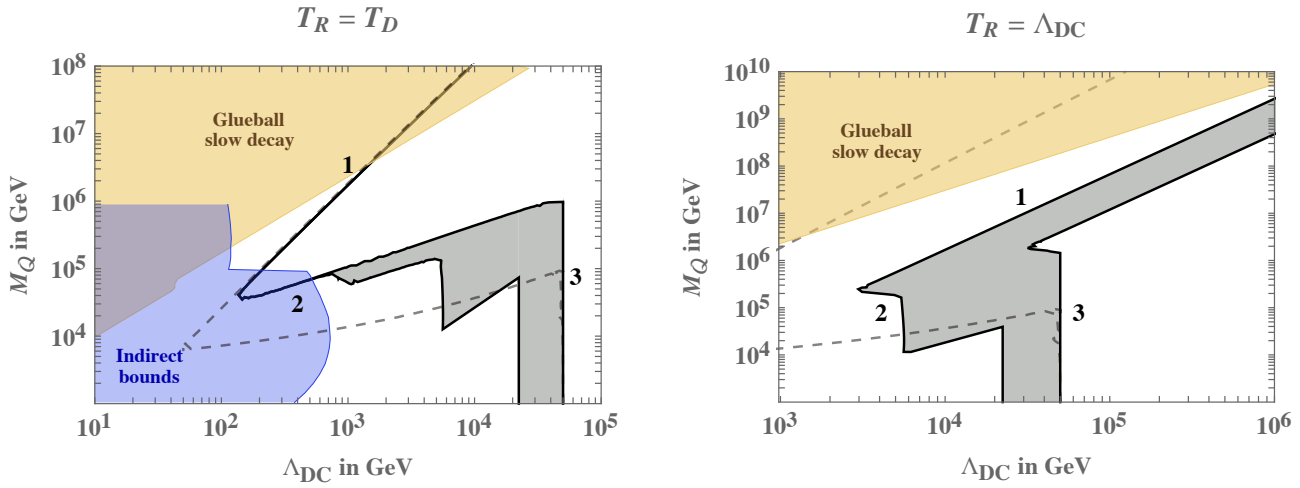


Figure 5.4: *On the black solid line* $\Omega_\chi = \Omega_{\rm DM}$. *We also report (dashed line) the isocurve* $\Omega_\chi = \Omega_{\rm DM}$ *for the case where re-annihilation is not considered. The numbers indicate the three thermal histories described in the text. In the yellow region the glueballs are either stable or have a lifetime bigger than* 1 s. *In the first case they will over-close the Universe while in the latter they will spoil BBN, both cases are therefore forbidden. The blue region is ruled out by indirect searches, namely modifications of the CMB power spectrum, 21-cm line observables and indirect detection (see section 5.4.3).*

## 5.3 Estimate of the Relic density

The cosmological evolution of gluequarks is determined by the interplay of the mechanisms described in the previous section and depends on the two fundamental parameters $M_\mathcal{Q}$ and $\Lambda_{\rm DC}$. For each point in the plane $(\Lambda_{\rm DC}, M_\mathcal{Q})$ one can thus in principle reconstruct the thermal history of the Universe and compute the DM abundance $\Omega_\chi$. In this section we will sketch the different possible thermal histories and give an estimate for $\Omega_\chi$. As a reference model we consider the minimal module with a triplet of $\mathrm{SU}(2)_L$ (see Table 5.1). We will assume the theory to be outside its conformal window, so that the regime of light dark quarks is well defined. We will discuss at the end how the picture changes for different SM representations and when the theory is in the conformal window or is not asymptotically free.

We will try to quantify the large uncertainties that arise in the determination of the cosmological evolution and of the relic density as a consequence of the non-perturbative nature of the processes involved. As anticipated in section 5.2.3, one of the largest uncertainties comes from the identification of the re-annihilation temperature $T_R$. We will consider the two previously discussed benchmarks: $T_R = T_D$, the most plausible one according to our estimates, and $T_R = T_{dc}$. We reconstruct for each of them the different possible cosmological evolutions obtained by varying $M_\mathcal{Q}$ and $\Lambda_{\rm DC}$. Our estimate of the DM abundance for both benchmarks is reported in Fig. 5.4, where we show the isocurve $\Omega_\chi h^2 = 0.119$ reproducing the experimentally observed density.

Let us consider first the case $T_R = T_D$. There are three possible thermal histories that can be realized (they are correspondingly indicated in the left plot of Fig. 5.4):

1. For very large $M_{\mathcal{Q}}/\Lambda_{\rm DC}$ the Universe undergoes a first perturbative freeze-out at $T_{\rm f.o.} \sim M_{\mathcal{Q}}/25$, then dark confinement occurs at $T \sim \Lambda_{\rm DC}$ followed by an epoch of dilution between $T_i$ and $T_f = T_D = T_R$ [9]. Glueballs decay at $T \lesssim T_D$, and the number density of gluequarks is too small, as a consequence of the dilution, to ignite a phase of non-perturbative re-annihilation. The DM density is therefore given by

$$\Omega_{\rm DM} \simeq \frac{n(T_{\rm f.o.})M_\chi}{\rho_{\rm crit}} \left(\frac{T_0}{T_{\rm f.o.}}\right)^3 \mathcal{F}\,, \tag{5.31}$$

   where the number density at freeze-out is estimated by solving the Boltzmann equations numerically and approximately given by eq. (5.11). By using the dilution factor reported in eq. (5.26), setting $M_\chi = M_{\mathcal{Q}}$, $T_{\rm f.o.} = M_{\mathcal{Q}}/25$, and $T_{dc} = \Lambda_{\rm DC}$ as indicated by lattice studies [271], one obtains

$$\Omega_{\rm DM}h^2 \sim 0.1 \left(\frac{0.1}{\alpha_{\rm DC}}\right)^2 \left(\frac{\Lambda_{\rm DC}}{\rm TeV}\right)^{3/2} \left(\frac{100\,\Lambda_{\rm DC}}{M_{\mathcal{Q}}}\right)^2\,, \tag{5.32}$$

   which describes well the slope of the upper part of the relic density isocurve in the left panel of Fig. 5.4. Because of the extreme dilution happening during the early epoch of matter domination, the experimental DM abundance is reproduced in this case for very large DM masses, of order of hundreds of TeV or more, above the naive unitarity bound.

2. For smaller values of $M_{\mathcal{Q}}/\Lambda_{\rm DC}$ (but still with $M_{\mathcal{Q}}/\Lambda_{\rm DC} \gtrsim 25$), the dilution between $T_{\rm f.o.}$ and $T_D$ is not enough to prevent re-annihilation (*i.e.* condition (5.29) is met). The latter thus occurs at $T \simeq T_D$, washing out any dependence of $\Omega_\chi$ from the previous stages of cosmological evolution; the corresponding DM relic density is

$$\Omega_{\rm DM} \simeq \frac{n_\chi(\bar{T})M_\chi}{\rho_{\rm crit}} \left(\frac{T_0}{\bar{T}}\right)^3 \qquad \text{for } T_0 < \bar{T} \ll T_R. \tag{5.33}$$

   The first factor corresponds to the gluequark energy density at the end of the re-annihilation (given by eq.(5.30)), and the second one encodes the standard dilution due to the Universe expansion. We evaluate the re-annihilation cross section by using the semiclassical model described in Appendix H.1; this gives

$$\sigma_{\rm rea}^{model} = \frac{4\pi}{\Lambda_{\rm DC}^2}\left[\varepsilon_\Phi(\Lambda_{\rm DC}, M_{\mathcal{Q}}, T_R) + \alpha_2\,\varepsilon_V(\Lambda_{\rm DC}, M_{\mathcal{Q}}, T_R)\right]\,. \tag{5.34}$$

   The parameters $\varepsilon_\Phi$ and $\varepsilon_V$ are smaller than 1 and encode the suppression from energy

[9] Here we are implicitly assuming that the re-heating temperature at the end of inflation is larger than $M_{\mathcal{Q}}$, so that the number density of dark quarks after the perturbative freeze-out is thermal.

and angular momentum conservation respectively for the recombination processes $\chi\chi \to QQ^* + \Phi$ and $\chi\chi \to QQ^* + V$. While eq.(5.34) is the result of a rather sophisticated analysis of the re-annihilation dynamics and represents our best estimate for $\sigma_{\rm rea}$, it is subject to large theoretical uncertainties, as discussed in Appendix H.1. We thus also consider the extreme situation where the re-annihilation cross section is always large and saturated by its geometric value

$$\sigma_{\rm rea}^{geo} = \frac{4\pi}{\Lambda_{\rm DC}^2}\,. \tag{5.35}$$

Varying $\sigma_{\rm rea}$ between the values in eqs.(5.34) and (5.35) will quantify the uncertainty on $n_\chi(\bar{T})$. By using eq.(5.30) and setting $M_\chi = M_\mathcal{Q}$ and $T_R = T_D \sim \sqrt{M_{\rm Pl}\Gamma_\Phi}$, eq. (5.33) takes the form:

$$\Omega_{\rm DM}h^2 \sim 0.1 \left(\frac{\Lambda_{\rm DC}}{\rm GeV}\right)^{11/4} \left(\frac{M_\mathcal{Q}}{1000\,\Lambda_{\rm DC}}\right)^{15/2} \frac{4\pi/\Lambda_{\rm DC}^2}{\sigma_{\rm rea}(M_\mathcal{Q}, \Lambda_{\rm DC})}\,. \tag{5.36}$$

This formula describes the intermediate part of the isocurve in the left plot of Fig. 5.4. Initially (*i.e.* for $150\,{\rm GeV} \lesssim \Lambda_{\rm DC} \lesssim 800\,{\rm GeV}$) the re-annihilation is dominated by the process $\chi\chi \to QQ^* + \Phi$ and $\varepsilon_\Phi \simeq 1$; in this case the last factor in (5.36) can be well approximated with 1 (the electroweak contribution to $\sigma_{\rm rea}^{model}$ is small) and the estimated uncertainty on the gluequark relic density is negligible. For larger $\Lambda_{\rm DC}$ re-annihilation into $QQ^*$ plus a glueball becomes kinematically forbidden in our semiclassical model, and $\varepsilon_\Phi$ quickly drops to zero (see Appendix H.1). In this region $\varepsilon_V \simeq 1/10$ and varying $\sigma_{\rm rea}$ between $\sigma_{\rm rea}^{model}$ and $\sigma_{\rm rea}^{geo}$ spans the gray region. The extension of the latter quantifies the uncertainty of our estimate of the relic density.

3. When $M_\mathcal{Q}/\Lambda_{\rm DC} \leqslant 25$, the perturbative freeze-out does not take place. If $M_\mathcal{Q}$ is bigger than $\Lambda_{\rm DC}$, then the Universe undergoes a first epoch of annihilation of dark quarks for $T \gtrsim M_\mathcal{Q}$, followed after confinement by the annihilation of gluequarks, until thermal freeze-out of these latter occurs at $T \simeq M_\chi/25$. If $M_\mathcal{Q} < \Lambda_{\rm DC}$, on the other hand, the theory is in its light quark regime and the only epoch of annihilation is that of gluequarks after dark confinement, again ending with a freeze-out at $T \simeq M_\chi/25$. Afterwards $n_\chi$ is diluted by the Universe expansion without any enhancement from the decay of glueballs (these are too short lived to give an early stage of matter domination). The expression for the DM relic density is formally the same as in eq.(5.31) with $\mathcal{F} = 1$. Setting $T_{\rm f.o.} = M_\chi/25$, one obtains

$$\Omega_{\rm DM}h^2 \approx 0.1\,\frac{4\pi/\Lambda_{\rm DC}^2}{\sigma_{\rm ann}} \left(\frac{\Lambda_{\rm DC}}{100{\rm TeV}}\right)^2\,. \tag{5.37}$$

For $1 \lesssim M_\mathcal{Q}/\Lambda_{\rm DC} \lesssim 25$ the non-perturbative annihilation of gluequarks proceeds through the same recombination processes of eq.(5.10). According to the model of Appendix H.1, only the final state with a vector boson is kinematically allowed, and $\varepsilon_V \simeq \alpha_2/10$. This implies $\sigma_{\rm ann} \simeq (\alpha_2/10)\,4\pi/\Lambda_{\rm DC}^2$, so that the DM relic density turns out to be independent of $M_\mathcal{Q}$. If instead the re-annihilation cross section is estimated by eq.(5.35), then by

continuity with the previous cosmological evolution one must take $\sigma_{\rm ann} \simeq 4\pi/\Lambda_{\rm DC}^2$, which also corresponds to a relic density independent of $M_{\mathcal{Q}}$. Varying $\sigma_{\rm ann}$ between these two values gives the largest vertical portion of the gray region in the left plot of Fig. 5.4.

As soon as one enters the light quark regime, $M_{\mathcal{Q}} < \Lambda_{\rm DC}$, the annihilation of gluequarks proceeds through the direct annihilation of their constituents (the theory at $M_{\mathcal{Q}}$ is non-perturbative) with a cross section $\sigma_{\rm ann} = 4\pi c/\Lambda_{\rm DC}^2$, where $c$ is an order 1 coefficient. We vary $1/5 < c < 1$ to quantify the uncertainty in this last non-perturbative process. We thus obtain the narrower vertical portion of the gray region in the left plot of Fig. 5.4, which extends down to arbitrarily small $M_{\mathcal{Q}}$. The observed relic density in this regime is reproduced for $\Lambda_{\rm DC} \simeq 50\,\text{TeV}$, similarly to the light quark regime in baryonic DM models [178].

Let us turn to the case $T_R = T_{dc} = \Lambda_{\rm DC}$. As for $T_R = T_D$ one can identify three possible thermal histories (correspondingly indicated in the right panel of Fig. 5.4):

1. For $M_{\mathcal{Q}}/\Lambda_{\rm DC} \gg 25$ the Universe goes first through a perturbative freeze-out of dark quarks at $T_{\rm f.o.} \simeq M_{\mathcal{Q}}/25$, then re-annihilation occurs right after confinement for $T \simeq \Lambda_{\rm DC}$. Finally, dilution takes place between $T_i$ and the temperature of the glueball decay $T_D$. The DM relic density is given by the expression in eq.(5.33) times the dilution factor $\mathcal{F}$. Numerically one has
$$\Omega_{\rm DM}h^2 \simeq 5\cdot 10^{-2}\,\frac{\Lambda_{\rm DC}^4}{\xi\, M_{\mathcal{Q}}^{5/2}}\,\frac{4\pi/\Lambda_{\rm DC}^2}{\sigma_{\rm rea}(M_{\mathcal{Q}},\Lambda_{\rm DC})}\,. \tag{5.38}$$
In this case, our semiclassical model estimates $\varepsilon_\Phi \simeq 1/100$ throughout the parameter space of interest. By varying $\sigma_{\rm rea}$ between $\sigma_{\rm rea}^{model}$ and $\sigma_{\rm rea}^{geo}$ we thus obtain the upper portion of the gray region in the right plot of Fig. 5.4.

2. For smaller $M_{\mathcal{Q}}/\Lambda_{\rm DC}$ (but still with $M_{\mathcal{Q}}/\Lambda_{\rm DC} > 25$), the glueballs are too short lived to ignite the dilution, and the DM relic density is given by eq.(5.33). Setting $T_R = \Lambda_{\rm DC}$ one obtains
$$\Omega_{\rm DM}h^2 \simeq 10^{-10}\,\frac{\Lambda_{\rm DC}M_{\mathcal{Q}}}{\text{GeV}^2}\left(\frac{M_{\mathcal{Q}}}{\Lambda_{\rm DC}}\right)^{1/2}\frac{4\pi/\Lambda_{\rm DC}^2}{\sigma_{\rm rea}(M_{\mathcal{Q}},\Lambda_{\rm DC})}\,. \tag{5.39}$$

3. When $M_{\mathcal{Q}}/\Lambda_{\rm DC} < 25$ the cosmological evolution of the Universe is the same as thermal history 3 in the case $T_R = T_D$. The DM relic density is given by eq.(5.37), corresponding to the vertical gray regions of the right plot of Fig. 5.4.

The plots of Fig. 5.4 graphically summarize our estimate of the DM relic density including the uncertainty from the value of $T_R$ (left vs right panel), and from the value of the cross sections for gluequark re-annihilation and annihilation in the light-quark regime (gray region). Reducing substantially the uncertainty on the re-annihilation process (both the cross section and the value of $T_R$) is not simple and would require a dedicated and in-depth study of the recombination and de-excitation rates, and an extensive study of the system of Boltzmann equations, which is

beyond the scope of the present work. An improved precision in the context of our semiclassical model, on the other hand, could be obtained from a more accurate knowledge of the spectrum of states in the strong sector, in particular of the masses of the glueball and gluequark; this can be obtained through dedicated lattice simulations. Notice also that the plots of Fig. 5.4 have been obtained by assuming a dark color gauge group $SU(3)$, for which the confinement temperature $T_{dc}$ and the non-perturbative matrix element relevant for the glueball decay rate are known from lattices studies. Extending our results to other dark gauge groups would in general require to determine these inputs with dedicated simulations, in absence of which there would be further theoretical uncertainties (both in the estimate of the DM relic density, through the expression of the dilution factor in eq. (5.26), and in the exclusion region from the glueball lifetime).

As a last remark we notice that the qualitative picture derived in this section is largely independent of the details of the specific model. However, the quantitative results can change significantly in models with Yukawa couplings, where the glueball lifetime is much shorter. In particular, the exclusion region from the glueball lifetime moves further up left and branch 1, where dilution occurs, becomes vertical (so that the relic density is uniquely fixed in terms of $\Lambda_{\rm DC}$). Finally, models that, in the limit of zero quark masses, are infrared free or in the conformal window are constrained to be in the regime $M_{\mathcal{Q}} > \Lambda_{\rm DC}$.

## 5.4 Phenomenology and Experimental Constraints

In this section we outline the main phenomenological signatures for collider physics and cosmology of the models with gluequark DM. In general, the phenomenology has analogies to the one of baryonic DM studied in Refs. [178,58]. Given the large gluequark masses needed to reproduce the DM relic density both in the light and heavy quark regimes, searches at colliders are not promising, whereas cosmological observations provide interesting bounds.

### 5.4.1 Collider searches

The dark sector has a rich spectrum of states which, in principle, one would like to study at colliders.

The lightest states in the spectrum, with mass given by eq.(5.8), are the NGBs from the $\mathrm{SU}(N_F) \to \mathrm{SO}(N_F)$ global symmetry breaking in the light quark regime. In the case of the $V$ model, the five NGBs form a multiplet with weak isospin 2, and one expects $m_\varphi \gtrsim \Lambda_{\rm DC}/5$. The phenomenology of a quintuplet of NGBs was studied recently in Ref. [261]. These states are pair produced at hadron collider in Drell-Yan processes through their electroweak interactions, and decay to pairs of electroweak gauge bosons through the anomalous coupling

$$\frac{2N_{\rm DC}}{\sqrt{3}}\frac{\alpha_2^2}{4\pi}\frac{\varphi_{ab}}{f}W^a_{\mu\nu}\tilde{W}^{b\,\mu\nu}\,. \tag{5.40}$$

A promising discovery channel studied by Ref. [261] is $pp \to \varphi^0\varphi^\pm \to 3\gamma W^\pm$; the doubly charged

states decay into same-sign $W$ pairs and are somewhat more challenging to see experimentally. The LHC has an exclusion reach up to TeV masses, while a 100 TeV collider would test the light quark scenario approximately up to 5 TeV. In this regime colliders could start probing the thermal region.

The lightest states in the heavy quark regime are the glueballs. They couple to the SM only through higher-dimensional operators, and are rather elusive at colliders. In models without Yukawa couplings, where interactions with the SM occur through dimension-8 operators, the production cross section via vector boson fusion (VBF) or in association with a SM vector boson is too small to observe a signal in current or future colliders (for example, the VBF cross section at a 100 TeV collider is of order $\sigma(pp \to \Phi + jj) \lesssim 10^{-9}$ fb for $M_{\mathcal{Q}}/\Lambda_{\rm DC} = 10$ and $M_\Phi > 500$ GeV). In models with Yukawa couplings the glueballs mix with the Higgs boson and production via gluon-fusion becomes also possible. While this leads to larger cross sections, the corresponding rate is too small to see a signal at the LHC and even high-intensity experiments like SHiP can only probe light glueballs in a region of parameter space that is already excluded by EW precision tests, as discussed in section 4.4.5.

Mesons can give interesting signatures in both light and heavy quark regimes. Bound states made of a pair of dark quarks, $QQ$, can be singly produced through their EW interactions. While the production of spin-0 mesons is suppressed since they couple to pairs of EW gauge bosons, spin-1 resonances mix with the SM gauge bosons of equal quantum numbers and can be produced via Drell-Yan processes. In the narrow width approximation the cross section for resonant production can be conveniently written in terms of the decay partial widths as

$$\sigma(pp \to QQ) = \frac{(2J_{QQ}+1)D_{QQ}}{sM_{QQ}} \sum_{\mathcal{P}} C_{\mathcal{P}\mathcal{P}} \Gamma(QQ \to \mathcal{P}\mathcal{P}) \,, \tag{5.41}$$

where $D_{QQ}$ is the dimension of the representation, $J_{QQ}$ the spin, $\mathcal{P}$ the parton producing the resonance and $C_{\mathcal{P}\mathcal{P}}$ are the dimension-less parton luminosities.

In the heavy quark regime the $QQ$ bound state is perturbative and its decay width can be computed by modelling its potential with a Coulomb plus a linear term. For $\alpha_{\rm DC} M_{\mathcal{Q}} > \Lambda_{\rm DC}$ the decay width of the lowest-lying s-wave bound states scales as

$$\Gamma(QQ \to \mathcal{P}\mathcal{P}) \sim D_{QQ} \alpha_{SM}^2 \alpha_{\rm DC}^3 M_{\mathcal{Q}} \,, \tag{5.42}$$

where $\alpha_{\rm DC}^3$ originates from the non-relativistic Coulombian wave-function. When $\alpha_{\rm DC} M_{\mathcal{Q}} < \Lambda_{\rm DC}$, the effect of the linear term in the potential becomes important and eq.(5.42) gets modified; since confinement enhances the value of the wave function at the origin, the width becomes larger in this regime. Using the Coulombian approximation thus provides conservative bounds. Explicit formulas for the rates were given in section 4.4.4 of the previous chapter. For example, in the $V$ model the decay width of the s-wave spin-1 $QQ$ resonance (isospin 1 in light of the Majorana

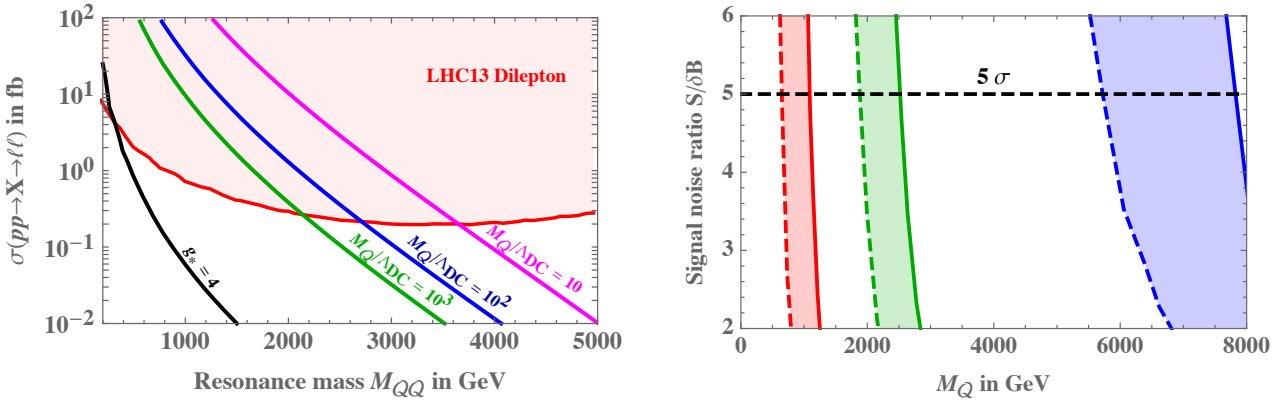


Figure 5.5: **Left:** *ATLAS bounds on the cross section for the direct production of a spin-1 QQ resonance decaying into muons and electrons [222].* **Right:** *Estimated reach on gluequark pair production obtained by recasting the limits of Ref. [272] from disappearing tracks searches at the HL-LHC (red), the HE-LHC (green) and a* 100 TeV *collider (blue). The solid (dashed) lines assume a* 20% *(*500%*) uncertainty on the background estimate.*

.

nature of $V$) into a left-handed fermion doublet is

$$\Gamma^{(n)}\left(QQ^{J=1}_{I=1}\to f\bar{f}\right)=(N^5_{\rm DC}-N^3_{\rm DC})\frac{\alpha_2^2\alpha_{\rm DC}^3}{24n^3}M_{\mathcal{Q}}\,, \tag{5.43}$$

where $n$ refers to the radial quantum number. The tiny energy splitting between levels is irrelevant at colliders and the total rate is dominated by the lowest-lying Coulombian ones. The branching ratio into pairs of leptons is about 7% and the strongest bounds currently arise from searches of spin-1 resonances at the LHC decaying into electrons and muons. We show the limits in the left plot of Fig. 5.5 and find that the LHC excludes masses up to $2-3.5\,$TeV depending on the ratio $M_{\mathcal{Q}}/\Lambda_{\rm DC}$ (or equivalently on the value of $\alpha_{\rm DC}(M_{\mathcal{Q}})$).

In the light quark regime the lightest spin-1 state is the $\rho$ meson with mass $M_\rho\sim\ \Lambda_{\rm DC}$. The widths scale as [273]

$$\begin{aligned}\Gamma(\rho\to\varphi\varphi)&\sim\frac{g_*^2}{8\pi}M_\rho\\ \Gamma(\rho\to f\bar{f})&\sim\alpha_{SM}^2\left(\frac{4\pi}{g_*^2}\right)M_\rho\,,\end{aligned} \tag{5.44}$$

where $g_*$ characterizes the interaction strength among bound states. For moderately large $g_*$, as suggested by large-$N_{DC}$ counting $g_*\sim 4\pi/\sqrt{N_{DC}}$, the decay into light NGBs dominates while final states with leptons are suppressed. It thus follows a weaker bound than in the heavy quark regime, as illustrated in Fig. 5.5 for $g_*=4$.

Gluequarks can also be pair produced at colliders through their EW interactions. In the

heavy quark regime the energy threshold is much higher than the confinement scale and quarks are produced in free pairs. Because dark quarks are in the adjoint representation of dark color, when they get separated by a distance of $O(1/\Lambda_{\rm DC})$ they hadronize producing color singlets that fly through the detector. On the contrary, dark quarks in the fundamental representation would not be able to escape, leading to quirks/hidden valley phenomenology [274, 179, 58]. The phenomenology of the open production is then identical to the one of an elementary electroweak multiplet except that the cross-section is enhanced by the multiplicity of the dark color adjoint representation, i.e. $N_{\rm DC}^2 - 1$ for SU($N_{\rm DC}$). Such enhancement factor is not present for gluequark pair production near threshold in the light quark regime. In general, an electroweak triplet can be searched for in monojet and monophoton signals or disappearing tracks, the latter being more constraining. We derived the reach of the high-luminosity LHC (HL-LHC), the high-energy LHC (HE-LHC) and the proposed 100 TeV collider by recasting the results of Ref. [272] for the $V$ model in the heavy quark regime, see the right plot of Fig. 5.5. We find that the HL-LHC could discover gluequark triplets up to $\sim 600$ GeV while a 100 TeV collider could reach $\sim 7$ TeV. Such bounds are typically weaker than the ones from the production of $QQ$ spin-1 resonances decaying to leptons.

### 5.4.2 DM Direct Detection

From the point of view of DM direct detection experiments, where the momentum exchanged is less than 100 KeV, the gluequark behaves as an elementary particle with the same electroweak quantum numbers as the constituent quark. The main difference from elementary candidates with same quantum numbers is that the relic abundance is not controlled by the electroweak interaction, leading to a different thermal region.

For a triplet of SU(2) the spin-independent cross-section is $\sigma_{\rm SI} = 1.0 \times 10^{-45}\,{\rm cm}^2$, which is below the neutrino floor for masses $M_\chi > 15$ TeV. For an SU(2) doublet tree-level $Z$-mediated interactions induce a spin-independent cross section on nucleons $\sigma_{\rm SI} \approx 10^{-40}\,{\rm cm}^2$, which is ruled out for $M_\chi \lesssim 10^8$ GeV [26]. Dark quark masses large enough to make the doublet model viable can be obtained only in the scenario where $T_R = \Lambda_{\rm DC}$, while the scenario with $T_R = T_D$ is ruled out (see Appendix I for more details).

### 5.4.3 DM Annihilation and Decay

After freeze-out, decays or residual annihilations of gluequarks can give rise to indirect detection signals.

In the region of parameter space relevant for our purposes, annihilation processes set constraints on theories in the heavy quark regime, and we thus focus on that case to analyse them. As discussed in section 5.2.3 (and more extensively in Appendix H), the annihilation can be either direct ($\chi\chi \to n\Phi/{\rm SM}$) or mediated by the formation of a $\mathcal{Q}\mathcal{Q}^*$ bound state that subsequently decays ($\chi\chi \to \mathcal{Q}\mathcal{Q}^* \to n\Phi/{\rm SM}$). In the former case the annihilation cross section is perturbative (see eq.(G.2)) and, given the relatively high mass of the gluequark, it does not

lead to any interesting indirect detection signatures. The latter case, instead, because of the enhanced annihilation cross section, could lead to an interesting phenomenology and it is worth further study.

As discussed in section 5.2.3 and in Appendix H, for angular momenta $\ell \gg 1$ the recombination cross section is of order $\sigma_{\rm rea} \simeq \varepsilon\, 4\pi/\Lambda_{\rm DC}^2$. However, given the small velocities relevant for indirect searches ($v_{\rm rel} \sim 10^{-6}\sqrt{\rm TeV/M_{\mathcal{Q}}}$ at the CMB epoch and $v_{\rm rel} \sim 10^{-3}$ in our galaxy), the angular momentum of the colliding particles $\ell \sim M_{\mathcal{Q}} v_{\rm rel}/\Lambda_{\rm DC}$ is of order unity in a large region of the parameter space. In this case only s-wave processes take place and $\sigma_{\rm rea} v_{\rm rel}$ rather than $\sigma_{\rm rea}$ is constant. In this regime the value of the cross section is very uncertain, and we chose to estimate it in terms of two benchmark scenarios (see Appendix H.1):

$$\langle \sigma_{\rm ann} v_{\rm rel} \rangle \sim \begin{cases} \dfrac{1}{\Lambda_{\rm DC}^2} \\ \pi R_B^2 \approx \dfrac{\pi}{(\alpha_{\rm DC}^2 M_{\mathcal{Q}}^2)}\,. \end{cases} \tag{5.45}$$

Once formed, the $\mathcal{Q}\mathcal{Q}^*$ bound states de-excite and in general decay into dark gluons, SM gauge bosons or SM fermions. The branching ratios can be derived in terms of the perturbative annihilation cross section of dark quarks into the corresponding final states, see eq.(G.2). In the region of interest $\alpha_{\rm DC} > \alpha_2$ and one finds

$$\mathrm{BR}(GG) \sim 1 + \mathcal{O}\left(\frac{\alpha_2}{\alpha_{\rm DC}}\right), \qquad \mathrm{BR}(WW/\Psi\Psi) \sim \frac{\alpha_2^2}{\alpha_{\rm DC}^2}, \qquad \mathrm{BR}(ZG) \sim \frac{\alpha_2}{\alpha_{\rm DC}}\,, \tag{5.46}$$

where $G$ denotes a dark gluon. For the specific case of the $V$ model, the tree-level decay into SM fermions and $ZG$ is forbidden (the $\chi_0$ has vanishing coupling to the $Z$) and use of eq.(G.2) thus gives

$$\langle \sigma v_{\rm rel} \rangle_{\chi_0\chi_0 \to WW} \sim \langle \sigma_{\rm ann} v_{\rm rel} \rangle \times \frac{6}{27}\frac{\alpha^2}{\alpha_{\rm DC}^2}\,, \tag{5.47}$$

where the last factor is from the branching ratio of $QQ$ into $WW$.

Similarly to residual annihilations, decays of the gluequark could give rise to indirect signals. The $\chi^0$ decays mostly to $h\nu$ plus glueballs in the heavy quark regime, and to $h\nu$ or $h\nu + \varphi$ in the light quark regime (see eqs.(5.4),(5.9)). Both glueballs and NGBs in turn decay into SM particles and ultimately the gluequark decay leads to the production of light SM species which can be observed experimentally. Bounds can be avoided, on the other hand, if some mechanism is at work that makes the $\chi^0$ absolutely stable or give it a much longer lifetime than the one estimated in eq. (5.4) and (5.9).

Fig. 5.6 summarizes the constraints in the plane $(\Lambda_{\rm DC}, M_{\mathcal{Q}})$ that arise from experiments probing DM decay and annihilation. The red exclusion regions from DM annihilation have been derived for the two benchmark values of $\langle \sigma_{\rm ann} v_{\rm rel} \rangle$ in eq. (H.2), while the blue ones from DM decay were obtained by setting $\Lambda_{UV}/g_{UV} = \bar{M}_{\rm Pl} = 2.4 \times 10^{18}\,\mathrm{GeV}$ and $f_\chi = 3\Lambda_{\rm DC}/(4\pi)$ when evaluating $\tau_{\rm DM}$ from eqs. (5.4),(5.9). Experimental bounds are given in terms of the DM mass

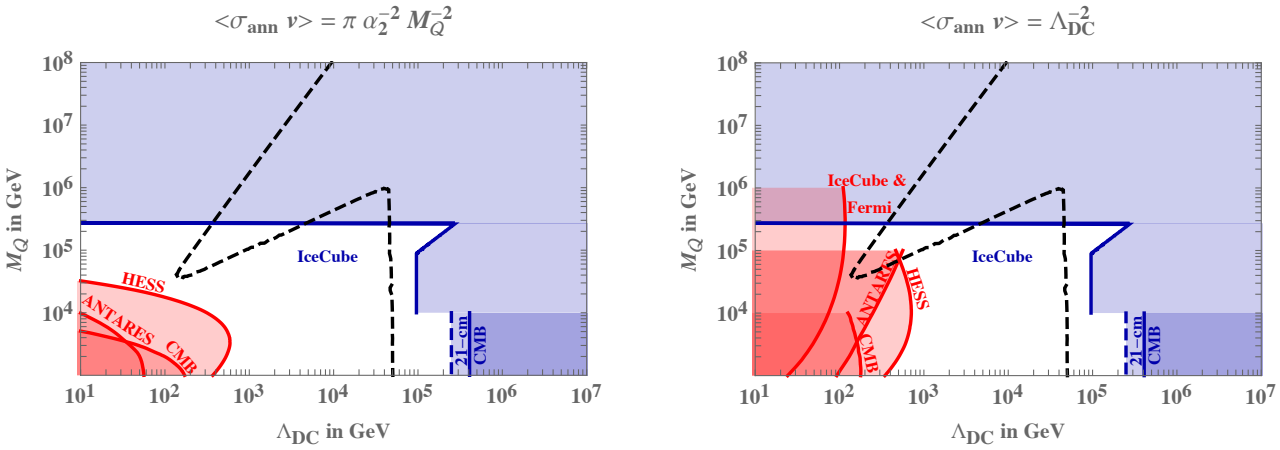


Figure 5.6: *Exclusion limits from experimental searches sensitive to the DM annihilation (red regions) and decay (blue regions). The limits from DM annihilation respectively in the left and right panels have been obtained by adopting the two benchmarks of eq.* (H.2)*, while limits from DM decay were derived by setting* $\Lambda_{UV}/g_{UV} = \bar{M}_{\rm Pl} = 2.4\times 10^{18}\, GeV$ *and* $f_\chi = 3\Lambda_{DC}/(4\pi)$ *in eqs.* (5.4),(5.9).

$M_\chi$; in order to translate them into the $(\Lambda_{\rm DC}, M_{\mathcal{Q}})$ plane we set $M_\chi = M_{\mathcal{Q}}$ in the heavy quark regime and $M_\chi = \Lambda_{\rm DC}$ in the light quark regime.

The constraints from DM annihilation are characterized by a large theoretical uncertainty, as one can easily see by comparing the left and right panels in the figure. Resolving such uncertainty would require a precise determination of the recombination cross section, which does not seem an easy task in general and is beyond the scope of this work. Also the exclusion curve from DM decay has a sizable theoretical uncertainty, which largely comes from the unknown relation between $M_\chi$ and $\Lambda_{\rm DC}$ in the light quark regime (needed to translate the experimental bounds into the $(\Lambda_{\rm DC}, M_{\mathcal{Q}})$ plane), and from the absence of a calculation of the gluequark decay constant (which controls the size of the DM decay rate and for which we were only able to give an order-of-magnitude estimate). In this case, however, dedicated lattice simulations could determine these quantities and thus drastically reduce the theoretical error on the blue exclusion curves.

The results of Fig. 5.6 stem from three classes of experiments, which are discussed in the following.

### Cosmic Rays Experiments

Given the large gluequark mass needed to reproduce the DM relic density in the heavy quark regime, the strongest indirect detection bounds on DM annihilation come from the ANTARES neutrino telescope [20], HESS [25] and the multi-messenger analysis made by the Fermi gamma-

ray telescope and IceCube [275]. The bounds can be roughly summarized as follows [10]:

$$\begin{aligned} \langle \sigma_{\rm ann} v_{\rm rel} \rangle &\lesssim 10^{-7}\,{\rm GeV}^{-2} \quad \text{(from ANTARES, HESS)} \\ \langle \sigma_{\rm ann} v_{\rm rel} \rangle &\lesssim 10^{-5}\,{\rm GeV}^{-2} \quad \text{(from Fermi-ICeCube)}\,. \end{aligned} \tag{5.48}$$

Indirect searches also place bounds on the lifetime of heavy DM candidates. In the high-mass range, Ice-Cube provides the most stringent bounds [15]. For $M_\chi = (10^5 \div 10^7)\,{\rm GeV}$, they are roughly given by

$$\tau(\chi^0) \gtrsim 10^{26} \left(\frac{M_\chi}{100\,{\rm TeV}}\right)^{3/2} {\rm s}\,. \tag{5.49}$$

### CMB power spectrum

The energy released by gluequark annihilations and decays around the epoch of recombination modifies the CMB power spectrum. This, similarly to indirect detection experiments, constrains the lifetime and the annihilation rate of the DM. The annihilation cross section is constrained to be smaller than [206]

$$\langle \sigma_{\rm ann} v_{\rm rel} \rangle \lesssim 10^{-8} \left(\frac{M_\chi}{100\,{\rm GeV}}\right) {\rm GeV}^{-2}\,, \tag{5.50}$$

while the limits on the DM lifetime are [12]

$$\tau\left(\chi^0\right) \gtrsim 10^{24}\,{\rm s}\,. \tag{5.51}$$

These bounds are slightly less stringent than the ones coming from indirect detection, but have the advantage to be free from astrophysical uncertainties. They are provided for DM masses up to 10 TeV, but are expected to be approximately mass-independent for masses above this value [276]. The CMB bounds shown in Fig. 5.6 have been obtained under this assumption.

### 21 cm line

While CMB is sensitive to sources of energy injection at the epoch of recombination, the cosmic 21-cm spectrum is sensitive to sources of energy injection during the dark ages. The recent observation of an absorption feature in this spectrum, if confirmed and in agreement with standard cosmology, can be used to put bounds on both the lifetime and the DM annihilation cross section. Conservative limits can be derived by neglecting astrophysical heating sources; the one on annihilation is of order [21, 17]:

$$\langle \sigma_{\rm ann} v_{\rm rel} \rangle \lesssim 10^{-5} \left(\frac{M_\chi}{10\,{\rm TeV}}\right) {\rm GeV}^{-2}, \tag{5.52}$$

[10] Here and in eqs. (5.51),(5.53) we omit for simplicity the mild dependence that the bounds have on the DM mass. The exclusion curves of Fig. 5.6 have been obtained by using the exact expressions without performing such approximation.

while the one on the DM lifetime is [18, 17, 13]

$$\tau\left(\chi^0\right) \gtrsim 10^{25}\,\mathrm{s}. \tag{5.53}$$

The latter is independent of astrophysical uncertainties on the distribution of DM.

As for the case of CMB, these bounds are provided up to $M_\chi = 10\,\mathrm{TeV}$ and to obtain Fig. 5.6 we assumed that they are constant at higher masses. Differently from the previous case, however, this assumption is not completely justified and further studies are needed to provide solid bounds in the high-mass range [276].

### 5.4.4 Glueball lifetime

In the region of the parameter space that we consider, $\Lambda_{\mathrm{DC}} \gtrsim$ GeV, glueballs with lifetime larger than 1 s are excluded by a combination of bounds. Cosmologically stable glueballs have a too large relic density and overclose the Universe. Long-lived glueballs, on the other hand, are constrained by BBN observations [210] in the range $1\,\mathrm{s} < \tau_\Phi < 10^{12}\,\mathrm{s}$ and by observations of the diffuse gamma-ray spectrum [213] in the range $10^{12}\,\mathrm{s} < \tau_\Phi < 10^{17}\,\mathrm{s}$.

These bounds constrain the high-mass region of the $V$ model as shown in Fig. 5.4. Notice, however, that they could be potentially relaxed if glueballs decay through dimension-6 operators (generated for example in models with Yukawa couplings).

## 5.5 Summary

In this chapter we continued the systematic study of gauge theories with fermions in real or vector-like representations, initiated in Ref. [178], where a DM candidate arises as an accidentally stable bound state of the new dynamics. We considered in detail the gluequark DM candidate, a bound state of adjoint fermions with a cloud of gluons, stable due to dark fermion number. What makes this scenario special in the context of accidental DM is that the physical size of DM, that controls the low-energy interactions, is determined by the dynamical scale of the gauge theory independently of its mass. In the heavy quark regime the DM mass and size can be vastly separated leading to an interesting interplay of elementary and composite dynamics. In particular, cross sections much larger than the perturbative unitarity bound of elementary particles can arise, modifying the thermal abundance and producing potentially observable signals in indirect detection experiments. Gluequarks display a rich and non-standard cosmological history and could be as heavy as PeV if their abundance is set by thermal freeze-out.

Our estimates show that the observed DM density can be reproduced by gluequarks both in the light and heavy quark regimes. The mass of the DM is of order 100 TeV or larger, which makes the models difficult to be directly tested at present and future colliders. On the other hand, indirect experiments sensitive to the decay and the annihilation of the DM are a powerful probes of gluequark theories. We found that these experiments can already set important limits, excluding part of the curve which reproduces the observed DM density, depending on

the value of the annihilation cross section and if the naive estimate for the gluequark decay rate is assumed (see Fig. 5.6). This suggests that gluequark theories in the very heavy quark regime require non-generic UV completions to ensure the accidental stability of the DM at the level of dimension-6 operators. For example, the dark parity could be gauged in the UV (see Appendix I), or its violation could be generated only by non-perturbative gravitational effects in a weakly-coupled UV completion. Similar arguments are put forward also in the context of axion models concerning the quality of the Peccei-Quinn symmetry, see [277]. Assuming that an appropriate UV completion exists, gluequark models are interesting examples where the DM density can be generated thermally after inflation by very heavy particles. This can be contrasted with other scenarios, such as Wimpzillas [278], where ultra heavy DM candidates are never in thermal equilibrium.

The low-energy dynamics and the spectrum of gluequarks are non-perturbative and we were only able to give rough estimates of various effects. In particular, in the heavy quark regime, the quantitative estimate of the re-annihilation relevant for the thermal relic abundance and indirect detection of DM is highly uncertain, as it depends on the details of the spectrum and on the rates of non-perturbative transitions. A more firm conclusion would require a better knowledge of the recombination cross sections and of the de-excitation rates of bound states, as well as an extensive study of the system of Boltzmann equations. In the light-quark regime, a non-perturbative calculation of the annihilation cross section would lead to a sharp prediction of the dynamical scale of the dark sector. The precise knowledge of the spectrum of gluequarks, mesons and pions would then give valuable information for indirect detection and collider studies.

In this chapter we studied gluequarks as thermal relic candidates and focused on the simplest, minimal theories of Tab. 5.1. Investigating non-minimal models would be certainly interesting and important under several aspects. For example, SM gauge couplings unify at high energies with less precision in the minimal blocks of Tab. 5.1 than in the SM. Achieving precision unification thus necessarily requires extending the models to include additional matter with SM quantum numbers. Furthermore, while the thermal relic abundance hints to a large DM mass, this conclusion can be modified in more general gluequark theories where the DM is asymmetric (this requires a larger accidental symmetry than dark parity) or where the DM abundance is determined by the decay of unstable heavier states. These theories would have a smaller mass gap and could be tested at the LHC and at future colliders. We leave an investigation along these directions to a future work.

# Chapter 6

# Conclusions

The focus of this thesis has been on the study of bound states in the phenomenology of DM models. We have considered both their model independent consequences in the context of a thermally produced relic and their role as composite DM candidates. While a detailed discussion of the results can be found in the concluding sections of Chapters 1, 2, 3, 4 and 5, here we summarize again the most relevant results.

In the first part of the work we provided a formalism to include bound states effects in the cosmological history of DM particles produced through thermal freeze-out. Compared to previous works on the subject, our results apply to both abelian and non-abelian gauge theories (both in the perturbative, see Chapter 1, and non-perturbative regime, see Chapter 2). Moreover, in our treatment the whole tower of bound states levels is included, providing a more precise computation of the effect. This formalism is then applied to some benchmark DM candidates (such as an electroweak triplet and quintuplet, and a neutralino co-annihilating with a colored partner) finding that bound state effects can give order one corrections to the DM mass required to reproduce the observed cosmological abundance. We also recast the bounds on long-lived relic gluinos including non-perturbative bound states effects which reduce their cosmological abundance by few orders of magnitude.

In the second part of the work, we considered scenarios where bound states do not only give corrections to the cosmological history of the DM but they also provide a viable composite DM candidate. This is either realized introducing new fermionic particles charged under QCD interactions (see Chapter 3) or a whole new dark sector featuring new matter fields charged under a new confining force (see Chapter 4 and 5).

Specifically, in the first scenario we extended the SM by adding a new Dirac fermion in the adjoint representation of QCD and neutral under electroweak interactions, we dubbed this new particle *quorn*. The DM candidate of the model is provided by the bound state of two quorn; this state is indeed electrically neutral and colorless. However, the quorn can also form stable hybrid states by binding with gluons or quark-antiquark pairs. These states have a large QCD-

like cross section to be captured into normal nuclei, and therefore are subject to very stringent experimental bounds. Because of this, to be successful the model should reproduce the observed DM relic density with the one of quorn bound states and, at the same time, predict a highly suppressed abundance of hybrid states. We showed that, thanks to post-confinement effects, for a quorn mass around 12.5 TeV the abundance of quorn bound states reproduces the one of DM, while the hybrids abundance is suppressed by four orders of magnitude (which is enough to evade the bounds). The DM candidate of the model interacts with normal nuclei through chromo dipole moments induced by the color charge of the constituents. Future direct detection experiments will be able to test this interaction. At colliders quorns can be pair produced through QCD interactions giving rise, after hadronization, to charged and neutral tracks. A 100 TeV collider is expected to test quorn masses up to 15 TeV. An interesting phenomenology is also expected in indirect detection experiments, where annihilation of quorn bound states proceeds through recombination of the constituents.

In the second scenario, the SM is extended by adding new fermions charged under both the electroweak group and a new confining dynamic (*dark color*). The mass of these new fermions, dubbed *dark quarks*, is assumed to be larger than the confining scale of the dark color. Such that, after confinement, the lightest states of the spectrum are dark glueballs. Dark glueballs can decay into SM particles through higher dimensional operator induced by a loop of dark quarks. If sufficiently long-lived, glueballs can lead to an early matter-dominated era in the evolution of the Universe and, upon decaying, dilute the density of preexisting relics thus allowing for very large DM masses. Depending on the assignment of dark quarks quantum numbers, we can have different DM candidates with vastly different phenomenologies.

In Chapter 4, we considered dark quarks in the fundamental representation of an $\mathrm{SU}(N)$ ($\mathrm{SO}(N)$) dark color group. In this scenario, the DM candidate is a dark baryon made of $N$ dark quarks. Dark baryons are stable thanks to an accidental $\mathrm{U}(1)$ ($\mathbb{Z}_2$) symmetry that guarantees dark baryon number conservation. The relic density of the dark baryons is fixed by a freeze-out of perturbative annihilations among dark quarks and a second stage of annihilations between dark baryons after the dark color confinement. This relic density (eventually diluted by glueball decays) matches the one of the DM for dark quarks masses of order 10 TeV.

In Chapter 5, we take dark quarks in the adjoint representation of the dark color group. In this scenario the DM candidate is a bound state made of one dark quark and a cloud of dark gluons, we call this state gluequark. The stability of the gluequark is guaranteed by an accidental dark parity that acts on the dark quarks. Contrary to baryons and mesons, the physical size of the gluequark is determined by the confinement scale independently of its mass. This implies a physical size larger than its Compton wavelength. The annihilation cross section for such a large and heavy bound state can be geometric, much larger than the perturbative unitarity bound of elementary particles. This, in turn, modifies the thermal relic abundance and can lead to significant effects in indirect detection experiments.

To sum up, we have shown that bound states can play a crucial role in the DM phenomenol-

ogy. Both in the case where the DM is an elementary particle, by providing a new annihilation channel through the formation and subsequent decay of unstable bound states. Both in the case where the DM is a composite object, by providing an accidentally stable candidate. It is therefore crucial, in the effort to explore all the possible solutions to the DM puzzle and provide accurate target regions for experiments, to take bound states into account.

While our understanding of bound states production in the perturbative regime is quite complete, a more precise understanding of post-confinement effects is needed in the case non-perturbative dynamics. Specifically, a better knowledge of the recombination cross sections and decay rates is required to reduce the uncertainties that plague these scenarios.

# Acknowledgements

I am deeply grateful to Roberto Contino for his careful and patient supervision during these years, and the precious time he dedicated to my education as a physicist. I will never forget the many stimulating and enlightening discussions we had in his office.
I am also indebted with Michele Redi who helped me take the first steps into the world of scientific research. I owe him a lot if during these years, from being one of his students, I became one of his collaborators.
In these years I had the luck to work with many great physicists: Alessandro Strumia, from which I learned that in physics crazy ideas are not always that crazy; Alessandro Podo, which I thank not only for the stimulating discussions but also for his friendship; Juri Smirnov, with whom I had a long and fruitful collaboration; Rashmish Mishra, that with his enthusiastic attitude towards research lead me to broaden my interests; Valerio De Luca, I had a lot of fun working with you; Christian Gross, Bryan Ostdiek, and Layne Bradshaw. Thank you all.
I also need to thank Scuola Normale Superiore for providing the incredibly stimulating environment in which I had the privilege to spend the last three years. During this time I met wonderful people that eventually became invaluable friends.
Finally, I want to thank my family and all my lifelong friends for their patient and unconditional support.

# Chapter A

## Wave functions in a potential mediated by a vector

In this appendix we collect the relevant formulas used throughout the first chapther.

If the vector is massless, the radial wave functions of a bound state in the Coulomb potential are

$$R_{n\ell}(r) = \left(\frac{2}{na_0}\right)^{3/2} \sqrt{\frac{(n-\ell-1)!}{2n(n+\ell)!}} e^{-r/na_0} \left(\frac{2r}{na_0}\right)^{\ell} L^{2\ell+1}_{n-\ell-1}(\frac{2r}{na_0}) \tag{A.1}$$

where $a_0 = 2/\alpha_{\rm eff} M_\chi$ is the Bohr radius and $L$ are Laguerre polynomials. If the vector has mass $M_V$, an analytic solution is obtained approximating the Yukawa potential with a Hulthen potential

$$V_{\rm Hulthen} = \frac{\kappa\, M_V e^{-\kappa M_V r}}{1 - e^{-\kappa\, M_V r}}. \tag{A.2}$$

The radial wave functions of bound states in the Hulthen potential are

$$R_{n\ell}(r) = N_{n\ell} e^{-r\kappa M_V q_{n\ell}} \frac{(1-e^{-r\kappa M_V})^{\ell+1}}{r} P^{2q_{n\ell},1+2\ell}_{n-\ell-1}(1-2e^{-r\kappa M_V}) \tag{A.3}$$

where $q_{n\ell} = \sqrt{M_\chi E_{n\ell}}/\kappa M_V$, $N_{n\ell}$ is the normalization factor such that $\int dr\, r^2 R_{n\ell} R_{n'\ell} = \delta_{nn'}$, and $P$ are the Jacobi polynomials[1] which equal unity for $\ell = n-1$. For $\ell = 0$ one has

$$q_{n0} = \frac{1-n^2 y}{2ny}, \qquad N_{n0} = \sqrt{\kappa M_V \frac{1-n^4y^2}{2y^3 n^5}}. \tag{A.4}$$

In particular, the ground-state wave function is

$$R_{10}(r) = \sqrt{\kappa M_V \frac{1-y^2}{2y^3}} e^{-r\kappa M_V q_{10}} \frac{1-e^{-r\kappa M_V}}{r}. \tag{A.5}$$

The normalisation factor for $\ell = 1$ is $N_{n1} = N_{n0}\sqrt{(1-n^2y^2)/(n^2-1)n^2y^2}$.

[1] Implemented in `Mathematica` as $P_a^{b,c}(x)$ = `JacobiP[a, b, c, x]`. The value of $c$ differs from [67].

The normalized radial wave function of a free state in the Hulthen potantial is [73, 67]

$$\begin{aligned} R_\ell(r) &= \sqrt{\frac{4\pi}{2\ell+1}}\frac{(1-e^{-\kappa M_V r})^{\ell+1}}{M_\chi r}e^{-iM_\chi v_{\rm rel} r/2}\,{}_2F_1(a^-,a^+,2(\ell+1),1-e^{-\kappa M_V r})\times \\ &\times\frac{1}{(2\ell)!}\frac{\sqrt{S}}{\alpha_{\rm eff}}\prod_{k=0}^{\ell}\sqrt{(\frac{\alpha_{\rm eff}M_\chi}{\kappa M_V})^2+k^2(\frac{v_{\rm rel}M_\chi}{\kappa M_V})^2(1-\frac{2\kappa M_V\alpha_{\rm eff}}{M_\chi v_{\rm rel}^2})+k^4} \end{aligned} \tag{A.6}$$

where $S$ is the Sommerfeld factor for $\ell=0$ given in eq. (1.27), $F$ is the hypergeometric function[2] and its arguments are

$$a^\pm = 1+\ell+iM_\chi\frac{v_{\rm rel}}{2\kappa M_V}\left(1\pm\sqrt{1-\frac{4\kappa M_V\alpha_{\rm eff}}{M_\chi v_{\rm rel}^2}}\right). \tag{A.7}$$

The function $R_\ell(r)$ is real, and in the limit $\alpha_{\rm eff}=0$ it reproduces the free partial wave expansion $e^{i\vec{r}\cdot\vec{p}}=\sum_\ell i^\ell R_\ell(r)Y_{\ell 0}(\theta)$ where $R_\ell(r)=\sqrt{4\pi(2\ell+1)}i^\ell j_\ell(pr)$. Here $\theta$ is the angle between $\vec{r}$ and $\vec{p}$, $p=M_\chi v_{\rm rel}/2$ and $j_\ell$ are spherical Bessel functions $j_\ell(z)=\sqrt{\pi/2z}J_{\ell+1/2}(z)$ (equal to $j_0(z)\simeq\sin(z)/z$ for large $z$). Furthermore, in the massless limit $M_V=0$, $R_\ell$ reproduces the Coulomb partial wave expansion

$$e^{\pi\alpha_{\rm eff}/2v_{\rm rel}}\Gamma(1-i\alpha_{\rm eff}/v_{\rm rel})\,{}_1F_1\left[i\alpha_{\rm eff}/v_{\rm rel},1,i(pr-\vec{p}\cdot\vec{r})\right]e^{i\vec{r}\cdot\vec{p}}=\sum_\ell i^\ell R_\ell(r)Y_{\ell 0}(\theta) \tag{A.8}$$

where

$$R_\ell(r)=\frac{\sqrt{4\pi(2\ell+1)\,S}}{\Gamma(2\ell+2)}e^{-ipr}(2pr)^\ell\;{}_1F_1[\ell+1+i\alpha_{\rm eff}/v_{\rm rel},2\ell+2,2ipr]\prod_{k=1}^{\ell}|\ell-k+1-i\alpha_{\rm eff}/v_{\rm rel}|\,. \tag{A.9}$$

Such analytic solution of the wave function for the Hulthen potential is only exact if $\ell=0$. If $\ell$ is not zero, an extra approximation for the centrifugal term is needed, such that the behaviour at large $r$ becomes only approximate. This is not a problem for the bound state wave function, as it is exponentially suppressed at large $r$. However, for the free state this approximation leads to unphysical results that become relevant in the case of bound state production from a $p$-wave and $d$-wave partial waves. In order to correct for this inaccuracy we multiply the resulting cross sections, as was suggested in [73] by

$$L_\ell=\frac{w^{2\ell}}{\prod_{k=0}^{k=\ell-1}((\ell-k)^2+w^2)}\qquad\text{with}\qquad w=\frac{M_\chi\,v_{\rm rel}}{\kappa M_V}\approx\frac{p}{M_V}\,. \tag{A.10}$$

This function is controlled by the critical momentum $M_V$ so that, once the momentum of the dark matter particles drops below the mediator mass, the production cross sections from higher $\ell$ states are suppressed.

[2] Implemented in `Mathematica` as ${}_2F_1(a,b;c;x)$ = `Hypergeometric2F1[a, b, c, x]`.

# Chapter B

## Non-abelian bound states

Production cross sections and decay widths of two-body bound states due to perturbative non-abelian gauge interactions have been given in Chapter 1, for bound states with low angular momentum $\ell$. Following the same notations, in appendix we generalize the decay widths to any $\ell$. We consider emission of a single-vector $V^a$ in dipole approximation, such that the angular momenta of the initial and final states differ by $\Delta\ell = \pm 1$. We denote with $\alpha$ the non-abelian gauge coupling, with $M_a$ the vector mass, and with $M$ the common mass of the two particles which form the bound state.

The decay widths of a bound state through single-vector emission are obtained from the previous expressions substituting the free-particle final state wave function $R_{p\ell}$ with the wave-function of the desired final bound states. Assuming again degenerate (or massless) vectors and a bound state in a representation $R$ with dimension $d_R$, we find

$$\begin{aligned}\Gamma(n,\ell\to n',\ell-1) = \frac{1}{d_R}\frac{8\ell}{(2\ell+1)}\frac{\alpha k}{M^2}\left(1-\frac{k^2}{3\omega^2}\right)\times \\ \times\sum_{aMM'}\left|\int r^2 dr R^*_{n',\ell-1}\left(C_{\mathcal{J}}^{aMM'}\left(\partial_r+\frac{\ell+1}{r}\right)+C_{\mathcal{T}}^{aMM'}\frac{\alpha M}{2}e^{-M_a r}\right)R_{n\ell}\right|^2\end{aligned} \tag{B.1}$$

and

$$\begin{aligned}\Gamma(n,\ell\to n'',\ell+1) = \frac{1}{d_R}\frac{8(\ell+1)}{(2\ell+1)}\frac{\alpha k}{M^2}\left(1-\frac{k^2}{3\omega^2}\right)\times \\ \times\sum_{aMM'}\left|\int r^2 dr R^*_{n''\ell+1}\left(C_{\mathcal{J}}^{aMM'}\left(\partial_r-\frac{l}{r}\right)+C_{\mathcal{T}}^{aMM'}\frac{\alpha M}{2}e^{-M_a r}\right)R_{n\ell}\right|^2 .\end{aligned} \tag{B.2}$$

# Chapter C

## Hydrogen decay rates

We summarize the known results for the hydrogen decay rates in dipole tree-level approximation [279]. We denote the initial state as $(n, \ell)$, and the final states as $(n', \ell')$. Their energy gap is

$$\Delta E(n, n') = \frac{\alpha^2 \mu}{2}\left(\frac{1}{n^2} - \frac{1}{n'^2}\right) \tag{C.1}$$

where $\mu$ is the reduced mass. The spontaneous emission rate, in dipole approximation, is

$$\Gamma(n, \ell \to n', \ell') = \frac{4\alpha}{3}\frac{\Delta E^3}{2\ell + 1}\sum_{m,m'} |\langle n', \ell', m'|\, \vec{r}\, |n, \ell, m\rangle|^2. \tag{C.2}$$

Selection rules imply $\Delta\ell = \pm 1$, and the matrix element are

$$\sum_{m'} |\langle n', \ell - 1, m'|\, \vec{r}\, |n, \ell, m\rangle|^2 = \frac{\ell}{2\ell + 1}\frac{1}{(\alpha\mu)^2}\left(R_{n,\ell}^{n',\ell-1}\right)^2 \tag{C.3}$$

$$\sum_{m'} |\langle n', \ell, m'|\, \vec{r}\, |n, \ell - 1, m\rangle|^2 = \frac{\ell}{2\ell - 1}\frac{1}{(\alpha\mu)^2}\left(R_{n,\ell-1}^{n',\ell}\right)^2 \tag{C.4}$$

where

$$R_{n\ell}^{n'\ell'} = (\alpha\mu)\int_0^\infty dr\, r^3\, R_{n\ell} R_{n'\ell'} \tag{C.5}$$

with $R_{n\ell}(r)$ the radial part of the hydrogen wave-function. These integrals are given by

$$\begin{aligned} R_{n\ell}^{n',\ell-1} \;=\; & \frac{(-1)^{n'-\ell}}{4(2\ell-1)!}\sqrt{\frac{(n'+\ell-1)!(n+\ell)!}{(n'-\ell)!(n-\ell-1)!}}\frac{(4nn')^{\ell+1}(n-n')^{n+n'-2\ell-2}}{(n+n')^{n+n'}} \times \\ & \left[{}_2F_1\left(-n+\ell+1, -n'+\ell, 2\ell, -\frac{4nn'}{(n-n')^2}\right) - \right. \\ & \left. + \left(\frac{n-n'}{n+n'}\right)^2 {}_2F_1\left(-n+\ell-1, -n'+\ell, 2\ell, -\frac{4nn'}{(n-n')^2}\right)\right] \end{aligned} \tag{C.6}$$

where ${}_2F_1$ is the `Hypergeometric2F1` function. A similar formula can be obtained for $R^{n',\ell}_{n,\ell-1}$ by the interchange of the indices $n$ and $n'$. The total decay rate and energy loss rate from an initial state $(n, \ell)$ is obtained by summing over all available lower-energy states with $n' < n$.

# Chapter D

## Toy redecoupling

We here show that the chromodark-synthesis mechanism is absolutely unavoidable by discussing a toy model that allows one to analytically understand some of its features. We consider formation of one bound state $B_{\mathcal{Q}\mathcal{Q}}$ containing two DM quarks $\mathcal{Q}$ from two bound states $B_{\mathcal{Q}}$ containing one DM quark:[1]

$$B_{\mathcal{Q}} + B_{\mathcal{Q}} \leftrightarrow B_{\mathcal{Q}\mathcal{Q}} + X \tag{D.1}$$

where $X$ denotes any other SM particles, such as pions. We define $\delta \equiv 2M_{B_{\mathcal{Q}}} - M_{B_{\mathcal{Q}\mathcal{Q}}}$. In the real situation described in section 3.2, many bound states with a semi-classical discretuum of binding factors $\delta$ can be produced. We simplify the problem by considering just one of them, with $\delta \sim \Lambda_{\rm QCD}$ such that the QCD cross section for the above process is large, $\sigma_{\mathcal{Q}\mathcal{Q}} \sim 1/\delta^2$. One then reaches thermal equilibrium

$$\frac{n_{B_{\mathcal{Q}\mathcal{Q}}}}{n^2_{B_{\mathcal{Q}}}} = \frac{n^{\rm eq}_{B_{\mathcal{Q}\mathcal{Q}}}}{n^{\rm eq2}_{B_{\mathcal{Q}}}} = \frac{g_{B_{\mathcal{Q}\mathcal{Q}}}}{g^2_{B_{\mathcal{Q}}}} \left(\frac{4\pi}{M_{\mathcal{Q}}T}\right)^{3/2} e^{\delta/T}. \tag{D.2}$$

This means that the $B_{\mathcal{Q}}$ dominantly form $B_{\mathcal{Q}\mathcal{Q}}$ at the redecoupling temperature

$$T_{\rm redec} = \frac{\delta}{A} \qquad \text{where} \qquad A = \ln \frac{Y_\pi}{Y_{\mathcal{Q}}} \sim 40 \tag{D.3}$$

is an entropy factor that describes how much formation of $B_{\mathcal{Q}\mathcal{Q}}$ gets delayed by having a plasma with much more particles $X$ than can break it, than particles $B_{\mathcal{Q}}$ that can form it. This is analogous to how $e, p$ bind in hydrogen at $T \lesssim \delta/\ln(n_\gamma/n_p)$, and to how $p, n$ bind in deuterium at $T \lesssim \delta/\ln(n_\gamma/n_p)$, where $\delta$ are the binding energies of hydrogen and deuterium respectively.[2]

In the toy model, the residual density of $B_{\mathcal{Q}}$ is estimated as its thermal equilibrium value at the redecoupling temperature where the interaction rate $\Gamma_{\mathcal{Q}\mathcal{Q}} \sim n_{B_{\mathcal{Q}}} \sigma_{\mathcal{Q}\mathcal{Q}} v_{\rm rel}$ for the process of eq. (D.1) becomes smaller than the Hubble rate. Imposing $\Gamma_{\mathcal{Q}\mathcal{Q}} \sim H$ with $H \sim T^2/M_{\rm Pl}$, $v_{\rm rel} \sim \sqrt{T/M_{\mathcal{Q}}}$ and

[1] Similar considerations apply to formation of $B_{\mathcal{Q}\mathcal{Q}}$ from free $\mathcal{Q}$ at $T \gtrsim \Lambda_{\rm QCD}$, but this phase is not relevant for the final DM abundance.

[2] In the numerical computation such entropy factor was accounted in section 3.1.5 by imposing a small time allowed to radiate enough energy down to an unbreakable state. To keep the argument simple we here ignore the Boltzmann suppression in the $\pi$ abundance at $T \lesssim m_\pi$ (in the full numerical computation this is taken into account and increases the $\sigma_{\rm fall}$ computed in section 3.1.5, consequently suppressing the hybrid abundances).

$n_{B_\mathcal{Q}} \sim Y_{B_\mathcal{Q}} T^3$ gives

$$Y_{B_\mathcal{Q}}^{\rm relic}|_{\rm toy} \sim \frac{1}{\sigma_{\mathcal{Q}\mathcal{Q}} M_{\rm Pl} T_{\rm redec} \sqrt{T_{\rm redec}/M_\mathcal{Q}}} \sim A^{3/2} \frac{\sqrt{\delta M_\mathcal{Q}}}{M_{\rm Pl}} \sim 10^{-16} \sqrt{\frac{M_\mathcal{Q}}{10\,{\rm TeV}} \frac{\delta}{\Lambda_{\rm QCD}}}. \tag{D.4}$$

This shows that re-annihilation is dominated by bound states with smaller $\delta \sim \Lambda_{\rm QCD}$, rather than by deep states. In the full computation many bound states contribute to the depletion of $Y_{B_\mathcal{Q}}$, that gets about 2 orders of magnitude smaller than the toy-model estimate of eq. (D.4). In turn, the unavoidable toy-value is much smaller than what obtained by including only perturbative QCD annihilations at $T \sim T_{\rm dec} \gg \Lambda_{\rm QCD}$.

# Chapter E

## Chromo-polarizability of $\mathcal{QQ}$ DM

Eq. (3.40) provides the formula for the polarizability of a QCD bound state. We here evaluate it for our DM, the $\mathcal{QQ}$ singlet bound state $|B\rangle = |1, s, \alpha_{\rm eff}\rangle$ with energy $E_{10} = -\alpha_{\rm eff}^2 M_Q/4$, where $\alpha_{\rm eff} = 3\alpha_3$. By emitting a gluon it becomes a $p$-wave octet, with free Hamiltonian $H_8 = \vec{p}^2/M_\chi - \alpha_8/r$ where $\alpha_8 = 3\alpha_3/2$, whose eigenvalues are $E_{8n} = -\alpha_8^2 M_Q/4n^2$ for bound states and $\vec{p}^2/M_\chi$ for positive energy states. To evaluate the matrix element in eq. (3.40) we insert the completeness relation for the octet eigenstates

$$\mathbf{1}_8 = \sum_{n,\ell,m} |n,\ell,m,\alpha_8\rangle\langle n,\ell,m,\alpha_8| + \frac{1}{3}\sum_{\ell,m}\int \frac{d^3p}{(2\pi)^3}|\vec{p},\ell,m,\alpha_8\rangle\langle\vec{p},\ell,m,\alpha_8| \tag{E.1}$$

where the first (second) term is the contribution from bound (free) states. The factor 1/3 is introduced not to double count the angular momentum states. In coordinate space $\langle\vec{r}|n,\ell,m\rangle = R_{n\ell}(r)Y_{\ell m}(\theta,\phi)$ for bound states and $\langle\vec{r}|\vec{p},\ell,m\rangle = R_{p\ell}(r)Y_{\ell m}(\theta,\phi)$ for continuum positive energy states, where $Y_{\ell m}(\theta,\phi)$ are spherical harmonics. The Coulombian wave-functions are

$$R_{n\ell\alpha_i}(r) = \left(\frac{2}{na_i}\right)^{3/2}\sqrt{\frac{(n-\ell-1)!}{2n(n+\ell)!}}e^{-r/na_i}\left(\frac{2r}{na_i}\right)^\ell L^{2\ell+1}_{n-\ell-1}\left(\frac{2r}{na_i}\right) \tag{E.2}$$

$$R_{p\ell\alpha_i}(r) = \sqrt{4\pi}\sqrt{2\ell+1}\frac{\Gamma[1+\ell-i/a_ip]}{\Gamma[2(\ell+1)]}e^{\pi/(2a_ip)}e^{-ipr}(2ipr)^\ell\,{}_1F_1[1+\ell+\frac{i}{a_ip}, 2(\ell+1), 2ipr] \tag{E.3}$$

where ${}_1F_1$ is the `Hypergeometric1F1` function; $a_i = 2/(\alpha_i M_\chi)$ are the Bohr radii in each channel with effective coupling $\alpha_i = \{\alpha_{\rm eff}, \alpha_8\}$ and $L^{2\ell+1}_{n-\ell-1}$ are Laguerre polynomials.

Angular momentum conservation implies that only $p$-wave intermediate states contribute to the polarizability. The bound state contribution thereby is

$$\langle B|\vec{r}\frac{1}{H_8 - E_{10}}\vec{r}|B\rangle_{\rm bound} = \sum_{n\geqslant 2}\frac{|\langle 1,s,\alpha_{\rm eff}|\vec{r}|n,p,\alpha_8\rangle|^2}{E_{8n}-E_{10}} \tag{E.4}$$

where the matrix element is

$$|\langle 1,s,\alpha_1|\vec{r}|n,p,\alpha_8\rangle|^2 = |\int_0^\infty dr\, r^3\, R_{10\alpha_{\rm eff}}(r)R_{n1\alpha_8}(r)|^2. \tag{E.5}$$

Performing numerically the integral and the sum one finds

$$\langle B|\vec{r}\frac{\alpha_3}{H_8 - E_{10}}\vec{r}|B\rangle_{\rm bound} = 0.359a^3. \tag{E.6}$$

The contribution of unbound $E > 0$ intermediate states is found generalizing the formulæ in [280]

$$\begin{aligned}\langle B|\vec{r}\frac{\alpha_3}{H_8 - E_{10}}\vec{r}|B\rangle_{\rm free} &= \frac{1}{3}\int\frac{d^3p}{(2\pi)^3}\frac{\alpha_3}{p^2/M_{\mathcal{Q}} - E_{10}}\left|\int_0^\infty dr\, r^3\, R_{10\alpha_{\rm eff}}(r)R_{p1\alpha_8}(r)\right|^2 \\ &= a^3\frac{512}{C}\rho(\rho+2)^2\int_0^\infty p^3\frac{(1+\rho^2/p^2)e^{-4\rho/p\arctan p}}{(e^{2\pi\rho/p}-1)(1+p^2)^7}\,dp = 1.17a^3\end{aligned} \tag{E.7}$$

where $C = 3$ and $\rho = -\alpha_8/\alpha_{\rm eff} = -1/2$ for our color octets. In the case of the hydrogen atom ($C = 1$, $\rho = -1$) one finds [170] $c_E|_{\rm hydrogen} = 8\pi(5.49 + 1.26)a^3/3 = 18\pi a^3$. The $\mathcal{QQ}$ chromo-polarizability is smaller than what suggested by a naive rescaling of the abelian result computed for the hydrogen atom $c_E|_{\rm naive} = 18\pi a^3 C/(N_c^2 - 1) = 6.75\pi a^3$.

# Chapter F

## Boltzmann equations for baryonic DM

To describe the cosmological evolution of dark quaks at $T > \Lambda_{\rm DC}$ we need to generalize the results of section 1.1 to include also stable bound states. As discussed in section 1.1, the joint evolution of the dark quarks and bound states number densities is described by eq.(3.13) and (1.5) which we report here for convenience:

$$\begin{aligned} sHz\frac{dY_{\mathcal{Q}}}{dz} &= -2\gamma_{\rm ann}\left[\frac{Y_{\mathcal{Q}}^2}{Y_{\mathcal{Q},\rm eq}^2}-1\right]-2\sum_I\gamma_I\left[\frac{Y_{\mathcal{Q}}^2}{Y_{\mathcal{Q},\rm eq}^2}-\frac{Y_I}{Y_{I,\rm eq}}\right] \\ sHz\frac{dY_I}{dz} &= n_I^{\rm eq}\left\{\langle\Gamma_{I\rm break}\rangle\left[\frac{Y_{\mathcal{Q}}^2}{Y_{\mathcal{Q},\rm eq}^2}-\frac{Y_I}{Y_{I,\rm eq}}\right]+\langle\Gamma_{I\rm ann}\rangle\left[1-\frac{Y_I}{Y_{I,\rm eq}}\right]+\sum_J\langle\Gamma_{I\to J}\rangle\left[\frac{Y_J}{Y_{J,\rm eq}}-\frac{Y_I}{Y_{I,\rm eq}}\right]\right\}. \end{aligned} \tag{F.1}$$

where $Y_{\mathcal{Q},I} = n_{\mathcal{Q},I}/s$ with $s$ the entropy density, $z = m_{\mathcal{Q}}/T$. We define as $n^{\rm eq}$ and $Y^{\rm eq}$ the thermal equilibrium value of $n$ and $Y$ respectively and $\gamma$ is the space-time density of interactions in thermal equilibrium. The first term describes $\mathcal{Q}\bar{\mathcal{Q}}$ annihilations to SM particles; the second term describes formation of the bound state identified by the index $I$ that collectively denotes its various quantum numbers: angular momentum, spin, gauge group representation, etc.

The effect of rapidly unstable bound states can be encoded in an effective annihilation rate, $\gamma_{\rm ann}^{\rm eff}$, that substitutes $\gamma_{\rm ann}$, such that their Boltzmann equations can be dropped, as shown in Chapter 1. However, the present study contains a new feature: some bound states (such as $\mathcal{Q}\mathcal{Q}$) do not decay, and can only be formed or broken by interactions. We then need to separately evolve the Boltzmann equations for their abundances. We define $\gamma_{\rm bsf-stable} = \sum_I \gamma_I$ with the sum running over the unstable bound states, and similarly for the stable ones. In the non-relativistic limit the space-time densities $\gamma$ get approximated as

$$2\gamma \overset{T\ll M_\chi}{\simeq} (n_{\mathcal{Q}}^{\rm eq})^2\langle\sigma v_{\rm rel}\rangle \tag{F.2}$$

such that the Boltzmann equations simplify to

$$\begin{cases} \dfrac{1}{\lambda}\dfrac{dY_{\mathcal{Q}}}{dz} = -\dfrac{S_{\rm eff-unstable}}{z^2}\left(Y_{\mathcal{Q}}^2-Y_{\mathcal{Q},\rm eq}^2\right)-\dfrac{S_{I,\rm bsf}}{z^2}\left(Y_{\mathcal{Q}}^2-Y_I\dfrac{Y_{\mathcal{Q},\rm eq}^2}{Y_{I,\rm eq}}\right) \\ \dfrac{1}{\lambda}\dfrac{dY_I}{dz} = \dfrac{S_{I,\rm bsf}}{z^2}\left(Y_{\mathcal{Q}}^2-Y_I\dfrac{Y_{\mathcal{Q},\rm eq}^2}{Y_{I,\rm eq}}\right), \end{cases} \tag{F.3}$$

where we introduced the dimension-less factors $S_{\rm eff-unstable} = S_{\rm ann} + S_{\rm bsf-unstable}$ and

$$S_X(z) = \frac{\langle \sigma_X v_{\rm rel} \rangle}{\sigma_0}, \qquad \lambda = \frac{\sigma_0 s}{H}\Big|_{T=M_\chi} = \sqrt{\frac{g_{\rm SM}\pi}{45}}\sigma_0 M_{\rm Pl} M_\chi \,. \tag{F.4}$$

Here $g_{\rm SM}$ is the number of degrees of freedom in thermal equilibrium at $T = M_\chi$ ($g_{\rm SM} = 106.75$ at $T \gg M_Z$).

Stable bound states $I$ are kept into thermal equilibrium by fast dark gauge interactions, so that they decouple at a $z_I$ much later than DM freeze-out, that occurs at $z_f \sim 25$. Thereby for $z \ll z_I$ we obtain a single Bolztmann equation

$$\frac{1}{\lambda}\frac{dY_{\mathcal{Q}}}{dz} = -\frac{S_{\rm eff}}{z^2}\left(Y_{\mathcal{Q}}^2 - Y_{\mathcal{Q},\rm eq}^2\right), \qquad S_{\rm eff} = S_{\rm ann} + S_{\rm bsf-unstable} + S_{\rm bsf-stable} \tag{F.5}$$

approximatively solved by

$$Y_{\mathcal{Q}}(z) = \frac{1}{\lambda}\left(\int_{z_f}^{z} \frac{S_{\rm eff}(z)}{z^2}dz + \frac{S_{\rm eff}(z_f)}{z_f^2}\right)^{-1} . \tag{F.6}$$

We now compute $z_I$, showing that it is so large that later annihilations are negligible. The value of $z_I$ is needed to estimate the fraction of dark quarks bound in stable states.

Assuming that $dY_I/dz \approx 0$ is violated at $z_I$ so large that annihilation processes are negligible, we have $Y_{\mathcal{Q}}(z) + 2Y_I(z) = Y_{\mathcal{Q}}(z_I) = Y_c$ at temperatures $z > z_I$ at which the stable bound states are no longer in thermal equilibrium. This leads to an effective single Boltzmann equation

$$\frac{1}{\lambda}\frac{dY_{\mathcal{Q}}}{dz} = -S_{\rm I,bsf}(z)\left(2Y_{\mathcal{Q}}(z)^2 - \frac{A g_{\mathcal{Q}}^2 z^{3/2}(Y_c - Y_{\mathcal{Q}}(z))e^{-z\Delta}}{g_I}\right), \tag{F.7}$$

where $\Delta = E_B/M_\chi$ and $A = 90/((2\pi)^{7/2} g_{\rm SM}^*)$. The value of $z_I$ is defined by imposing that the leading order term in the $1/\lambda \ll 1$ expansion of the solution $Y_{\mathcal{Q}}(z) \approx Y_{\mathcal{Q}}^0(z) + Y_{\mathcal{Q}}^1(z)/\lambda$ is comparable to the second order term. The leading order term is simply defined by the condition that the derivative of $Y_{\mathcal{Q}}(z)$ vanishes

$$Y_{\mathcal{Q}}^0(z) = A\, z^{3/2}\,\frac{g_{\mathcal{Q}}}{4g_I} e^{-z\Delta}\left(\sqrt{\left(g_{\mathcal{Q}}^2 + 8\frac{z^{-3/4}\,Y_c}{A} g_I e^{z\Delta}\right)} - g_{\mathcal{Q}}\right). \tag{F.8}$$

Inserting the assumptions in eq. (F.7), solving for $Y_{\mathcal{Q}}^1(z)$ and evaluating $Y_{\mathcal{Q}}^0(z_I) = Y_{\mathcal{Q}}^1(z_I)/\lambda$ defines $z_I$. Such equation can be simplified assuming $z \gg 1$ and reads

$$z_I = \frac{1}{\Delta}\ln\left(\frac{32 A g_{\mathcal{Q}}^2 \lambda^2 S_{\rm I,bsf}(z_I)^2 Y_c}{\Delta^2 g_I z_I^{5/2}}\right). \tag{F.9}$$

For a typical value $\Delta \equiv E_B/M_\chi \approx 10^{-3}$ we find $z_I \approx 10^5$, which justifies our initial assumptions, since $z_f \approx 25$ and the annihilation has no effect at $z > 10^4$. Now the second effective eq. (F.7) which describes the recombination effect can be integrated in the same manner as the first and leads, after

the appropriate asymptotic matching, to

$$Y_{\mathcal{Q}}(\infty) = \left( 2\lambda \int_{z_I}^{\infty} \frac{S_{\mathrm{bsf-stable}}(z)}{z^2} dz + \frac{1}{Y^0_{\mathcal{Q}}(z_I)} \right)^{-1} \qquad Y_I(\infty) = \frac{1}{2} \left( Y_{\mathcal{Q}}(z_I) - Y_{\mathcal{Q}}(\infty) \right) . \tag{F.10}$$

Using this method we find that, in the models considered, the relic abundance of stable dark di-quark states is at most at the percent level of the abundance of free dark quarks at confinement. In conclusion, perturbative production of stable bound states negligibly affects the final dark matter relic abundance.

# Chapter G

# Dark Quark Annihilation Cross Section

In this appendix we report the formulas for the annihilation cross section of dark quarks, which are useful to study the perturbative freeze-out and DM indirect detection.

Dark quarks can annihilate into dark gluons and into SM final states (mainly $VV$, $Vh$, $hh$ and $\psi\bar{\psi}$, where $V = W, Z, \gamma$). These latter contribute significantly to the total cross section in the case of perturbative freeze-out whenever $M_{\mathcal{Q}}/\Lambda_{\rm DC} \gg 1$ and thus the dark color interaction strength does not exceed much the electroweak one. Final states into SM particles are also expected to be important for direct detection even though they have a smaller rate compared to DM annihilation into glueballs.

The tree-level annihilation cross-section of dark quarks $\chi_i\chi_j$ in a representation $(A_{\rm DC}, R_{\rm SM})$ of the dark color and $\mathrm{SU}(2)_L$ groups into massless vectors at low energy reads,

$$\begin{aligned} \langle\sigma v_{\rm rel}\rangle_{ij\to VV} &= \frac{A^1_{ij} + A^2_{ij}}{16\pi}\frac{1}{M^2_{\mathcal{Q}}} \\ A^1_{ij} &\equiv \left[T^a T^a T^b T^b\right]_{ij}\,, \qquad A^2_{ij} \equiv \left[T^a T^b T^a T^b\right]_{ij} \end{aligned} \tag{G.1}$$

where the generators are written as $T \equiv (g_{\rm DC} T_{\rm DC} \otimes 1) \oplus (1 \otimes g_{\rm SM} T_{\rm SM})$. Selecting the neutral component in the equation above and averaging over dark color gives the perturbative annihilation cross-section of DM today. Averaging over all initial states as required for the thermal freeze-out one finds,

$$\begin{aligned} \langle\sigma v_{\rm rel}\rangle_{\rm ann} = \frac{\pi}{M^2_{\mathcal{Q}}}\Bigg[ &\frac{\alpha^2_{\rm DC}}{d(R_{\rm SM})}\frac{K_1(R_{\rm DC}) + K_2(R_{\rm DC})}{g_\chi d(R_{\rm DC})^2} + \frac{\alpha_2^2}{d(R_{\rm DC})}\frac{K_1(R_{\rm SM}) + K_2(R_{\rm SM})}{g_\chi d(R_{\rm SM})^2} \\ &+ \alpha_{\rm DC}\alpha_2 \frac{4C(R_{\rm DC})C(R_{\rm SM})}{g_\chi d(R_{\rm SM}) d(R_{\rm DC})}\Bigg], \end{aligned} \tag{G.2}$$

where

$$K_1(R) = d(R)C(R)^2, \quad K_2(R) = K_1(R) - \frac{d(A)C(A)T(R)}{2}, \quad d(R) = dim(R)\,. \tag{G.3}$$

and $A$ stands for the adjoint representation. $T(R)$ and $C(R)$ are respectively the Dynkin index and the quadratic Casimir of the representation $R$, and $g_\chi = 2(4)$ for real (complex) representations.

Dark quarks can also annihilate into final states with SM fermions and Higgs bosons through their SM gauge and Yukawa interactions. These channels have been included in eq. (5.12).

# Chapter H

## Reannihilation

As discussed in section 5.2.3, a second stage of annihilation involving gluequarks can occur after confinement. The annihilation can proceed in a single step into glueballs or SM vector and Higgs bosons:

- $\chi + \chi \to n\Phi/nV$: in the heavy quark regime this process has a perturbative cross section; indeed the exchanged momentum in the interaction is of $\mathcal{O}(M_{\mathcal{Q}})$ with $M_{\mathcal{Q}} \gg \Lambda_{\rm DC}$, thus the interaction strength is governed by $g_{\rm DC}(M_{\mathcal{Q}})$ which is perturbative.

Alternatively, it can take place in two steps, a non-perturbative recombination followed by de-excitation and decay into SM particles:

- $\chi + \chi \to \mathcal{Q}\mathcal{Q}^* \dashrightarrow$ SM: the recombination is two to one and energy conservation implies $M_{\mathcal{Q}\mathcal{Q}^*} > 2M_\chi$, therefore the opposite decay process is always allowed. The matrix element for the inverse decay is non-perturbative and the corresponding rate is expected to be much larger than the rate of the de-excitation process $\mathcal{Q}\mathcal{Q}^* \to \mathcal{Q}\mathcal{Q} + n\Phi/nV$.

- $\chi + \chi \to \mathcal{Q}\mathcal{Q}^* + \Phi/V \dashrightarrow$ SM: the recombination takes place with the emission of one electroweak gauge boson or, if kinematically allowed, one glueball. Bound states with $M_{\mathcal{Q}\mathcal{Q}^*} < 2M_\chi$ will in general be formed which cannot decay back into gluequarks. They can de-excite and decay into SM particles. The corresponding re-annihilation rate is expected to be non-perturbative and potentially large.

Only the last of the three processes described above can ignite an epoch of re-annihilation. The dynamics of re-annihilation is described by a set of coupled Boltzmann equations of the form

$$\begin{aligned}
\frac{dY_\chi}{dz} &= -\frac{s\langle\sigma_{\rm rec}v\rangle}{Hz}\left(Y_\chi^2 - Y_{\chi,eq}^2\frac{Y_{\mathcal{Q}\mathcal{Q}^*}Y_\Phi}{Y_{\mathcal{Q}\mathcal{Q}^*}^{eq}Y_\Phi^{eq}}\right), \\
\frac{dY_{\mathcal{Q}\mathcal{Q}^*}}{dz} &= \frac{1}{2}\frac{s\langle\sigma_{\rm rec}v\rangle}{Hz}\left(Y_\chi^2 - Y_{\chi,eq}^2\frac{Y_{\mathcal{Q}\mathcal{Q}^*}Y_\Phi}{Y_{\mathcal{Q}\mathcal{Q}^*}^{eq}Y_\Phi^{eq}}\right) - \frac{\Gamma_{\mathcal{Q}\mathcal{Q}^*}}{Hz}(Y_{\mathcal{Q}\mathcal{Q}^*} - Y_{\mathcal{Q}\mathcal{Q}^*}^{eq}) \\
\frac{dY_\Phi}{dz} &= \frac{1}{2}\frac{s\langle\sigma_{\rm rec}v\rangle}{Hz}\left(Y_\chi^2 - Y_{\chi,eq}^2\frac{Y_{\mathcal{Q}\mathcal{Q}^*}Y_\Phi}{Y_{\mathcal{Q}\mathcal{Q}^*}^{eq}Y_\Phi^{eq}}\right) - \frac{\Gamma_\Phi}{Hz}(Y_\Phi - Y_\Phi^{eq}).
\end{aligned} \tag{H.1}$$

These expressions are simplified in that the actual system of equations involves the number densities of all possible $\mathcal{Q}\mathcal{Q}^*$ bound states. Furthermore, we have omitted the effect of the recombination into EW vector bosons and of the corresponding inverse process. Equation (H.1) will be however sufficient for our discussion, and the generalization to the full case is straightforward.

In order to annihilate into SM particles with an unsuppressed rate, an excited $\mathcal{Q}\mathcal{Q}^*$ bound state needs to reach first a state with low angular momentum. Consequently, re-annihilation is efficient only when the rate of de-excitation is larger than the one of dissociation[1].

Obtaining a precise estimate of the ratio between the de-excitation and dissociation rates is difficult because: *i)* the dynamics of these processes is non-perturbative and the lifetime depends on the different initial and final $\mathcal{Q}\mathcal{Q}^*$ states considered; *ii)* the rate of the dissociation process initiated by EW vector bosons depends on their energy, which follows a thermal distribution and thus varies with the temperature. The result is that the re-annihilation process can be efficient for some of the $QQ^*$ states and inefficient for others, and it becomes more and more efficient as the temperature decreases.

This can be effectively described as a non-perturbative re-annihilation process happening with a temperature-dependent cross section that saturates to a maximal value when dissociation becomes inefficient for all the bound states. Since the evolution of the relic density takes place on relatively short time scales, the final abundance after this second freeze-out can be approximately characterized by two parameters: the final (maximal) value of the cross section, and the temperature at which this final cross section is reached. These two quantities will be dubbed respectively as the re-annihilation cross section, $\sigma_{\rm rea}$, and the re-annihilation temperature, $T_R$.

During the last stage of re-annihilation, for sufficiently large $\Gamma_\Phi$ or $\Gamma_{\mathcal{Q}\mathcal{Q}^*}$, the system of equations given in eq. (H.1) simplifies. The abundance of gluequarks can be described by a single equation, see eq. (5.28).

# H.1 Estimate of the Re-annihilation Cross Section

In this appendix we try to estimate $\sigma_{\rm rea}$ using considerations based on energy and angular momentum conservation and simplified phenomenological models.

First of all, it is useful to determine if (depending on value of the temperature, $\Lambda_{\rm DC}$ and $M_{\mathcal{Q}}$) the recombination process takes place in a semiclassical or fully quantum regime. If the De Broglie wavelength of the particle $\lambda = h/p$ is of order or larger than the typical interaction range $R \sim 1/\Lambda_{\rm DC}$ the collision is fully quantum mechanical, otherwise a semiclassical picture can be adopted. The condition for a semiclassical behaviour can be recast as $l_{\rm max} \sim M_\chi v R \gg 1$, where $l_{\rm max}$ is the maximum angular momentum of the process given the short-range nature of the interaction. We find that the processes occurring in the very early Universe (at $T = T_R$) are always in the semiclassical regime in the region of parameter space where the DM experimental density can be reproduced. Recombination processes occurring at the CMB or at later times, instead, turn out to be quantum mechanical because of the much lower gluequark velocity.

In the quantum regime, the lowest partial wave is expected to dominate in the low momentum

[1] In the opposite regime of fast dissociation, and much before the glueball decay, the last term in the second and third lines of eq. (H.1) can be neglected. The solution to the Boltzmann equations is thus given by non-thermal equilibrium values for the three populations which are close to their initial conditions at dark confinement.

limit $k \to 0$. In the case of exothermic reactions [2], as the one considered here, general arguments of scattering theory suggest that the cross section scales as $1/k$ for $k \to 0$ if the process can take place in $s$-wave [281]. In the non-relativistic limit we thus expect a cross section $\sigma \propto 1/v$. Since the process is non-perturbative it is not possible to compute this cross section from first principles; furthermore, since two different scales ($M_{\mathcal{Q}}$ and $\Lambda_{\rm DC}$) appear in the problem, it is not clear what is the cross section scaling[3]. In light of this we adopt two different benchmark scenarios:

$$\langle \sigma_{\rm ann} v_{\rm rel} \rangle \sim \begin{cases} \dfrac{1}{\Lambda_{\rm DC}^2} \\ \\ \pi R_B^2 \approx \dfrac{\pi}{(\alpha_{\rm DC}^2 M_{\mathcal{Q}}^2)} \,. \end{cases} \tag{H.2}$$

In the first one the cross-section is controlled by the size of the gluequark while in the latter is the size of the $s$-wave ground state which fixes the cross section.

In the semiclassical regime we estimate the re-annihilation cross section using a simple dynamical model. We first discuss the process $\chi + \chi \to QQ^* + \Phi$ and then analyse the recombination into EW vector bosons. Our semiclassical model is defined in terms of the following simplified assumptions:

- The gluequarks are modelled as hard spheres with radius of order $R \sim 1/\Lambda_{\rm DC}$, colliding with impact parameter $b$ and thermal velocity $v$.

- The interaction is short range, therefore the maximum impact parameter for which an interaction occurs is $b_{\rm max} = 2R \sim 2/\Lambda_{\rm DC}$. We define a corresponding geometric total cross section

$$\sigma_{\rm total} = \pi b_{\rm max}^2 = \frac{4\pi}{\Lambda_{\rm DC}^2} \,. \tag{H.3}$$

  For thermal velocities, $b_{\rm max}$ can be converted into a maximum angular momentum $l_{\rm max} = b_{\rm max} M_\chi v \sim 2(M_\chi/\Lambda_{\rm DC})\sqrt{3T/M_\chi}$ for the colliding particles.

- Energy conservation implies that only some bound states can be formed. Among these we identify the states with maximum angular momentum $l_*$ allowed by energy conservation and by the short range constraint $l_* \leqslant l_{\rm max}$.

- Angular momentum conservation implies that only interactions with impact parameter smaller than $b_* \approx (l_* + 1)/(M_\chi v)$ can lead to bound state formation [4]. The short range interaction constraint then forces $b_* \leqslant b_{\rm max}$. If no bound state is allowed by energy conservation we take $b_* = 0$.

- The recombination cross section is estimated by the geometrical value $\sigma = \pi b_*^2$.

[2] Exothermic reactions are those where the particles in the final states are lighter than those in the initial state.

[3] The electroweak process $\chi + \chi \to QQ^* + V$ has a close nuclear analogue given by $p + n \to d + \gamma$. Explicit calculations reproduce the expected $1/v$ velocity dependence [282]. The non-perturbative constant in that case can be predicted using elastic nucleon scattering data.

[4] The factor $(l_* + 1)$ takes into account the quantization of $l_*$ and ensures that the cross section is not underestimated for small angular momenta.

The model predicts a re-annihilation cross section into glueballs that can be conveniently expressed in terms of a suppression factor $\varepsilon_\Phi$ as follows:

$$\sigma_{\mathrm{rea},\Phi} = \pi b_*^2 = \left(\frac{b_*}{b_{\max}}\right)^2 \sigma_{\mathrm{total}} \equiv \varepsilon_\Phi \, \sigma_{\mathrm{total}} \,, \tag{H.4}$$

where $\varepsilon_\Phi$ is computed to be

$$\varepsilon_\Phi = \begin{cases} 1 & \text{if} \quad l_* > l_{\max} - 1, \\ \dfrac{\Lambda_{\mathrm{DC}}^2}{4} \dfrac{(l_*+1)^2}{M_\chi^2 v^2} & \text{if} \quad l_* < l_{\max} - 1, \\ 0 & \text{if} \quad l_* \text{ does not exist.} \end{cases} \tag{H.5}$$

Notice that $\varepsilon_\Phi$ is a function of $M_\mathcal{Q}$, $\Lambda_{\mathrm{DC}}$ and indirectly of the temperature through the value of $l_*$ and $v$.

In order to determine $l_*$ we use the energy balance equation in the center-of-mass frame:

$$2M_\chi + 2K_\chi \geqslant M_{\mathcal{Q}\mathcal{Q}^*} + M_\Phi \,, \tag{H.6}$$

where $K_\chi$ is the kinetic energy of the colliding gluequarks. The gluequark mass can be written in terms of the quark mass plus a binding energy $B_\chi$:

$$M_\chi = M_\mathcal{Q} + B_\chi \,. \tag{H.7}$$

Similarly, the mass of the di-quark bound state is decomposed as

$$M_{\mathcal{Q}\mathcal{Q}^*} = 2M_\mathcal{Q} + B_{\mathcal{Q}\mathcal{Q}^*} \,. \tag{H.8}$$

We set the gluequark binding energy to the value computed in QCD lattice simulations of SU(3) gauge theories: $B_\chi = 3.5\,\Lambda_{\mathrm{DC}}$ [255] [5]. The binding energy of the $\mathcal{Q}\mathcal{Q}^*$ bound state, $B_{\mathcal{Q}\mathcal{Q}^*}$, is instead approximated by the energy levels of a confining model with a Coulomb potential plus a linear term [143]

$$V(r) = -\frac{\alpha_{\mathrm{eff}}}{r} + \sigma r, \tag{H.9}$$

with $\alpha_{\mathrm{eff}} = \alpha_{\mathrm{DC}}(M_\mathcal{Q})$ and $\sigma = 2.0\, N_{\mathrm{DC}} \Lambda_{\mathrm{DC}}^2$. Therefore, $B_{\mathcal{Q}\mathcal{Q}^*}$ is computed numerically as a function of the principal and orbital quantum numbers of the bound state. The energy balance of eq.(H.6) can be rewritten as

$$B_{\mathcal{Q}\mathcal{Q}^*} \leqslant 2B_\chi + 2K_\chi - M_\Phi \,, \tag{H.10}$$

[5] The bare quark mass and binding energy are renormalization scheme dependent. Here we quote the result of reference [255] valid in the RS scheme which, according to the authors, smoothly converges to the $\overline{MS}$ scheme in the perturbative regime. Since we are interested in just an order-of-magnitude determination of the relic density, we neglect the scheme dependence of $B_\chi$ in what follows. We notice however that our numerical estimate of the re-annihilation cross section is rather sensitive to the value of $B_\chi$, hence the scheme dependence can have a strong impact. We take such theoretical uncertainty effectively into account by considering different benchmark scenarios, as explained in section 5.2.3.

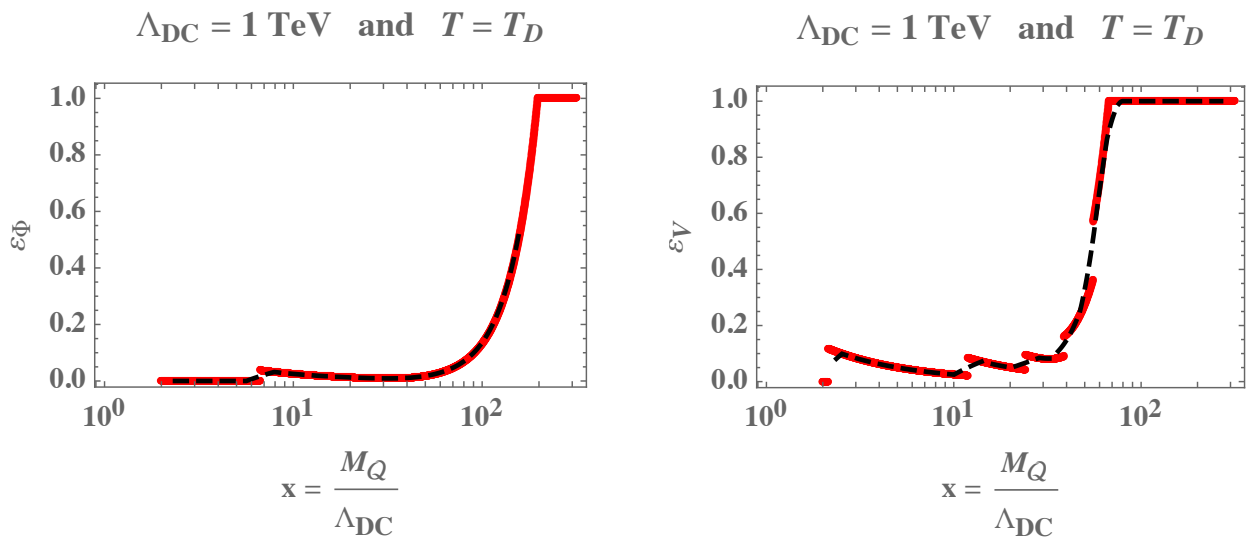


Figure H.1: *Suppression factors $\varepsilon_\Phi$ (left panel) and $\varepsilon_V$ (right panel) at $T = T_D$ as a function of the ratio $M_Q/\Lambda_{DC}$ for $\Lambda_{DC} = 1\,\text{TeV}$. In red the results of the numerical computation and in black the interpolation used to compute the relic density. Discontinuities in the numerical results are due to the integer nature of $l_*$.*

and implies a constraint on the maximal angular momentum $l_*$ (as well as on the principal number). In general one should also impose the additional condition $M_{QQ^*} < 2M_\chi$, to ensure that the decay of the $QQ^*$ state back into gluequarks is kinematically forbidden. In terms of binding energies, this condition reads

$$B_{QQ^*} < 2B_\chi\,. \tag{H.11}$$

The average gluequark kinetic energy in eq. (H.10) is of order of the temperature, which in turn is smaller than $\Lambda_{\rm DC}$. We set the glueball mass to its value computed on the lattice in SU(3) Yang-Mills theories, $M_\Phi \simeq 7\Lambda_{\rm DC}$, and thus find $2K_\chi - M_\Phi < 0$. As a consequence, the condition (H.10) is always stronger than (H.11).

Since eq. (H.10) depends on the gluequark kinetic energy, which we set to $K_\chi = T$ in our numerical computation, the value of $l_*$ will have a dependence on $T$. For illustration we show in Fig. H.1 the value of $\varepsilon_\Phi$ as a function of $M_Q/\Lambda_{\rm DC}$ obtained at $T = T_D$ for $\Lambda_{\rm DC} = 1\,\text{TeV}$. Changing $\Lambda_{\rm DC}$ while keeping the temperature fixed leads to very small variations of $\varepsilon_\Phi$. For $T = \Lambda_{\rm DC}$, on the other hand, $\varepsilon_\Phi$ turns out to be small and of order of a few$\times 10^{-2}$ in the region of interest ($100\,\text{GeV} < \Lambda_{\rm DC} < 10\,\text{TeV}$ and $1 < M_Q/\Lambda_{\rm DC} < 100$).

In the case of the recombination with the emission of a vector boson, $\chi + \chi \to QQ^* + V$, we expect the re-annihilation cross section to be suppressed by at least a factor $\alpha_2$. Clearly, this process becomes relevant only when the recombination with glueball emission is strongly suppressed or forbidden for kinematic reasons. The transitions $\chi + \chi \to QQ^* + V$ that are relevant for re-annihilation are those where the $QQ^*$ is sufficiently light so that it cannot decay back in two $\chi$'s. Such bound states satisfy the condition (H.11), which requires the kinetic energy of the emitted vector boson to be larger than the sum of the kinetic energies of the colliding gluequarks ($K_V > 2K_\chi$). The re-annihilation cross section

can be written as

$$\sigma_{\mathrm{rea},V} = \varepsilon_V \alpha_2 \frac{4\pi}{\Lambda_{\mathrm{DC}}^2}\,, \tag{H.12}$$

and the suppression factor $\varepsilon_V$ can be estimated using our semiclassical model by following a procedure similar to the one described for the case of glueball emission. We find that $\varepsilon_V$ has a behaviour similar to $\varepsilon_\Phi$ as a function of its variables, and a slightly larger absolute value, see Fig. H.1.

## H.2 Re-annihilation temperature

The temperature at which the re-annihilation cross section saturates and the relic abundance freezes out is determined by two competing processes: de-excitation and dissociation. The cross section saturates when the former dominates over the latter for all the bound states with $M_{\mathcal{Q}\mathcal{Q}^*} < 2M_\chi$. We will now try to argue that for $T > T_D$ there are states for which the dissociation rate is larger than the de-excitation one. Therefore, the most reasonable scenario is one in which the re-annihilation cross section saturates at $T_R \lesssim T_D$.

States with $M_{\mathcal{Q}\mathcal{Q}^*} > 2M_\chi - M_\Phi$ can be dissociated by glueballs with vanishing kinetic energy. Therefore, these states are the most easily dissociated since all the glueballs present in the Universe contribute to their breaking rate

$$\Gamma_{\mathrm{dis}} = n_\Phi \langle \sigma_{\mathrm{dis}} v \rangle\,, \tag{H.13}$$

where $\sigma_{\mathrm{dis}} \sim \Lambda_{\mathrm{DC}}^{-2}$ and $n_\Phi$ is the number density of glueballs which, at $T > T_D$, is dominated by the population coming form the confinement of dark gluons: $n_\Phi \sim T^3$. The de-excitation rate can be estimated using the well known result for spontaneous emission [6]

$$\Gamma_{\mathcal{Q}\mathcal{Q}^*} \sim \alpha_2\, \Delta E^3\, |\langle R_f | \vec{r} | R_i \rangle|^2\,, \tag{H.14}$$

where $\Delta E$ is the difference of energy levels. A reasonable estimate for this rate can be given for transitions between these states and the ground level. In this case $\Delta E \sim \Lambda_{\mathrm{DC}} + \alpha_{\mathrm{DC}}^2 M_{\mathcal{Q}}$, while the matrix element is a fraction of the Bohr radius, $r_b \sim 1/(\alpha_{\mathrm{DC}} M_{\mathcal{Q}})$. This estimate gives $\Gamma_{\mathcal{Q}\mathcal{Q}^*}$ smaller than $\Gamma_{\mathrm{dis}}$ and suggests that for $T > T_D$ re-annihilation cannot proceed through the formation of these states. At $T \sim T_D$ glueballs start to decay. Their number density decays exponentially and the dissociation process becomes soon inefficient. Therefore all the states can contribute to the re-annihilation process and the cross section saturates.

After the decay of the primordial glueballs, dissociation processes involving electroweak gauge bosons can play a role. However their cross section is suppressed by an electroweak factor and, moreover, their energy distribution is thermal. At $T \lesssim T_D$ one needs vector bosons in the tail of the Bose-Einstein distribution in order to have enough energy to dissociate the bound states. As a result, the rate of this process is exponentially suppressed by a factor $\exp[-(2B_\chi - B_{\mathcal{Q}\mathcal{Q}^*})/T]$ and, even if it is efficient at $T_D$, it becomes soon inefficient.

For these reasons, we consider the case in which the reannihilation occurs at $T_D$ as the most

[6] This rate corresponds to dipole transitions and is associated to the usual atomic selection rules. Higher multipole transitions can be considered, but we limit our discussion to the case of the dipole since we are interested only in an order-of-magnitude estimate.

plausible. This is in agreement with what suggested in Ref. [241]. Due to the large uncertainties on the estimates of the rates, however (especially for what concerns $\Gamma_{\mathcal{Q}\mathcal{Q}^*}$, where neither $\Delta E$ nor the matrix element can be computed from first principles), we do not exclude the possibility that the dissociation processes are never efficient and re-annihilation takes place directly at $\Lambda_{\rm DC}$.

# Chapter I

# A model with hypercharge

In this article we focused on the minimal block $V$ of Table 5.1 as a benchmark for our analysis. However, the $L \oplus \bar{L}$ model has many peculiarities and deserves a separate discussion. In particular, in this case the DM candidate has non-vanishing hypercharge and interacts at tree level with the $Z$ boson.

## Higher-dimensional operators

This model has a $U(1)_D$ accidental symmetry, comprising dark parity as a subgroup, under which the dark quarks $L$ and $\bar{L}$ have charge $\pm 1$. Differently from the other models, this symmetry is broken by higher-dimensional operators with classical dimension $[\mathcal{O}_{\rm dec}] = 5$ of the form

$$\mathcal{O}_{\rm dec} = \ell \mathcal{G}_{\mu\nu} \sigma^{\mu\nu} L \,.$$

In order to have a stable DM candidate and make the model viable, one can gauge the $U(1)_D$ in the ultraviolet and break it spontaneously to the dark parity subgroup by means of a scalar field. For instance, if a scalar $\phi$ with charge 2 acquires a vacuum expectation value the symmetry is broken according to the pattern:

$$U(1)_D \to \mathbb{Z}_2 .$$

At the scale of the spontaneous breaking only operators that are dark-parity even are generated, hence the gluequark is absolutely stable.

## $Z$-boson mediated direct detection

Below the confinement scale, the spectrum comprises a composite Dirac fermion with SM quantum numbers $2_{1/2}$, whose EM neutral component is identified with the DM. The non-zero hypercharge induces a tree-level interaction with the $Z$ boson which is strongly constrained by direct searches. The corresponding spin-independent elastic cross section on nuclei $\mathcal{N}$ is given by [159]:

$$\sigma = \frac{G_{\rm F}^2 M_{\mathcal{N}}^2}{8\pi} \Big( N - (1 - 4 \sin^2 \theta_W) Z \Big)^2 ,$$

where $Z$ and $N$ are the number of protons and neutrons in the nucleus $\mathcal{N}$ and $M_{\mathcal{N}}$ is its mass. This cross section is excluded by direct detection experiments for masses $M_\chi \lesssim 10^8\,\text{GeV}$ [26]. This bound rules out the model in the scenario $T_R = T_D$, corresponding to the left panel of Figure 5.4, but can be satisfied in the scenario $T_R = \Lambda_{\text{DC}}$.

In fact, the constraint from direct detection experiments can be also avoided by introducing a heavy singlet gluequark. In this case the presence of Yukawa couplings induces a splitting among the electromagnetically neutral Majorana fermions. The DM is the lightest among these fermions, so that tree-level elastic scattering mediated by the $Z$ boson cannot exist due to its Majorana nature. Inelastic scatterings are kinematically forbidden if the splitting is large enough; this is easily realized for $M_{\text{N}} \lesssim y^2 \times 10^5\,\text{TeV}$, where $y$ is the Yukawa coupling. This scenario is analogous to Higgsino DM in supersymmetry, see [178, 58] for an extensive discussion.

## Accidentally stable mesons

If the model is not in the conformal window, it is possible to consider the light quark regime. In this case, the model is characterized by the presence of NGBs made of $LL$ or $\bar{L}\bar{L}$ constituents which have $U(1)_D$ number $\pm 2$ and therefore cannot decay. If the accidental $U(1)_D$ is gauged in the UV and spontaneously broken to dark parity, then dimension-5 operators can be generated which let the NGBs decay while keeping the gluequarks stable.

# Bibliography


[1] J. Oort, *"The force exerted by the stellar system in the direction perpendicular to the galactic plane and some related problems"* Bull. Astron. Inst. Neth. 16 (1960) 45 4

[2] F. Zwicky, *"Die Rotverschiebung von extragalaktischen Nebeln"*, Helvetica Physica Acta, 6 (1933) 110 4

[3] van Dokkum, P., Danieli, S., Cohen, Y., et al. "*A galaxy lacking Dark Matter*" 2018, Nature, 555, 629 [arXiv:1803.10237]. 4

[4] van Dokkum, P., Danieli, S., Abraham, R., et al., "*A Second Galaxy Missing Dark Matter in the NGC 1052 Group*", AJL, **874** (2019), L5 [arXiv:1901.05973]. 4

[5] Trujillo, I., Beasley, M. A. Beasley, Borlaff, et al., "*A distance of 13 Mpc resolves the claimed anomalies of the galaxy lacking dark matter*", Monthly Notices of the Royal Astronomical Society , **486** (2019), 1192 [arXiv:1806.10141]. 4

[6] Planck Collaboration, "*Planck 2018 results. VI. Cosmological parameters*", [arXiv:1807.06209]. 4, 8

[7] S. Tremaine, J.E. Gunn, *"Dynamical Role of Light Neutral Leptons in Cosmology"*, Phys. Rev. Lett. 42 (1979) 407 [InSpires:Tremaine:1979we]. 5

[8] J. Madsen, "*Generalized Tremaine-Gunn limits for bosons and fermions*", Phys. Rev. D **44** (1991) 999. [InSpires:Madsen:1991mz]. 5

[9] T.D. Brandt, *"Constraints on MACHO Dark Matter from Compact Stellar Systems in Ultra-Faint Dwarf Galaxies"*, Astrophys. J. 824 (2016) L31 [arXiv:1605.03665]. 5

[10] S.M. Koushiappas, A. Loeb, *"Dynamics of Dwarf Galaxies Disfavor Stellar-Mass Black Holes as Dark Matter"*, Phys. Rev. Lett. 119 (2017) 041102 [arXiv:1704.01668]. 5

[11] J. A. Dror, H. Ramani, T. Trickle and K. M. Zurek, "*Pulsar Timing Probes of Primordial Black Holes and Subhalos*", [arXiv:1901.04490] 5

[12] T.R. Slatyer, C-L. Wu, *"General Constraints on Dark Matter Decay from the Cosmic Microwave Background"*, Phys. Rev. D95 (2017) 023010 [arXiv:1610.06933]. 5, 6, 161

[13] A. Mitridate, A. Podo, *"Bounds on Dark Matter decay from 21 cm line"*, JCAP 1805 (2018) 069 [arXiv:1803.11169]. 5, 6, 65, 162

[14] T. Cohen, K. Murase, N.L. Rodd, B.R. Safdi, Y. Soreq, *"$\gamma$ -ray Constraints on Decaying Dark Matter and Implications for IceCube"*, Phys. Rev. Lett. 119 (2017) 021102 [arXiv:1612.05638]. 6, 7

[15] IceCube Collaboration, *"Search for neutrinos from decaying dark matter with IceCube"*, Eur. Phys. J. C78 (2018) 831 [arXiv:1804.03848]. 6, 161

[16] J.D. Bowman, A.E.E. Rogers, R.A. Monsalve, T.J. Mozdzen, N. Mahesh, *"An absorption profile centred at 78 megahertz in the sky-averaged spectrum"*, Nature 555 (2018) 67 [InSpires:Bowman:2018yin]. 6, 65

[17] H. Liu, T.R. Slatyer, *"Implications of a 21-cm signal for dark matter annihilation and decay"*, Phys. Rev. D98 (2018) 023501 [arXiv:1803.09739]. 6, 65, 161, 162

[18] S. Clark, B. Dutta, Y. Gao, Y-Z. Ma, L.E. Strigari, *"21 cm limits on decaying dark matter and primordial black holes"*, Phys. Rev. D98 (2018) 043006 [arXiv:1803.09390]. 6, 65, 162

[19] Fermi-LAT Collaboration, *"Searching for Dark Matter Annihilation from Milky Way Dwarf Spheroidal Galaxies with Six Years of Fermi Large Area Telescope Data"*, Phys. Rev. Lett. 115 (2015) 231301 [arXiv:1503.02641]. 7

[20] A. Albert *et al.*, *"Results from the search for dark matter in the Milky Way with 9 years of data of the ANTARES neutrino telescope"*, Phys. Lett. B769 (2017) 249 [arXiv:1612.04595]. 7, 160

[21] G. D'Amico, P. Panci, A. Strumia, *"Bounds on Dark Matter annihilations from 21 cm data"*, Phys. Rev. Lett. 121 (2018) 011103 [arXiv:1803.03629]. 7, 8, 161

[22] T.R. Slatyer, *"Indirect dark matter signatures in the cosmic dark ages. I. Generalizing the bound on s-wave dark matter annihilation from Planck results"*, Phys. Rev. D93 (2016) 023527 [arXiv:1506.03811]. 7, 117

[23] M. Cirelli, T. Hambye, P. Panci, F. Sala, M. Taoso, *"Gamma ray tests of Minimal Dark Matter"*, JCAP 1510 (2015) 026 [arXiv:1507.05519]. 7, 42, 44

[24] G. Giesen, M. Boudaud, Y. Génolini, V. Poulin, M. Cirelli, P. Salati, P.D. Serpico, *"AMS-02 antiprotons, at last! Secondary astrophysical component and immediate implications for Dark Matter"*, JCAP 1509 (2015) 023 [arXiv:1504.04276]. 7

[25] HESS Collaboration, *"Search for dark matter annihilations towards the inner Galactic halo from 10 years of observations with H.E.S.S"*, Phys. Rev. Lett. 117 (2016) 111301 [arXiv:1607.08142]. 7, 118, 160

[26] Xenon1T Collaboration, *"Dark Matter Search Results from a One Ton-Year Exposure of XENON1T"*, Phys. Rev. Lett. 121 (2018) 111302 [arXiv:1805.12562]. 8, 9, 158, 189

[27] M. Battaglieri *et al.*, "*US Cosmic Visions: New Ideas in Dark Matter 2017: Community Report*", [arXiv:1707.04591]. 10

[28] R. Essig, T. Volansky, T-T. Yu, *"New Constraints and Prospects for sub-GeV Dark Matter Scattering off Electrons in Xenon"*, Phys. Rev. D96 (2017) 043017 [arXiv:1703.00910]. 10

[29] J. Tiffenberg *et al.* [SENSEI Collaboration], "*Single-electron and single-photon sensitivity with a silicon Skipper CCD*", Phys. Rev. Lett. **119** (2017) no.13, 131802 [arXiv:1706.00028]. 10

[30] DAMIC Collaboration, *"Direct Search for Low Mass Dark Matter Particles with CCDs"*, Phys. Lett. B711 (2012) 264 [arXiv:1105.5191]. 10

[31] SuperCDMS Collaboration, *"Search for Low-Mass Weakly Interacting Massive Particles with SuperCDMS"*, Phys. Rev. Lett. 112 (2014) 241302 [arXiv:1402.7137]. 10

[32] Y. Hochberg, Y. Zhao, K.M. Zurek, *"Superconducting Detectors for Superlight Dark Matter"*, Phys. Rev. Lett. 116 (2016) 011301 [arXiv:1504.07237]. 10

[33] K. Schutz, K.M. Zurek, *"Detectability of Light Dark Matter with Superfluid Helium"*, Phys. Rev. Lett. 117 (2016) 121302 [arXiv:1604.08206]. 10

[34] S. Knapen, T. Lin, M. Pyle, K.M. Zurek, *"Detection of Light Dark Matter With Optical Phonons in Polar Materials"*, Phys. Lett. B785 (2018) 386 [arXiv:1712.06598]. 10

[35] Y. Hochberg, T. Lin, K.M. Zurek, *"Detecting Ultralight Bosonic Dark Matter via Absorption in Superconductors"*, Phys. Rev. D94 (2016) 015019 [arXiv:1604.06800]. 11

[36] Y. Hochberg, T. Lin, K.M. Zurek, *"Absorption of light dark matter in semiconductors"*, Phys. Rev. D95 (2017) 023013 [arXiv:1608.01994]. 11

[37] I.M. Bloch, R. Essig, K. Tobioka, T. Volansky, T-T. Yu, *"Searching for Dark Absorption with Direct Detection Experiments"*, JHEP 1706 (2017) 087 [arXiv:1608.02123]. 11

[38] M. Battaglieri *et al.*, *"US Cosmic Visions: New Ideas in Dark Matter 2017: Community Report"* [arXiv:1707.04591]. 11

[39] P. Sikivie, *"Experimental Tests of the Invisible Axion"*, Phys. Rev. Lett. 51 (1983) 1415 [InSpires:Sikivie:1983ip]. 12

[40] P. Sikivie, N. Sullivan, D.B. Tanner, *"Proposal for Axion Dark Matter Detection Using an LC Circuit"*, Phys. Rev. Lett. 112 (2014) 131301 [arXiv:1310.8545].

[41] D. Budker, P.W. Graham, M. Ledbetter, S. Rajendran, A. Sushkov, *"Proposal for a Cosmic Axion Spin Precession Experiment (CASPEr)"*, Phys. Rev. X4 (2014) 021030 [arXiv:1306.6089]. 12

[42] P.W. Graham, D.E. Kaplan, J. Mardon, S. Rajendran, W.A. Terrano, *"Dark Matter Direct Detection with Accelerometers"*, Phys. Rev. D93 (2016) 075029 [arXiv:1512.06165]. 12

[43] P.W. Graham, S. Rajendran, *"New Observables for Direct Detection of Axion Dark Matter"*, Phys. Rev. D88 (2013) 035023 [arXiv:1306.6088]. 12

[44] A. Arvanitaki, P.W. Graham, J.M. Hogan, S. Rajendran, K. Van Tilburg, *"Search for light scalar dark matter with atomic gravitational wave detectors"*, Phys. Rev. D97 (2018) 075020 [arXiv:1606.04541]. 12

[45] W. Tucker, P. Blanco, S. Rappoport, L. David, D. Fabricant, E.E. Falco, W. Forman, A. Dressler, M. Ramella, *"1e0657-56: a contender for the hottest known cluster of galaxies"*, Astrophys. J. 496 (1998) L5 [InSpires:Tucker:1998tp]. 11

[46] M. Markevitch, A.H. Gonzalez, L. David, A. Vikhlinin, S. Murray, W. Forman, C. Jones, W. Tucker, *"A Textbook example of a bow shock in the merging galaxy cluster 1E0657-56"*, Astrophys. J. 567 (2001) L27 [InSpires:Markevitch:2001ri]. 11

[47] A.H.G. Peter, M. Rocha, J.S. Bullock, M. Kaplinghat, *"Cosmological Simulations with Self-Interacting Dark Matter II: Halo Shapes vs. Observations"*, Mon. Not. Roy. Astron. Soc. 430 (2012) 105 [arXiv:1208.3026]. 11

[48] D. Harvey, R. Massey, T. Kitching, A. Taylor, E. Tittley, *"The non-gravitational interactions of dark matter in colliding galaxy clusters"*, Science 347 (2015) 1462 [arXiv:1503.07675]. 11

[49] S.W. Randall, M. Markevitch, D. Clowe, A.H. Gonzalez, M. Bradac, *"Constraints on the Self-Interaction Cross-Section of Dark Matter from Numerical Simulations of the Merging Galaxy Cluster 1E 0657-56"*, Astrophys. J. 679 (2007) 1173 [arXiv:0704.0261]. 12

[50] S. Tulin, H-B. Yu, *"Dark Matter Self-interactions and Small Scale Structure"*, Phys. Rept. 730 (2018) 1 [arXiv:1705.02358]. 12

[51] R. A. Flores and J. R. Primack, "*Observational and theoretical constraints on singular dark matter halos*", Astrophys. J. **427** (1994) L1 [arXiv:astro-ph/9402004]. 12

[52] J.F. Navarro, C.S. Frenk, S.D.M. White, *"A Universal density profile from hierarchical clustering"*, Astrophys. J. 490 (1996) 493 [InSpires:Navarro:1996gj]. 12

[53] K. A. Oman *et al.*, *"The unexpected diversity of dwarf galaxy rotation curves"*, Mon. Not. Roy. Astron. Soc. 452 (2015) 3650 [arXiv:1504.01437]. 12

[54] M. Rocha, A.H.G. Peter, J.S. Bullock, M. Kaplinghat, S. Garrison-Kimmel, J. Onorbe, L.A. Moustakas, *"Cosmological Simulations with Self-Interacting Dark Matter I: Constant Density Cores and Substructure"*, Mon. Not. Roy. Astron. Soc. 430 (2012) 81 [arXiv:1208.3025]. 12

[55] A. Mitridate, M. Redi, J. Smirnov, A. Strumia, *"Cosmological Implications of Dark Matter Bound States"*, JCAP 1705 (2017) 006 [arXiv:1702.01141]. 13, 99, 146

[56] C. Gross, A. Mitridate, M. Redi, J. Smirnov, A. Strumia, *"Cosmological Abundance of Colored Relics"*, Phys. Rev. D99 (2019) 016024 [arXiv:1811.08418]. 13

[57] V. De Luca, A. Mitridate, M. Redi, J. Smirnov, A. Strumia, *"Colored Dark Matter"*, Phys. Rev. D97 (2018) 115024 [arXiv:1801.01135]. 13, 145

[58] A. Mitridate, M. Redi, J. Smirnov, A. Strumia, *"Dark Matter as a weakly coupled Dark Baryon"*, JHEP 1710 (2017) 210 [arXiv:1707.05380]. 13, 143, 155, 158, 189

[59] R. Contino, A. Mitridate, A. Podo and M. Redi, "*Gluequark Dark Matter*", JHEP **1902** (2019) 187 [arXiv:1811.06975] 13

[60] K.M. Belotsky, M.Y. Khlopov, S.V. Legonkov, K.I. Shibaev, *"Effects of new long-range interaction: Recombination of relic heavy neutrinos and antineutrinos"*, Grav. Cosmol. 11 (2005) 27 [InSpires:Belotsky:2005dk]. 15

[61] J. Hisano, S. Matsumoto, M. Nagai, O. Saito, M. Senami, *"Non-perturbative effect on thermal relic abundance of dark matter"*, Phys. Lett. B646 (2006) 34 [InSpires:Hisano:2006nn]. 15, 37, 38, 39

[62] M. Cirelli, A. Strumia, M. Tamburini, *"Cosmology and Astrophysics of Minimal Dark Matter"*, Nucl. Phys. B787 (2007) 152 [arXiv:0706.4071]. 15, 42, 119, 127

[63] M.B. Wise, Y. Zhang, *"Stable Bound States of Asymmetric Dark Matter"*, Phys. Rev. D90 (2014) 055030 [arXiv:1407.4121]. 15

[64] B. von Harling, K. Petraki, *"Bound-state formation for thermal relic dark matter and unitarity"*, JCAP 1412 (2014) 033 [arXiv:1407.7874]. 15, 23

[65] K. Petraki, M. Postma, M. Wiechers, *"Dark-matter bound states from Feynman diagrams"*, JHEP 1506 (2015) 128 [arXiv:1505.00109]. 15, 23

[66] J. Ellis, F. Luo, K.A. Olive, *"Gluino Coannihilation Revisited"*, JHEP 1509 (2015) 127 [arXiv:1503.07142]. 15

[67] P. Asadi, M. Baumgart, P.J. Fitzpatrick, E. Krupczak, T.R. Slatyer, *"Capture and Decay of Electroweak WIMPonium"*, JCAP 1702 (2017) 005 [arXiv:1610.07617]. 15, 23, 25, 34, 40, 168, 169

[68] M. Cirelli, A. Strumia, *"Minimal Dark Matter: Model and results"*, New J. Phys. 11 (2009) 105005 [arXiv:0903.3381]. 17, 44

[69] M. Cirelli, A. Strumia, M. Tamburini, *"Cosmology and Astrophysics of Minimal Dark Matter"*, Nucl. Phys. B787 (2007) 152 [arXiv:0706.4071]. 20, 36, 37, 38, 39, 41, 42, 44

[70] E. Del Nobile, M. Nardecchia, P. Panci, *"Millicharge or Decay: A Critical Take on Minimal Dark Matter"*, JCAP 1604 (2016) 048 [arXiv:1512.05353]. 20

[71] A. De Simone, G.F. Giudice, A. Strumia, *"Benchmarks for Dark Matter Searches at the LHC"*, JHEP 1406 (2014) 081 [arXiv:1402.6287]. 20, 47, 50, 146

[72] R. Iengo, *"Sommerfeld enhancement: General results from field theory diagrams"*, JHEP 0905 (2009) 024 [arXiv:0902.0688]. 22

[73] S. Cassel, *"Sommerfeld factor for arbitrary partial wave processes"*, J. Phys. G37 (2009) 105009 [arXiv:0903.5307]. 22, 169

[74] F. J. Rogers, H. C. Graboske, and D. J. Harwood, *"Bound eigenstates of the static screened coulomb potential"*, Phys. Rev. A 1 (1970) 1577. 23

[75] M. Beneke, *"Perturbative heavy quark - anti-quark systems"*, PoS hf8 (1999) 009 [arXiv:hep-ph/9911490]. 25

[76] A.V. Manohar, I.W. Stewart, *"Running of the heavy quark production current and 1 / v potential in QCD"*, Phys. Rev. D63 (2000) 054004 [InSpires:Manohar:2000kr]. 25

[77] J. Harz, K. Petraki, *"Radiative bound-state formation in unbroken perturbative non-Abelian theories and implications for dark matter"*, JHEP 1807 (2018) 096 [arXiv:1805.01200]. 25

[78] H. An, M.B. Wise, Y. Zhang, *"Effects of Bound States on Dark Matter Annihilation"*, Phys. Rev. D93 (2016) 115020 [arXiv:1604.01776]. 25

[79] G. Lindblad, "*On the generators of quantum dynamical semigroups*", Commun. Math. Phys. 48, 119 (1976). 35

[80] N. Gisin and I. C. Percival, *"The quantum-state diffusion model applied to open systems"*, J. Phys. A 25, 5677 (1992). 49

[81] L. Stodolsky, *"The Unnecessary wave packet"*, Phys. Rev. D58 (1998) 036006 [arXiv:hep-ph/9802387]. 36

[82] P.M. Chesler, A. Gynther, A. Vuorinen, *"On the dispersion of fundamental particles in QCD and N=4 Super Yang-Mills theory"*, JHEP 0909 (2009) 003 [arXiv:0906.3052]. 36

[83] S. Kim, M. Laine, *"On thermal corrections to near-threshold annihilation"*, JCAP 1701 (2017) 013 [arXiv:1609.00474]. 36, 37, 52

[84] Y. Yamada, *"Electroweak two-loop contribution to the mass splitting within a new heavy SU(2)(L) fermion multiplet"*, Phys. Lett. B682 (2009) 435 [arXiv:0906.5207]. 37

[85] M. Ibe, S. Matsumoto, R. Sato, *"Mass Splitting between Charged and Neutral Winos at Two-Loop Level"*, Phys. Lett. B721 (2013) 252 [arXiv:1212.5989]. 37

[86] A. Strumia, *"Sommerfeld corrections to type-II and III leptogenesis"*, Nucl. Phys. B809 (2008) 308 [arXiv:0806.1630]. 39

[87] D. Buttazzo, G. Degrassi, P.P. Giardino, G.F. Giudice, F. Sala, A. Salvio, A. Strumia, *"Investigating the near-criticality of the Higgs boson"*, JHEP 1312 (2013) 089 [arXiv:1307.3536]. 39, 43

[88] Fermi-LAT Collaboration, *"Updated search for spectral lines from Galactic dark matter interactions with pass 8 data from the Fermi Large Area Telescope"*, Phys. Rev. D91 (2015) 122002 [arXiv:1506.00013]. 45

[89] C. Garcia-Cely, A. Ibarra, A.S. Lamperstorfer, M.H.G. Tytgat, *"Gamma-rays from Heavy Minimal Dark Matter"*, JCAP 1510 (2015) 058 [arXiv:1507.05536]. 44

[90] V. Lefranc, E. Moulin, P. Panci, F. Sala, J. Silk, *"Dark Matter in $\gamma$ lines: Galactic Center vs dwarf galaxies"*, JCAP 1609 (2016) 043 [arXiv:1608.00786]. 44

[91] E.J. Chun, J-C. Park, S. Scopel, *"Non-perturbative Effect and PAMELA Limit on Electro-Weak Dark Matter"*, JCAP 1212 (2012) 022 [arXiv:1210.6104]. 44

[92] M. Duerr, P. Fileviez Perez, J. Smirnov, *"Gamma Lines from Majorana Dark Matter"*, Phys. Rev. D93 (2016) 023509 [arXiv:1508.01425]. 45

[93] M. Duerr, P. Fileviez Pérez, J. Smirnov, *"Scalar Dark Matter: Direct vs. Indirect Detection"*, JHEP 1606 (2016) 152 [arXiv:1509.04282]. 45

[94] Y. Akamatsu, A. Rothkopf, *"Stochastic potential and quantum decoherence of heavy quarkonium in the quark-gluon plasma"*, Phys. Rev. D85 (2011) 105011 [arXiv:1110.1203]. 49

[95] Y. Kats, M.D. Schwartz, *"Annihilation decays of bound states at the LHC"*, JHEP 1004 (2009) 016 [arXiv:0912.0526]. 49

[96] J. Ellis, F. Luo, K.A. Olive, *"Gluino Coannihilation Revisited"*, JHEP 1509 (2015) 127 [arXiv:1503.07142]. 51, 52

[97] S.P. Liew, F. Luo, *"Effects of QCD bound states on dark matter relic abundance"*, JHEP 1702 (2017) 091 [arXiv:1611.08133]. 51

[98] N. Arkani-Hamed, S. Dimopoulos, *"Supersymmetric unification without low energy supersymmetry and signatures for fine-tuning at the LHC"*, JHEP 0506 (2004) 073 [arXiv:hep-th/0405159]. 53, 145

[99] N. Arkani-Hamed, S. Dimopoulos, G.F. Giudice, A. Romanino, *"Aspects of split supersymmetry"*, Nucl. Phys. B709 (2004) 3 [arXiv:hep-ph/0409232]. 53

[100] A. Arvanitaki, C. Davis, P.W. Graham, A. Pierce, J.G. Wacker, *"Limits on split supersymmetry from gluino cosmology"*, Phys. Rev. D72 (2005) 075011 [arXiv:hep-ph/0504210]. 53, 63

[101] J. Kang, M.A. Luty, S. Nasri, *"The Relic abundance of long-lived heavy colored particles"*, JHEP 0809 (2006) 086 [arXiv:hep-ph/0611322]. 53, 66, 78, 80, 112, 145

[102] M. Toharia, J.D. Wells, *"Gluino decays with heavier scalar superpartners"*, JHEP 0602 (2005) 015 [InSpires:Toharia:2005gm]. 54

[103] P. Gambino, G.F. Giudice, P. Slavich, *"Gluino decays in split supersymmetry"*, Nucl. Phys. B726 (2005) 35 [arXiv:hep-ph/0506214]. 54

[104] K. Griest, M. Kamionkowski, *"Unitarity Limits on the Mass and Radius of Dark Matter Particles"*, Phys. Rev. Lett. 64 (1989) 615 [InSpires:Griest:1989wd]. 55, 68

[105] M. Geller, S. Iwamoto, G. Lee, Y. Shadmi, O. Telem, *"Dark quarkonium formation in the early universe"*, JHEP 1806 (2018) 135 [arXiv:1802.07720]. 55, 145

[106] W. Fischler, *"$q$-$\bar{q}$ Potential in QCD"*, Nucl. Phys. B129 (1977) 157 [InSpires:Fischler:1977yf]. Y. Schroder, *"The Static potential in QCD to two loops"*, Phys. Lett. B447 (1998) 321 [arXiv:hep-ph/9812205]. 57

[107] P. Bicudo, *"The QCD string tension curve, the ferromagnetic magnetization, and the quark-antiquark confining potential at finite Temperature"*, Phys. Rev. D82 (2010) 034507 [arXiv:1003.0936]. P. Petreczky, *"Lattice QCD at non-zero temperature"*, J. Phys. G39 (2012) 093002 [arXiv:1203.5320]. S. Aoki et al., *"Review of lattice results concerning low-energy particle physics"*, Eur. Phys. J. C77 (2017) 112 [arXiv:1607.00299]. 57, 58, 76

[108] R.L. Hall, *"Simple eigenvalue formula for the Coulomb plus linear potential"*, Phys. Rev. D30 (1984) 433 [InSpires:Hall:1984wk]. 58, 77, 78

[109] G. Bhanot, M.E. Peskin, *"Short Distance Analysis for Heavy Quark Systems. 2. Applications"*, Nucl. Phys. B156 (1979) 391 [InSpires:Bhanot:1979vb]. 62

[110] M. Kawasaki, K. Kohri, T. Moroi, *"Big-Bang nucleosynthesis and hadronic decay of long-lived massive particles"*, Phys. Rev. D71 (2004) 083502 [InSpires:Kawasaki:2004qu]. 64

[111] M. Kawasaki, K. Kohri, T. Moroi, Y. Takaesu, *"Revisiting Big-Bang Nucleosynthesis Constraints on Long-Lived Decaying Particles"*, Phys. Rev. D97 (2018) 023502 [arXiv:1709.01211]. 64

[112] M. Pospelov, *"Particle physics catalysis of thermal Big Bang Nucleosynthesis"*, Phys. Rev. Lett. 98 (2006) 231301 [InSpires:Pospelov:2006sc]. 64, 71

[113] M. Kusakabe, T. Kajino, T. Yoshida, G.J. Mathews, *"Effect of Long-lived Strongly Interacting Relic Particles on Big Bang Nucleosynthesis"*, Phys. Rev. D80 (2009) 103501 [arXiv:0906.3516]. 64

[114] M. Kawasaki, T. Moroi, *"Electromagnetic cascade in the early universe and its application to the big bang nucleosynthesis"*, Astrophys. J. 452 (1994) 506 [InSpires:Kawasaki:1994sc]. 64

[115] E. L. Wright *et al.*, *"Interpretation of the COBE FIRAS spectrum"*, Astrophys. J. 420 (1993) 450 [InSpires:Wright:1993re]. 65

[116] W. Hu, J. Silk, *"Thermalization constraints and spectral distortions for massive unstable relic particles"*, Phys. Rev. Lett. 70 (1993) 2661 [InSpires:Hu:1993gc]. 65

[117] J. C. Mather *et al.*, *"Measurement of the Cosmic Microwave Background spectrum by the COBE FIRAS instrument"*, Astrophys. J. 420 (1993) 439 [InSpires:Mather:1993ij]. 65

[118] D.J. Fixsen, E.S. Cheng, J.M. Gales, J.C. Mather, R.A. Shafer, E.L. Wright, *"The Cosmic Microwave Background spectrum from the full COBE FIRAS data set"*, Astrophys. J. 473 (1996) 576 [InSpires:Fixsen:1996nj]. 65

[119] M. Cirelli, G. Corcella, A. Hektor, G. Hutsi, M. Kadastik, P. Panci, M. Raidal, F. Sala, A. Strumia, *"PPPC 4 DM ID: A Poor Particle Physicist Cookbook for Dark Matter Indirect Detection"*, JCAP 1103 (2010) 051 [arXiv:1012.4515]. 65, 66

[120] A. Kogut *et al.*, *"The Primordial Inflation Explorer (PIXIE): A Nulling Polarimeter for Cosmic Microwave Background Observations"*, JCAP 1107 (2011) 025 [arXiv:1105.2044]. 65

[121] T.R. Slatyer, C-L. Wu, *"General Constraints on Dark Matter Decay from the Cosmic Microwave Background"*, Phys. Rev. D95 (2017) 023010 [arXiv:1610.06933]. 65

[122] V. Poulin, J. Lesgourgues, P.D. Serpico, *"Cosmological constraints on exotic injection of electromagnetic energy"*, JCAP 1703 (2017) 043 [arXiv:1610.10051]. 65

[123] T. Cohen, K. Murase, N.L. Rodd, B.R. Safdi, Y. Soreq, *"$\gamma$ -ray Constraints on Decaying Dark Matter and Implications for IceCube"*, Phys. Rev. Lett. 119 (2017) 021102 [arXiv:1612.05638]. 66

[124] M. Foster, C. Michael, *"Hadrons with a heavy color adjoint particle"*, Phys. Rev. D59 (1998) 094509 [InSpires:Foster:1998wu]. 66, 141

[125] G.R. Farrar, R. Mackeprang, D. Milstead, J.P. Roberts, *"Limit on the mass of a long-lived or stable gluino"*, JHEP 1102 (2010) 018 [arXiv:1011.2964]. 66

[126] S. Polikanov, C.S. Sastri, G. Herrmann, K. Lutzenkirchen, M. Overbeck, N. Trautmann, A. Breskin, R. Chechik, Z. Frankel, *"Search for supermassive nuclei in nature"*, Z. Phys. A338 (1991) 357 [InSpires:Polikanov:1990sf]. 66, 92

[127] E. Bagnaschi, G.F. Giudice, P. Slavich, A. Strumia, *"Higgs Mass and Unnatural Supersymmetry"*, JHEP 1409 (2014) 092 [arXiv:1407.4081]. 66

[128] ATLAS Collaboration, *"Reinterpretation of searches for supersymmetry in models with variable R-parity-violating coupling strength and long-lived R-hadrons"* [InSpires:ATLAS:2018yey]. 67

[129] ATLAS Collaboration, *"Search for new phenomena in dijet events using 37 $fb^{-1}$ of pp collision data collected at $\sqrt{s}$ =13 TeV with the ATLAS detector"*, Phys. Rev. D96 (2017) 052004 [arXiv:1703.09127] 67

[130] M. Papucci, K. Sakurai, A. Weiler, L. Zeune, *"Fastlim: a fast LHC limit calculator"*, Eur. Phys. J. C74 (2014) 3163 [arXiv:1402.0492]. 67

[131] S. El Hedri, A. Kaminska, M. de Vries, J. Zurita, *"Simplified Phenomenology for Colored Dark Sectors"*, JHEP 1704 (2017) 118 [arXiv:1703.00452].

[132] A. Delgado, G.F. Giudice, G. Isidori, M. Pierini, A. Strumia, *"The light stop window"*, Eur. Phys. J. C73 (2013) 2370 [arXiv:1212.6847]. 69

[133] Y. Jia, *"Variational study of weakly coupled triply heavy baryons"*, JHEP 0610 (2006) 073 [arXiv:hep-ph/0607290]. 109

[134] S. Meinel, *"Prediction of the Omega$_{bbb}$ mass from lattice QCD"*, Phys. Rev. D82 (2010) 114514 [arXiv:1008.3154]. 109

[135] M. Pospelov, J. Pradler, *"Big Bang Nucleosynthesis as a Probe of New Physics"*, Ann. Rev. Nucl. Part. Sci. 60 (2010) 539 [arXiv:1011.1054]. 71

[136] M.L. Perl, E.R. Lee, D. Loomba, *"Searches for fractionally charged particles"*, Ann. Rev. Nucl. Part. Sci. 59 (2009) 47 [InSpires:Perl:2009zz]. 75

[137] E. Witten, *"Cosmic Separation of Phases"*, Phys. Rev. D30 (1984) 272 [InSpires:Witten:1984rs]. 75

[138] G.R. Farrar, *"Stable Sexaquark"* [arXiv:1708.08951]. 75

[139] M. Cirelli, N. Fornengo, A. Strumia, *"Minimal dark matter"*, Nucl. Phys. B753 (2005) 178 [arXiv:hep-ph/0512090]. 75, 108, 119

[140] P.J. Fox, A.E. Nelson, N. Weiner, *"Dirac gaugino masses and supersoft supersymmetry breaking"*, JHEP 0208 (2002) 035 [arXiv:hep-ph/0206096]. 76

[141] J.E. Kim, *"Weak Interaction Singlet and Strong CP Invariance"*, Phys. Rev. Lett. 43 (1979) 103 [InSpires:Kim:1979if]. M.A. Shifman, A.I. Vainshtein, V.I. Zakharov, *"Can Confinement Ensure Natural CP Invariance of Strong Interactions?"*, Nucl. Phys. B166 (1980) 493 [InSpires:Shifman:1979if]. 76

[142] M. Farina, D. Pappadopulo, A. Strumia, *"A modified naturalness principle and its experimental tests"*, JHEP 1308 (2013) 022 [arXiv:1303.7244]. 76

[143] E. Eichten, K. Gottfried, T. Kinoshita, J.B. Kogut, K.D. Lane, T-M. Yan, *"The Spectrum of Charmonium"*, Phys. Rev. Lett. 34 (1974) 369 [InSpires:Eichten:1974af]. 76, 184

[144] H.S. Bali, *"Casimir scaling of* SU(3) *static potentials"*, JHEP D62 (2000) 114503 [arXiv:hep-lat/0006022]. 76

[145] G.S. Bali, *"Casimir scaling or flux counting?"*, Nucl. Phys. Proc. Suppl. 83 (1999) 422 [arXiv:hep-lat/9908021]. 76

[146] M. Kusakabe, T. Takesako, *"Resonant annihilation of long-lived massive colored particles through hadronic collisions"*, Phys. Rev. D85 (2011) 015005 [arXiv:1112.0860]. 79, 112

[147] C.B. Dover, T.K. Gaisser, G. Steigman, *"Cosmological constraints on new stable hadrons"*, Phys. Rev. Lett. 42 (1979) 1117 [InSpires:Dover:1979sn]. 89

[148] D.A. Dicus, V.L. Teplitz, *"Primordial synthesis of anomalous nuclei"*, Phys. Rev. Lett. 44 (1980) 218 [InSpires:Dicus:1979xm]. 89

[149] R.N. Mohapatra, V.L. Teplitz, *"Primordial nucleosynthesis constraint on massive, stable, strongly interacting particles"*, Phys. Rev. Lett. 81 (1998) 3079 [InSpires:Mohapatra:1998nd]. 89

[150] M. Kusakabe, T. Kajino, T. Yoshida, G.J. Mathews, *"Effect of Long-lived Strongly Interacting Relic Particles on Big Bang Nucleosynthesis"*, Phys. Rev. D80 (2009) 103501 [arXiv:0906.3516]. 89, 90

[151] E. Epelbaum, H-W. Hammer, U-G. Meissner, *"Modern Theory of Nuclear Forces"*, Rev. Mod. Phys. 81 (2008) 1773 [arXiv:0811.1338]. 89

[152] E. Epelbaum, *"Nuclear Forces from Chiral Effective Field Theory: A Primer"* [arXiv:1001.3229]. 89

[153] R. Machleidt, *"The High precision, charge dependent Bonn nucleon-nucleon potential (CD-Bonn)"*, Phys. Rev. C63 (2000) 024001 [InSpires:Machleidt:2000ge]. 89

[154] T. Miyamoto *et al.*, *"$\Lambda_c N$ interaction from lattice QCD and its application to $\Lambda_c$ hypernuclei"*, Nucl. Phys. A971 (2018-03) 113 [arXiv:1710.05545]. 89

[155] G.R. Farrar, G. Zaharijas, *"Non-binding of flavor-singlet hadrons to nuclei"*, Phys. Lett. B559 (2003) 223 [arXiv:hep-ph/0302190]. 89

[156] T. K. Hemmick *et al.*, *"A Search for Anomalously Heavy Isotopes of Low Z Nuclei"*, Phys. Rev. D41 (1989) 2074 [InSpires:Hemmick:1989ns]. 92

[157] R.H. Cyburt, B.D. Fields, V. Pavlidou, B.D. Wandelt, *"Constraining strong baryon dark matter interactions with primordial nucleosynthesis and cosmic rays"*, Phys. Rev. D65 (2002) 123503 [arXiv:astro-ph/0203240]. 90

[158] G.D. Starkman, A. Gould , R. Esmailzadeh, S. Dimopoulos, *"Opening the Window on Strongly Interacting Dark Matter"*, Phys.Rev. 3594 (1990) D41 [InSpires:Starkman:1990nj]. 90

[159] M.W. Goodman, E. Witten, *"Detectability of Certain Dark Matter Candidates"*, Phys. Rev. 3059 (1985) D31 [InSpires:Goodman:1984dc] 90, 188

[160] G.D. Mack, J.F. Beacom, G. Bertone, *"Towards Closing the Window on Strongly Interacting Dark Matter: Far-Reaching Constraints from Earth's Heat Flow"*, Phys. Rev. D76 (2007) 043523 [arXiv:0705.4298]. 91

[161] R.N. Mohapatra, S. Nussinov, *"Possible manifestation of heavy stable colored particles in cosmology and cosmic rays"*, Phys. Rev. D57 (1997) 1940 [arXiv:hep-ph/9708497].

[162] E.B. Norman, S.B. Gazes, D.A. Bennett, *"Searches for Supermassive X- Particles in Iron"*, Phys. Rev. Lett. 58 (1986) 1403 [InSpires:Norman:1986ux]. 92

[163] S. Burdin, M. Fairbairn, P. Mermod, D. Milstead, J. Pinfold, T. Sloan, W. Taylor, *"Non-collider searches for stable massive particles"*, Phys. Rept. 582 (2015) 1 [arXiv:1410.1374]. 92

[164] P.F. Smith, J.R.J. Bennett, G.J. Homer, J.D. Lewin, H.E. Walford, W.A. Smith, *"A search for anomalous hydrogen in enriched $D_2O$, using a time-of-flight spectrometer"*, Nucl. Phys. B206 (1982) 333 [InSpires:Smith:1982qu]. 92

[165] M. Heine *et al.*, *"Determination of the neutron-capture rate of $^{17}C$ for r-process nucleosynthesis"*, Phys. Rev. C95 (2017) 014613 [arXiv:1604.05832]. 94

[166] IceCube Collaboration, *"Search for annihilating dark matter in the Sun with 3 years of IceCube data"*, Eur. Phys. J. C77 (2017) 146 [arXiv:1612.05949]. 95

[167] P. Baratella, M. Cirelli, A. Hektor, J. Pata, M. Piibeleht, A. Strumia, *"PPPC 4 DMν: a Poor Particle Physicist Cookbook for Neutrinos from Dark Matter annihilations in the Sun"*, JCAP 1403 (2014) 053 [arXiv:1312.6408]. 95

[168] J. Hisano, R. Nagai, N. Nagata, *"Effective Theories for Dark Matter Nucleon Scattering"*, JHEP 1505 (2015) 037 [arXiv:1502.02244]. 96

[169] XENON1T Collaboration, *"First Dark Matter Search Results from the XENON1T Experiment"*, Phys. Rev. Lett. 119 (2017) 181301 [arXiv:1705.06655]. 96

[170] M.E. Peskin, *"Short Distance Analysis for Heavy Quark Systems. 1. Diagrammatics"*, Nucl. Phys. B156 (1979) 365 [InSpires:Bhanot:1979vb]. M.B. Voloshin, *"On Dynamics of Heavy Quarks in Nonperturbative QCD Vacuum"*, Nucl. Phys. B154 (1979) 365 [InSpires:Voloshin:1978hc]. A. Dalgarno, J.T. Lewis, *"The exact calculation of long-range forces between atoms by perturbation theory"*, Proc. Royal Soc. 233 (1955) 70. 96, 98, 176

[171] CTA Collaboration, *"Prospects for Indirect Dark Matter Searches with the Cherenkov Telescope Array (CTA)"*, PoS ICRC2015 (2015) 1203 [arXiv:1508.06128]. 97

[172] M. Cirelli et al., *"PPPC 4 DM ID: A Poor Particle Physicist Cookbook for Dark Matter Indirect Detection"*, JCAP 1103 (2010) 051 [arXiv:1012.4515]. P. Baratella et al., *"PPPC 4 DMν: a Poor Particle Physicist Cookbook for Neutrinos from Dark Matter annihilations in the Sun"*, JCAP 1403 (2014) 053 [arXiv:1312.6408]. 97

[173] D.L. Morgan, V.W. Hughes, *"Atomic processes involved in matter-antimatter annihilation"*, Phys. Rev. D2 (1970) 1389 [InSpires:Morgan:1970yz]. D.L. Morgan, V.W. Hughes, *"Atom-Antiatom Interactions"*, Phys. Rev. A7 (1973) 1811 [InSpires:Morgan:1973zz]. P. Froelich et al., *"Hydrogen-Antihydrogen Collisions"*, Phys. Rev. Lett. 84 (2000) 4577. S. Jonsell, A. Saenz, P. Froelich, *"Low-energy hydrogen anti-hydrogen collisions"*, Nucl. Phys. A663 (2000) 959 [InSpires:Jonsell:2000wb]. 98

[174] L. Schiff, "*Quantum Mechanics*", section 27. This can also be seen classically as the Keesom interaction between rotating dipoles. 98

[175] H. Fujii, D. Kharzeev, *"Long range forces of QCD"*, Phys. Rev. D60 (1999) 114039 [arXiv:hep-ph/9903495]. 98

[176] See e.g. CMS Collaboration, *"Search for heavy stable charged particles with* 12.9 $\text{fb}^{-1}$ *of 2016 data"*, CMS-PAS-EXO-16-036. ATLAS Collaboration, *"Reinterpretation of searches for supersymmetry in models with variable R-parity-violating coupling strength and long-lived R-hadrons"*, ATLAS-CONF-2018-003. 99

[177] G. Grilli di Cortona, E. Hardy, A.J. Powell, *"Dirac vs Majorana gauginos at a 100 TeV collider"*, JHEP 1608 (2016) 014 [arXiv:1606.07090]. 99

[178] O. Antipin, M. Redi, A. Strumia, E. Vigiani, *"Accidental Composite Dark Matter"*, JHEP 1507 (2015) 039 [arXiv:1503.08749]. 102, 142, 144, 154, 155, 162, 189

[179] M.J. Strassler, K.M. Zurek, *"Echoes of a hidden valley at hadron colliders"*, Phys. Lett. B651 (2006) 374 [arXiv:hep-ph/0604261] 102, 158

[180] G.D. Kribs, T.S. Roy, J. Terning, K.M. Zurek, *"Quirky Composite Dark Matter"*, Phys. Rev. D81 (2009) 095001 [arXiv:0909.2034].

[181] O. Antipin, M. Redi, A. Strumia, *"Dynamical generation of the weak and Dark Matter scales from strong interactions"*, JHEP 1501 (2015) 157 [arXiv:1410.1817]. 102

[182] Appelquist:2014jch, *"Composite bosonic baryon dark matter on the lattice: SU(4) baryon spectrum and the effective Higgs interaction"*, Phys. Rev. D89 (2014) 094508 [arXiv:1402.6656]. 102

[183] R. Huo, S. Matsumoto, Y-L. Sming Tsai, T.T. Yanagida, *"A scenario of heavy but visible baryonic dark matter"*, JHEP 1609 (2016) 162 [arXiv:1506.06929]. 102

[184] J.M. Cline, W. Huang, G.D. Moore, *"Challenges for models with composite states"*, Phys. Rev. D94 (2016) 055029 [arXiv:1607.07865]. 102

[185] G.D. Kribs, E.T. Neil, *"Review of strongly-coupled composite dark matter models and lattice simulations"*, Int. J. Mod. Phys. A31 (2016) 1643004 [arXiv:1604.04627]. 102

[186] J.M. Berryman, A. de Gouvêa, K.J. Kelly, Y. Zhang, *"Dark Matter and Neutrino Mass from the Smallest Non-Abelian Chiral Dark Sector"*, Phys. Rev. D96 (2017) 075010 [arXiv:1706.02722]. 102, 105, 112

[187] K. Harigaya, M. Ibe, K. Kaneta, W. Nakano, M. Suzuki, *"Thermal Relic Dark Matter Beyond the Unitarity Limit"*, JHEP 1608 (2016) 151 [arXiv:1606.00159]. 102, 106, 111, 116, 145

[188] B. Lucini, M. Teper, U. Wenger, *"The High temperature phase transition in SU(N) gauge theories"*, JHEP 0401 (2003) 061 [arXiv:hep-lat/0307017]. O. Aharony, J. Marsano, S. Minwalla, K. Papadodimas, M. Van Raamsdonk, *"A First order deconfinement transition in large N Yang-Mills theory on a small 3 sphere"*, Phys. Rev. D71 (2005) 125018 [arXiv:hep-th/0502149]. 102

[189] Y. Bai, R.J. Hill, *"Weakly Interacting Stable Pions"*, Phys. Rev. D82 (2010) 111701 [arXiv:1005.0008]. 104

[190] O. Antipin, M. Redi, A. Strumia, E. Vigiani, *"Accidental Composite Dark Matter"*, JHEP 1507 (2015) 039 [arXiv:1503.08749]. 104, 105, 112, 113, 121

[191] T. Appelquist *et al.*, *"Stealth Dark Matter: Dark scalar baryons through the Higgs portal"*, Phys. Rev. D92 (2015) 075030 [arXiv:1503.04203]. 105

[192] D. Tucker-Smith, N. Weiner, *"Inelastic dark matter"*, Phys. Rev. D64 (2001) 043502 [InSpires:TuckerSmith:2001hy]. 106, 121

[193] C.J. Morningstar, M.J. Peardon, *"The Glueball spectrum from an anisotropic lattice study"*, Phys. Rev. D60 (1999) 034509 [arXiv:hep-lat/9901004] 107

[194] A. Soni, H. Xiao, Y. Zhang, *"Cosmic selection rule for the glueball dark matter relic density"*, Phys. Rev. D96 (2017) 083514 [arXiv:1704.02347]. 107

[195] D. Spier Moreira Alves, S.R. Behbahani, P. Schuster, J.G. Wacker, *"The Cosmology of Composite Inelastic Dark Matter"*, JHEP 1006 (2010) 113 [arXiv:1003.4729]. 110

[196] E. Witten, *"Baryons in the 1/n Expansion"*, Nucl. Phys. B160 (1979) 57 [InSpires:Witten:1979kh]. 110, 111

[197] D.L. Morgan, V.W. Hughes, *"Atomic processes involved in matter-antimatter annihilation"*, Phys. Rev. D2 (1970) 1389 [InSpires:Morgan:1970yz]. 111, 145

[198] D.L. Morgan, V.W. Hughes, *"Atom-Antiatom Interactions"*, Phys. Rev. A7 (1973) 1811 [InSpires:Morgan:1973zz]. 111

[199] P. Froelich et al., *"Hydrogen-Antihydrogen Collisions"*, Phys. Rev. Lett. 84 (2000) 4577. 111

[200] S. Jonsell, A. Saenz, P. Froelich, *"Low-energy hydrogen anti-hydrogen collisions"*, Nucl. Phys. A663 (2000) 959 [InSpires:Jonsell:2000wb]. 111

[201] C. Jacoby, S. Nussinov, *"The Relic Abundance of Massive Colored Particles after a Late Hadronic Annihilation Stage"* [arXiv:0712.2681]. 112, 145

[202] J. Polchinski, *"Introduction to cosmic F- and D-strings"* [arXiv:hep-th/0412244]. 112, 116

[203] B. Lucini, M. Teper, U. Wenger, *"The High temperature phase transition in SU(N) gauge theories"*, JHEP 0401 (2003) 061 [arXiv:hep-lat/0307017]. 114

[204] B.R. Webber, *"A QCD Model for Jet Fragmentation Including Soft Gluon Interference"*, Nucl. Phys. B238 (1984) 492 [InSpires:Webber:1983if]. 115

[205] B. Andersson, G. Gustafson, G. Ingelman, T. Sjostrand, *"Parton Fragmentation and String Dynamics"*, Phys. Rept. 97 (1983) 31 [InSpires:Andersson:1983ia]. 115

[206] Planck Collaboration, *"Planck 2015 results. XIII. Cosmological parameters"*, Astron. Astrophys. 594 (2016) A13 [arXiv:1502.01589]. 117, 118, 161

[207] G. Mangano, P.D. Serpico, *"A robust upper limit on $N_{\rm eff}$ from BBN, circa 2011"*, Phys. Lett. B701 (2011) 296 [arXiv:1103.1261]. 117

[208] M.A. Buen-Abad, G. Marques-Tavares, M. Schmaltz, *"Non-Abelian dark matter and dark radiation"*, Phys. Rev. D92 (2015) 023531 [arXiv:1505.03542]. 117, 132

[209] J. Lesgourgues, G. Marques-Tavares, M. Schmaltz, *"Evidence for dark matter interactions in cosmological precision data?"*, JCAP 1602 (2016) 037 [arXiv:1507.04351]. 117

[210] K. Jedamzik, *"Big bang nucleosynthesis constraints on hadronically and electromagnetically decaying relic neutral particles"*, Phys. Rev. D74 (2006) 103509 [arXiv:hep-ph/0604251]. 117, 118, 162

[211] T.R. Slatyer, N. Padmanabhan, D.P. Finkbeiner, *"CMB Constraints on WIMP Annihilation: Energy Absorption During the Recombination Epoch"*, Phys. Rev. D80 (2009) 043526 [arXiv:0906.1197]. 118

[212] G.F. Giudice, A. Romanino, *"Electric dipole moments in split supersymmetry"*, Phys. Lett. B634 (2005) 307 [arXiv:hep-ph/0510197]. 118, 126

[213] G.D. Kribs, I.Z. Rothstein, *"Bounds on longlived relics from diffuse gamma-ray observations"*, Phys. Rev. D55 (1996) 4435 [arXiv:hep-ph/9610468]. 118, 162

[214] W. Detmold, M. McCullough, A. Pochinsky, *"Dark Nuclei I: Cosmology and Indirect Detection"*, Phys. Rev. D90 (2014) 115013 [arXiv:1406.2276]. W. Detmold, M. McCullough, A. Pochinsky, *"Dark nuclei. II. Nuclear spectroscopy in two-color QCD"*, Phys. Rev. D90 (2014) 114506 [arXiv:1406.4116]. G. Krnjaic, K. Sigurdson, *"Big Bang Darkleosynthesis"*, Phys. Lett. B751 (2015) 464 [arXiv:1406.1171]. E. Hardy, R. Lasenby, J. March-Russell, S.M. West, *"Big Bang Synthesis of Nuclear Dark Matter"*, JHEP 1506 (2015) 011 [arXiv:1411.3739]. E. Hardy, R. Lasenby, J. March-Russell, S.M. West, *"Signatures of Large Composite Dark Matter States"*, JHEP 1507 (2015) 133 [arXiv:1504.05419]. 119

[215] R.J. Hill, M.P. Solon, *"WIMP-nucleon scattering with heavy WIMP effective theory"*, Phys. Rev. Lett. 112 (2014) 211602 [arXiv:1309.4092]. 119

[216] M. Cirelli, E. Del Nobile, P. Panci, *"Tools for model-independent bounds in direct dark matter searches"*, JCAP 1310 (2013) 019 [arXiv:1307.5955]. 120

[217] J.M. Alarcon, J. Martin Camalich, J.A. Oller, *"The chiral representation of the $\pi N$ scattering amplitude and the pion-nucleon sigma term"*, Phys. Rev. D85 (2011) 051503 [arXiv:1110.3797]. 120

[218] J.M. Alarcon, L.S. Geng, J. Martin Camalich, J.A. Oller, *"The strangeness content of the nucleon from effective field theory and phenomenology"*, Phys. Lett. B730 (2014) 342 [arXiv:1209.2870]. 120

[219] S. Fichet, *"Shining Light on Polarizable Dark Particles"*, JHEP 1704 (2017) 088 [arXiv:1609.01762]. 121

[220] T. Appelquist *et al.*, *"Detecting Stealth Dark Matter Directly through Electromagnetic Polarizability"*, Phys. Rev. Lett. 115 (2015) 171803 [arXiv:1503.04205]. 121

[221] R. Franceschini, G.F. Giudice, J.F. Kamenik, M. McCullough, A. Pomarol, R. Rattazzi, M. Redi, F. Riva, A. Strumia, R. Torre, *"What is the $\gamma\gamma$ resonance at 750 GeV?"*, JHEP 1603 (2016) 144 [arXiv:1512.04933]. 121, 125

[222] ATLAS collaboration, *"Search for new high-mass phenomena in the dilepton final state using 36.1 $fb^{-1}$ of proton-proton collision data at $\sqrt{s}$ = 13 TeV with the ATLAS detector"* [InSpires:ATLAS:2017wce]. 121, 157

[223] J. Kang, M.A. Luty, *"Macroscopic Strings and 'Quirks' at Colliders"*, JHEP 0911 (2008) 065 [arXiv:0805.4642]. 123

[224] J.E. Juknevich, D. Melnikov, M.J. Strassler, *"A Pure-Glue Hidden Valley I. States and Decays"*, JHEP 0907 (2009) 055 [arXiv:0903.0883]. 123

[225] J.E. Juknevich, *"Pure-glue hidden valleys through the Higgs portal"*, JHEP 1008 (2009) 121 [arXiv:0911.5616]. 123, 141

[226] L. Forestell, D.E. Morrissey, K. Sigurdson, *"Non-Abelian Dark Forces and the Relic Densities of Dark Glueballs"*, Phys. Rev. D95 (2017) 015032 [arXiv:1605.08048]. 123

[227] SHiP Collaboration, *"A facility to Search for Hidden Particles at the CERN SPS: the SHiP physics case"*, Rept. Prog. Phys. 79 (2016) 124201 [arXiv:1504.04855]. 124

[228] F.J. Botella, L.M. Garcia Martin, D. Marangotto, F.M. Vidal, A. Merli, N. Neri, A. Oyanguren, J.R. Vidal, *"On the search for the electric dipole moment of strange and charm baryons at LHC"*, Eur. Phys. J. C77 (2017) 181 [arXiv:1612.06769]. 124

[229] Y. Yang, *"Constraints on the basic parameters of dark matter using the Planck data"*, Phys. Rev. D91 (2015) 083517 [arXiv:1504.01195]. 126

[230] R. Essig, E. Kuflik, S.D. McDermott, T. Volansky, K.M. Zurek, *"Constraining Light Dark Matter with Diffuse X-Ray and Gamma-Ray Observations"*, JHEP 1311 (2013) 193 [arXiv:1309.4091]. K.K. Boddy, J. Kumar, *"Indirect Detection of Dark Matter Using MeV-Range Gamma-Ray Telescopes"*, Phys. Rev. D92 (2015) 023533 [arXiv:1504.04024]. Fermi-Lat Collaboration, *"Updated search for spectral lines from Galactic dark matter interactions with pass 8 data from the Fermi Large Area Telescope"*, Phys. Rev. D91 (2015) 122002 [arXiv:1506.00013]. 126

[231] O. Antipin, M. Redi, *"The Half-composite Two Higgs Doublet Model and the Relaxion"*, JHEP 1512 (2015) 031 [arXiv:1508.01112]. 126, 143

[232] A. Agugliaro, O. Antipin, D. Becciolini, S. De Curtis, M. Redi, *"UV complete composite Higgs models"*, Phys. Rev. D95 (2017) 035019 [arXiv:1609.07122]. 126

[233] ACME Collaboration, *"Order of Magnitude Smaller Limit on the Electric Dipole Moment of the Electron"*, Science 343 (2013) 269 [arXiv:1310.7534]. 127

[234] J. Hisano, S. Matsumoto, M. Nagai, O. Saito, M. Senami, *"Non-perturbative effect on thermal relic abundance of dark matter"*, Phys. Lett. B646 (2006) 34 [arXiv:hep-ph/0610249]. 127

[235] K.M. Belotsky, M.Y. Khlopov, S.V. Legonkov, K.I. Shibaev, *"Effects of new long-range interaction: Recombination of relic heavy neutrinos and antineutrinos"*, Grav. Cosmol. 11 (2005) 27 [arXiv:astro-ph/0504621]. 127

[236] S. El Hedri, A. Kaminska, M. de Vries, *"A Sommerfeld Toolbox for Colored Dark Sectors"*, Eur. Phys. J. C77 (2017) 622 [arXiv:1612.02825]. 127

[237] M. Cirelli, A. Strumia, *"Minimal Dark Matter: Model and results"*, New J. Phys. 11 (2009) 105005 [arXiv:0903.3381]. 133

[238] Pamela Collaboration, *"An anomalous positron abundance in cosmic rays with energies 1.5-100 GeV"*, Nature 458 (2008) 607 [arXiv:0810.4995]. M. Cirelli, M. Kadastik, M. Raidal, A. Strumia, *"Model-independent implications of the e+-, anti-proton cosmic ray spectra on properties of Dark Matter"*, Nucl. Phys. B813 (2013) 1 [arXiv:0809.2409]. AMS Collaboration, *"First Result from the Alpha Magnetic Spectrometer on the International Space Station: Precision Measurement of the Positron Fraction in Primary Cosmic Rays of 0.5–350 GeV"*, Phys. Rev. Lett. 110 (2013) 141102 [InSpires:Aguilar:2013qda]. 135

[239] A. Falkowski, J. Juknevich, J. Shelton, *"Dark Matter Through the Neutrino Portal"* [arXiv:0908.1790]. 137

[240] K.K. Boddy, J.L. Feng, M. Kaplinghat, T.M.P. Tait, *"Self-Interacting Dark Matter from a Non-Abelian Hidden Sector"*, Phys. Rev. D89 (2014) 115017 [arXiv:1402.3629]. 137, 138, 143

[241] K.K. Boddy, J.L. Feng, M. Kaplinghat, Y. Shadmi, T.M.P. Tait, *"Strongly interacting dark matter: Self-interactions and keV lines"*, Phys. Rev. D90 (2014) 095016 [arXiv:1408.6532]. 137, 138, 143, 187

[242] S.B. Gudnason, C. Kouvaris, F. Sannino, *"Towards working technicolor: Effective theories and dark matter"*, Phys. Rev. D73 (2006) 115003 [InSpires:Gudnason:2006ug]. 138

[243] C. Kouvaris, *"Dark Majorana Particles from the Minimal Walking Technicolor"*, Phys. Rev. D76 (2007) 015011 [arXiv:hep-ph/0703266]. 138

[244] M. Cirelli, N. Fornengo, A. Strumia, *"Minimal dark matter"*, Nucl. Phys. B753 (2005) 178 [InSpires:Cirelli:2005uq]. 139

[245] S. Catterall, L. Del Debbio, J. Giedt, L. Keegan, *"MCRG Minimal Walking Technicolor"*, Phys. Rev. D85 (2011) 094501 [arXiv:1108.3794]. 140

[246] G. Bergner, P. Giudice, G. Münster, I. Montvay, S. Piemonte, *"Spectrum and mass anomalous dimension of SU(2) adjoint QCD with two Dirac flavors"*, Phys. Rev. D96 (2017) 034504 [arXiv:1610.01576]. 140

[247] G. Bergner, P. Giudice, G. Münster, P. Scior, I. Montvay, S. Piemonte, *"Low energy properties of SU(2) gauge theory with $N_f = 3/2$ flavours of adjoint fermions"*, JHEP 1801 (2018) 119 [arXiv:1712.04692]. 140

[248] A. Athenodorou, E. Bennett, G. Bergner, B. Lucini, *"Infrared regime of SU(2) with one adjoint Dirac flavor"*, Phys. Rev. D91 (2015) 114508 [arXiv:1412.5994]. 140

[249] G. Bergner, P. Giudice, G. Münster, I. Montvay, S. Piemonte, *"The light bound states of supersymmetric SU(2) Yang-Mills theory"*, JHEP 1603 (2016) 080 [arXiv:1512.07014]. 140

[250] T. DeGrand, *"Lattice tests of beyond Standard Model dynamics"*, Rev. Mod. Phys. 88 (2015) 015001 [arXiv:1510.05018]. 140

[251] S. Ali, G. Bergner, H. Gerber, P. Giudice, I. Montvay, G. Munster, S. Piemonte, *"Simulations of N=1 supersymmetric Yang-Mills theory with three colours"*, PoS LATTICE2016 (2016) 222 [arXiv:1610.10097]. 140

[252] G. Bergner, P. Giudice, I. Montvay, G. Münster, S. Piemonte, *"Spectrum and mass anomalous dimension of SU(2) gauge theories with fermions in the adjoint representation: from $N_f = 1/2$ to $N_f = 2$"*, PoS LATTICE2016 (2017) 237 [arXiv:1701.08992]. 140

[253] D. Nogradi, A. Patella, *"Strong dynamics, composite Higgs and the conformal window"*, Int. J. Mod. Phys. A31 (2016) 1643003 [arXiv:1607.07638]. 140

[254] T. DeGrand, Y. Shamir, B. Svetitsky, *"Near the Sill of the Conformal Window: Gauge Theories with Fermions in Two-Index Representations"*, Phys. Rev. D88 (2013) 054505 [arXiv:1307.2425]. 140

[255] G.S. Bali, A. Pineda, *"QCD phenomenology of static sources and gluonic excitations at short distances"*, Phys. Rev. D69 (2003) 094001 [InSpires:Bali:2003jq]. 141, 184

[256] C.J. Morningstar, M.J. Peardon, *"The Glueball spectrum from an anisotropic lattice study"*, Phys. Rev. D60 (1999) 034509 [InSpires:Morningstar:1999rf]. 141

[257] J.E. Juknevich, D. Melnikov, M.J. Strassler, *"A Pure-Glue Hidden Valley I. States and Decays"*, JHEP 0907 (2009) 055 [arXiv:0903.0883]. 141

[258] H.B. Meyer, *"Glueball matrix elements: A Lattice calculation and applications"*, JHEP 0901 (2008) 071 [arXiv:0808.3151]. 141

[259] D.B. Kaplan, H. Georgi, *"SU(2) ⊗ U(1) Breaking by Vacuum Misalignment"*, Phys. Lett. 136B (1984) 183 [InSpires:Kaplan:1983fs]. 143

[260] C. Kilic, T. Okui, R. Sundrum, *"Vectorlike Confinement at the LHC"*, JHEP 1002 (2009) 018 [arXiv:0906.0577]. 143

[261] D. Barducci, S. De Curtis, M. Redi, A. Tesi, *"An almost elementary Higgs: Theory and Practice"*, JHEP 1808 (2018) 017 [arXiv:1805.12578]. 143, 155

[262] S. Bolognesi, M. Shifman, *"The Hopf Skyrmion in QCD with Adjoint Quarks"*, Phys. Rev. D75 (2007) 065020 [arXiv:hep-th/0701065]. 143

[263] R. Auzzi, S. Bolognesi, M. Shifman, *"Skyrmions in Yang-Mills Theories with Massless Adjoint Quarks"*, Phys. Rev. D77 (2008) 125029 [arXiv:0804.0229]. 143

[264] R.J. Scherrer, M.S. Turner, *"Decaying Particles Do Not Heat Up the Universe"*, Phys. Rev. D31 (1984) 681 [InSpires:Scherrer:1984fd]. 144

[265] M. Kamionkowski, M.S. Turner, *"Thermal relics: do we know their abundances?"*, Phys. Rev. D42 (1990) 3310 [InSpires:Kamionkowski:1990ni]. 144

[266] J. McDonald, *"WIMP Densities in Decaying Particle Dominated Cosmology"*, Phys. Rev. D43 (1989) 1063 [InSpires:McDonald:1989jd]. 144

[267] G.F. Giudice, E.W. Kolb, A. Riotto, *"Largest temperature of the radiation era and its cosmological implications"*, Phys. Rev. D64 (2000) 023508 [arXiv:hep-ph/0005123]. 144

[268] R.T. Co, F. D'Eramo, L.J. Hall, D. Pappadopulo, *"Freeze-In Dark Matter with Displaced Signatures at Colliders"*, JCAP 1512 (2015) 024 [arXiv:1506.07532]. 144, 148

[269] M. Cirelli, Y. Gouttenoire, K. Petraki, F. Sala, *"Homeopathic Dark Matter, or how diluted heavy substances produce high energy cosmic rays"*, JCAP 1902 (2019) 014 [arXiv:1811.03608]. 144

[270] A. Zenoni *et al.*, *"New measurements of the anti-p p annihilation cross-section at very low-energy"*, Phys. Lett. B461 (1999) 405 [InSpires:Zenoni:1999st]. 146

[271] G. Boyd, J. Engels, F. Karsch, E. Laermann, C. Legeland, M. Lutgemeier, B. Petersson, *"Thermodynamics of SU(3) lattice gauge theory"*, Nucl. Phys. B469 (1996) 419 [arXiv:hep-lat/9602007]. 152

[272] T. Han, S. Mukhopadhyay, X. Wang, *"Electroweak Dark Matter at Future Hadron Colliders"*, Phys. Rev. D98 (2018) 035026 [arXiv:1805.00015]. 157, 158

[273] R. Contino, T. Kramer, M. Son, R. Sundrum, *"Warped/composite phenomenology simplified"*, JHEP 0705 (2006) 074 [arXiv:hep-ph/0612180]. 157

[274] J. Kang, M.A. Luty, *"Macroscopic Strings and 'Quirks' at Colliders"*, JHEP 0911 (2008) 065 [arXiv:0805.4642]. 158

[275] K. Murase, J.F. Beacom, *"Constraining Very Heavy Dark Matter Using Diffuse Backgrounds of Neutrinos and Cascaded Gamma Rays"*, JCAP 1210 (2012) 043 [arXiv:1206.2595]. 161

[276] T.R. Slatyer private communication 161, 162

[277] M. Redi, R. Sato, *"Composite Accidental Axions"*, JHEP 1605 (2016) 104 [arXiv:1602.05427]. 163

[278] D.J.H. Chung, E.W. Kolb, A. Riotto, *"Superheavy dark matter"*, Phys. Rev. D59 (1998) 023501 [arXiv:hep-ph/9802238]. 163

[279] For recent works see S. Olszewski and T. Kwiatkowski, *"Semi-classical approach to intensity spectrum of atomic hydrogen"*, Z. Phys. D21 (1991) 201. M. Seidl, P.O. Lipas, *"Semiclassical interpretation of spontaneous transitions in the hydrogen atom"*, Eur. J. Phys. 17 (1996) 25. See also the references therein. 171

[280] N. Brambilla, G. Krein, J. Tarrús Castellà, A. Vairo, *"Long-range properties of* $1S$ *bottomonium states"*, Phys. Rev. D93 (2016) 054002 [arXiv:1510.05895]. 176

[281] S. Weinberg, *"The Quantum theory of fields. Vol. 1: Foundations"* [InSpires:Weinberg:1995mt]. 183

[282] D.B. Kaplan, *"Five lectures on effective field theory"* [InSpires:Kaplan:2005es]. 183